PHOSPHOPROTEOMICS OF MAMMARY GLAND DURING DIFFERENT STAGES OF DEVELOPMENT AND ITS ROLE IN LACTATION

THESIS SUBMITTED TO THE
ICAR-NATIONAL DAIRY RESEARCH INSTITUTE, KARNAL
(DEEMED UNIVERSITY)
IN PARTIAL FULFILMENT OF THE REQUIREMENTS
FOR THE AWARD OF THE DEGREE OF

DOCTOR OF PHILOSOPHY
IN
ANIMAL BIOTECHNOLOGY
BY

SYED AZMAL ALI
M.Sc. (Biotechnology)

ANIMAL BIOTECHNOLOGY CENTER
ICAR-NATIONAL DAIRY RESEARCH INSTITUE
(DEEMED UNIVERSITY)
KARNAL-132001 (HARYANA), INDIA

2021

Regn. No. 14-P-BT-07

PHOSPHOPROTEOMICS OF MAMMARY GLAND DURING DIFFERENT STAGES OF DEVELOPMENT AND ITS ROLE IN LACTATION

By

SYED AZMAL ALI

THESIS SUBMITTED TO THE
ICAR-NATIONAL DAIRY RESEARCH INSTITUTE, KARNAL
(DEEMED UNIVERSITY)
IN PARTIAL FULFILMENT OF THE REQUIREMENTS
FOR THE AWARD OF THE DEGREE OF

DOCTOR OF PHILOSOPHY
IN
ANIMAL BIOTECHNOLOGY

Approved by

External Examiner

(Dr. Ashok K. Mohanty)
Major Advisor

Members of Advisory Committee

1. **Dr. Jai K Kaushik**
   Principal Scientist,
   Animal Biotechnology Center

2. **Dr. Sudarshan Kumar**
   Scientist,
   Animal Biotechnology Center

3. **Dr. Manishi Mukesh**
   Principal Scientist,
   ICAR-NBAGR, Karnal

4. **Dr. Ajay K Dang**
   Principal Scientist,
   Dairy Cattle Physiology Division

5. **Dr. Suneel Kumar Onteru**
   Senior Scientist,
   Animal Biochemistry Division

ANIMAL BIOTECHNOLOGY CENTER
ICAR-NATIONAL DAIRY RESEARCH INSTITUTE
(DEEMED UNIVERSITY)
KARNAL-132001, HARYANA, INDIA

Dr. Ashok K. Mohanty
Principal Scientist

CERTIFICATE

This is to certify that the thesis entitled **"Phosphoproteomics of Mammary Gland during different stages of development and its role in Lactation"** submitted by **Syed Azmal Ali** towards the partial fulfilment of the requirement for the award of the degree of Doctor of Philosophy in **Animal Biotechnology** of the **ICAR-National Dairy Research Institute (Deemed University), Karnal (Haryana), India,** is a bonafide research work carried out by him under my supervision and no part of the thesis has been submitted for any other degree or diploma.

Date: 28/01/21

Dr. Ashok K Mohanty
Major Advisor

Phone: 0184-2259538, Fax: 0184-2250042, *Email:Ashok.Mohanty@icar.gov.in*

ACKNOWLEDGEMENT

All Praise to ALLAH, the Almighty, for giving me the blessing, the strength, the chance and endurance to complete this study.

I would like to express my sincere gratitude to my advisor Dr Ashok K Mohanty, for the continuous support for my PhD research.

I convey special acknowledgement to Director ICAR-N.D.R.I. (deemed university), Karnal and Head, Animal Biotechnology Centre for providing necessary facilities for carrying out this study and financial assistance in the form of N.D.R.I. Institutional fellowship during my PhD programme.

I owe my sincere thanks to my advisory committee members for their valuable suggestions and encouragement throughout the research period.

One year of financial assistance from the Indian Council of Medical Research (ICMR) is gratefully acknowledged. I am very thankful to the All Indian Institute of Medical Science (AIIMS) to use their central facilities for Transmission Electron Microscopy (TEM). I am highly thankful to Pradeep and Kuldeep for the TEM analysis of my samples and helping nature.

I am very much thankful to Referral Lab, ICAR-NDRI, Karnal, for allowing me to use their central facilities for LC-MS/MS and Fluorescent ELISA Plate Reader.

My sincere thanks also go to Dr Sanjeeva Srivastava, Principal Scientist, Animal Biotechnology Centre, who gave me access to LC-MS/MS facilities at his laboratory. Without his support, it would be very hard to conduct Proteomics during my research.

I want to mention my best friend Karmveer for his help and support during my entire PhD, for meaningful discussion about research, professional, and personal life. I am feeling lucky to have a friend like him.

I am highly thankful to my friend Parul Singh for her outstanding contributions in helping me write the thesis and complete proofreading.

My sincere thanks also go to my colleague Deepti Mittal, Harpreet Kaur and Vanya Bushan for their continuous support and love.

I am incredibly thankful to Gurjeet Kaur to help me in animal rearing, feeding, breeding and experimentation, while continuously giving her strong support, insights and encouragement.

I could not have finished this study without the full support of my beloved family. Neither language nor space is sufficient to express my deepest gratitude and heartfelt thanks to My father, Syed Arshad Ali and Mummy, Tanveer Ali, for their blessing, inspiration, encouragement and love that always given me a new step to move forward. I have no words to express my feelings towards my brother Syed Akmal Ali to help me learn the basics concept of computer science. He is the most logical person in my life. I like to take this opportunity to thank my sister Ateka Firdos, who always encourages me to think higher and given her complete support while taking care of my family when I am always away from my parents (home).

Thank you all of you for your great support and encouragement to complete this journey

CONTENTS

LIST OF TABLES

LIST OF FIGURES

LIST OF ABBREVIATIONS

%	Percent
@	At the rate of
°C	Degree centigrade
Abs	Absorbance
ANOVA	Analysis of variance
ATP	Adenosine tri-phosphate
BAX	BCL2 Associated X
BCL2	B-cell lymphoma 2
BSA	Bovine Serum albumin
Ca^{2+}	Calcium ions
cAMP	Cyclic adenosine monophosphate
CO_2	Carbon dioxide
DF	Dilution factor
DMEM/ F12	Dulbecco's Modified Eagle Medium/Nutrient Mixture F-12
DMSO	Dimethyl Sulfoxide
DNA	Deoxyribonucleic Acid
DPBS	Dulbecco's Modified phosphate buffered saline
DTT	Dithiothreitol
EDTA	Ethylenediamine tetraacetic acid
EtBr	Ethidium bromide
g	Gram
G	Gravitational force
GAPDH	Glyceraldehyde 3-phosphate dehydrogenase
GD	Gestation day
GPX	Glutathione peroxidase
h	hour
HEPES	(4-(2-hydroxyethyl)-1-piperazineethanesulfonic acid)
IHC	Immunohistochemistry
ISO	International Organization for Standardization
iTRAQ	Isobaric tags for relative and absolute quantitation
L	Litre

LC	Lethal Concentration
Ltd	Limited
M	Molar
m^3	Meter cube / cubic meter
mg	Milli gram
Mg^{++}	Magnesium ion
Min	Minutes
mL	Millilitre
mm	Millimeter
mM	Millimolar
MG	Mammary gland
mRNA	Messenger RNA
MS	Mass Spectrometry
NGS	Next generation sequencing
HT	High-throughput
MTT	3-(4,5-dimethylthiazol-2-yl)-2,5-diphenyl tetrazolium bromide
NR	Neutral Red
DCFH-DA	carboxy-2',7'-dichloro-dihydro-fluorescein diacetate
N	Normality
NDRI	National Dairy Research Institute
ng	Nanogram
nm	Nanometre
NO	Nitric oxide
No.	Number
NRU	Neutral red Uptake
OD	Optical density
OECD	Organisation for Economic Co-operation and Development
PBS	Phosphate buffered saline
PCR	Polymerase chain reaction
PGA	Polyglutamic acid
pH	Negative log of hydrogen ion concentration

PLG	Poly lacto-glycolide
PND	Postnatal day
PVA	Polyvinyl alcohol
PVP	Polyvinyl pyrrolidone
Pvt.	Private
qPCR	Quantitative PCR
RNA	Ribonucleic acid
ROS	Reactive Oxygen Species
rpm	Revolutions per minute
RT	Room Temperature
Sec	Second
SEM	Standard error of mean
SD	Standard Deviation
SOD	Super oxide dismutase
TEM	Transmission electron microscopy
TiO_2	Titanium dioxide
TNF-α	Tumor necrosis factor alpha
TMT	Tandem Mass Tags
UV	Ultraviolet
v/v	volume/volume
w/v	weight/volume
µ	Micron
µg	Microgram
µL	Microlitre
µm	Micrometer

PHOSPHOPROTEOMICS OF MAMMARY GLAND DURING DIFFERENT STAGES OF DEVELOPMENT AND ITS ROLE IN LACTATION

ABSTRACT

The mammary gland is apocrine undergoes series of morphological changes during the lifetime of a female. It is the only organ whose complete development takes place after birth in response to reproductive hormones. In the phase of the pregnancy-lactation-involution cycle, the drastic remodelling occurs. The phosphoproteomics based study of mammary gland development resulted in the discovery of 6235 phosphoproteins, 20,328 phosphopeptides and ~25,000 phosphosites using five search engines. The phosphorylation occupancy localization ratio was found to be 10:7:3 in STY amino acid, respectively. We discovered kinases (N=256) and phosphatases (N=80) cross-talk for the mammary gland's lactation function. The tSNE machine-learning algorithm showed the 19 critical proteins in the phosphoproteome data. TEM microscopy details the crucial role of nucleus associated phosphoproteins. Upon hormonal changes, the mammary gland's remodelling occurs with six unique phosphorylated ubiquitin proteins in each different stage: Rnf7; Cop1; Trim30c; Bmi1; Rnf133; and Dtx1. The combined phosphopeptide analysis identified 2552 common while unique 14287 and 7060 in EpH4 and BuMEC. The total phosphoproteome in EpH4 and BuMEC is 8,468 and 7,036, respectively. Lactogenic differentiation resulted in the discovery of 5,451 phosphorylated proteins containing 13,855 phosphopeptides in BuMEC further 5,189 phosphorylated proteins; 16,194 phosphopeptides with more than 25,000 phosphosites in EpH4 cell line. Upon hormonal differentiation ten and eight milk, associated phosphoproteins are identified in the BuMEC and EpH4 cell lines, respectively. MFGE8 is one of the highlighted essential common connecting phosphoprotein identified among these studies. MFG-E8 suppression results in reduced mammary epithelial cells' growth by an autocrine/paracrine mechanism and induction of transcription factors such as cyclins D1, FOXA1, ZNF652, and AURKB for modulating the cytoskeleton-associated proteins and cell cycle regulators. We conclude that mammary gland remodelling's metabolic activity is regulated by adipogenesis and epithelial cells trans-differentiation by shifting the phosphorylation event in different stages. The phosphoproteomics data provide new insight into the cell polarization linked to the PI3K-Akt; mTOR; Cadherin; JAK/STAT; Oxytocin receptor-mediated; LIF; and Wnt signalling pathways commonly regulated between in-vivo and in-vitro studies. Our findings brighten up the concept regarding the importance of MFGE8 protein in overall mammary gland development. We finally anticipate that our comprehensive datasets will serve as a valuable foundation for further validation and mechanistic exposition of many novel proteins involved in the mammary gland development signalling.

विकास के विभिन्न चरणों और स्तनपान में इसकी भूमिका के दौरान स्तन ग्रंथि के फॉस्फोप्रोटोमिक्स

सार

स्तन ग्रंथि एक महिला के जीवनकाल के दौरान रूपात्मक परिवर्तनों की श्रृंखला है। यह एकमात्र अंग है जिसका पूरा विकास प्रजनन हार्मोन के जवाब में जन्म के बाद होता है। गर्भावस्था-स्तनपान-चालन चक्र के चरण में, कठोर रीमॉडेलिंग होती है। स्तन ग्रंथि के विकास के फास्फोटोप्रोटिक्स पर आधारित अध्ययन में पांच खोज इंजनों का उपयोग करते हुए 6235 फॉस्फोप्रोटीन, 20,328 फॉस्फोपेप्टाइड और ~ 25,000 फॉस्फोसिट्स की खोज हुई। फॉस्फोराइलेशन ऑक्यूपेंसी स्थानीयकरण अनुपात क्रमशः STY एमिनो एसिड में 10: 7: 3 पाया गया। हमने स्तन ग्रंथि के लैक्टेशन फ़ंक्शन के लिए काइनेज (एन = 256) और फॉस्फेटेस (एन = 80) क्रॉस-टॉक की खोज की। tSNE मशीन-लर्निंग एल्गोरिथ्म ने फॉस्फोप्रोटेम डेटा में 19 महत्वपूर्ण प्रोटीन दिखाए। TEM माइक्रोस्कोपी नाभिक से जुड़े फॉस्फोप्रोटीन की महत्वपूर्ण भूमिका का विवरण देता है। हार्मोनल परिवर्तनों पर, स्तन ग्रंथि की रीमॉडेलिंग प्रत्येक अलग-अलग चरण में छह अद्वितीय फॉस्फोराइलेटेड यूबिकिटिन प्रोटीन के साथ होती है: Rnf7; Cop1; Trim30c; Bmi1; Rnf133; और Dtx1। संयुक्त फॉस्फोपेप्टाइड विश्लेषण ने 2552 सामान्य है, जबकि अद्वितीय 14287 और 7060 ने EpH4 और BuMEC में होने की पहचान की । EpH4 और BuMEC में कुल फॉस्फोप्रोटेम क्रमशः 8,468 और 7,036 है। लैक्टोजेनिक भेदभाव के परिणामस्वरूप 5,451 फॉस्फोराइलेटेड प्रोटीन की खोज हुई, जिसमें BuMEC में 13,855 फॉस्फोपेप्टाइड, 5,189 फॉस्फोराइलेटेड प्रोटीन; EpH4 कोशिका की परत में 25,000 से अधिक फॉस्फोसाइट्स के साथ 16,194 फॉस्फोपेप्टाइड शामिल हैं । हार्मोनल विभेदीकरण क्रमशः दस और आठ दूध से संबंधित फॉस्फोप्रोटीन BuMEC और EpH4 सेल लाइनों में पहचान की गई। MFGE8 इन अध्ययनों में पहचाने जाने वाले फ़ॉस्सोप्रोटीन को उजागर करने वाले आवश्यक सामान्य में से एक है। एमएफजी-ई 8 (MFGE8) के दमन के परिणामस्वरूप एक स्तनधारी / पैरासरीन तंत्र द्वारा स्तनधारी उपकला कोशिकाओं की वृद्धि कम हो जाती है और साइटोस्केलेटन से जुड़े प्रोटीन और सेल चक्र नियामकों को संशोधित करने के लिए प्रतिलेखन कारकों जैसे कि cyclins D1, FOXA1, ZNF652, और AURKB को शामिल किया जाता है। हम निष्कर्ष निकालते हैं कि स्तन ग्रंथि रीमॉडेलिंग की चयापचय गतिविधि को अलग-अलग चरणों में फॉस्फोराइलेशन घटना को स्थानांतरित करके एडिपोजेनेसिस और उपकला कोशिकाओं को ट्रांस-भेदभाव द्वारा नियंत्रित किया जाता है। फॉस्फोटोप्रोटिक्स डेटा PI3K-Akt से जुड़े सेल ध्रुवीकरण में नई अंतर्दृष्टि प्रदान करता है; mTOR; केडरहिन; JAK / STAT; ऑक्सीटोसिन रिसेप्टर-मध्यस्थता; LIF; और आमतौर पर इन-विवो और इन-विट्रो अध्ययनों के बीच सिग्नलिंग मार्ग को विनियमित नहीं करना चाहिए। हमारे निष्कर्ष समग्र स्तन ग्रंथि के विकास में MFGE8 प्रोटीन के महत्व के बारे में अवधारणा को उज्ज्वल करते हैं। हम अंत में अनुमान लगाते हैं कि हमारे व्यापक डेटासेट स्तन ग्रंथि विकास सिग्नलिंग में शामिल कई उपन्यास प्रोटीनों के आगे सत्यापन और यंत्रवत प्रदर्शनी के लिए एक मूल्यवान आधार के रूप में काम करेंगे।

CHAPTER –1

Introduction

INTRODUCTION

The mammary gland produces and delivers milk from mother to newborn. The only organ after which an entire class of animals has been named, the mammary gland is responsible for the success of mammalian evolution. Primarily due to nutritional and nutraceutical properties of milk (Peaker, 2002). Lactation, the synthesis and secretion of milk, is made possible by the architecture of the gland. The mammary gland uses fluid transport through the mammary epithelium structure that develops into an elaborate network of branched ducts which maximize surface area within a constrained volume like other organs. The mature mammary duct consists of an outer layer of myoepithelial cells and an inner layer of luminal epithelial cells that surround a hollow lumen and differentiate into milk-producing alveoli. It releases milk through duct upon hormone-triggered contraction of the myoepithelium (Forsyth and Neville, 2009). The epithelial ductal tree is enveloped by a basement membrane (Williams and Daniel, 1983) and embedded within a complex stroma, the mammary fat pad, which contains fibroblasts, adipocytes, blood vessels, nerves and various immune cells, all of which are important for normal mammary development and function (Polyak and Kalluri, 2010).

Mammary development occurs in three distinct and differentially regulated stages: embryonic, pubertal and adult. In many animals, embryonic mammary development begins mid-gestation by forming pairs of placodes in the epithelial layer that invaginate into the underlying mesenchyme to form the mammary buds anlagen (Robinson 2007; Watson and Khaled, 2008). The mammary bud then proliferates and extends 10–20 sprouts (Hens and Wysolmerski, 2005), thus transforming into a rudimentary ductal structure. After birth, the rudimentary gland enters a phase of morphogenetic quiescence. Puberty is perhaps the most striking stage of mammary morphogenesis. Prompted by elevated levels of ovarian hormones, including oestrogen, the rudimentary ducts' ends proliferate and swell into distinct multilayered epithelial structures known as terminal end buds (TEBs) (Hinck and Silberstein, 2005). These ductal structures then undergo

successive rounds of elongation, bifurcation and lateral branching until reaching the fat pad's limit, thus forming a full epithelial tree (Sternlicht, 2006). During pregnancy, the luminal epithelium proliferates and differentiates into milk-producing secretory alveoli (Brisken et al., 1999; Lu and Werb, 2008). Massive apoptosis then removes up to 80% of the epithelium during post lactational involution (Davies et al., 2002; Affolter et al., 2009). Remarkably, the mammary gland maintains its ability to perform this dramatic remodelling during the pregnancy–lactation–involution cycle for several decades in animals.

Post-translational modifications (PTMs) are essential mechanisms used by eukaryotic cells to regulate their protein functions and dynamically coordinate their signalling networks. Defects in PTMs have been linked to numerous developmental disorders and diseases, highlighting the importance of PTMs in maintaining normal cellular states. This is important to understanding the role of PTMs (glycosylation, phosphorylation, acetylation, and methylation) in regulating cellular signalling and pathways. Protein Phosphorylation is one of the PTM that plays a fundamental role in signal transduction and is a crucial regulator of essential cellular processes including metabolism, growth, cell cycle progression, migration and apoptosis (Cohen 2001; Manning et al. 2002; Ubersax and Ferrell 2007). Disruption of signalling pathways is associated with the pathology of many diseases, including invasion of pathogens, cancer, diabetes, autoimmune diseases and neurodegenerative conditions (Cohen 2001). Hence, understanding the activity of signal transduction pathways can lead to identifying novel therapeutic targets and biomarkers. Such biomarkers may be used to stratify ill animal according to their signalling defects, therefore enabling the implementation of targeted treatments based on the activity status and circuitry of affected cells (Cutillas and Jorgensen 2011).

In the present study, we focus on development during puberty to involution, paying close attention to phosphoproteins mechanisms that establish the mammary epithelial tree's pattern. Some of the elegant mechanisms that drive mammary patterning might be conserved across branched epithelia, and others that will pave the way for new paradigms in the study of morphogenesis. We have also discussed the role proteins and collective cellular phosphoproteome in branching of mammry ducts and how they are involved in signalling networks, specifically lactation (Milk Production). The principles that

will emerge should help us build comprehensive models for mammary development and important foreplay of phosphoproteomics, particularly milk production and organogenesis in general. Keeping this view in mind, the present study is designed for "**Phosphoproteomics of Mammary Gland during different stages of development and its role in Lactation**" with the following objectives:

I. Comparative phosphoproteome analysis of mammary epithelial cells for identification of ubiquitous expression of phosphoproteins.

II. Time-resolved identification of Phosphoproteome in Mammary gland at six stages of development.

III. Targeted validation of an important Phosphoprotein in cell line involved in lactation.

CHAPTER –2

Review of Literature

2.1 The mammary gland

The class Mammalian is especially called Mammals due to the presence of uniquely characterised anatomical structures that are globally termed as mammary glands. The presence of this unique glandular organ separates the mammals from other animals. In the case of farm animals, it is called Udder, and in humans, it is called Breast. This organ's vital role is to nourish the new-born offspring by producing and secreting milk. It is the only organ whose maturation takes place outside the mother's uterus, i.e., postnatal life, hence it provides the unique model system for the biologist to study the organ developmental/organogenesis and specificity.

The mammary gland transformation warrants inductive cell-cell communication between epithelium and mesenchyme via molecules or respective receptors in terms of growth, development, differentiation, and oncogenesis. This present-day idea is almost 100 years old, and it was estimated that the evolution of the mammary gland most likely took place from apocrine sweat glands over 300 million years ago (Oftedal, 2002). It has been identified very long that mammary mesenchyme is the induction of overlying ectoderm, upon specified differentiation it developed into mammary bud formation (Propper and Gomot, 1967). Therefore, it appears as a rudimentary thicken structure in the fetus body and limited to a small ventral epidermis or ectoderm area, which resulted in the mammary "framework". After birth, depending on the hormonal response during the female's puberty stage, the gland initiates branching into the fat pad. It is essential here to report that mammary gland development or organogenesis is not only in the context of growth but also in cellular functional differentiation and glandular structural regression in response to the female reproductive cycle (Daniel and Smith, 1999). Before the gonadal hormone release and at the initial period of the puberty, the development of mammary gland is equivalent to the overall animal body ratio. In mice's case, at the age of 4 weeks, during the dawn of puberty, the terminal end buds (TEBs) structures are observed, which result in ductal

extension and branching. TEBs are mainly growing ducts at the tip and morphologically look like large club-shaped specialised structures which contain two distinct cell types, body and cap cells. Later, body cells differentiate into mammary epithelial cells, and cap cells differentiate into myoepithelial precursors (Humphreys et al., 1996). The category of TEBs which contains high regeneration powers impels ductal tree extension and further embraces a layer of luminal epithelial cells that build the transport channel for milk ejaculation at lactation. However, primary ducts are encircled by a sheet of myoepithelial cells and at maturation gets discontinuous by secondary/tertiary ducts and the TEBs **(Figure 1)**.

The mammary gland is the only organ which undergoes extensive structural and functional changes during the lifetime of the female and attractive model for molecular interrogation. Majority of these changes occur during postnatal life and are driven by **circadian rhythmicity of mammary gland clock** in oestrous/menstrual hormones cues. However, dramatic alterations seen in pregnancy, lactation and involution cycles **(Figure 1).** All these stages are mainly responsible for mammary gland cellular proliferation, differentiation or regression/programmed cell death in response to chemically induce timely hormonal stimulus, finally, resulting in significant glandular tissue architectural remodelling. In this regard, it is natural that this organ system study provides a platform to understand the mechanism of cell fate regulation and specification, cellular polarity, tissue remodelling, branching like tree morphogenesis, and, most importantly, apoptosis through involution of a functional organ. Interestingly, several dysregulated molecular signalling pathways observed in breast cancer progression mimic similar those surveyed at the distinct phases of development normal mammary gland/breast development and its remodelling. Hence, the study of normal mammary gland/breast development is of high interest to developmental and cancer biologists.

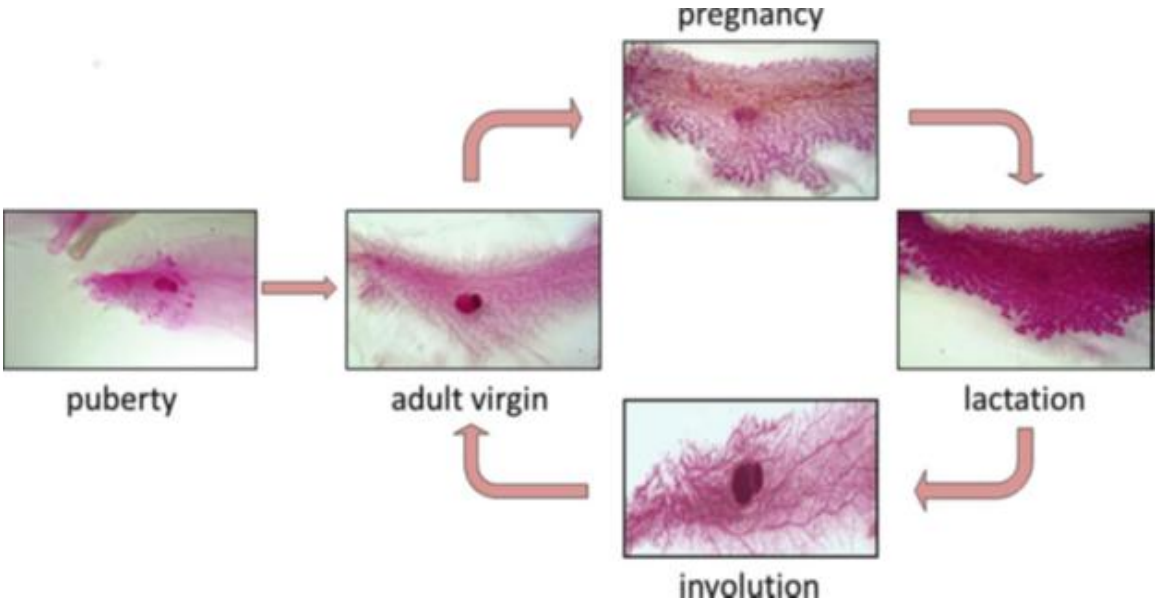

Figure 2.1. Carmine alum-stained mouse mammary gland whole-mounts showing the changes in mammary ductal development during puberty, pregnancy, lactation, and involution

This review will focus on mainly rodent and comparison with human and cattle mammary gland morphogenesis and remodelling, three critical stages of development—starting from an early embryonic stage to puberty up till involution (reproductive) stages. Our understanding of these biological processes is mostly from studies carried out in mice, giving the information for other mammals too, including human breasts and cattle udders. Nonetheless, there are quite a few differences concerning the architectural and hormonal signalling among mouse, human and cattle's mammary glands. However, many scientists, including our lab employed the rodent's organism mammary gland as a model system to understand and investigate the molecular mechanism of glandular development as it is easily accessible to complicated in vivo and in vitro investigations. These mammary gland stages predominantly consist of epithelial and mesenchymal cells that maintain the respective developmental phase’s equilibrium.

However, depending on the phase, mammary gland receives the stimuli in terms of systemic hormones regulatory controls, autocrine and paracrine growth factors, cytokines, epithelial-mesenchymal interactions, and the surrounding microenvironment cell-cell communication. Epithelial and mesenchymal cells lead to the assembly of collecting ducts with hollow alveolar ductules comprising

terminal duct lobular units that function to synthesise and expel milk. At the period of genesis, these cells coordinate to generate parenchyma and stroma precursor's cells too. Majorly postnatal mammary gland organogenesis consists of six stages: puberty, virgin (adulthood), pregnancy, lactation involution and menopause (in rodent retired female) **(Figure. 2)** (Humphreys et al., 1998; Richert et al., 2000). An explicit set of stimulus guides regulates all these stages to significantly dynamic morphogenetic alterations in glandular structure and function. The glandular system's remodelling majorly occurs via rounds of cell proliferation, differentiation, and apoptosis until the female menopause phase gets completed. Hence, the mammary gland accumulates substantial diverse cell varieties: including epithelial cells, adipocytes, fibroblasts, vascular endothelial cells, and immune cells. Fascinatingly, these changes are similar in the physiological responses of inflammation and pathological episodes such as tumorigenesis are noteworthy. Here, in my project work, I studied how these fundamental processes contour the gland's composition and function at every development point using proteomics, phosphoproteomics, transcriptomics, and miRNAomics techniques.

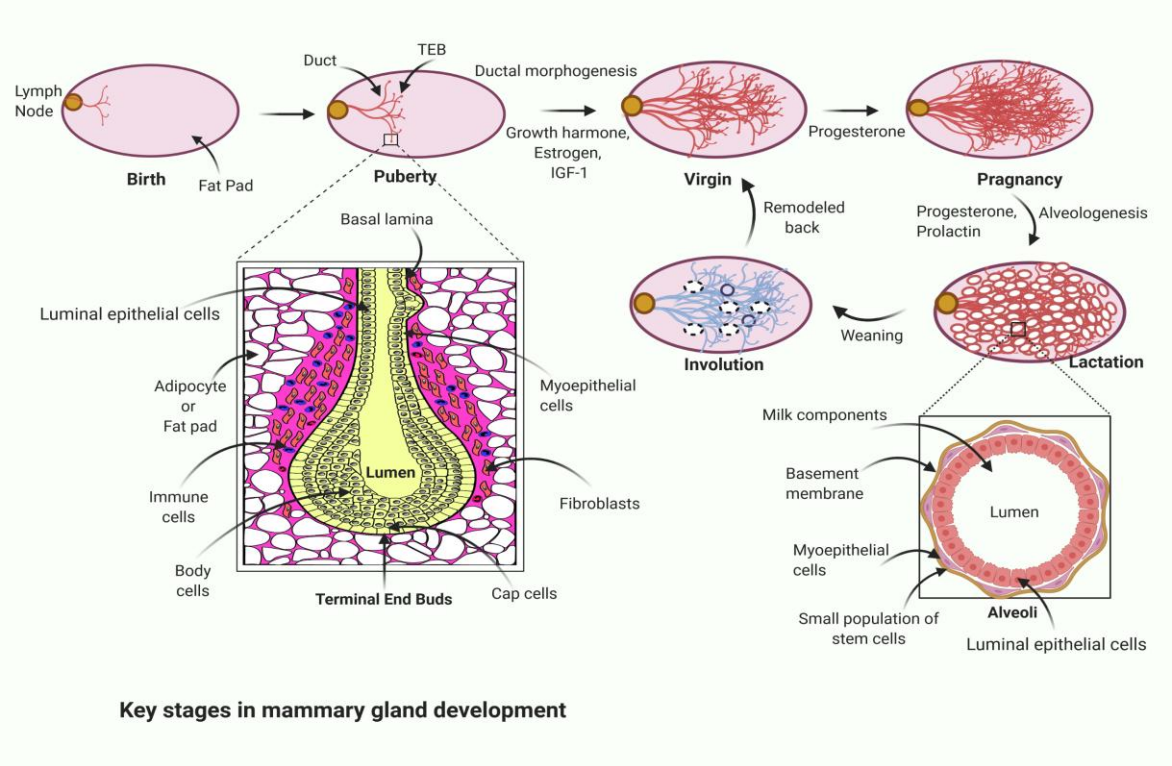

Key stages in mammary gland development

Figure 2.2. Drawing portrayal of the stages of postpartum exocrine gland development. At birth, the exocrine gland epithelial tissue is rudimentary, consisting of solely many tiny ducts that grow allometrically till pubescence (4 weeks in mice). With the onset of pubescence, expansive growth in an exceedingly method known as ductal ontogenesis fills the fat pad with the animal tissue exocrine gland tree. This development is influenced by human growth hormone (GH), estrogen, and a protein, insulin-like growth factor-1 (IGF1). Within the mature virgin, formation of short tertiary branches underneath the influence of progesterone. Still, alveologenesis solely happens upon the physiological state with the induction of lactogenic hormone (PRL), which, beside Lipo-Lutin, fuels alveolar cell's growth. PRL stimulation continues into the lactogenesis stage, culminating in milk production that continues till a scarcity of demand at substitution signals involution and also the exocrine gland is remodelled back to its original adult state.

This complex secretory organ contains extensive morphological lobulo-alveolar regeneration, especially during ductal branching at pregnancy, however, at early lactation, alveolar and ductal cells endure a series of cell division (Humphreys et al., 1998). Finally, results into the functional differentiation of cells during parturition for the synthesis and secretion of milk during lactation, in this way during pregnancy, lactation and involution alveolar cells switch quickly through energetic proliferation, differentiation, and apoptosis **(Figure 2**) (Strange et al., 1992). The complete involution of the lobulo-alveolar epithelial cells remodelling occurs when the pups stop taking milk from mother (weaning) and the mammary gland's regression, which again bears a resemblance to the virgin-like morphology.

In 1924, two developmental biologists H. Spemann and H. Mangold definitively generated the notion of embryonic induction when they wrote a seminal paper (Spemann et al., 2001). They experimented using separate newt gastrula's microsurgical transplantation from the dorsal grey crescent quarter to the ventral portion of the different newt gastrula. The outcome of the investigation inferred the fluctuations in the fate of nearby master cells from non-neural to the neural tissue and suggested that processes between embryonic tissues controlled cell differentiation and morphogenesis. In 1935, this discovery

led them to a Nobel Prize in Physiology or Medicine for Spemann. However, nobody was able to identify the molecule that signals the message for which Spemann dubbed the "primary embryonic organiser".

After a long time in the 1950s, Clifford Grobstei identified that organogenesis of the glandular tissues during the prenatal stage of mice required morphogenetic interactions between mesenchyme and epithelium (Grobstein, 1953; Grobstein, 1967). He experimented with sorted two tissues from embryonic day 13 (E13) submandibular and E11 metanephric rudiments with proteolytic enzymes and microsurgery. Further, the membrane filters were used to block the immediate connection within homogeneous and heterogeneous mixtures of these epithelial and mesenchymal in "on-the-clot" tissue cultures and resulted in no growth in either tissue. The outcomes implied that morphogenesis of dichotomous branching canals in submandibular epithelium depended on particular effectors from its analogous mesenchyme. Conversely, the epithelial transformation of metanephric mesenchyme in coiled tubules, a fantastic few converted to glomeruli, turned on explicit effectors from its analogous epithelium. Although differentiation of one tissue likely wanted diffusible molecules from the neighbouring tissue, the effector's essence was undiscovered. Consequently, epithelial-mesenchymal communications fitted as a burning problem for developmental biologists globally. (Freischmajer and Billingham, 1968). From 1967 to 1981, similar experiments were done on the pancreas (Wessells and Cohen, 1967), kidney (Saxen, 1970; Ekblom, 1984), digestive tract (Fukamachi et al., 1979; Simon-Assmann et al., 1988), prostate (Cunha et al., 1980) and teeth (Slavkin et al., 1981).

Combinational transplantation of isografts of E16 mouse mammary epithelium with either E16 mammary mesenchyme or E14 salivary mesenchyme syngeneic recipients (Sakakura et al., 1976) further solved the mystery. The experiment result showed that mammary gland morphogenesis is mesenchyme-dependent, and its cytodifferentiation also epithelium-specific. Distinct cell types form the organ and review eternally-improving understanding of stroma–epithelial intercommunications, how external factors decide the glandular microenvironment, and influence cell fate and function in mammary gland biology. Here, I bestow mammary gland development and remodelling

information, highlighting the significant morphological changes related to the inductive capacity and supportive function of mammary mesenchyme in normal development.

2.1.1 Morphology of mammary gland

The description is mostly about the mouse mammary gland (MG); however, whenever it is possible, we will discuss the human and cattle mammary gland development. The mammary gland comprises two cellular compartments, epithelial and stromal cells from the embryonic ectoderm and mesoderm, respectively (Hennighausen and Robinson, 2001). There are five mammary fat pad pairs between the forelimb and hindlimb of the mouse beneath the skin on the mammary line, mostly embroidered with fat, connective tissue, and rudimentary ductal branches in a tree-like structure (Parmar and Cunha, 2004)**.** The mammary line or milk line is the thickened epidermis between the mid-ventral region of the embryo. It contains three thoracic and two lingual fat pad pairs. The first pair of mammary glands is minimally differentiated.

In contrast, the fifth pair is correctly differentiated in the arrangement, describing the specification's gradient (Bolander, 1990). All of the pairs contains the lymph node and can be observed deftly in whole-mount staining of the glands (Russo IH, Russo, 1996). The mammary gland's arrangement in nature is such a way that, in all the mammals, the fat pad in the predominant epithelial duct bridge to the nipple and functions for the release of milk during the period of lactation (Daniel et al., 1987; Sakakura et al., 1987). However, interestingly, to report that mice have five pairs, human one and cattles are with two pairs; however, all the organisms contain similar epithelial cells. A summary of the knowledge for different phases of mammary gland development is detailed below section starting from inside the uterus from the embryonic development to puberty till pregnancy-lactation-involution cycle.

2.1.2 Embryonic mammary gland development

During embryogenesis, changes were governed by mesenchyme; however, puberty onset and adulthood were directed by the circulating hormones, which is the synthesis and secreted by the pituitary and ovary and released into the bloodstream. Mammary epithelium comprises two main types

of cells, named basal and luminal. Basal epithelium embodies mainly myoepithelial cells, which participate as the gland's outer layer, and a few stem cells that generate different cell types. Contrarily, luminal epithelium majorly form ducts and secretory unit i.e.alveoli, and also comprises a small set of the population that defines their hormone receptor status. The epithelium generated by luminal and basal cells bilayer forms the tubular structure, making it the finest suitable structure for milk-producing unit function. During milk secretion, outer myoepithelial cells contract themselves to squeeze the milk from the inner alveolar luminal cells. The embryonic mouse and the human mammary gland's development was similar, and the placode-derived mammary epithelial bud invades the underlying mesenchyme. However, human development is more complicated than that of the mouse and is characterized by ten phases defined by the fetal length (Russo and Russo, 2004).

2.1.3 The role of dermal mesenchyme in the induction of mammary development

In the late 90s, it was identified that development of mouse mammary gland starting to grow on E10–11, where basal cells of ectoderm enlarged and developed into **mammary bands** (Turner et al., 1933) and also leading to the formation of mammary streaks on both sides of the body from the upper to the lower limb buds in the rat (Myers, 1917), human (Raynaud, 1961), and rabbit (Propper, 1978) embryos. In the stage of E11–12 embryo, the cells of ectoderm develop the five pairs of lens-shaped structures called as placodes epidermal cell migration along with the mammary bands (Balinsky, 1950), as further development of placodes structure leads to the formation of buds (Veltmaat et al., 2003). However, the epithelium explants dissected and cultured from the placodes area do not give rise to mammary buds, which clear the fact that only ectoderm cells do not have the competence to initiate the placodes formation (Sakakura, 1987). In this context, the question is what other outside factors are required for the epithelium to complete the mammogenesis.

To understand the answer, Klaus Kratochwil in 1969 used the recombinant cultures of embryo day 12–16 mouse mammary epithelium with E12 mammary mesenchyme with a monopodial branching duct and identified the

characteristic mammary gland morphogenesis (Kratochwil. 1969). On the other hand, the epithelial cells co-culture with salivary mesenchymal cells displayed the dichotomous branching at terminal buds, a salivary epithelium representative structure, in the absence of mesenchymal cells, the epithelial cells deteriorated. While the identified finding implies that mesenchyme persuades a mammary fate in the epithelium, remains unclear. However, in the experiments, the mesenchymal cells were used from 1-2 days of embryos after mammary band and placode generation indicates that it might have stimulated the differentiation in mesenchymal cells. Few years, later in 1967, Propper and Gomot identified buds' formation in *in-vitro* mesenchymal cells co-cultured with epithelial cells isolated from the dermal head/neck section (Propper and Gomot, 1967). They provided the decisive proof that dermal mesenchymal cells decide the providence's epithelial cells for their structural formation and functional differentiation.

Additional reports described the succeeding grafts of recombinants heterotopic and heterospecific tissue (Koller and Fisher, 1980; Neubauer et al., 1983; Kusakabe et al., 1985). In 1978, it was reported that chick embryo epidermis synthesized keratin proteins explicit to feather when combined with feather dermis and grafted on the chorioallantoic membrane (Dhouailly et al., 1978). Ablation in genetic makeup in the placode of the embryonic mammary gland in mice showed the best model to deduce the mesenchymal cues that promote mammogenesis. It affirms the role of fibroblast growth factor 10 (FGF10) in the formation of E10.5–E11.5 hypaxial somitic buds (Mailleux et al., 2002). While its expression is under the control of transcription factor Gli3 of bilaterally paired blocks of paraxial mesoderm and in the combination of both resulted in the formation of placode 3 (Veltmaat et al., 2006). However, it is still unclear, how the other four placode pairs formation occurs? What factors and signals from the mesenchyme regulate the complete formation of the early embryonic placodes mammary gland?

2.2 What is explicitly mammary mesenchyme?

Mainly the organs are a combination of two distinct tissue types that are parenchyma and stroma. First are particularly epithelial cells majorly responsible for all main biochemical activities and regulation of the organ. Second is the

cellular scaffold's fundamental component creating the connective tissue of fibrous proteins for the interstitial matrix. Stroma provides the amorphous basal substance for structural support and also holds circulatory, lymphatic, and nervous system components for the whole organ system. Mesenchyme conventionally leads to the rise of stromal cells, scattered unorganized undifferentiated cells from embryonic mesoderm. They are majorly progenitors of native connective tissue cells such as fibroblasts and adipocytes. In vivo and cell, culture-based transplantation investigations manifest the importance of reciprocal interactions between epithelium and stroma for organogenesis (Grobstein, 1967; Freischmajer and Billingham, 1968). Mesenchyme is vital for deciding the mammary epithelium development's fate and in turn, the morphogenesis of the overall mammary gland (Sakakura et al., 1976; Kratochwil, 1969).

An interplay signalling between mesenchymal and epithelial is necessary to establish the mammary gland's early developmental stages in the mouse embryo. Five pairs of ectodermal placodes initiate to appear along with two milk lines between the E10 and E11 (embryonic day 10th and 11th), which pass ventrally inside the limbs from the genital to the neck. Some studies believe that ectodermal cells drift to the location of the formation of placodes, also ectodermal cells merely intensify the cell proliferation in the mouse embryo (Parmar and Cunha, 2004). The embryonic mammary gland contains **two classes of mesenchymal tissue** (Sakakura et al., 1982). In the first class, the ectodermal cells, around E12 days of embryonic development, the dermal mesenchyme signals and generates the primary mammary mesenchyme consisting of **densely packed fibroblasts neighbouring the mammary epithelium**. The second class is the **fat pad precursor tissue**, which is generated below the dermal mesenchyme around E14 days. It majorly comprises preadipocytes and also surrounds primary mammary mesenchyme. In the subcutaneous area of the trunk, the fat pad precursor tissue inhabits half of the space. It is relatively loose arranged and larger in size, from the days between E14-E16 epithelial cells impales precursor fat pad tissue and differentiate into adipocytes that configured fatty stroma from 2 to 3 days following parturition (Veltmaat et al., 2003; Sakakura et al., 1982).

At the embryonic stage, the mammary gland comprises two cellular compartments, including epithelial surrounded by stromal. These different compartmental tissues originate embryologically from ectoderm and mesoderm, respectively. The actual development of mouse mammary gland initiated at E10 represents the formation of bilateral stripes (milk lines) of multilayered ectoderm that pass anterior-to-posterior from the forelimb bud to hindlimb bud on the ventral surface of the embryo. At embryonic day E11.5 mammary line starts to resolve into five pairs of placodes at reproducible points which develop asynchronously with the third pair of placodes emerging first, followed by the fourth pair, then the first and fifth pairs simultaneously, with the second pair in the end. These pairs are not identical and are believed to appear as thick plates of ectoderm, consisting of numerous columnar shaped cells that arise and aggregation by the migration of ectodermal cells at the mammary line (Balinsky, 1950; Propper, 1978). At the time of the first trimester in humans, these mammary lines form giving a single pair of placodes (Howard and Gusterson, 2000). In mice, these placodes eventually form buds carry on with the increase in size up to E15 (Sakakura et al., 1987). Mammary gland development is temporarily halted once mammary buds formation complete in female mice. On the other hand, in male embryos, mammary epithelium promotes the mesenchymal expression of androgen receptor and sensitivity toward testosterone at E13. Moreover, at a similar day of embryonic development, the irreversible condensation of mesenchymal occurs around the bud, followed by the degeneration of bud epithelium during E13.5 and E15.5 (Kratochwil, 1971).

Although in humans, embryonic development of glands in both male and females develop similarly in the uterus (Howard and Gusterson, 2000). At the embryonic development of day 15.5 to 16, every individual bud initiates to elongate through proliferation specifically at the bud tip and form sprout or cord type stature which invade the fat pad precursor (Parmar and Cunha, 2004). Contrarily in mice females, these sprouts pass on to the skin surface to mark the location where the nipple will form via the epidermal invagination process. Each sprout appears at E16 followed by quick transformation into small glands that will

present at the time of birth, at that time each fat pad accommodates at least 15-20 branched ducts (Veltmaat et al., 2003).

2.2.1 Dense Mammary Mesenchyme

It is well known that primary mesenchyme is responsible for the induction of epithelial morphogenesis. Earlier, it was found that the co-culture experiment of mammary E12 along with E12–16 epithelium generates a pattern of ducts with a monopodial branching (Kratochwil, 1969). In a similar experiment, a combination of mammary E16 epithelium with E14 salivary mesenchyme was transplanted under a foster female's kidney capsule and resulted in typical salivary gland morphology. Histological evidence supports that after pregnancy, the graft generates milk in recombinant females, and it is due to the stimulations to hormones of pregnancy (Sakakura et al., 1976).

We can collectively say that primary mesenchyme from these organs can influence the glandular morphology; moreover, mammary epithelial function's developmental decision is decided before E16. The reason could be because native cells of compact mammary mesenchyme express the extracellular matrix glycoproteins such as fibronectin (Kimata et al., 1985), tenascin (Inaguma et al., 1988; Chiquet-Ehrismann et al., 1986), and receptors for sex hormones such as androgens and estrogens (Kratochwil and Schwartz, 1976). Afterwards, evoke the paracrine signal to govern the epithelial growth and ductal morphogenesis. In the case of the development of a male mouse embryo, this stage is critical, in which androgen secreted by testes results in dense mammary mesenchyme to compact and degenerate to suppress the rudiment mammary gland.

Besides, it is essential to note that at E15.5, the dense mesenchyme that neighbours the proximal end of mammary sprout interacts with the overspread epidermis to trigger nipple differentiation inhibits prompt hair follicles. It was also reported that these mesenchymal induce the elongation of bud/bulb into sprout through signalling parathyroid hormone-related peptide (PTHrP) and its type 1 receptor. Hence, binding between the BMP antagonist Noggin protein, bone morphogenetic protein 4 (BMP4), and PTHrP, govern the ductal outgrowth, nipple formation, hair follicle formation (Foley et al., 2001; Hens et al., 2007; Mayer 2008). Moreover, the mammary bud's epithelial cells initiate to produce

PTHrP results in the enhanced formation of dense mammary mesenchyme. Along with this, PTHrP also sensitises mesenchyme cells to respond to BMP 4 through stimulating to express BMP 1A receptors. On the other hand, Noggin protein decreases the BMP signal in the epithelium, which reduces the level of PTHrP. These interactions' elaborateness may be critical to define the molecular basis of cell fate determination and differentiation in embryonic mammary gland epithelium and mesenchymal.

During the onset of female puberty, mammary gland ducts initiate multiplying and forming end buds surrounded by numerous layers of fibroblasts. Tenascin glycoprotein again reappears in the dense mesenchyme, which looks like that of the embryonic mammary gland (Inaguma et al., 1988). Transplantation of mammary epithelium from E14 mice with dense mammary mesenchyme demonstrates the formation of nodular mass. This nodular mass contains ducts with abnormal short branching. Dense mesenchymal does not support the morphogenesis of regular branches and its elongation, which could reside in fat pad precursor tissue.

2.2.2 The prepubertal mammary gland

Till here, we have described the importance and development of the embryonic mammary gland. Now, we will report the importance of proteins and phosphoproteins in the postembryonic development of MG development. Until puberty, the mammary gland remains in the quiescent state, even in humans and cattle. During this period mouse mammary glands mostly residency the connective tissue and stromal fibroblast with the company of a simple primary ductal network that occupies the only fraction of the fat pad. This rudimentary ductal network graves itself in the parenchyma (this is the functional tissue of a gland distinguished from the connective and supporting tissue). At this stage, each branch consists of a lumen surrounded by the single epithelial cell layers. Both stroma and parenchyma compartments are separated from each other with the help of laminin containing basement membrane. Here, the layer of myoepithelial cells stacks over the layer of epithelial cells. In mice, mammary glands, epithelial cells can be identified through immunohistochemistry by using distinct biomarkers such as keratin 8, 11, 20, and 22 proteins. On the other hand, both human and myoepithelial mouse cells expressed cytokeratin 5, 14,

alpha-smooth muscle actin, and p63 (Radice et al., 1997). One difference between human and mice mammary gland is that at birth, various minor ductal networks were observed at the nipple in human contrarily in mice a single network is found (Howard and Gusterson, 2000).

2.2.3 Pubertal mammary gland development

Until puberty, the mammary gland remains in the primitive stage; however, it is entirely competent to produce milk. In some cases, fetal exposure to maternal hormones can provoke milk protein expression known as witch's milk or witch milk proteins. This endocrine influence makes glands grow allometrically until puberty comes. Mammary glands grow in pace with overall body development, till extensive proliferation initiates and fills the fad pad under the hormonal clues and growth factor-mediated signalling. Furthermore, terminal end buds (TEBs), form a club-shaped structure at the tip of growing ducts that perforate into the fat pad, by the uninterrupted proliferation of a single layer of cap cells the tip of TEB and by underneath pre-luminal epithelium. Further surrounding stroma governs the TEB bifurcation of primary ductal structure. Cap cells of TEB are differentiated into myoepithelial cells to form the outer layer of the ductal bilayer, which enclose inner luminal cells (Williams and Daniel, 2001).

In the later episode of the development, the secondary branches multiplied laterally from primary ducts and resulted in tree-like patterns in ductal morphogenesis. This tree-like structure occupies up to 60% of the niche, rest space filled with stroma under the influence of pregnancy hormones. Under the control of cyclic ovarian stimulation, only short tertiary branches can form, rest full development of alveolar buds occurs only after the pregnancy hormone secretion. Cattle and humans also exhibit similar extensive mammary trees during puberty. Branching further led to terminal ducts that bring about the terminal ductal-lobular unit, consisting of various blind-ended ductules named acini (Howard and Gusterson, 2000). These acini are implanted fibroblastic intralobular stroma that is more noticeable in case of humans than in mice in which adipocyte rich stroma is neighbouring the branches of rodent mammary tree.

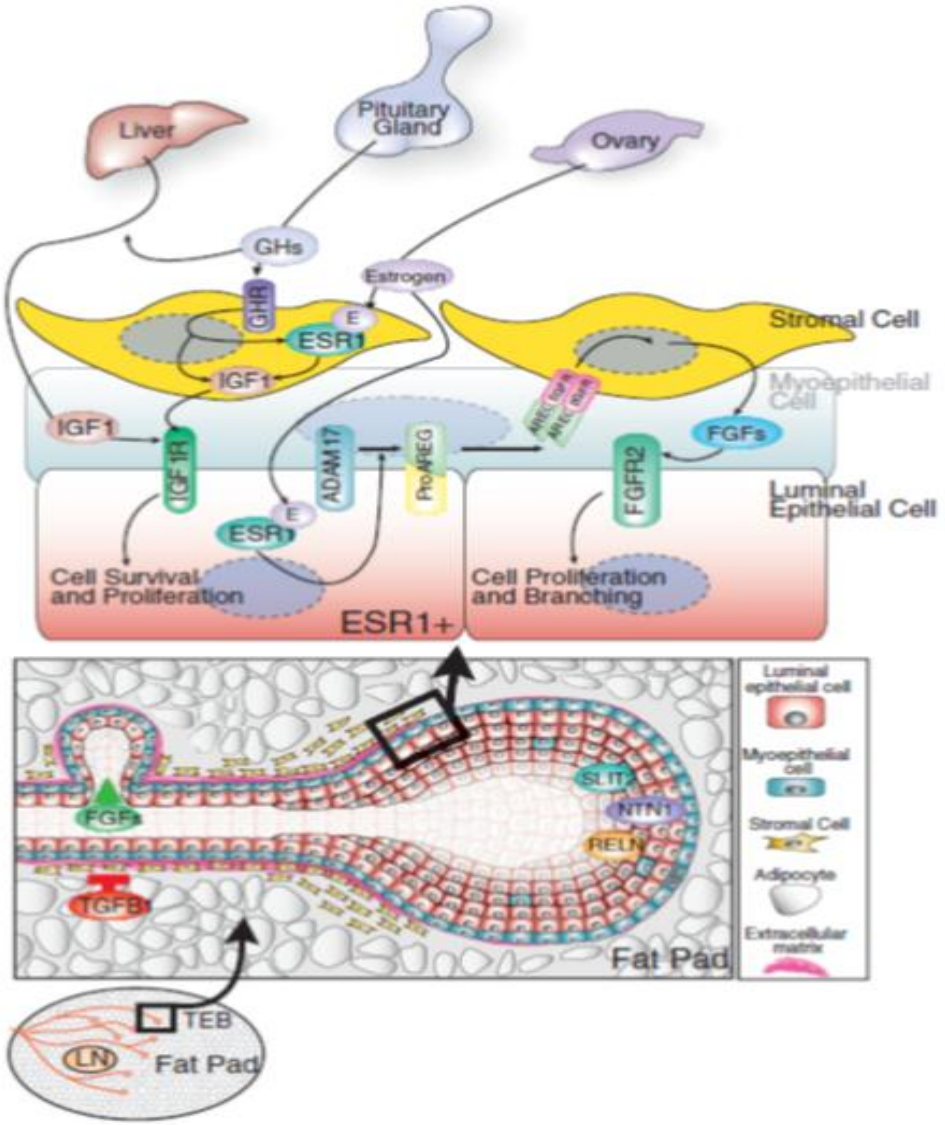

Figure 2.3. Schematic read of the events occurring throughout the time of pubertal development. Terminal finish buds (TEBs) grow through the exocrine gland fat pad, oxyacetylene by cell proliferation (diagram at the bottom). Growth hormone (GH) regulates cell proliferation by causation insulin-like growth factor-1 (IGF1) expression in each the liver and exocrine gland stroma. IGF1 acts, along with oestrogen secreted from the ovary, to induce vegetative cell proliferation (diagram at the top). Oestrogen signalling through its receptor (ESR1) acts via a paracrine fashion to stimulate the discharge of dermal protein (EGF) friend, amphiregulin (AREG), that issue to bind its receptor on stromal cells and induce expression of FGFs. FGFs, in turn, to stimulate luminal cell proliferation. Alternative factors, like TGFB1, Reelin (RELN), Slit2, and Netrin1

(NTN1), contribute to mammary architecture by ultimately or negatively regulating cell proliferation and maintaining cell-cell interactions. For details, see text.

In this way, the pubertal mouse mammary gland presents the absolute model for organ development, differentiation, and morphogenesis. In the fifth week in mice and 9-12th years in humans, primary glandular branching morphogenesis occurs, integrating epithelial cell differentiation, proliferation, and apoptosis. During puberty, swift expansion of pre-existing rudimentary mammary epithelium brings out substantial ductal networks, including branch initiation, followed by elongation and invasion of mammary mesenchyme. Similarly, in human females, during the arrival of puberty restarting in growth has been noticed in both mammary stroma (fatty and fibrous tissue) and glandular tissue, including ductal elongation and branching. The process is the hallmark of branching morphogenesis that symbolizes puberty in both humans and rodent mammary glands. Mammary gland specific molecular networks elucidate the received signal in cytokines or growth factors from the surrounding stromal and epithelial microenvironment. It is primarily orchestrated by secreted ovarian and pituitary hormones.

Ovarian hormones, such as estrogen, trigger the swift proliferation and expansion of branches during branching morphogenesis. The TEB majorly guides this expansion precisely. For example, in mice, primary ducts elongate at the tip of TEB, later on, bifurcate, which represents primary branching of TEB to generate additional primary ducts. Later these primary branchings were subjected to lateral and secondary branching (Ingman and Robertson, 2008). As sexual maturity reached approximately fifth weeks in the mice and 11–14th years in humans, even though ductal trees continue to develop, it exceeds the point until it touches the maximum space limit in the gland's room. It is expected to continue until the age of eight weeks in the mouse and 18–24th years in the human mammary gland (Russo and Russo, 2011; Brisken and Duss, 2007). After reaching the fat pad's extremities, end buds shrink in their size and become

mitotically quiescent, indicating completion of the pubertal growth phase (Sternlicht et al., 2006; Silberstein et al., 1990). To know more about the molecular signalling and associated regulator of TEB formation, please follow the following article (McNally and Martin, 2011).

Steroid hormones, local growth factors, cytokines, and pituitary hormones fuel the initiation and establishment of pubertal mammary gland development (Topper YJ, Freeman, 1980). Also, the mammary gland's ductal morphogenesis process is characterized by extensive estrogen requirement (Sternlicht et al., 2006; Brisken, 2002). Hence ovariectomized mice at five weeks of age fail to develop a full ductal tree of the mammary gland. Nevertheless, this effect can be reversed upon exogenous supplementation of estrogen pellet into mammary, which stimulate ductal growth (Daniel et al., 1987; Deroo et al., 2009). In mice ductal tree found deficient in ERα which gravely undersized because of complete failure to invade into the stroma, even adult mammary gland exhibit resemblance to the mammary gland of new-born female (Couse and Korach, 1999; Bocchinfuso and Korach, 1997).

Moreover, $ERα^{-/-}$ epithelial cells are incapable of developing mammary tree at puberty when transplanted into $ERα^{+/+}$ fat pad. Nevertheless, in contrarily, $ERα^{+/+}$ epithelial cells potentiate to trigger the ductal outgrowth when transplanted in the $ERα^{-/-}$ fat pad, suggesting the requirement of ERα in the epithelium but not in stroma. In terms of ductal morphogenesis in the pubertal mammary gland, it is mandated that epithelial ERα is required to function in a paracrine fashion validated by $ERα^{-/-}$ epithelial cells. These cells will only carry on in the mammary tree when transplanted into a fat pad with $ERα^{+/+}$ cells (Mallepell et al., 2006).

It is not just ductal expansion dependent on ovarian steroids and pituitary hormones during the pubertal mammary gland. However, these two hormones act as the mediator for mammary stem cell fate decisions. To find detailed information on 'molecular regulators of pubertal gland development' detailed

information is provided in a review article (McNally and Martin, 2011). A comprehensive review of the impact of regulators of pubertal mammary gland development on stem cell compartments and breast cancer progression (LaMarca and Rosen, 2008).

In mature virgin glands, an extensive ductal tree with basic building structures is named terminal duct lobular units (TDLUs) in humans and alveolar buds in mice (Britt et al., 2007). In humans, these TDLUs act as basic functional units of Breasts that resemble the bunch of grapes. One TDLUs represents the acini group (from one single terminal duct) that grave in the intra-lobular stroma (Parmar and Cunha, 2004). Sufficient room still available to this tree can further support the tertiary lateral branches, occur during diestrus (cycle time) and at the time of pregnancy (Ingman and Robertson, 2008; Atwood et al., 2000). One significant difference among human and mice mammary gland at the time of puberty is that lobules structures can be seen in human Breast at puberty whereas mice lobules only show during pregnancy onset (Silberstein, 2001).

The key regulators direct lateral secondary branching events that require strict control, including adequate space which must remain in postpubertal gland to prop up lobular alveolar development. This event is governed by restricting the number of branching events. The endogenous inhibitory morphogen, TGFβ, acts as the controller of a spatial geometry of branching morphogenesis (Nelson et al., 2006). TGFβ has been demonstrated to interact with the extracellular matrix (ECM) molecules specifically in the area where budding for new branching initiates. It inhibited budding by preventing excessive branching and invasion of the advancing ductal network in the fat pad. In those areas where morphogenesis is restricted there are concentrated chondroitin sulfate and type 1 collagen deposits Silberstein et al., 1990) and recently, strong upregulation of the chondroitin sulfate proteoglycan was found upregulated in versican cap cells during puberty (Olijnyk et al., 2014).

The Scatter factor (SF)/cytokine hepatocyte growth factor (HGF) acts as a positive regulator of branching morphogens, and also pushes proliferation and EMT (epithelial to mesenchymal transition) phenomena in the mammary gland. Fibroblast population is a known source of HGD/SC, in both humans and mice. Precisely, HGF/SF is a stromal-derived paracrine mediator that enhances morphogenesis *in vitro* and *in vivo*, in Ras pathway-dependent manner (Soriano et al., 1998; Pollard, 2001). Moreover, TGFβ signalling is thought to be a cumulative role of both cytokine and HGF/SF, governing the limits of branching spacing in the mammary gland. Please refer to more detail about the growth factor and hormonal control of pubertal mouse mammary gland side-branching (McNally and Martin, 2011).

2.2.4 Adult mammary gland development

In adult/ postpubertal mice mammary gland, the release of ovarian hormones and each oestrous cycle assist in the alveolar buds development and lateral branching (Andres and Strange, 1999). In mice, an oestrous cycle lasts for 4-5 days, and as adult mammary gland development continues, alveolar buds initiate to subdivide into the rudimentary alveolar structure. After completing the pubertal developmental stage, during pregnancy which represents the second postnatal mammary development stage, ductal branches start to expand from alveolar buds in mice or TDLUs in humans (Russo et al., 1990). In humans' case, the branching process is more complex and starts from nipple primary duct to connect segmental ducts, subsidiary ducts, and subsegmental ducts, and finally reaches the TDLUs (Howard and Gusterson, 2000). Another species difference noted was that humans' mammary stroma consists of comparative less adipocyte than mice, but composed of more fibrous connective tissue (Visvader, 2009). Therefore non-lactating human Breast contains near to 80% stroma (Parmar and Cunha, 2004). Moreover, ducts in both species dominantly made up of similar epithelial cells which surround central lumen (Richert et al., 2000). Also, luminal epithelial cells were found to express cytokeratin proteins 7,

8, 11, 15, 18, 19, 20, and 22 in both species (Asch and Asch, 1985; Moll et al., 1958).

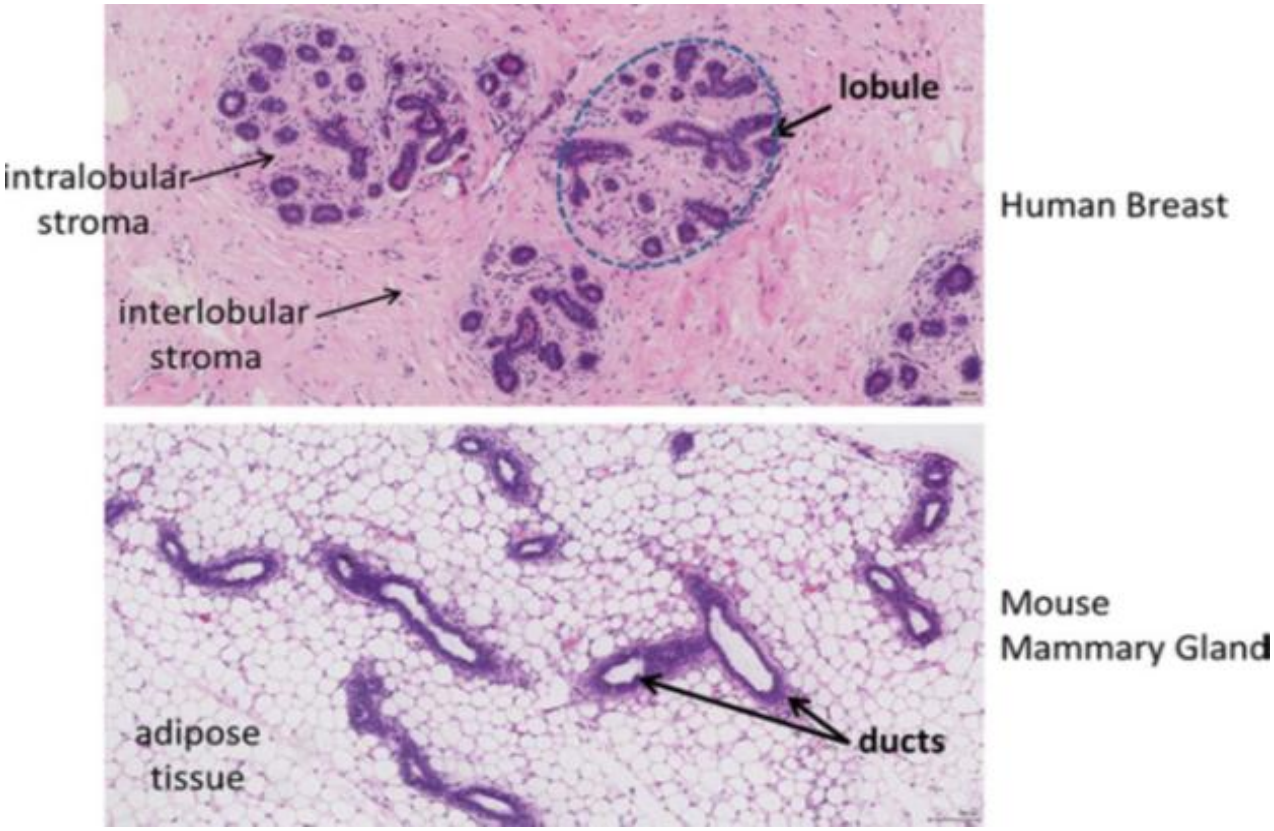

Figure 2.4. Hematoxylin and eosin-stained sections of somebody's breast (top) and a mouse duct gland (bottom). In contrast, the human breast section shows animal tissue lobules with a scleroprotein intralobular and interlobular stroma, the animal tissue ducts of the mouse duct gland area unit enclosed by a scleroprotein sheath inside associate degree adipocyte-rich tissue.

2.2.5 The pregnant mammary gland

During pregnancy, substantial tissue remodelling of the mammary gland were materialise. The initial phase of pregnancy was marked for ductal branch proliferation, remodelling of ECM and further development of alveolar buds. In mice at day 19-21th days of pregnancy, mammary gland differentiation peaks along with alveoli's growth (Nandi, 1958). Pregnancy triggers gland cause growth of alveolar buds at the tips of tertiary branches, which is well potentiated to produce and secrete milk after parturition and lactation (Richert et al., 2000).

The pregnant stage is well documented for the functional differentiation of mammary gland under hormonal control. Majorly oestrogen and progesterone are two hormones which secrete from the corpus luteum. Then somatotropin, adrenocorticoids and prolactin secreted from the placenta, adrenal gland and pituitary, respectively. There estrogen signalling participates indirectly in alveolar proliferation, alveologenesis (Brisken, 2002).

A tightly regulated balance between progesterone and prolactin signalling has been observed during pregnancy, which resulted in the formation of milk secretory unit (Neville et al., 2002). Pituitary originated prolactin regulates the level of progesterone in early pregnancy via stimulation of ovarian progesterone. In mice, from the second to the sixth day of pregnancy, both of these hormones fuel the proliferative drive (Traurig, 1967). Progesterone receptor knockout and epithelial recombination experiment have shown progesterone's requirement during alveolar morphogenesis, and contrary epithelial cell proliferation hangs on the progesterone receptor (PR) activity of epithelial cells (Brisken et al., 1998). Incredibly reciprocal transplantation technology provide the results that epithelial PR is essentially required for lobuloalveolar development, whereas stromal PR may moderate the ductal growth (Brisken et al., 1998; Humphreys et al., 1997). Depletion of both progesterone receptor isoforms (PR-A and PR-B), consequently fail lobuloalveolar development and tertiary side branching formation during both pregnancy and adult stage. Moreover, selective knockout suggests the PR-B is critical isoform at this time (Conneely et al., 2003).

In cycling female adult non-pregnant mice, the ductal side branching and alveolar morphogenesis depend on progesterone signalling (Brisken, 2002). Progesterone signalling in its downstream acts as the activator of nuclear factor-kB ligand (RANKL) and Wnt4 (Wingless ligand) in a paracrine manner in mammary gland development. Moreover, in the absence of pregnancy, RANKL or Wnt4 ectopic expression causes tertiary branching (Bradbury et al., 1995; Fernandez-Valdivia et al., 2009). Hence, the deletion of RANKL or Wnt4 causes impairment in pregnancy driven side branching, and alveologenesis (Brisken et al., 2000; Fata et al., 2000) since the expression of these proteins is regulated by progesterone and therefore, their colocalisation with PR-positive luminal epithelial cells (Brisken et al., 2000; Mulac-Jericevicet a., 2003).

It has been found in several studies through prolactin receptor knockout mice (PrlKO) that epithelial PrlR is also essential for normal **lobulo-alveolar** differentiation. Altogether it suggests the nonessential role of stromal PrlR at this point. PrlR−/− mammary fats pads transplantation in wild-type fat pads fails the development of lobuloalveolar and milk synthesis during pregnancy, which indicates the crucial need of PrlR in alveolar morphogenesis (Brisken et al., 1999). Furthermore, during late pregnancy, alveolar development and lactogenesis, solely depends on the PRL signalling, whereas it seems not essential for the side branching and ductal outgrowth (Brisken et al., 1999). Socs, members of the suppressor of cytokine signalling gene family, are activated by the Prl signalling and act negatively for Prl action. Advanced mammary gland development has been seen in Socs1−/− during pregnancy in mice, further it was demonstrated that lobuloalveolar defect phenotype of Prlr+/− mice could be overcome bySocs1+/− mice (Ormandy et al., 2003). However, lactation defects in Prlr+/− mice can be improved by the Socs2 deletion (Harris et al., 2006).

In late pregnancy, single alveoli differentiate from continuing cleaved alveolar buds and later form alveoli, resulting in milk secretory lobules at the time of lactation. However, the myoepithelial cell's discontinuous layer is surrounded by alveolus in the mammary gland (Adams and Watt, 1993; Howlett and Bissell; 1993). Absolute lobuloalveolar differentiation needs direct interaction between the basement membrane and luminal cells (Fata et al., 2004). Moreover, GATA-3, known as the transcription factor, has been demonstrated as an essential ingredient during complete alveolar maturation. Its deletion causes alveolar/lactogenesis defect (Kouros-Mehr et al., 2006). Since approximately days 18 of pregnancy, the onset of a secretory activation phase takes place, at this time, most fat pads of the mammary gland replace with alveoli. Further, lipids and milk proteins are synthesised by alveolar epithelial cells to devise postpartum secretion (Richert et al., 2000; Nguyen et al., 2001).

Overall, spacious remodelling occurring during pregnancy in the mouse mammary gland and it is comparable to the cattle and human morphogenesis (mostly, at this particular moment). Lobules are found in the cattle and human female gland before pregnancy. Therefore female mammary gland is not

classified as completely differentiated till the first full-term pregnancy has attended its final stage (Russo and Russo, 1987). Inscriptionally, human breast cancers arise from the terminal ductal-lobular unit (TDLU). Hyperplastic enlarged lobular units (HELUs) progress from normal TDLU in the Breast, a prospective disease state (Lee et al., 2007). Transformation of TDLU to a HELU mostly routinely causes growth abnormality in the human female Breast (Lee et al., 2007; LaMarca and Rosen, 2007).

Differential gene expression profiling of HELU's in comparison to TDLU's reveal that especially two genes (estrogen receptor α (ERα) and amphiregulin (Areg)) level increased in HELUs (Lee et al., 2007). Functional involvement of ERα and Areg in governing epithelial cell expansion in mammary gland suggests possible two axes to gives to breast tumour progression; furthermore, Areg is established to increase in ERα- positive breast tumours (Lee et al., 2007; Johnston, 2006).

2.2.6 The lactating mammary gland

Table 2.1. Mammary gland specific hormones

Mammogenic	**Lactogenic**	**Lactopoietic (Galactopoietic)**
Estrogen	Prolactin	Growth hormones
Progesterone	Insulin	Glucocorticoids
Prolactin	Glucocorticoids	Insulin
Growth hormones		Prolactin
Human Placental Lactogen (HCS)		Thyroid hormones
		Parathyroid hormones
		Oxytocin

During lactation, the lobular alveoli (milk-producing architecture) differentiate from the terminal ductal-lobular unit (TDLUs) (in humans and cattle)

or alveolar buds (in mice). The structures are required to supply the nutrients to offspring from fully differentiated mammary glands. It is completed by PRL signalling for the final step of lactogenic differentiation in the gland (Neville et al., 2002). Consequently, in retaliation of suckling, which is the infant's induction, the release of Prl from the anterior pituitary resulted in the maintenance of the architecture of the "functional" mammary gland. PRL signalling mediators are signal transducer and activator of transcription 5 (Stat5) and Janus kinase 2 (Jak2) (Chen et al., 2012; Wagner et al., 2004). These molecules function through post-translation phosphorylation events and the upregulation of cyclin D1 and IGF-2, in response to Prl activity (Hovey et al., 2003; Brisken et al., 2002).

The milk synthesis machinery performs with the maximum tempo at this phase where secretory epithelial cells are fully functional at the lactation stage. In a replay to increase milk production, alveoli continue to dilate until they are entirely occupied and populate the glandular volume. Response from neonates suckling induces pituitary oxytocin, which further stimulates the contraction of myoepithelial cells. These contraction forces create sufficient force to squeeze milk into the ducts from alveoli (milk secretory unite). In this way, milk production is induced again by removing milk through suckling action (Richert et al., 2000; Prilusky and Deis, 1975; Mather and Keenan, 1998). At this lactation period, almost complete adipocytes present in the gland were metabolised, and maximally the MG was occupied by the expansion of alveoli. Lactation stage in the mouse mammary gland remains maintained at least for three weeks until pups are weaned. For this entire period, the fully developed alveolar structure remained intact than weaning resulted in the induction of signals for involution (Neville, 1999). In the next section, we have discussed the signals responsible for involution.

2.2.7 The involuting mammary gland

The involution stage (post-lactational) of mammary gland development is begun by absence by suckling stimulus (weaning) or lack of breastfeeding and reduction in buildup of **milk** within the Breast. Also, Prl status decreased after weaning courses arrest of milk secretory activity through Akt and Stat5 signalling

(Abell et al., 2005; Schwertfeger et al., 2001). Since the early involution stage is reversible, re-initiation of the suckling stimulus can reverse the involution stage to lactation (Li et al., 1997). On the other hand, the irreversible phase of involution begins after two days where regressive remodelling and extensive programmed cell death of epithelial cells occur. These involution phases generally govern at the molecular level by lack of survival factors and cell death mediators' gathering. Moreover, the lack of sucking stimulus further reduces the defined levels of lactogenic hormones and milk synthesis in the alveolar lumina (Feng et al., 1995). Both human and mice involution defines the removing of unnecessary epithelial cells in a highly regulated manner.

An early phase of involution is identified by the death of secretory epithelial cells of alveoli, in which approximately 80% of glandular epithelial cells remove by the lysosome-mediated programmed cell death followed by removal by efferocytosis process (Kreuzaler et al., 2011; Monks et al., 2005). Therefore, early involution signs can be seen instantly after 24 h of pup removal in rodents (Monks et al., 2008). Furthermore, involution associated gene expression alteration could be observable within 12 h after weaning (Clarkson et al., 2004). As consequences, alveolar distension happens, and alveoli start to collapse in the epithelial cluster at this particular time. On the other hand, this time, epithelial cells start to leave the fat pad's room to refill and expand in the gland (Richert et al., 2000).

Moreover, ducts grove in the dense stroma is prominent during the early phase, where the epithelium is disorganized. Besides, cell cycle-regulated genes have been detected upregulated at the time point (Marti et al., 1994; Marti et al., 1999), including clusterin and tissue inhibitor of metalloproteinases-1 (TIMP-1) (Lund et al., 1996), caspases (Marti et al., 1999) and acute-phase proteins (Stein et al., 2004). Furthermore, Akt/PKB's constitutive expression is the mediator of cell survival and restrict apoptosis in the involuting mammary gland (Schwertfeger et al., 2001). Dynamic of both survival and death signals in the epithelium is highly regulated. The level of activated Akt could be decreased in stat3 mediated activated PI3 kinase, which acts as negative regulatory subunits (Abell et al., 2005). Besides, at this point in involution epithelial cell death in mouse mammary gland also depends on the expression of Fas ligand (FasL),

macrophages and transforming growth factor β (TGFβ) signalling (Watson CJ, Kreuzaler, 2011; O'Brien et al., 2012).

Furthermore, the disintegration of both basement membrane and ECM characterises the secondary or late involution phase. Even decreased lobulo-alveolar structure simultaneously occurs with increased gene expression of the candidate gene associated with gland remodelling (Richert et al., 2000; Lund et al., 1996). In mice during the second phase of involution, after 48h of weaning and further established by the immigration of numerous immune cells such as neutrophils, plasma cells, macrophages, and eosinophils (Stein et al., 2004). After the compilation of involuntary stage, which approximately takes three weeks in mice, the mammary gland shows similarity to the adult stage (quiescent virgin gland), potentiating the increase in lobular alveoli. Hence, parous human mammary gland seems to contain larger lobules than non-porous, and therefore, it majorly composed of glandular tissue (Russo and Russo, 2004). Furthermore, alteration in gene profiling has been demonstrated for nulliparous and parous human Breast. Also, cyclic pregnancy further fuels the re-initiation of alveolar bud or TDLU expansion, lobular alveolar differentiation process and involution occurring at the end.

Another form of involution occurs in the mammary gland, independent of earlier lactational events, instead correlated with the female's age. This age-related lobular involution in case of humans occurs gradually with loss of epithelial tissue. This type of involution is a natural process that physiologically protects the female from breast cancer incidence. Existence clinical data suggest that postmenopausal women with delayed lobular involution show a higher risk of developing breast cancer than menopausal women experiencing partial or complete involution (Milanese et al., 2006). At this time mammary gland loss, its complexity and function whereas in humans, initial signs of lobular involution occur at perimenopause (Hutson et al., 1985). This phase generally accelerates during menopause, and its hallmark characteristic is the reduction in size and complexity of both TDLU's and ductal network (Hutson et al., 1985).

Although there were no studies about the phosphorylation of the proteins during mammary gland development, we highlighted the proteins that can

phosphorylate and activate the signalling pathway during the review. The above discussion and literature review climax the mouse mammary gland's morphological journey from embryonic development to puberty, pregnancy/lactation, and involution. Parallel this literature review tries to throw light and compare mammary glands of humans, cattle, and mice.

2.3 Proteome versus proteins

All organisms contain a single genome in virtually all its cells, and thus the difference between the numerous cell types within the same organisms are attributed mainly to epigenetics, genetic imprinting, transcriptional and post-transcriptional processes. Therefore, learning of all the protein molecules present in the living system or cell (termed proteomics) at any given time and the physiological condition can logically offer insights into life's mechanism to Associate in Nursing unexampled depth. Traditionally once proteins were studied 'one at a time' achieving a systems read of the cell or organelles was a frightening and effortful endeavour to undertake. Further, once the protein area unit is studied separately, the results may sometimes be unclear thanks to the crosstalk between the sign pathways and nodes (Taniguchi et al., 2006; Gossage and Eisen, 2010). tho' their area unit palmy structural biology technologies on a little scale and techniques like phage display system (Smith, 1985) and yeast two-hybrid (Luban and Goff, 1995) to characterize the protein-protein interaction at a bigger scale they are doing not offer a system-wide read establishing the interaction between proteins groups. Further, the false negative and false positive rates area unit is difficult to estimate, and also the info is also a smaller amount quantitative (if at all) to construct a stoichiometric protein complicated (Deane et al., 2002).

2.3.1 Mass spectrometry-based proteomics

Mass qualitative analysis (MS) - one in all the foremost sensitive analytical techniques - has competed for a colossal role in developing proteomics to its existing capabilities. The arrival of ESI and MALDI techniques primarily employs the mass spectrometry to the mass qualitative analysis employed for individual protein sequencing and identification of gel bands, therefore bit by bit commutation the Edman degradation technique. At first,

proteomics was related to 2-dimensional gel electrophoresis techniques (2DE) (Wilkins et al., 1996); however, 2DE has serious limitations (Corthals et al., 2000). Once protein and peptide (macromolecule and amide) separation techniques like liquid chromatography were combined with mass qualitative analysis through mess spectroscopy (Makarov and Scigelova, 2010), advanced macromolecule and amide mixtures were success analyzed, resulting in the emergence of MS-based proteomics (Aebersold and Mann, 2003; Gstaiger and Aebersold, 2009; Yates et al., 2009; Domon and Aebersold, 2006; Kocher and Superti-Furga, 2007). Complementary to advances in separation ways, new mass spectrometers, particularly the FT ICR (Marshall et al., 1998) and Orbitrap (Makarov and Scigelova, 2010; Makarov et al., 2006a; Makarov et al., 2006b; Makarov and Denisov, 2009; Hu et al., 2005) hybrid instruments, have expedited routine massive scale high accuracy and high-resolution MS.

Mass qualitative analysis through mass spectrometry is not quantitative by itself, and methods are developed to get relative quantification between conditions either victimization non-radioactive isotopes or the spectral data itself (Wilm, 2009; Bantscheff et al., 2007; Schulze and Usadel, 2010). Proteins or peptides are tagged with lightweight and different non-radioactive isotopes that are identical in terms of organic chemistry properties together with the ionization potency and differ solely by mass and distinguished within the spectrum (Ong and Mann, 2005; Steen and Pandey, 2002; Yan and Chen, 2005; Ong et al., 2003). Labelling may be performed by (1) the metabolic labeling of cells utilizing ^{15}N isotopes (Lahm and Lagen, 2000; Oda et al., 1999) or by stable isotope labeling of amino acids in cell culture (SILAC) (Mann, 2006; Ong et al., 2002) and (2) chemical labeling of peptides like Hys Tag (Olsen et al., 2004), isotope-coded affinity tags (ICAT) (Gygi et al., 1999), isobaric tags iTRAQ (Ross et al., 2004) and dimethyl labeling (Hsu et al., 2003). Recently, Hans Geiger et al. have incontestible the relevance of SILAC based mostly quantification to clinical samples (Geiger et al., 2010), that may probably result in a replacement paradigm of clinical proteomics. A label-free format quantification may be performed from the extracted ion chromatogram (XIC) for the peptides ('label-free quantification'). A broad range of algorithms is presently out there for label-

free quantification, creating this a horny strategy, particularly for clinical samples and samples that labelling is mostly not possible.

With coincident maturation in several sides, MS-based quantitative proteomics is currently set to become an essential tool in cell and systems biology. It is currently doable to spot complete or near-complete proteomes of being cells at intervals an inexpensive quantity of activity time (Wisniewski et al., 2009; Diamond State Godoy et al., 2008). Quantitative proteomics in its current state is habitually utilized in learning overall expression changes, classification of cell sorts (Luber et al., 2010), post-translational modification (PTM) (phosphorylation (Olsen et al., 2010; Olsen et al., 2006), cell signalling networks (Choudhary and Mann, 2010), protein-protein interactions (Hubner et al., 2010; Vermeulen et al., 2008; Butter et al., 2010; Bonaldi et al., 2008), ubiquitination (Xu et al., 2010), acylation (Choudhary et al., 2009), organelle-specific localization and macromolecule or protein turnover rates.

2.3.1.1 The Orbitrap analyzer

The Orbitrap analyzer is one of the most recent mass qualitative analysis developments and was fancied by Alexander Makarov and colleagues (Hu et al., 2005). The Orbitrap derives its basic style from the lure device delineate by K. H. Kingdon within the early Twenties named Kingdon lure or trap. Curiously as Makarov discerned within the lecture at International Mass qualitative analysis Conference, IMSC 2009, Bremen, the Orbitrap's construction long-faced such an immense amount of intimidating challenges that the project appeared doomed again and again. One such case was economical ion particle injection into the Orbitrap, which was solved by introducing a 'C-trap' or an arciform or curved linear trap device. The C lure 'squeezes' the ions in terms of house and time and shoots them into the Orbitrap through the z-lens perpendicular to the oblong section plane of the Orbitrap analyzer.

The Kingdon lure, from that the Orbitrap derives its fundamental principles, employs solely electric field by applying an electrical potential between an outer cylindrical conductor or electrode and a skinny inner wire that acts because of the central conductor. In distinction, the outer conductor is barrel-shaped within the Orbitrap analyser, whereas the inner conductor is

fusiform. As a result, the house between the two electrodes is not constant on the coordinate axis (length of the Orbitrap), implying that the electrical field is weakest within the middle wherever the house between the two electrodes is largest. Once the ions are injected in packages from the C-trap, they enter a circular motion due to the interaction of centripetal and centrifugal forces generated from the tangential movement and therefore the field of force between the electrodes. This electric field of force has two kinds of heterogeneousness. First, this field or sphere strength is variable on the coordinate axis within the wrong way from the centre of the Orbitrap analyzer, and second, the direction of electrical field vectors from totally different points on the coordinate axis is not parallel to every different. This unregularity ends up in the mass-dependent oscillation of ions on the coordinate axis synchronous to the central electrode's circular motion. This oscillation measures the mass of ions within the field between the electrodes detected as a picture current by the electrically isolated sections of the outer barrel electrodes. This frequency of oscillation is a freelance of energy and spatial unfold of ions.

Since the oscillating or periodic frequency may be a direct life of the ions' mass and freelance of the energy, the Orbitrap mass analyzer boosts a high-resolution power as long as the frequency may be measured with very high exactness. The Orbitrap analyzer has considerably higher particle trappings capability than the quadrupole particle lure and therefore the FT ICR instruments, thus abundant higher house charge tolerance. The Orbitrap mass analyzer contains a Low Mass deviation of habitually than three ppm. However, this mass accuracy of the Orbitrap needs high vacuum as collisions with background molecules will cause dephasing of ions and therefore deterioration of the mass accuracy and resolution. For this reason, ion particle activation by collision to neutral gas molecules is not typically doable in Orbitrap analysers. The Orbitrap analyzer has a comparative resolution to FT-ICR while not the necessity for cooling any superconducting magnets. In routine application, the Orbitrap analyser's mass accuracy is improved to sub-ppm level by period standardization with ions present in close or ambient air (lock masses) that are often present within the spectra throughout the chromatography gradient.

The mass-dependent frequencies of particle motions are given by the on top of equation, where, m is that the frequency in rad/s and k is an instrumental constant.

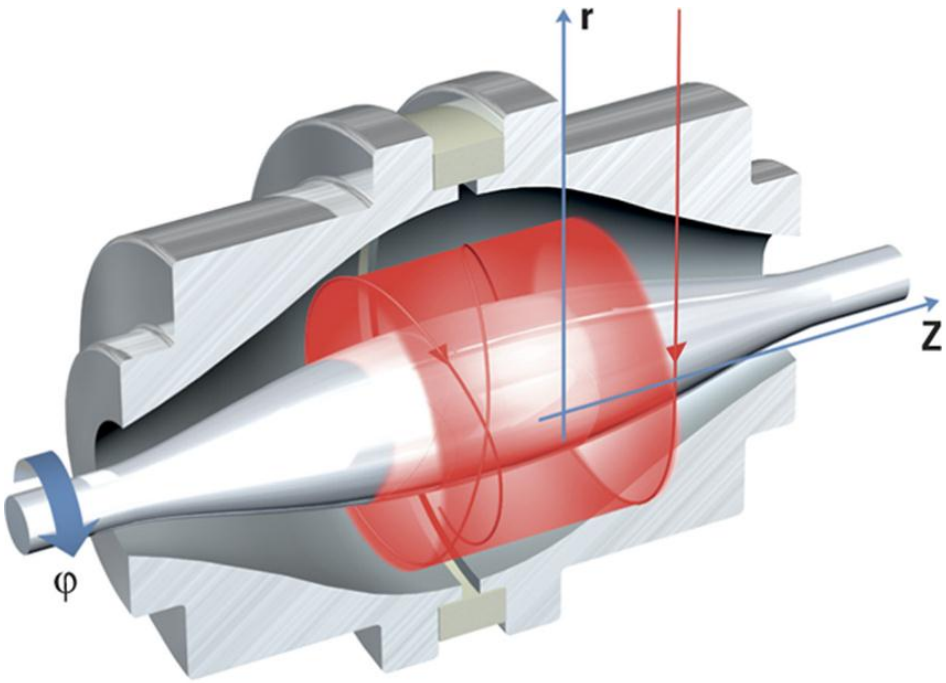

$$U(r,z) = \frac{k}{2} \cdot \left\{ z^2 - r^2/2 + R_m^2 \cdot \ln(r/R_m) \right\}$$

Figure 2.5. A cross-sectional view of the Orbitrap. The ions move each on the axis and round the central conductor shaded in orange. The outer barrel conductor is split into two electrically isolated halves to observe the image current.

2.3.1.1.1 Orbitrap is a hybrid instrument

The Orbitrap analyzer is commercially out there from Thermo Fisher Scientific during a cycle or random configuration coupled to a linear particle lure instrument. Since the Orbitrap has the only operate of detection (in principle, the Orbitrap is a fashionable detector), it cannot be used as a standalone device. It needs the C-trap for particle storage and injection.

In the hybrid configuration, the total scans square measure sometimes noninheritable within the Orbitrap analyzer whereas at the same time torrential amide (peptide) ions square measure selected, isolated, fragmented, and analysed within the particle lure. The particles square measure initial accumulated within the ion lure for the total scans then axially ejected into the C-trap and afterwards into the Orbitrap. Whereas the MS transients exploit the Orbitrap, the particle lure is programmed to perform many law enforcement agency fragmentation events and to scan out the following peptide fragments to the multipliers by lateral ejection. Within the latest version of the instrument (LTQ-Orbitrap Velos), the linear particle lure consists of 2 traps. This twin cell particle lure is maintained at differential pressure in order that the hard-hitting particle isolation and activation and nonaggressive scanning square measure performed (Perry et al., 2008).

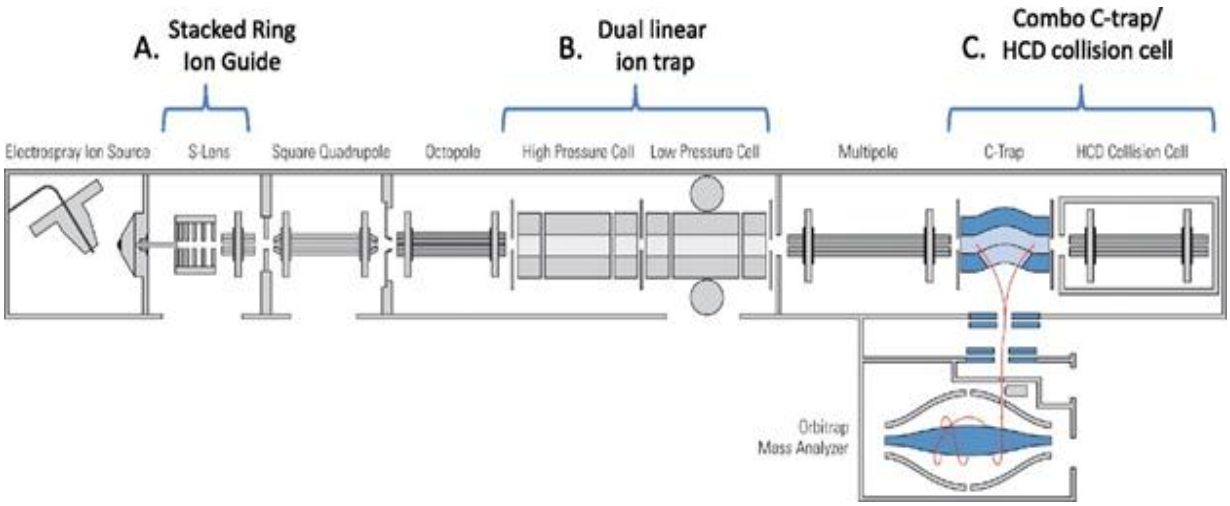

Figure 2.6. The hybrid mass spectroscope configuration of the LTQ-Orbitrap Velos. The twin cell linear particle entice intended for quick law enforcement agency fragmentation scans whereas a full high-resolution scan is noninheritable within the Orbitrap.

2.4 Large scale phospho-proteomics by higher energy collision dissociation

The Nobel Prize in Physiology or Medication in 1992 received by Edmond H. Fischer and Edwin G. Sir Hans Adolf Krebs for their discoveries regarding reversible supermolecule (protein) phosphorylation a biological regulative mechanism. Phosphorylation of proteins is one in all the essential post-translation modifications and is often studied by MS-based proteomics. Phosphorylation on serine and threonine (aminoalkanoic acid and essential amino acid) residues is labile, whereas phosphorylated tyrosine amino acid is comparatively stable. Over the years, the ion trap based tandem mass spectrometry (particle entices based mostly bicycle mass qualitative analysis) has gained quality and popularity over the quadrupole mass spectrometer. Therefore, most phosphoproteomics analysis is performed in an exceedingly low energy CID regime in particle entice (ion trap) instruments. The ion particle trap's blessings embody high sensitivity, quick scan speeds, and operation with the Orbitrap or FT instrument. However, since the phospho cluster is lost within the CID fragmentation (neutral loss), the analysis includes an extra fragmentation step referred to as pseudo MS^3 or multi-stage activation (MSA). This multi-stage activation ends up in advanced spectra, and any low mass cut-off precludes low mass communicator particle analysis. In distinction, HCD fragmentation yields high-resolution spectra probably at the price of lower sensitivity. We tend to examine the ductal mammary gland and associated massive scale phosphoproteome by HCD collision and detection of fragment ions within the Orbitrap instrument during this project. Our results knew thousands of phosphosites and phosphopeptides' initial time in mammary gland biology.

2.5 Pathway analysis

A pathway reveals the series of chemical reactions in the cell that result in an observable biological function. Protein's regulatory influence and their involvement in the chemical reaction are combined, known as pathway databases. Likewise, Gene ontology/enrichment analysis, where the gene or protein lists closely inspect pathway abundance, could be more meaningful because it interprets far from gene-centric instead of identifying functional biological implications. Additionally, the functional independent protein could

have superfluity in GO term correlation, such as very general terms, e.g. ‘cytoplasmic’ or ‘binging’. More number of database and resources available to draw the pathway restrict to the biological data.

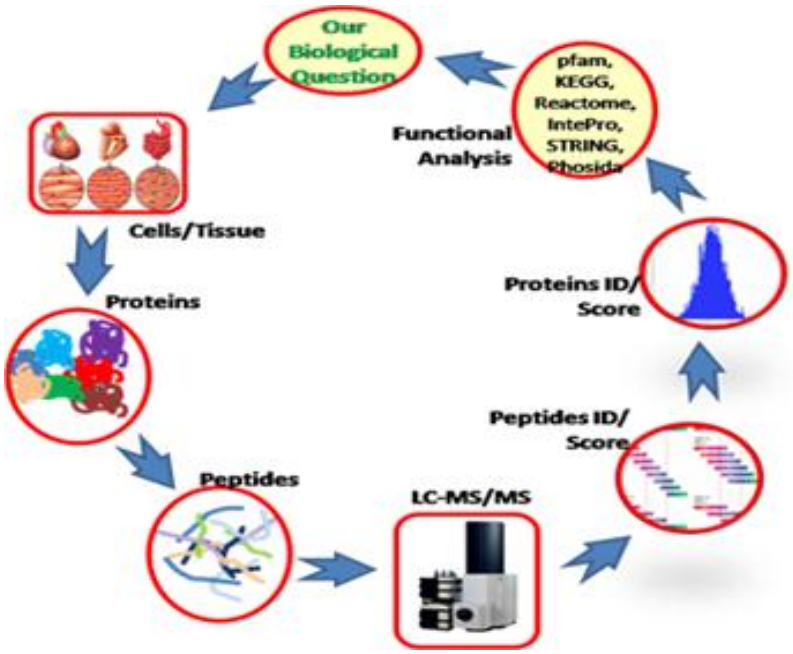

Figure 2.7: Pipeline of Proteomics Workflow

Furthermore, comprehensive pathways database, such as Reactome, KEGG, Ingenuity Pathway Knowledge Base, or BioCarta includes various diverse data. This data arises from the intracellular reactions, including genetic interactions or drug development, metabolism, or signalling pathways studies. Instead of these comprehensive studies or resources or particularly databases designed for signal transduction processes includes PANTHER, PID, or GenMAPP. Moreover recently various database also was created which containing the pathways active in cancer. That type of database is Netpath which should help identify cancer-associated proteins and genes from a complicated dataset. The publicly available database shows a high degree of correlation and connectivity and quickly distributes the novel finding.

This comprehensive list of approximately more than ~300 pathways and interaction databases is found on the pathguide website http://pathguide.org. Nevertheless, recently enrichment analyses are accessible with all pathways database resources, so that concern list of significantly concerning abundance and/or post-translational modifications, altered proteins, which is enough to

extract data on pathway abundance. Moreover, similar to the GO term annotation, identifying pathways act on under certain conditions highly dependent on the algorithm.

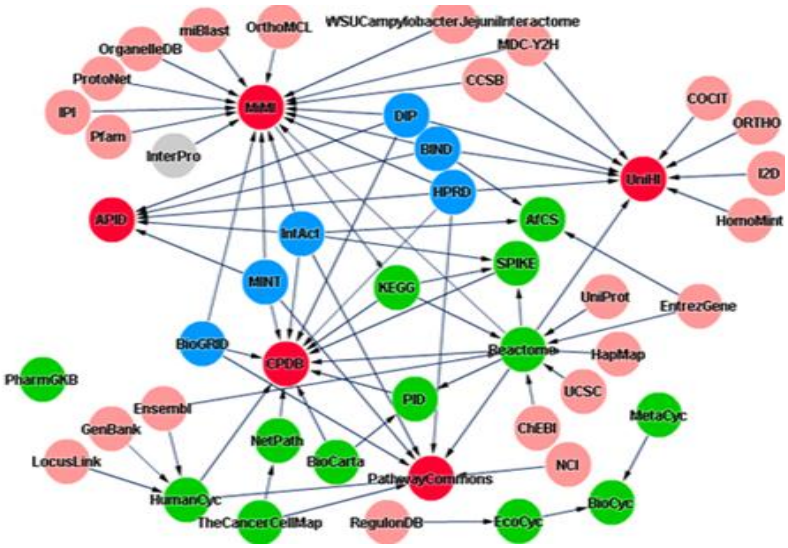

Figure 2.8: Network shows the interaction of the databases

2.6 Analysis of protein-protein-interactions

Almost all proteins do not work as independent entities, either they form transient or stable complexes with several other different or similar protein that regulates or scaffolds protein activity. Therefore a single protein could be involved in multiple complex to varying the composition of complexes. Hence, to thoroughly understand the biological system and analyze the large protein complexes, it is necessary to analyze the protein-protein interaction and networks.

As information about protein interaction in complexes is submitted in-network and interaction databases, such as IntAct or HRPD, MINT, BioGRID, and its associated biological process and function implication. It is not necessary, annotated interaction in public database is experimentally proof or observed. The search can find predicted interaction in a relatively higher percentage and interaction based on the database used, based on literature mining such as iRefWeb or STRING. Numerous literature mining tools such as PubMed have been developed with these intentions, among which mostly favoured are sciminer and chilibot. Thus these interactions are getting from sophisticated algorithms that are designed on an existing set of protein-protein interactions.

Moreover, an extensive interaction database has implicated the simplest algorithms that let annotate interaction of proteins on the database site. Protein interactions are frequently displayed as an extensive network which illustrates the high degree of connectivity or interaction and promiscuous hub proteins. The most widely used resource or database for interaction is STRING, which is not a database. Instead, it connects the various other data resources. It also potentiates literature mining.

Furthermore, STRING can take out a simple protein network based on the gene list provided and already available interaction in the database. Another tool cystoscope is an evolutionary powerful graphical tool to draw the conclusive interaction network of high complexity and further incorporate and compare databases from different experimental procedures. However, Cytoscape has its limitation because it has limited information stored, but it can interconnect excessively to other databases to obtain information. As noted from the beginning, the system-level snapshot of mammary gland proteome and phosphoproteome, associated molecular processes has a considerable amount of mechanistic information to connect different developmental stages. In this regard, a high-resolution mass spectrometer is a valuable tool for generating valuable information in phosphoproteins relative expression and provides better avenues for mammary gland development and organogenesis. About 20,000 genes encoded by the human genome and almost one third always remain phosphorylated at any point in time. This higher level of phosphoproteins expression resulted in identifying the thousands of the phosphosites that can be easily quantified with the sensitive and robust high-throughput MS/MS analyzer.

Thus, the present study uses a high-resolution mass spectrometer approach to investigate the molecular pathways underlying different developmental stages of the mammary gland to understand the role of phosphoproteins in lactation. We decided to take the rat as an *in vitro* model developmental phosphoproteomics study. Rodent derives mammary cell EpH4, and buffalo mammary gland derived cell line BuMEC for in vitro comparison. Several identified proteins were validated in the immune histochemistry. Finally, for targeted validation and identification of pursuing pathways, we selected the MFGE8 and Slug protein to knock down and identified the downstream response using the MS/MS analysis combined with several assays, qRT-PCR and western blot.

CHAPTER –3

Materials & Methods

3.1 MATERIALS

3.1.1 Plastic wares and Glasswares

All the glassware used in the present study were made of high-grade Pyrex glass and were procured from Borosil Glass Works Ltd., India. The glasswares, wherever used, were thoroughly cleaned, rinsed with ultrapure water and then heat sterilised at 250°C for 4 h. All the plastic ware was purchased from Tarsons Pvt. Ltd., Abdos Labtech Pvt. Ltd. and Eppendorf, India. Disposable plastic syringes were non-toxic and non-pyrogenic from BD lifesciences (Norm-Ject, Henke-Sass Wolf GmbH, Germany). Syringe filters 0.22 µm were purchased from Sartorious, Germany. Autoclavable disposable tips for micropipettes were obtained from Tarsons, India. For *in vitro* experiments, cell culture flask (25 cm^2), multiwell plates (6, 12 and 96) and plastic dishes were purchased from Eppendorf, India. The black flat bottom black plates were purchased from Cell Clone TMGenetix Biotech Asia Pvt Ltd. Real-time PCR plates were purchased from Thermo Fisher Scientific.

3.1.2 Chemicals and Supplements

Estrogen (Cas. No., E8875-1G), Progesterone (Cas. No., P0130-25G), Prolactin (Cas. No., SRP4688-50UG), Dexamethasone (Cas. No., D4902-25MG), Hydrocortisone (Cas. No., H0888-5G), Bovine Insulin (Cat. No., I6634-25MG), Neutral red (Cat no.-N4638), 3-(4,5-dimethylthiazol-2-yl)-2,5-diphenyl tetrazolium bromide (MTT) (Cat no.-M2128), Trypan Blue (TB), Ethylenediaminetetraacetic acid (EDTA), carboxy-2',7'-dichloro-dihydro-fluorescein diacetate (DCFHDA), TRIzol (T9424), Gentamicin (cat no.- G1272), Isopropanol (cat no.-CAS-67-63-0) were purchased from Sigma Aldrich, St. Louis, MO, USA). Bengaluru. Fetal bovine serum (FBS, Cat. No. CCS-500-SA-U), Modified Eagle's medium (DMEM) 1X with 4.5 g/L glucose, 4.0 mM L-glutamine, and sodium pyruvate (Cat. No. CC3004.05L), Dimethyl sulphoxide (DMSO, Cat. No. PG-1320-500mL) all were purchased from CellClone TM Genetix Biotech Asia Pvt Ltd. India. Dulbecco's phosphate buffer saline (DPBS,

Cat. No.SH30013.02) without calcium and magnesium was obtained from Hyclone Laboratories (Logan, UT).

TMT six-plex isobaric tags (TMT sixplex™ Isobaric Label Reagent Set, 1 × 0.8mg, Thermo Fisher Scientific, Catalog number: 9006), revert Aid First Strand cDNA Synthesis Kit (K1622) and Maxima SYBR Green/ROX qPCR Master Mix (K0251) was purchased from Fermantas, Thermo Fisher Scientific. All other chemicals purchased were of the highest analytical or molecular biology grade available. All the chemicals used in the study include NaCl, KCl, $MgCl_2$-$6H_2O$, NaH_2PO_4, KH_2PO_4, $NaHCO_3$, $CaCl_2$.2H2O, $CuSO_4$, K_2SO_4, Sodium Citrate Tribasic Dehydrate, Agarose, Ethidium bromide, $MnSO_4.2H_2O$ were of analytical and biochemical grade and purchased from Sigma Aldrich (U.S.A).

3.1.3 Reagents and buffers

Detail description of the media composition, buffers, reagents and stock solutions have been listed in Appendix I, and II.

3.1.4 Equipments

All the equipment used in the study have been listed in Appendix-III

3.2 METHODS

3.2.1 Objective 1: Time-resolved identification of phosphoproteome in the mammary gland at six stages of development

3.2.1.1 Animal husbandry and breeding

According to institutional guidelines for the laboratory animals, rats were maintained in the designated animal care facility at the ICAR-NDRI, Karnal, according to institutional guidelines. All experimental procedures for the use of Wistar rat were conducted according to the institutional animal ethics committee (IAEC, NDRI, Karnal). The IAEC, ICAR-NDRI, Karnal Institutional Animal Care and Use Committee (IACUC) approved the animal protocol describing these procedures. The IACUC approval number for this protocol is 16026 dated August 16, 2016.

All procedures were approved by the Institutional Animal Care and Use Committee. Wistar rats were housed with a 12 h light schedule and ad libitum access to food and water.

We sought to understand the remodelling of different stages of mammary gland and their respective differential changes in the phosphorylation status. Initially, to implement the experiment, we required accurate stage-specific females. Hence, the Wistar rats were timely mated for the isolation of the mammary gland on different stages such as puberty stage (60th day), virgin stage (90th day), pregnancy stage (10th day after a successful mating), early lactation stage (6th day after parturition), late lactation (18th day after parturition), and involution (4th day after weaning of the neonates) were selected. The detailed self-explanatory illustrative workflow for mammary gland isolation collection is depicted in Figure 1.

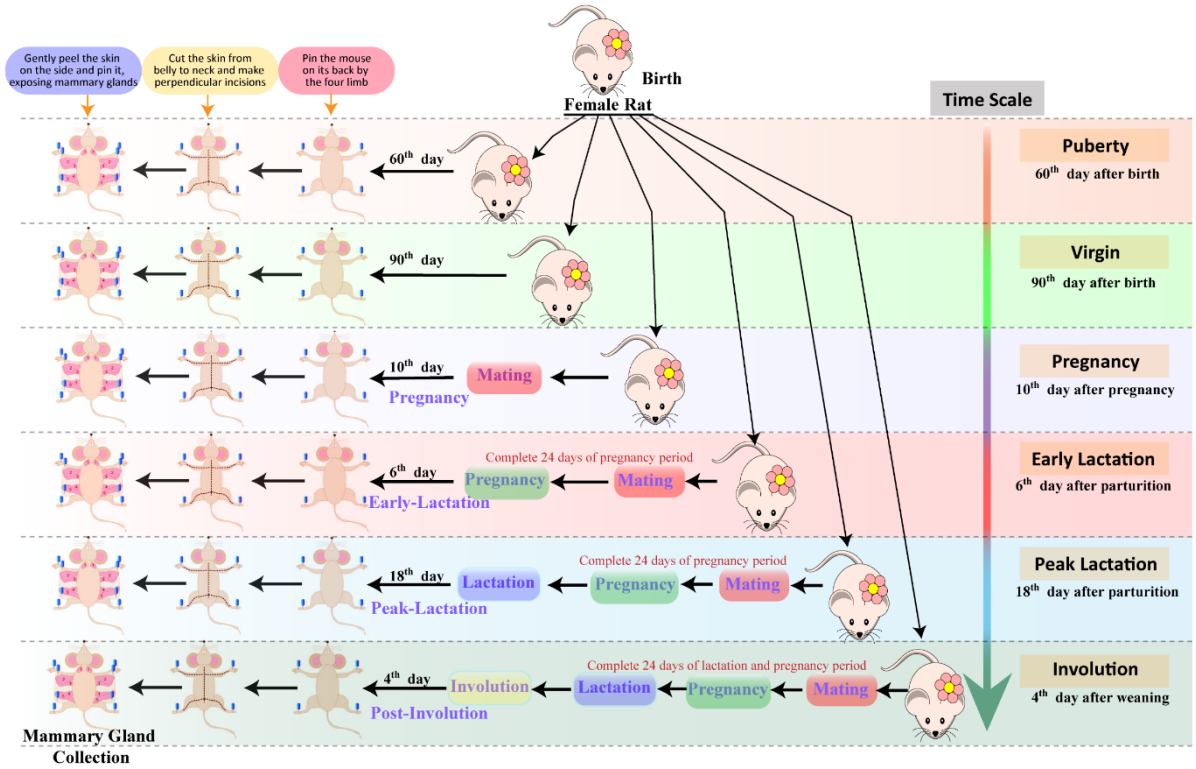

Figure 3.1: Tissue collection from six critical stages of mammary gland development

After completing the specific time duration mentioned above, the females were sacrificed to collect the inguinal gland (4th gland in the rodents). We marked the gland around the teats pairs (five or six) with black pen during the isolation

(please refer figure 2) and the glands were isolated after peeling of the skin around the teats (Figure 2).

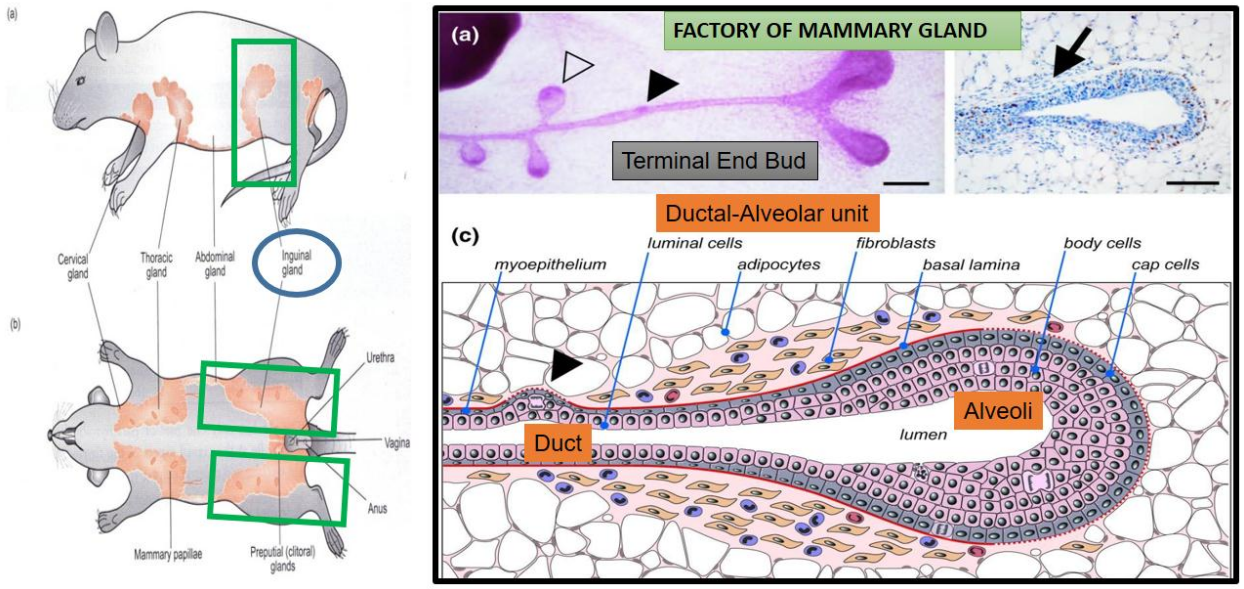

Figures 3.2: Rats were housed and timely mate for stage-specific mammary gland collection as previously defined. Dissection, collection, and mounting of Mammary Gland.

Estrous cycle was not taken into account for virgin samples. All rats were euthanised by CO2 asphyxiation followed by cervical dislocation. Mammary tissue was harvested from all glands. Samples consisted of all glands pooled from one mouse. Three samples for each stage of development were used.

3.2.1.2 Timed mating

In order to study mammary gland development at different stages of pregnancy, animals were time-mated. Pairs were co-housed in the late afternoon and females were checked for a vaginal plug early on the following morning. The day on which a vaginal plug was observed was designated pregnancy day 0 (P0). Females were singly housed from late pregnancy to prevent other animals from destroying newborn pups. The day on which offspring were first observed was designated lactation day 1 (L1).

3.2.1.3 Oestrous staging

To determine the oestrous stage of virgin animals, vaginal smears were stained with Diff Quick (Lab-Aids, Australia). Oestrus is characterised by a

relative predominance of the enucleated cell, while predominance of the leukocytes characterised dioestrus.

3.2.1.4 Mammary gland whole-mount preparation, imaging and morphometric analysis

Mammary glands (inguinal mammary gland) were mounted on glass slides and then fixed overnight in 10% neutral buffered. Fat was removed by acetone washes (3x2h then overnight), and the glands were rehydrated (70% ethanol 1h, water rinse) before staining with carmine alum (0.2% carmine, 0.5% aluminium sulfate, 0.1% thymol) overnight. Following staining, glands were dehydrated in ethanol (70% 2h, 95% 2h, 100% 2h, 100% overnight) and cleared in Slide Brite (Sasco, Albany GA USA) for 1h prior to storage in methylsalicylate (Ajax Fine chem, Taren Point NSW Australia).

Mammary whole-mounts were visualised using a Leica MZ12.5 stereomicroscope and imaged using a Leica DCDFC420C digital camera. Mammary whole mounts were then rehydrated in ethanol (overnight incubations in 100%, 95% and 70%), peeled off the slides and paraffin-embedded.

Inguinal mammary glands were harvested, mounted on glass slides, stained with Carmine alum. Whole mounts were imaged using a Leica MZFLIII dissecting microscope, Adobe Photoshop, and ImageJ to process images.

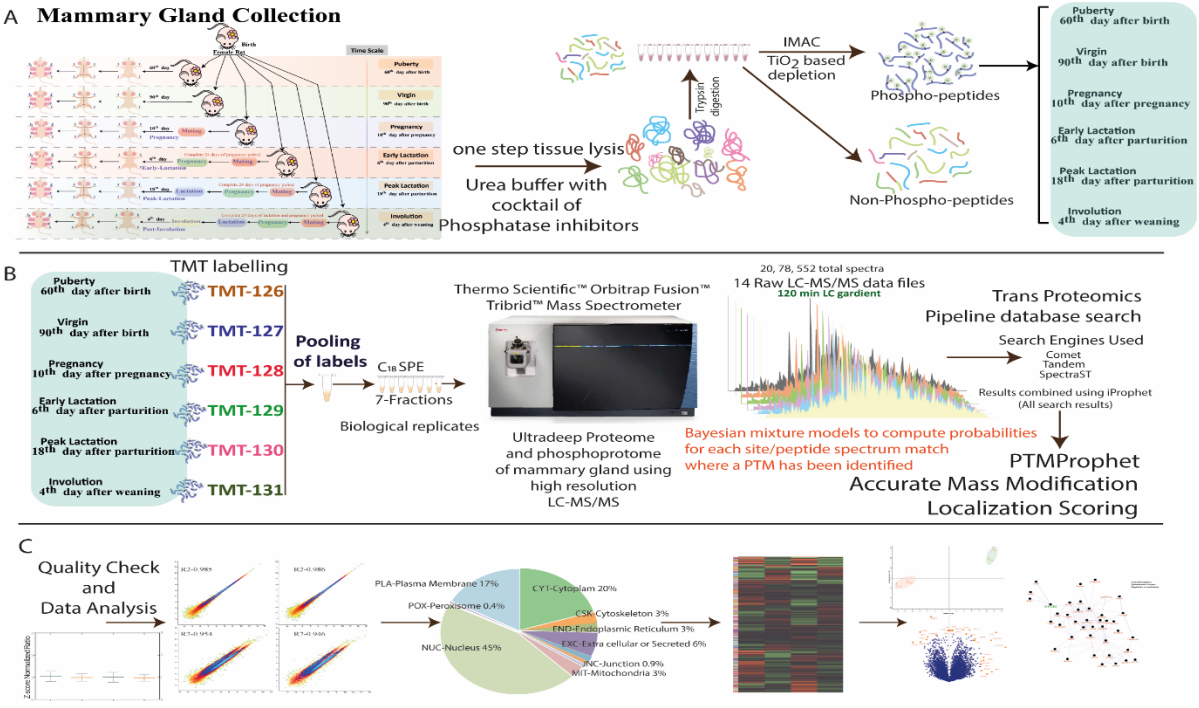

Figures 3.3: Schematic flow chart of phosphoproteome analysis

3.2.1.5 Protein isolation and digestion

Prior to the enzymatic digestion, protein quantification was performed using Bradford assay (Bio-Rad) following the manufacturer's instructions. One hundred micrograms of lysed protein sample from each six group (puberty, virgin, pregnancy, lactation I and lactation II, and Involution) were denatured using 15 µl of 6M urea. The denatured proteins were reduced by adding tris (2-carboxyethyl) phosphine (TCEP) (Sigma Aldrich) to a final concentration of 20mM and were incubated at 37 °C for 60 min. The reduced samples were alkylated by adding iodoacetamide [(IAA), Sigma Aldrich] to a final concentration of 40mM and incubated at room temperature in the dark 30min. The samples were then diluted eight times with 50mM ammonium bicarbonate buffer, and trypsin (Pierce Trypsin) was added to a 1:50 ratio (trypsin: protein) for performing in-solution digestion. Samples were incubated at 37 °C for 18 h for efficient digestion. The digestion was quenched by adding formic acid to a final concentration of 1%. Subsequently, sample cleaning was performed by using C18 Zip tip. Activation of the C18 cartages was done using 50% ACN in 0.1% FA,40 µl, 1 min, 1500g thrice, followed by 99% ACN in 0.1% FA 40 µl, 1 min, 1500g thrice. Equilibration of zip tip by using 0.1% FA 40 µl, 1 min, 1500g was done thrice. Sample addition in zip tip up to 80 µl volume max, 1 min, 1000g five times. Cleanup using 0.1% FA 40 µl, 1 min, 1500g thrice. Elution by using 50% ACN in 0.1% FA60 µl, 1 min, 1000g twice and 50% ACN in 0.1% FA 60 µl, 3 min, 4000g.

3.2.1.6 Phosphopeptides enrichment and purification

IMAC Enrichment. The multi-step IMAC enrichment was performed. Briefly, 30µL Phos-Select iron affinity gel (IMAC beads) (Sigma-Aldrich, St Louis, MO, USA) were washed 3 times with a 10x volume of IMAC binding buffer (40% ACN, 25 mM FA in H2O), and resuspended in IMAC binding buffer to make a 50% gel slurry. Using the 100:1 (mg/µl) peptide-to-IMAC ratio optimised, 3 mg of desalted, lyophilised whole-cell digest were resuspended in 360µL of IMAC binding buffer and incubated with 30 µl of bead slurry for 60min with vigorous shaking. After washing with 360 µl of binding buffer three times, phosphopeptides were eluted by shaking 5min in 40µL of 50mM K_2HPO_4/NH_4OH, pH10. The elution step was repeated three times to recover the phosphopeptides fully, and the combined eluates were immediately acidified with

40µL of 10% formic acid. The second round of IMAC enrichment was performed with the supernatant of the first round of IMAC enrichment, while the third round of IMAC enrichment was performed with the supernatant from the second round of IMAC enrichment. At each step, the supernatant was applied directly to new beads as soon as it was removed from the beads' previous aliquot. According to the manufacturer's, the eluates from each round of the multi-step IMAC enrichment were then lyophilised and desalted with C18 ZipTips (Millipore, Billerica, MA) instructions for LC-MS/MS analysis.

3.2.1.7 TiO2 Enrichment

TiO2 Tips were used to enrich the phosphopeptides. The detailed protocol are as follows. Initially, the required amounts of TiO2 beads (GL Sciences, Tokyo, Japan) were washed with 500 µL loading buffer (65% ACN/2% TFA/saturated by glutamic acid) three times resuspended in 200 µL loading buffer to make bead slurries. To optimise the TiO2 conditions, different amounts of TiO2 slurries were added to 3 mg of peptides according to the indicated peptide-to-TiO2 ratio (µg/ µg). The peptides were resuspended in 200 µL loading buffer and incubated with the indicated amounts of TiO2 beads slurries at room temperature for 20 minutes while shaking. After incubation, the beads were then washed with 800 µL wash buffer I (65% ACN/0.5% TFA) once and 800 µL wash buffer II (65% ACN/0.1% TFA) twice. The TiO2 beads were then incubated with 200 µL elution buffer I (300 mM NH4OH/50% ACN) once and 200 µL elution buffer II (500 mM NH4OH/60% ACN) twice at room temperature for 20 minutes each time while shaking to elute the phosphopeptides. The eluates were combined and immediately acidified with formic acid. For multi-step TiO2 enrichment, the first round of TiO2 enrichment was completed with 3 mg of peptides from whole-cell lysates, and phosphopeptides were enriched with the optimized 1:2 peptide-to-TiO2 ratio (µg/ µg). The second enrichment was performed with supernatant from the first TiO2 enrichment, while the third round of enrichment was performed with the supernatant from the second TiO2 enrichment. The eluates from each round were then lyophilised and desalted with C18 ZipTips for LC-MS/MS analysis.

3.2.1.8 TMT-based quantitative proteomics analysis

TMT six-plex isobaric tags (TMT sixplex™ Isobaric Label Reagent Set, 1 × 0.8mg, Thermo Fisher Scientific, Catalog number: 9006) were used labelling of

enriched phosphopeptides from six samples as per the manufacturer's instructions. In brief, digested phosphopeptides were reconstituted in dissolution buffer and were vortexed to mix well. A pooled sample was prepared from each sample and considered a reference for performing normalisation of the different mass spectrometric datasets. TMT reagents were reconstituted in 40 µl of anhydrous acetonitrile (ACN). The reagents were added to the corresponding aliquot of digested protein sample following the labelling strategy; 15 µg of each digested phosphopeptides sample was labelled at ~1:13 ratio (digested phosphopeptides: TMT reagents) for performing efficient labelling. The solution was mixed well and incubated at room temperature (RT) for 1 h. The reactions were quenched by adding 2 µl of 5% hydroxylamine and were incubated for 15 min at RT. All the respective samples were pooled and were dried completely.

3.2.1.9 Liquid chromatography-mass spectrometry (LC-MS/MS) acquisition.

Multiplexed TMT-labeled samples (6-plex) were analysed as biological replicates using an Orbitrap Fusion Tribrid mass spectrometer interfaced with an Easy-nLC 1200 system (Thermo Fisher Scientific). The mobile phase consisted of milli-Q water with 0.1% formic acid as solvent A and 0.1% formic acid/80% acetonitrile as solvent B. Each fraction was reconstituted in 15 µl of solvent A, and 1µg of digested peptides were loaded on to a pre-analytical column (100 µm × 2 cm, nano Viper C18, 5 µm, 100 A; Thermo Fisher Scientific). Isocratic gradient of 10–35% B in 103 min, 35–95% B in 2 min and holds at 95% B for 15 min at 300 nl/min flow rate were used on an analytical column (75 µm × 50 cm, 3 µm particle, and 100 Å pore size; Thermo Fisher Scientific). A single Orbitrap MS scan from 375 to 1700m/z at a resolution of 60,000 with automatic gain control (AGC) set at 5e was followed by up to 20 ms/ms scans at a resolution of 30,000 with AGCset at 4e. MS/MS spectra were collected with a normalised collision energy of 35% and an isolation width of 1.2m/z. Dynamic exclusion was set to 40 s, and the peptide match was set to on. Surveys scans were performed in the Orbitrap mass analyser, and data-dependent MS2 scans were performed in the Orbitrap mass analyser trap using higher-energy collisional dissociation (HCD) following isolation the instrument's quadrupole. The intensity threshold of the peptide was set 5e). Internal calibration was carried out using a lock mass option (m/z445.1200025) from ambient air.

3.2.1.10 Phosphoproteome analysis and data processing

All the acquired raw files were in .raw format and initially for identifying the peptides and parental protein commercially available MASCOT software (Matrix Science, London, UK; v. 2.3.02) adapted from MOWSE algorithm was employed. The parameters for peptide search were MS/MS ion search with utilising enzyme trypsin. For the identification of monoisotopic mass values with total protein mass. The peptide mass tolerance kept was +100 ppm with fragment mass tolerance of +0.5 Da. We allowed the 2 maximum missed cleavages. In the variable modification options, the selection was Gln- Glu-.pyro-Glu, ammonia-loss of the N-terminus and oxidation of histidine, methionine and tryptophan. The database taxonomy used was *Mus musculus* (mouse) from the updated Uniprot database. All the proteins reported were recognised using a reversed decoy database. Peptide identification was accepted if they threshold of more than 90% probability (p, 0.9). For further analysis proteins with a minimum, one unique peptide with an ion score of above 16 were selected. Proteins were further shortlisted based on phosphorylation sites.

Further validation of the identification of mass spectrometer data was performed in the open-source software Trans Proteomics Pipeline (TPP). It utilises the blended tool of TPP msconvert to change the raw files into open access mzML format and examined employing the TPP variant 5.1.0 with UniProt (*Mus musculus*) database and equal quantity of reversed protein sequences as decoy sequences from the primary database. The search was performed applying the various search engines in the platform, including the SpectraST, X! Tandem (MacLean et al., 2006), plus Comet. All the search engine utilises the identical parameters as mentioned for the Mascot search engine. However, the algorithm provides the peptides probability distributions to ascertain the mathematical validation of peptide-spectra-matches (PSM) and prudence of FDR at the PSM level.

Nevertheless, to calculate the possibilities, counts and implement a Gaussian pattern for the accurate classifications for both independently examined peptides and the corresponding proteins (Deutsch et al., 2010), the ProteinProphet^{TM} algorithms were applied. Above another filter criterion used for the authentication is that it should contain at least two top-ranked peptides specific with a peptide probability score of over 95%. Sequences received from

total engines were joined using the extra computational program, of iProphet (Nesvizhskii et al., 2003). A design of iProphet representation concerning the abundance of suitable identifications *versus* failure for definitive classification of the proteins, 0.99 iProphet probability was applied. More than 2 individual peptides per protein were weighed for proteins quantification to guarantee the quantitation with least false discovery rate.

An extra program was applied for the identical raw files in extension to the preceding processes for classification. The well-known MaxQuant suite 1.5.2.8 with the Intensity-Based Absolute Quantification implementation is the well popular algorithm employing the combined Andromeda search engine. All the parameter database decoy contaminant sequences were the same as the Mascot instruction search for the MS/MS spectra analysis. To warrant the confidence on the identifications of proteins, the FDR was applied at three levels: PSM, protein, and decoy fraction was set to less than 1%. As mentioned in the above analysis, the enzyme, maximum of two missed cleavages were allowed with trypsin as enzyme specificity. Furthermore, to authenticate and transmit identifications across different replicates, the 'match between runs' option was permitted in MaxQuant with a prolonged retention time frame of 0.7 minute and a placement time window of 20 minutes.

3.2.1.11 Preparation of histological sections

Histological sections were prepared from paraffin-embedded tissue by Ms Alice Boulghourjian. 4µm sections were cut using a Leica RM 2145 microtome and placed on Super frost glass slides (Lomb Scientific, Taren Point NSW Australia). Sections were baked at 62°C for 2h and stored at 4°C until required for staining.

3.2.1.12 Haematoxylin and eosin (H&E) staining

Mammary gland sections were baked at 80°C for 5min and placed in xylene for deparaffinisation. Slides were then rehydrated and stained with haematoxylin (Thermo Scientific) for the 30s, differentiated in acid alcohol (70% ethanol, 0.01M HCl) for 10s, blued in hot water for 30s and stained with alcoholic eosin Y (Sigma-Aldrich) for 2s, according to the manufacturers' guidelines. Slides were then dehydrated in ethanol, dried, and placed in xylene for 5min before mounting in Ultramount No. 4 (Fronine Laboratory Supplies, Riverstone

NSW Australia). All sections were visualised on a Leica DMRB light microscope and imaged using a Leica DFC420C camera.

3.2.1.13 Immunochemistry

Paraffin-embedded mammary tissues were sectioned and subjected to IHC. Antibodies concentration and species of origin with catalogue number are described in the table below. IHC was performed on mammary tissue sections, using primary antibodies and bound primary antibodies were detected with either horseradish peroxidase (HRP)- conjugated secondary antibodies. Sections were counterstained with hematoxylin or dapi and mounted. Cells were fixed in a 3.7% formalin solution at room temperature for 15 min, followed by PBS washing. 0.25% Triton X-100 permeabilised the cells in PBS for 10 min, and nonspecific binding of antibodies was blocked with 5% donkey serum for 1 h at room temperature. Cells were incubated with primary antibodies overnight at 4^{o}C. Labelling was visualised with fluorescent label-conjugated secondary antibodies and slides were mounted in Prolong GOLD and cured for 24 h before imaging. The images of immunohistochemical staining were captured using a Leica DM2500 light microscope fitted with a Qimaging Retiga 2000R camera (Qimaging). These images were minimally processed on Adobe Photoshop version 8.

Table 3.1: Details for antibodies used in the study for the IHC staining.

Antibody origin	Type	Dilution	Company Name	Company catalogue
Rabbit	S100-A4 Antibody	1:100-500	Biorbyt	Orb6190
Mouse	Beta-Actin Antibody	1:300-500	Merk Sigma-Aldrich	A5316
Rabbit	Smooth Muscle Actin Antibody	1:20-50	Thermofisher	PAI-37023
Goat	p-Smad 2/3 (Ser 423/425) Antibody	1:50-500	Santa Cruz Biotechnology, Inc.	Sc-11769
Rabbit	p-Akt 1/2/3 (Ser 473) Antibody	1:50	Santa Cruz Biotechnology, Inc.	Sc-33437
Rabbit	Akt 1/2/3 (H-136)	1:50-500	Santa Cruz	Sc-8312

	Antibody		Biotechnology, Inc.	
Rabbit	Stat-3 (K-18) Antibody	1:50-500	Santa Cruz Biotechnology, Inc.	Sc-483
Rabbit	p-Stat-3 (Ser-727) Antibody	1:50-500	Santa Cruz Biotechnology, Inc.	Sc-8001
Rabbit	Twist (H-8) Antibody	1:50-500	Santa Cruz Biotechnology, Inc.	Sc-1593
Goat	E-Cadherin (CN-20) Antibody	1:50-500	Santa Cruz Biotechnology, Inc.	Sc-1500
Mouse	Vimentin (RV-203) Antibody	1:50-500	Santa Cruz Biotechnology, Inc.	Sc-58899
Rabbit	ZEB-1 Antibody	1:50-500	Santa Cruz Biotechnology, Inc.	Sc-25388
Mouse	SNAIL + Slug Antibody	1:500-1000	Abcam	Ab 78105
Mouse	LIF Antibody	1:100	emdmillipore	MAB4306
Goat	MFG-E8 Antibody (G-17)	1:100	Santa Cruz Biotechnology, Inc.	Sc-23999
Mouse	X Keratin Epithelial Antibody	1:100-500	Millipore Temecula California	MAB 1611

3.2.1.14 Image Quantification

Slides representing the different protein concentration in sections were analysed for the intensities quantification. ImageJ software was used for the quantification using the measure function, and the obtained results were statistically tested in Graph Pad Prism version 8.4.0.1.

3.2.1.15 TEM Analysis

We performed the TEM analysis to estimate the cellular features of internal tissue structures from different stages of development and experiments. The tissue was dissected from the animals and washed carefully thrice with PBS

and prefixed for 1 h in the fixative medium (2.5% glutaraldehyde and 2% paraformaldehyde in 0.1 M PBS (pH 7.4)), then extra tissue was removed by scraping and washed twice with PBS. The tissue ultra-sectioning was performed after-fixation by using, 1% osmium tetroxide for one hour. Dehydration was done with various ethanol concentration (30% 50%, 70%, 80%, and 95%) for 10 min at each gradient, and end up with three dehydration cycle using 100% ethanol for 10 min each. Furthermore, samples were embedded in Spurr resin and kept at 68 ºC for 15 h to get polymerised after that ultrathin sectioning was performed by ultra-microtome and visualised under TEM without staining.

3.2.1.16 Ovariectomy models and hormone treatment

Ovariectomy was performed on female rats at 60 days of age with the assistance of a veterinarian. Animals were anaesthetised with isoflurane at a 1L/min oxygen 4% isoflurane rate for induction and 1L/min oxygen 2% isoflurane for maintenance. The analgesics ketoprofen (0.1mg/mouse) was administered prior to surgery. A 1cm dorsal incision was made halfway between the middle of the back and the tail base. Scissors were then used to separate the skin from the subcutaneous tissue on either side of this incision. A 3mm incision was then made through the abdominal wall on either side of the spine. The ovaries and associated fat were located through these incisions, and each oviduct was cauterised to detach the ovary from the uterus. The main ovarian artery and the fat pad were then cauterised to remove the ovary. The abdominal wall incisions were sutured, and the incision in the skin was closed using wound clips. Bupivacaine (0.15mg/mouse) was applied to the surgical site for analgesia.

3.2.1.17 Hormone treatments

Slow-release hormone pellets were obtained from Innovative Research of America (Sarasota FL USA). Progesterone (Pg; 5mg/pellet, 60-day release) and estrogen E2 (0.1mg/pellet, 60-day release) pellets were implanted subcutaneously into the neck's lateral side between the ear and shoulder to all ovx rats. The control was treated with vehicle controls (oil or saline). Another set was created with normal females with the different treatment of hormones. The detailed pictorial protocol was provided in the below figure.

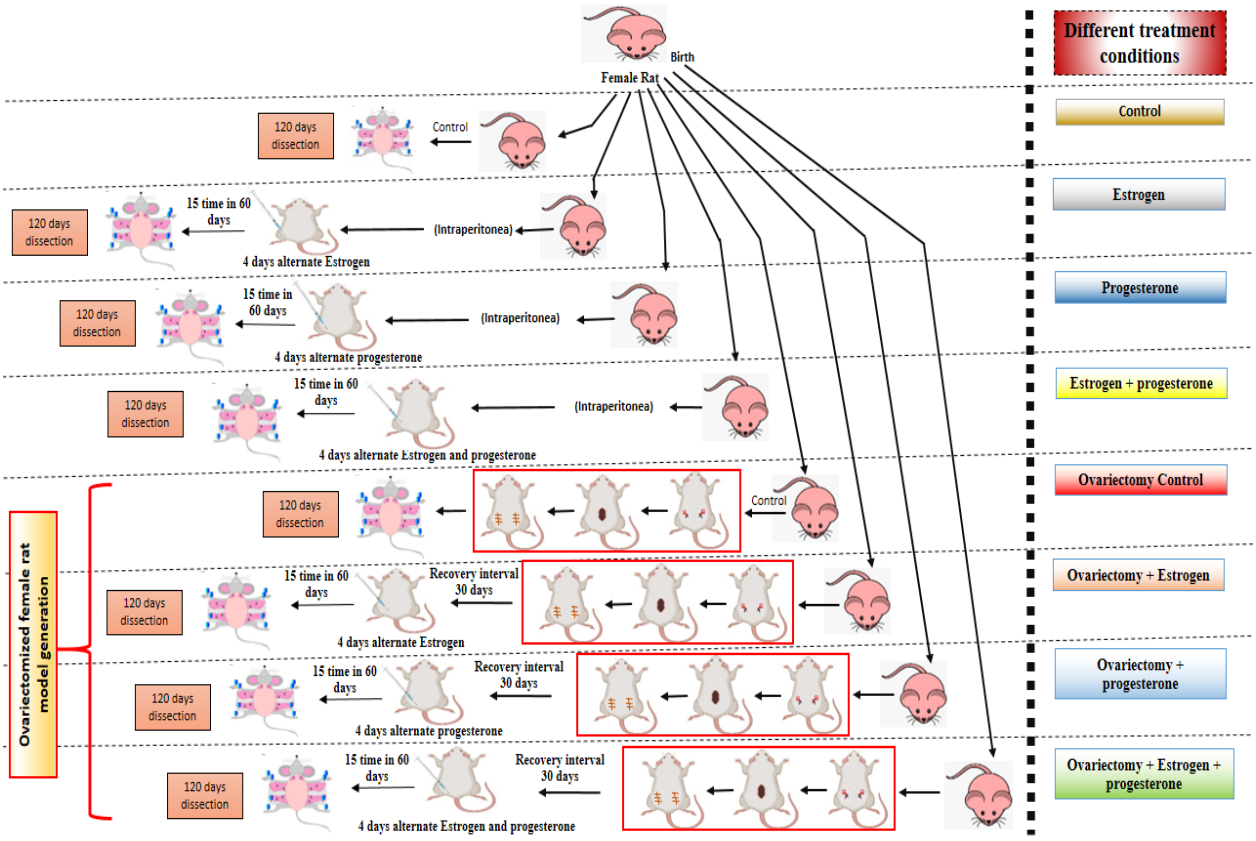

Figure 3.4: Ovariectomy model for hormone treatment.

3.2.1.18 Total RNA isolation, purification and library construction

The mammary gland extracted from the treatment ovx rats were used for the total RNA extracted using the RNeasy mini kit (Qiagen GMBH, Hilden, Germany) following the manufacturer's recommendations. Up to 5mg of tissue from each treatment were disrupted in Buffer RLT and homogenised. Ethanol was then added to the lysate, creating conditions that promote selective binding of RNA to the RNeasy membrane. The sample was then applied to the RNeasy Mini spin column. Total RNA binds to the membrane, contaminants were efficiently washed away, and high-quality RNA was eluted in RNAse-free water. The bind and wash steps were performed on a QIAvac 24, QIAvac 24 Plus, or QIAvac 6S vacuum manifold, and the final elution step was performed by centrifugation in a microcentrifuge. The integrity of total RNA was assessed using the Agilent 2100 bioanalyser. The NEBNext® UltraTM Directional RNA Library Prep Kit (New England Biolabs, MA, USA) was used to prepare the individual sample's RNA-sequencing library (Figure 3.5).

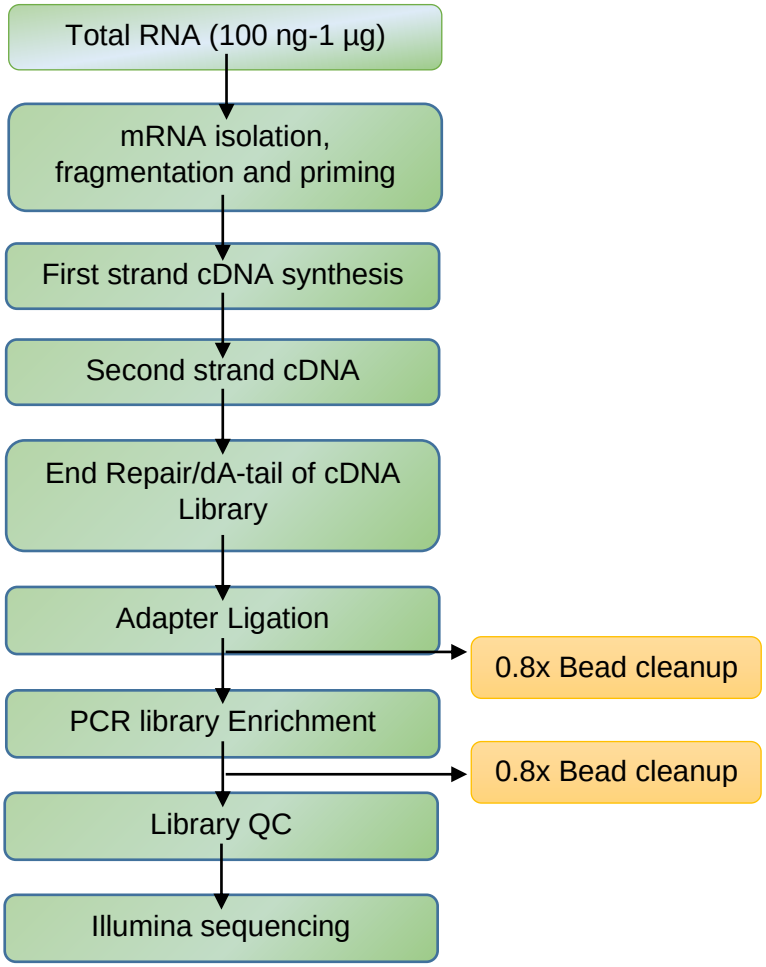

Figure 3.5: Workflow: NEBNext Ultra Directional RNA Library Preparation

1 µg of pooled total RNA was taken for mRNA isolation, fragmentation and priming. Fragmented and primed mRNA was further subjected to first-strand synthesis in Actinomycin D (Gibco, Life Technologies, CA, USA) followed by second-strand synthesis. The double-stranded cDNA was purified using HighPrep magnetic beads (Magbio Genomics Inc, USA). Purified cDNA was end-repaired, adenylated and ligated to Illumina multiplex barcode adapters. Adapter ligated cDNA was purified using HighPrep beads and was subjected to 12 cycles of Indexing-PCR (37 ˚C for 15mins followed by denaturation at 98˚C for 30 sec, cycling (98˚C for 10 sec, 65˚C for 75sec) and 65˚C for 5mins) to enrich the adapter-ligated fragments. The final PCR product (sequencing library) was purified with HighPrep beads, followed by library quality control check. The Illumina-compatible sequencing library was quantified by Qubit fluorometer (Thermo Fisher Scientific, MA, USA) and its fragment size distribution was analysed on Agilent 2200 Tape station.

3.2.1.19 RNA-sequencing data analysis

Analysis pipeline was based on Tuxedo software package. To identify and quantification of transcripts expressed in different condition. They were identifying the differentially expressed transcripts between the control and treated samples. The pipeline utilised for analysis is shown in figure 3.5. The generated RAW reads were first checked for the quality using FastQC (http://www.bioinformatics. babraham.ac.uk/projects/fastq) and pre-processed, which includes removing the adapter sequences and removing the low-quality bases (<q30). Pre-processing of the data is done with Cutadapt. HISAT is a fast and sensitive spliced alignment program that aligns the high-quality data to the reference genome (GRCm38.p6) with the default parameters. Reads are classified into aligned reads (which align to the reference genome) and unaligned reads. Then Cufflinks was used to estimate and calculate transcript abundance. It results in normalised read count in the form of FPKM values. FPKM is a unit measuring gene/transcript expression (Fragments Per Kilobase of transcript per Million mapped reads). Cuffdiff was used to calculate the differentially expressed transcripts and categorise them into UP, Down and Neutrally regulated based on the log2fold change values.

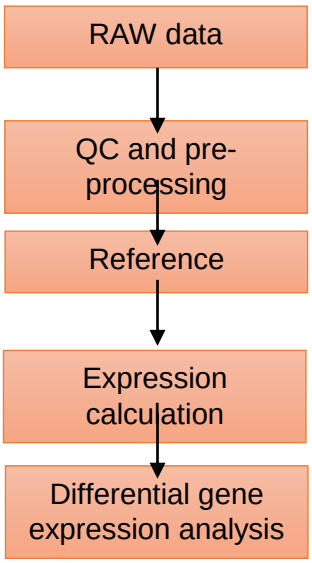

Figure 3.6: Overview of reference-based transcriptome pipeline schema

3.2.1.20 Functional enrichment analysis of nanoparticles induced transcriptome

For functional annotation analysis to the identified high-throughput NGS based sequencing data, we performed (Database for Annotation, Visualization and Integrated Discovery) by DAVID analysis (https://david.ncifcrf.gov/. Initially,

to gather information, we selected all transcripts more than and less than 3 fold change differentially regulated and submitted to DAVID web-based bioinformatics tool. The newly updated enrichment analytic algorithm measures the relationships among annotation terms based on their co-association genes' degrees to group similar, redundant, and heterogeneous annotation contents from the same or different resources into annotation groups. We calculated the fold enrichment by keeping the minimum number of 2 genes for the corresponding term and maximum EASE threshold/p-value of 0.1 using the multiple post-test including Bonferroni, Benjamini, and the Fisher Exact test the confidence of the annotation. We also calculated the corrected FDR values for all the tests mentioned above to reduce the burden of associating similar redundant terms and making the biological interpretation more focused on a group level. All the calculations for functional annotation clustering were performed in the background of the rat genome database. Additionally, other online tools like PANTHER gene list analysis (http://www.pantherdb.org/) and WebGestalt (WEB-based GEne SeT AnaLysis Toolkit) (http://www.webgestalt.org/) were also utilised.

3.2.1.21 Pathways enrichment and overrepresentation analysis of the transcriptome data

Enrichment analysis for differentially expressed genes was performed using clusterProfiler based R package. The package allows the statistical evaluation of enrichment of pathway at different levels, providing the platform to determine the resultant gene set in the transcriptomics data. Nonetheless, the use of a support vector machine learning model helps predict and give confidence. It considers the use of genome annotation data to increase the statistical power and biological relevance for enrichment analysis. The algorithm compares the analysed transcriptome data over the whole genome and creates enrichment values.

3.2.1.22 Preparation of Venn diagrams, Hierarchical clustering analysis and similarity matrix

The overall data was considered for the initial analysis against all the hormone-treated conditions. The terms found common for all were considered individually for further analysis. Unique and common genes were graphically

represented through Venn diagrams with the software Venny (http://bioinfogp.cnb.csic.es/tools/venny/index.html). The hierarchical clustering was performed considering the common genes. Clustering analysis was performed using hclust function in R, which uses the complete linkage method for hierarchical clustering by default. This clustering method defines the cluster distance between two clusters as the maximum distance between their components. At every stage of the clustering process, the two nearest clusters are merged into a new cluster. The process is repeated until the whole data set is agglomerated into one cluster to generate the HCA plot. After the HCA analysis if data is of type "clust", the distance matrix is extracted from the result and transformed to a similarity matrix. Possibly a range normalisation is performed. If data is of type "dist", it is also transformed into a similarity matrix, and the cluster is performed on the distances. If data is of type "sim", the data is transformed into a distance matrix on which clustering is performed. Once the similarity matrix is obtained, the cutoff value is applied, and a heatmap is drawn.

3.2.1.23 STRING network analysis for the individual selected process

All the common DEG's was considered for network analysis. The network analysis has been done using STRING (Search Tool for the Retrieval of Interacting Genes, https://string-db.org/) software. STRING is a database of known and predicted protein-protein interactions. The interactions include direct (physical) and indirect (functional) associations; they stem from computational prediction, from knowledge transfer between organisms, and interactions aggregated from other (primary) databases. Proteins and their functional interactions form the backbone of the cellular machinery. Their connectivity network needs to be considered to understand biological phenomena fully, but the available information on protein-protein associations is incomplete and exhibits varying levels of annotation granularity and reliability. The STRING generated a .tsv file as an output, which contained the node1, node 2, their interaction type and interacting combined score.

Data Sources

Interactions in STRING were derived from five primary sources:

1) Genomic Context Predictions
2) High-throughput Lab Experiments(Conserved)
3) Co-Expression

4) Automated Text mining

5) Previous Knowledge in Databases

All the selected processes were used for fetching the interaction of PPI networks to decipher the variation in the molecular connections.

3.2.1.24 Bioinformatics analysis and PPI network construction

The prediction of kinase pathways and explore the classified proteins, we performed the protein-protein interaction (PPI) investigation for kinome and its associated proteins. Initially, the complete protein sequences were regained, and properties were obtained from various PPI network databases, including STRING v 10.0, GeneMANIA, Reactome, and KEGG. Kinase close interacting companions were classified based on the Boolean interface design utilising degree, closeness, and betweenness centrality criteria. PPI network was created and conceived employing Cytoscape 3.2.1 program by consolidating all those characteristics. Hand-operated footnotes were prepared for the distinguished proteins in the PPI network employing the Reactome database for biologically appropriate processes. Furthermore, to classify the phospho positions and interplay motif in the proteins, the complete amino-acid sequence in FASTA format was examined on the GPS-phospho 1.0 engine's online program.

The biological association of the phosphoproteome collection was explained working with Reactome and WikiPath for the mark genes. Gene Ontology Enrichment Analysis Software Toolkit (GOEAST) released 2016-07-15 Version 11 was applied during the gene-term enrichment investigation. The fold enrichment was determined to utilise the expected value for an appropriate Gene Ontology (GO) classification based on the database's mentioned record. Consequently, the expectation ratio was defined applying a binomial statistic for p-values with the cutoff of 0.05. Further, the statistical analysis was performed using the two-sided hypergeometric distribution tests and Benjamini and Hochberg false discovery rate (FDR)-correction at <0.05 weight level.

3.2.1.25 Preparation of histological sections (mentioned above)

3.2.1.26 Haematoxylin and eosin (H&E) staining (mentioned above)

3.2.1.24 Immunochemistry (mentioned above)

3.2.2 Objective 2: Comparative phosphoproteome analysis of mammary epithelial cell line for identification of ubiquitous expression of proteins

3.2.2.1 Cell culture: Mammary epithelial cells (MEC) differentiation assay

All cell culture reagents were obtained from Invitrogen unless otherwise stated. EpH4 Cell line, *Mus musculus*, Mammary Epithelial cell line, were maintained in DMEM/F12 media supplemented with 10% fetal calf serum (FCS; Thermo Scientific, US), 25mM HEPES buffer, 2mM L-glutamine, 50U/ml penicillin and 50µg/ml streptomycin.

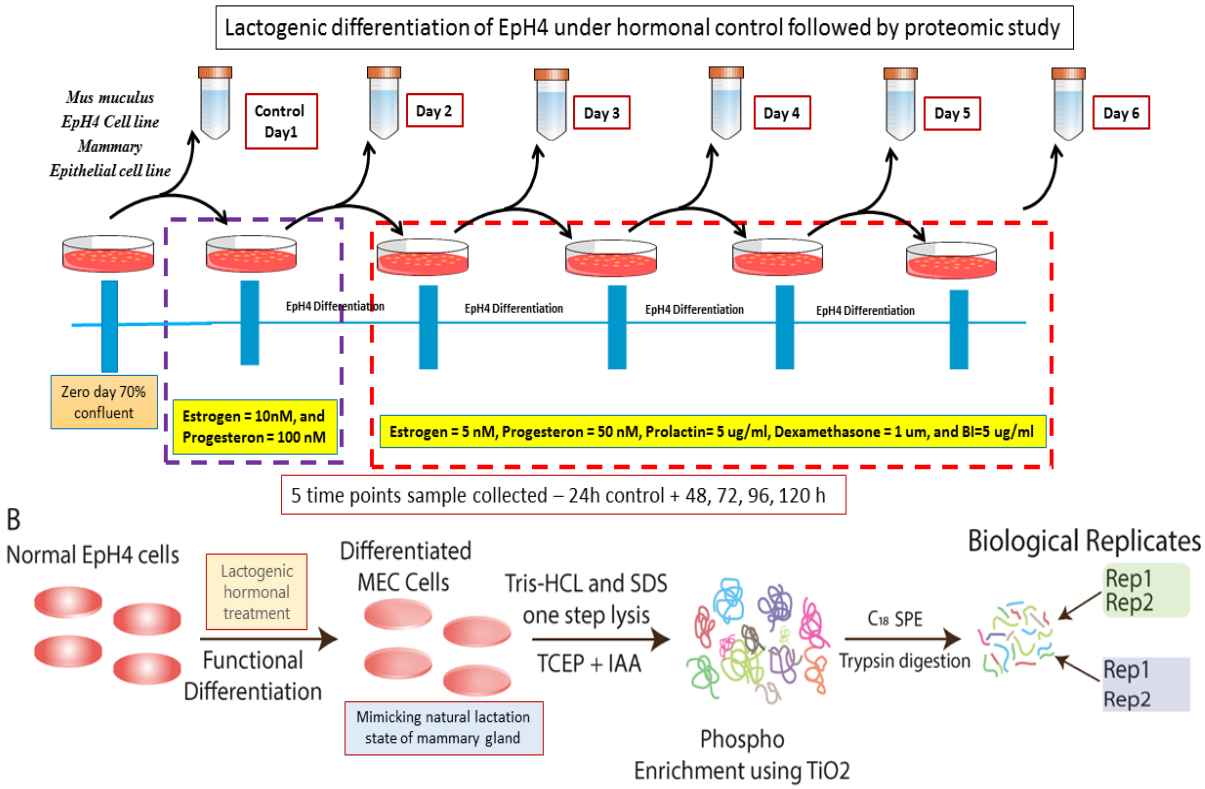

Figure 3.7: Overview of EpH4 treatment for lactogenic differentiation

BuMEC Cell line, *Bubalus Bubalis*, Buffalo Mammary Epithelial cell line cells were maintained in DMEM/F12 media (Thermo Scientific) supplemented with10% FCS, 6mML-glutamine and 5µg/ml insulin (Sigma-Aldrich, US),10ng/ml epidermal growth factor (EGF; BioScientific, US), 500 ng/mL of hydrocortisone, 0.1125% Na(CO3)2, 50U/ml penicillin and 50µg/ml streptomycin. For experiments involving oestrogen treatments, phenol red-free media, and charcoal-stripped FCS were used. For experiments involving hormone treatment,

FCS was heat-inactivated by 30min incubation at 50°C. All cell cultures were maintained in a 37°C, 5% CO2 humidified incubator.

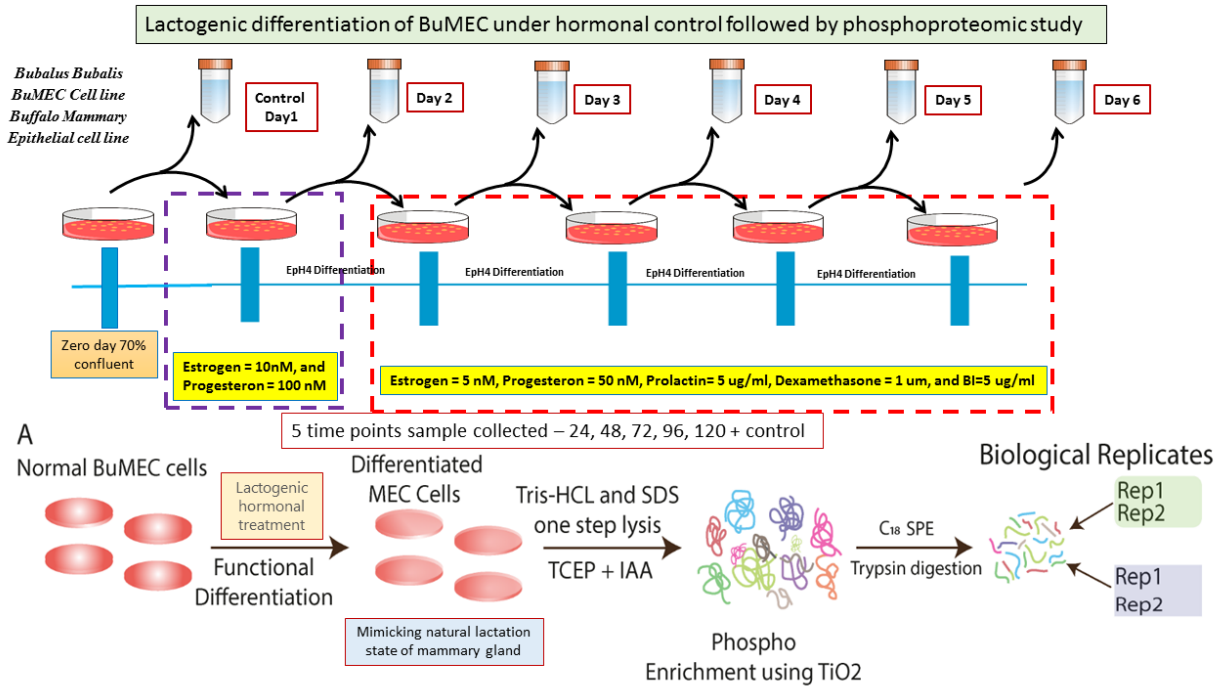

Figure 3.8: Overview of BuMEC treatment for lactogenic differentiation

Both the cell line at a density of $1x10^6$ cells/well seeded and allowed to grow for Day 1 to attend the 70-80% confluence and used as control. Day 2 was treated with Estrogen = 10nM, and Progesterone = 100 nM. From the third day onwards, the medium was changed to Estrogen = 5 nM, Progesteron = 50 nM, Prolactin= 5 ug/ml, Dexamethasone = 1 ug/ml, and BI=5 ug/ml. This treatment was repeated daily until day 6. The detailed protocol is described in the above figure 3.7 and 3.8.

3.2.2.2 Protein isolation and digestion

After growing to 80% confluence, cells were rinsed twice with ice-cold PBS and lysed with 8 M urea lysis buffer, which contained the final concentration of 8 M urea, 75 mM NaCl, 50 mM Tris-HCl (pH8.2), 1 mM NaF, 1 mM β-glycerophosphate, 1 mM sodium orthovanadate, 10 mM sodium pyrophosphate, 1 mM PMSF, and 1 tablet of EDTA-free protease inhibitors cocktail for every 10 mL of lysis buffer. Cell lysates were sonicated for 1 min followed by a 2 min rest interval, and this operation was repeated for 3 times. The mixture was centrifuged at 2500g for 10 min to remove cell debris. Protein concentrations

were confirmed with bicinchoninic acid (BCA) protein assay kit (Thermo Scientific Pierce, Rockford, IL), and 15 mg of protein was used in the SCX-IMAC experiment, while 3 mg of protein was used in multistep IMAC enrichment and multi-IMAC-HLB experiments. Proteins were treated with 5 mM DTT for 25 min at 56 °C to reduce their disulfide bonds. Then IAA was added to the protein mixtures to make a final concentration of 14 mM and reacted in the dark for 30 min at room temperature to allow the cysteine's alkylation. Another 5 mM DTT was added and allowed to react in the dark for 15 min to stop the IAA reaction. The protein mixture was then diluted with 25 mM Tris-HCl (pH 8.2) to achieve a final urea concentration of 1.8 M. Proteins were digested overnight with trypsin from bovine pancreas (Sigma-Aldrich, St Louis, MO) at 37 °C at a 50:1 protein to trypsin ratio (m/m) in the presence of 1 mM CaCl2. The digestion reaction was stopped by adding TFA to a final concentration of 0.4% (v/v). Samples were centrifuged at 2500g for 10 min to remove any precipitates.

3.2.2.3 Peptide fractionation

The peptides were then desalted by 500 mg reverse-phase tC18 Sep-Pak solid-phase extraction cartridges (Waters Corporation, Milford, MA). Strong Cation Exchange (SCX): The SCX steps were performed as described previously.18 Briefly, 15 mg of desalted peptides were resuspended in 500 µL of SCX Buffer A (30% ACN, 7 mM KH2PO4, pH 2.65) and loaded onto PolySULFOETHYL A column (9.4 × 200 mm, 5 µm particle size, 200 Å pore size) (PolyLC, Columbia, MD) with 5 injections. The separations were performed on a Waters Alliance e2695 System (Waters Corporation, Milford, MA) at a 1 mL/min flow rate. Liquid chromatography runs (120 min total time) included 2 min at 100% Buffer A, 33 min of a gradient from 0 to 25% Buffer B (30% ACN, 7 mM KH2PO4, 350 mM KCl, pH 2.65), 1 min of a jump from 35 to 100% Buffer B, 5 min of running at 100% Buffer B, 6 min of washing with 100% water, 11 min of washing with 100% Buffer C (50 mM K2HPO4, 500 mM NaCl, pH 7.5), 6 min of washing with 100% water, and 52 min of equilibration with 100% Buffer A. The chromatogram was recorded at 220 and 280 nm. The eluates from the first 52 min were collected at 4 min intervals to generate 13 fractions. The SCX fractions were then lyophilised to reduce the volume by 30% and desalted with 100 mg reverse-phase tC18 Sep-Pak solid-phase extraction cartridges (Waters Corporation, Milford, MA).

3.2.2.4 Phosphopeptides enrichment and purification (mentioned in 1st Objective)

3.2.2.5 TMT labelling (mentioned in 1st Objective)

3.2.2.6 Mass Spectrometer acquisition (mentioned in 1st Objective)

3.2.2.7 Bioinformatics Analysis (mentioned in 1st Objective)

3.2.3 Objective 3: Targeted validation of an important phosphoprotein in cell line involved in lactation

3.2.3.1 Cell culture and stable knockdown of MFGE-8 expression in BuMEC cells

The bovine macrophage (*BoMac) cell line* was the generous gift by Prof. J. R Stabel. The cells were cultured in RPMI medium with 10% (FBS) (Gibco BRL, USA). The Buffalo Mammary Epithelial Cell (BuMEC) was previously established in the lab (ExPASy accession: Buffalo 2012 (CVCL_M445)) and used for the experimental purpose. Briefly, cells were cultured in DMEM/F12 media (Gibco BRL, USA) supplemented with 8% (FBS) (Gibco BRL, USA), 5 µg/ml bovine insulin (Sigma, USA), 1 µg/ml hydrocortisone (Sigma, USA), 10 ng/ml EGF (Sigma, USA), 100 U/ml penicillin, and 5 µg/ml streptomycin were incubated with 5% CO_2 at 37°C in a humidified environment. The confluent monolayer after 4-5 days were sub-cultured at split ratio of 1:3 by seeding in $1x10^6$ cells/flasks ($25cm^2$ flasks) by trypsinization (0.5% trypsin and 0.05% EDTA). The fresh medium was changed in ever two alternate days regularly.

The designed three shRNA MFGE-8_1 (TCCCACAAGAAGAACATATTT), MFGE-8_2 (CGGTCAGGAGATAAGATATTT) and MFGE-8_3 (CAACAGCGGCCTGAAGATTAA) oligonucleotides were annealed in pLKO.1-puro-CMV-tGFP vector backbone individually and used for the transfection. For making the stable knockdown BuMECs ($3×10^5$) cell line, initially, cells were cultured in 24 well plates at 70% confluence, transfected with 3 µg of a non-target scramble and targeted shRNA pLKO.1-puro-CMV-tGFP recombinant plasmid using lipofectamine 2000 (Qiagen) using manufacturer protocol. After 24 hours, cells were shifted to complete medium containing 50 µg/mL of puromycin as a selective agent. After 48 h of transfection, cells were trypsinised and seeded at low density in puromycin-containing media and allowed to grow with regular media changed every 48 h. Colonies of transfected cells were selected

and further propagated in selection medium by retrograde passaging using clonal dilution till a stably transfected KD BuMEC_MFGE-8 cell line was established. The expression of GFP protein was observed under a fluorescent microscope (NikonTE2000, Japan). The knockdown effect was confirmed by analysing the low-level expression of MFGE-8 at different passages by quantitative real-time PCR. The cell line stably transfected with MFGE-8 shRNA pLKO.1-puro-CMV-tGFP was designated as KD_BuMEC_MFGE-8 (KD-cells) and the control transfected with scramble pLKO.1-puro-CMV-tGFP plasmids were named as Puro_BuMEC_MFGE-8 (WT-cells).

3.2.3.2 Sample preparation for proteomic analysis

For the preparation of proteomics sample, KD_BuMEC_MFGE-8 (KD-cells) and Puro_BuMEC_MFGE-8 cells (WT-cells) were cultured for 80% confluence, washed 3 times with PBS. The cells were harvested using 500 µL of lysis buffer [50 mM Tris-Cl (pH7.8), 0.3% SDS, 200 mM DTT, 1 mM PMSF, 1 mM EDTA] containing a protease inhibitor cocktail (Sigma-Aldrich) and vortexed. Subsequently, sonication was performed using the 10 cycles (pulse ON 5 sec and OFF 7 sec) with an interval of 120 sec. The undisrupted cells were removed by centrifugation at 2500g for 15 min, and the supernatant was transferred to another tube. Proteins were precipitated by adding 10 volumes of cold acetone followed by overnight incubation at -20^{0}C. The precipitated proteins were collected by centrifugation at 12,000g for 20 min. According to manufacturer protocol, the protein concentration in the cell-free extract was determined using a 2D Quant kit (GE Healthcare, Life Sciences).

3.2.3.3 Protein Digestion, iTRAQ labelling and RP-HPLC Fractionation

The iTRAQ labelling was performed as per the manufacturer protocol (AB Sciex). Briefly, the lyophilised protein sample (100 µg) from each group was resuspended in 20 µl of 2% sodium dodecyl sulfate (SDS) in 1 M triethylammonium bicarbonate (TEAB). The samples then reduced in 50 mM tris-(2-carboxyethyl) phosphine (TCEP) for 1 h at 56°C and cysteine-blocked with 200 mM iodoacetamide (IAA) at room temperature in the dark for 30 min. The proteins were digested using trypsin (Mass Spec Grade, Promega, Madison, WI) at 1:80 (trypsin: protein ratio) for 16 h at 37 °C. The prepared peptides were iTRAQ labelled in duplicate pairs with KD_BuMEC_MFG-E8 (KD1-114, and KD2-116) Puro_BuMEC_MFGE-8 (WT1-115, and WT2-117) for 1 h at room

temperature. The reaction was stopped by adding deionised water, and the labelled samples were pooled. RP fractionated the final combined sample- HPLC (Agilent 1100) using analytical column (Grace Smart RP, C18 (150 X 4.6mm), 5 µm). The mobile phase A (10 mM TEAB) and B (10 mM TEAB in 90% ACN) was used respectively for the peptides separation using following linear gradient : 0 to 2% in 5 min, 2 to 60% in 60 min, 60 to100% in 25 min and then 100 to 2% in 2 min. The collected 120 fractions were concatenated into 30 fractions, again lyophilised and reconstituted in 0.1% formic acid in water and subjected to desalting using C18 zip tip (Millipore, USA). Eluted peptides were lyophilised and re-dissolved in 0.4% FA and immediately used for MS/MS spectra generation.

3.2.3.4 Electrospray ionisation tandem mass spectrometry LC-MS/MS analysis

The reconstituted peptides were used for shotgun LFQ and iTRAQ proteomics experiments. The peptides were separated using nano-LC (Nano-Advance, Bruker, Germany) through a trap column (Bruker Magic C18 AQ, 0.1 × 20 mm, 3 µm, 200 Å) and a nano-analytical column (Bruker Magic C18 AQ, 0.1 × 150 mm, 3 µm, 200 Å) coupled with captive ion source (Bruker Captive Spray tip) spray in Maxis-HD qTOF (Bruker, Germany) mass spectrometer (MS) for identification with high mass accuracy and sensitivity. The elution was performed with 400 nL/min flow rate in a continuous gradient of 5-75% acetonitrile over 135 min. Solvent A was 100% water in the solvent system in 0.1% formic acid, and solvent B was 100% acetonitrile in 0.1% formic acid. The data-dependent mode was used for acquisition in a mass spectrometer to switch between MS and MS/MS acquisition automatically. The precursor ion MS spectra scan range of 300-1400 (m/z) was used in the Q-TOF with resolution R = 75, 000. The six most abundant precursor ions were searched for detection of different masses in the acquisition method and selected for fragmentation using collision-induced dissociation (CID) with a fixed cycle time of 3 sec and 2 min of release for exclusion filter (otof processing software, Bruker Daltonics).

3.2.3.5 Data Processing for iTRAQ analysis

With the above mentioned same parameter, the iTRAQ analysis was performed in the Maxquant with Andromeda environment. Simultaneously, the data were also analysed using the TPP pipeline. For TPP analysis, the obtained

otof generated raw (.d) files were converted to mzML format using MSconvertGUI using the default parameters. The converted mzML files were searched using the Trans-Proteomic Pipeline version 5.1.0 released on 2017-11-03 to in-house combined UniProt (Cow), and *Bubalus bubalis* (Buffalo) database together with common contaminant sequences were provided for MS/MS spectra search. The database was also appended with an equal number of decoy sequences (reversed proteins sequences from the original database). Initially, for the analysis, the peptide assignments were performed using multiple search engines using X! Tandem (with the *k*-score plug-in (MacLean et al., 2006)), **SpectraST and Comet**. For all the search engine the search parameters included semi-digested LysC and trypsin with two allowed miss cleavage, static modifications carbamidomethyl (Cys) and iTRAQ reagents (N-terminus and Lys), and dynamic modification oxidation (Met), Gln-pyro Glu and Glu-pyro Glu remaining parameter were kept as default.

The minimum peptide length parameter was set to 7 amino acid residue. Further PeptideProphet and ProteinProphet algorithms were used in the pipeline to computing the probabilities score for both individually searched peptides and the respective proteins. The accurate mass model in PeptideProphet was used for high confidence peptide identifications to boost peptides' probability (Deutsch et al., 2010). Another protein validation step was executed using both Peptide Prophet and Protein Prophet scores, where the protein was authenticated if it contains a minimum of two top-ranked peptides with each peptide probability score above 95%. All the search engines results were merged and validated using another computational method, termed iProphet. This method takes as the input of PeptideProphet spectrum-level results from multiple LC-MS/MS runs and then computes a new probability at the level of a unique peptide sequence (or protein sequence (Nesvizhskii et al., 2003)). This framework allows for the combination of results from multiple search tools and considers other supporting factors, including the number of sibling experiments identifying the same peptide ions, the number of replicate ion identifications, sibling ions, and sibling modification states. A model of iProphet performance concerning the number of

correct identifications *versus* error. An iProphet probability of more than 0.95 was used as the cutoff for final identification of the protein. For protein quantitation, ≥2 unique peptides per protein were considered to ensure high-quality quantitation.

3.2.3.6 Transcriptional analysis at mRNA level by qRT-PCR

The qRT-PCR analysis was performed as explained earlier (Ali et al., 2017). Cells were grown at 80% confluence, three times cold PBS washed, mild trypsinised and pelleted by centrifugation at 400 g for 2 min, and samples were collected for RNA isolation. RNA was extracted using the RNAeasy mini kit (Qiagen, Germany) followed by cDNA synthesis using cDNA Synthesis kit (MBI, Fermentas). The respective sets of primers were employed for selected proteins, and the GAPDH gene was used as an internal reference gene. The reactions were carried out for 25 µl total volume containing 1 µl template, 10 nM of 1.25 µl primers, 12.5 µl master mix (Thermo Fisher Scientific, USA) and 9 µl nuclease-free water keeping the standard conditions in 35 PCR cycle (Kaur et al., 2016). The associated fold change was measured using the 2–ΔΔCT method. The standard t-test statistic was applied to compare the expression of the gene ($p \geq 0.05$). Data were analysed using MS Excel 2007 and Prism software 5.01 (GraphPad Software, USA).

3.2.3.7 Cell viability tests: MTT; BrdU; Neutral Red; Caspase activity assay for apoptosis determination

We used four different principles based on apoptosis determination assay to assess MFGE8 KD and WT cells' cell viability. For all the assays cells were initially seeded in a cell count of 1×10^5 cells/ml in a 96-well plate with different intervals of time (12, 24, 36, 48, 60, and 72 h) including respective controls containing complete medium without cells. For MTT-assay (3-(4, 5-Dimethylthiazol-2-yl)-2, 5-diphenyltetrazolium bromide (MTT, Sigma) MTT solution of 0.5 mg/ml dissolved in PBS was added in accordance to the mentioned time intervals and incubated for 2 h at 37°C in 5% CO_2 followed by addition of the DMSO to dissolve the precipitated formazan and absorbances

were measured at 570 nm using NanoQuant plate reader (TECAN, Infinite 200 PRO, Mannedorf, Switzerland).

The BrdU (5-Bromo-2´-Deoxyuridine) assay was performed according to the manufacturer's protocol using the assay kit (Cat No. Q11A58, Calbiochem, USA). As mentioned above, cells were seeded in a 96-well plate but with 100 µl medium containing the density of 200 cells per well. The BrdU labels were incubated for 2 hours in the growing cells (KD and WT transfected) for integration followed by measuring the absorbance at 540 nm using Nano-quant plate reader.

For Neutral Red assay, cells were seeded as mentioned above, and in correspondence to mentioned intervals, 0.33% Neutral Red Solution (Sigma-N-2889) was added with 10% of the culture medium volume and incubated for 3 h at 37°C in 5% CO_2. After incubation, the cells were fixed using 0.1% $CaCl_2$ in 0.5% formaldehyde for 2 min. Further, the solution was removed, and integrated dye was solubilised using 100 µl of 1% acetic acid in 50% ethanol and incubated for 15 min at room temperature, and absorbances were measured at 540 nm.

To measure the degree active Caspase- 3/7 we used Caspase-Glo 3/7 activity assay (Promega Cat No. G8091 Madison USA) according to the manufacturer's protocol with minor changes as also described previously (Kaur et al., 2016). Briefly, cells were seeded and incubated as mentioned above in 96-well plate and after completion of individual incubation period, 100 µL of Caspase-Glo 3/7 reagent was added. Further, the plate was incubated for 3 h at room temperature, and luminescence intensities were measured using excitation wavelength 492 nm and emission wavelength 535 nm.

3.2.3.8 Cell confluence, Wound Healing, and Transwell assay

The number of $4x10^4$ KD, WT, KD+HA 14-1 and WT+HA 14-1 BuMEC cell were cultured in 24 well cell culture plates to ~10% of confluence. Cell proliferation was monitored every 7 hrs using Bio-Rad TC20^{TM} automated cell counting system (Bio-Rad, California, USA) up to 56 hrs for over 9-time points.

The migratory behaviour of KD and WT BuMEC cells was evaluated using the wound healing scratch assay. An equal number of cells were seeded on 6-

well plates in six biological replicates and allowed to reach 90% confluency. Upon reaching the suitable confluent stage, the cells were then 12 h serum-starved, creating the wound by spanning the line at the bottom of the individual wells using a sterile p-20 pipette tip. All the wells were rinsed gently with DPBS, and then one set of the KD and WT cells were treated with HA 14-1 a well-known apoptosis inducer as mock control cells were also preincubated with DMSO alone. The quantification was manually completed in the scratch cross-sectional area by measuring the number of cells migration.

In the transwell assay using transwell buckets (Millipore, USA) was covered to the bottom of the inner wells. A cell suspension ($5x10^4$ cells in 200 µL of DMEM without FBS) was added to the upper chamber, and DMEM with 10% FBS (500 µL) was added to the lower chamber. After 15 hrs., the migrated cells were stained with hematoxylin. The stained cells were analysed by microscope in five randomly selected fields/assay. The Image J software counted the cell numbers. Values represent the means ± SD from six replicates.

3.2.3.9 In vitro Phagocytic assay

The phagocytosis assay was performed using bovine macrophage (BoMAC) and BuMEC cell line (KD and WT) with the help of a previously published protocol Hanayama et al., 2002. The apoptosis was induced by HA 14-1 in the assay. The respective BuMEC ($1X10^6$ Cells) KD or WT with or without apoptotic inducer were added to $2X10^4$ macrophage cells previously cultured in eight well Lab-tec II chamber slides and incubated for 1.5 h followed by the fixation using 1% paraformaldehyde and TUNNEL staining was performed. The TUNNEL positive apoptotic cells per phagocytes were counted (phagocytosis index) by light microscopy in a total of 200 phagocytes, and the relative index was determined.

3.2.3.10 Western blots

Protein lysates were resolved by SDS/PAGE using the NuPage pre-cast gel system from Invitrogen. Proteins were transferred to PVDF membranes (Millipore; Billerica MA USA) using the wet tank Mini Trans-Blot Electrophoretic Transfer Cell from Bio-Rad. Membranes were then blocked for 1h at room temperature with either 5% skim milk powder or 1% bovine serum albumin

(Sigma-Aldrich) in TBS-Tween (10mM Tris base, 150mM NaCl, 0.1% Tween). Membranes were incubated with anti-milk (1:10000; Accurate Chemical, Westbury NY USA), anti-STAT5a (1:1000; Cell Signalling Technology, Danvers MA USA) or antiphospho- STAT5 (1:1000; Cell Signalling Technology) primary antibodies overnight at 4°C, and then washed 5 times 5min in TBS-Tween. Specific binding was detected following 2h incubation with horseradish peroxidase-conjugated secondary antibodies using Western Lightning chemiluminescence reagent (PerkinElmer, Waltham MA USA) and Fuji Medical X-ray Film (Fujifilm, Tokyo Japan). In some experiments, membranes were incubated in stripping buffer (62.5mM Tris base, 2% SDS, 100mM □-mercaptoethanol) for 30min at 50°C to remove bound antibodies, before being subjected to the second round of immunoblotting.

3.3 Statistical analysis

The statistical calculations were performed using the GraphPad Prism 4 software package (GraphPad Software, Inc., La Jolla, CA, USA). Data were shown in bar plot as mean with standard deviation (± SD) by calculated error bars with relative 100 per cent control. Statistical significance for MTT, BrdU, Neutral red, Caspase 3/7, and cell grown confluence assay was determined using 2way ANOVA test with Bonferroni post-test correction for false discovery rate (FDR)-correction at <0.05 significance level indicated by asterisk marks. For wound healing, transwell, and phagocytosis assay 1way ANOVA test with repeated measures along with post Turkey test for false discovery rate (FDR)-correction at <0.05 significance level indicated by asterisk marks.

Results are expressed as mean ± SD. Statistical significance was determined using a student's t-test, and two-sided hypergeometric distribution tests with Benjamini and Hochberg false discovery rate (FDR)-correction at <0.05 significance level whenever applicable. For Mass Spectrometer and qRT-PCR results, data are represented as relative log2 fold change. Transcripts CT values were normalised against the housekeeping gene β-actin, and fold change were calculated using the $2^{-\Delta\Delta}$CT method. All experiments were performed in triplicates. The significance of the differences in expression levels was tested using the non-parametric Mann–Whitney U test *p< 0.05, **p<0.01.

CHAPTER –4

Results

4.1 Time-resolved identification of phosphoproteome in the mammary gland at six stages of development

4.1.1 Structural anatomical features after isolation of mammary gland

Organ functioning and remodelling depend on the stage, time and stimulus. Predominantly, it is governed by the expression of proteome and allied post-translation modification such as phosphorylation. Protein phosphorylation is an essential cellular supervisory machinery, as numerous enzymes and receptors are activated/deactivated by phosphorylation and dephosphorylation events, employing kinases and phosphatases. In this regards, mammary gland act as the perfect organ system for the study of developmental biology and organogenesis. With this view, we sought to understand the remodelling of different mammary stages and their respective differential changes in the phosphorylation status. Initially, to implement the experiment, we required accurate stage-specific females. Hence, the Wistar rats were timely mated for the isolation of the mammary gland. For puberty stage 60th day, virgin stage 90th day, pregnant stage 10th day after a successful mating, early lactation stage 6th day after parturition, late lactation 18th day after parturition, and involution is the 4th day after weaning of the neonates were selected. The detailed self-explanatory illustrative workflow for mammary gland isolation collection was depicted in Figure 3.1. After completing the specific time duration mentioned above, the females were sacrificed to collect the inguinal gland (4th gland in the rodents). We marked the gland through black marks from the skin's upper side during the isolation based on the number of teats pairs (five or six) (please refer figure 3.2). Cut loose foreskin after pining the rat on four sides, and the glands were isolated (Figure 4.1).

4.1.2 Whole mammary gland mount

As expected, depending on the mammary gland physiological state stage, we found the branching of the mammary tree pattern (Figure 4.2). In the six stages, the peeled mammary gland showed the expected morphology. We found less branching in the puberty and virgin compare to pregnant and lactation stage. The involution showed the same pattern as the puberty or virgin like stage

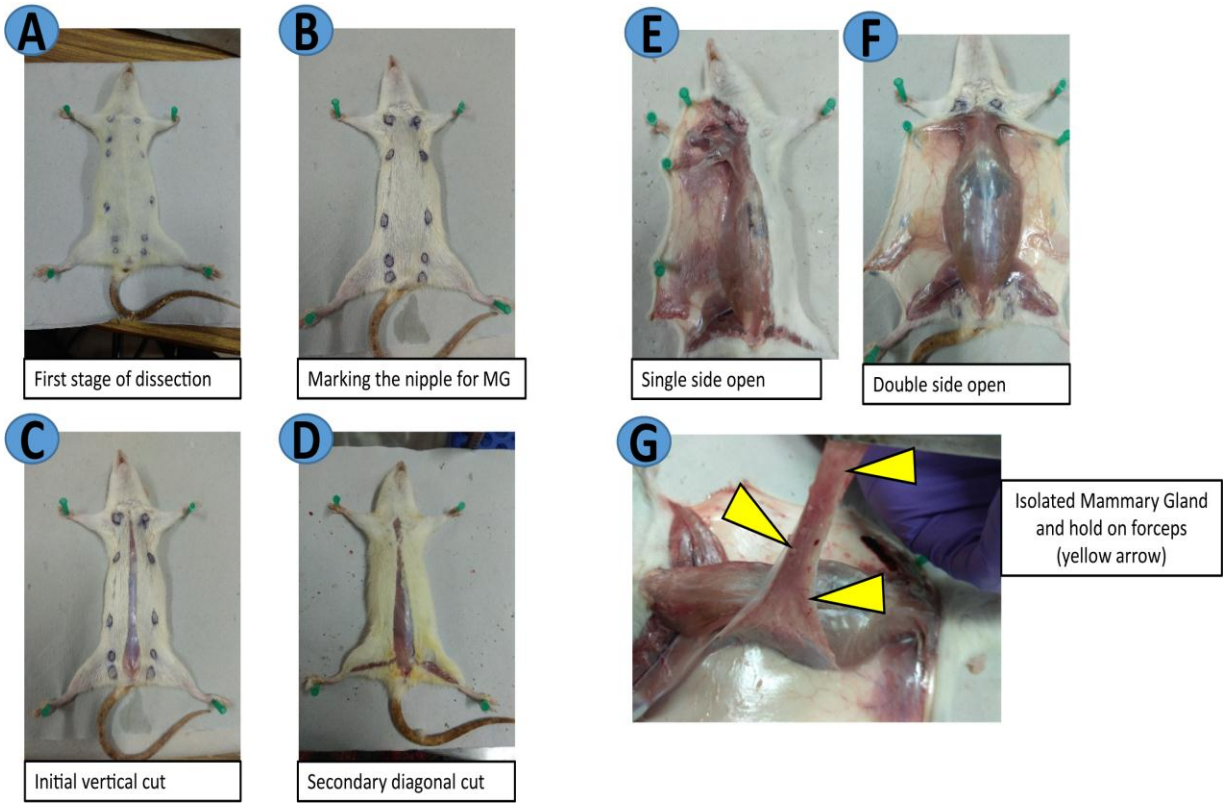

Figure 4.1: **Isolation of Inguinal Mammary gland**: Dissection steps for Isolation of Inguinal Mammary gland from the rat. Above photographs showing the collection of the mammary gland. Likewise, 300 female rats were sacrificed for the collection of mammary glands

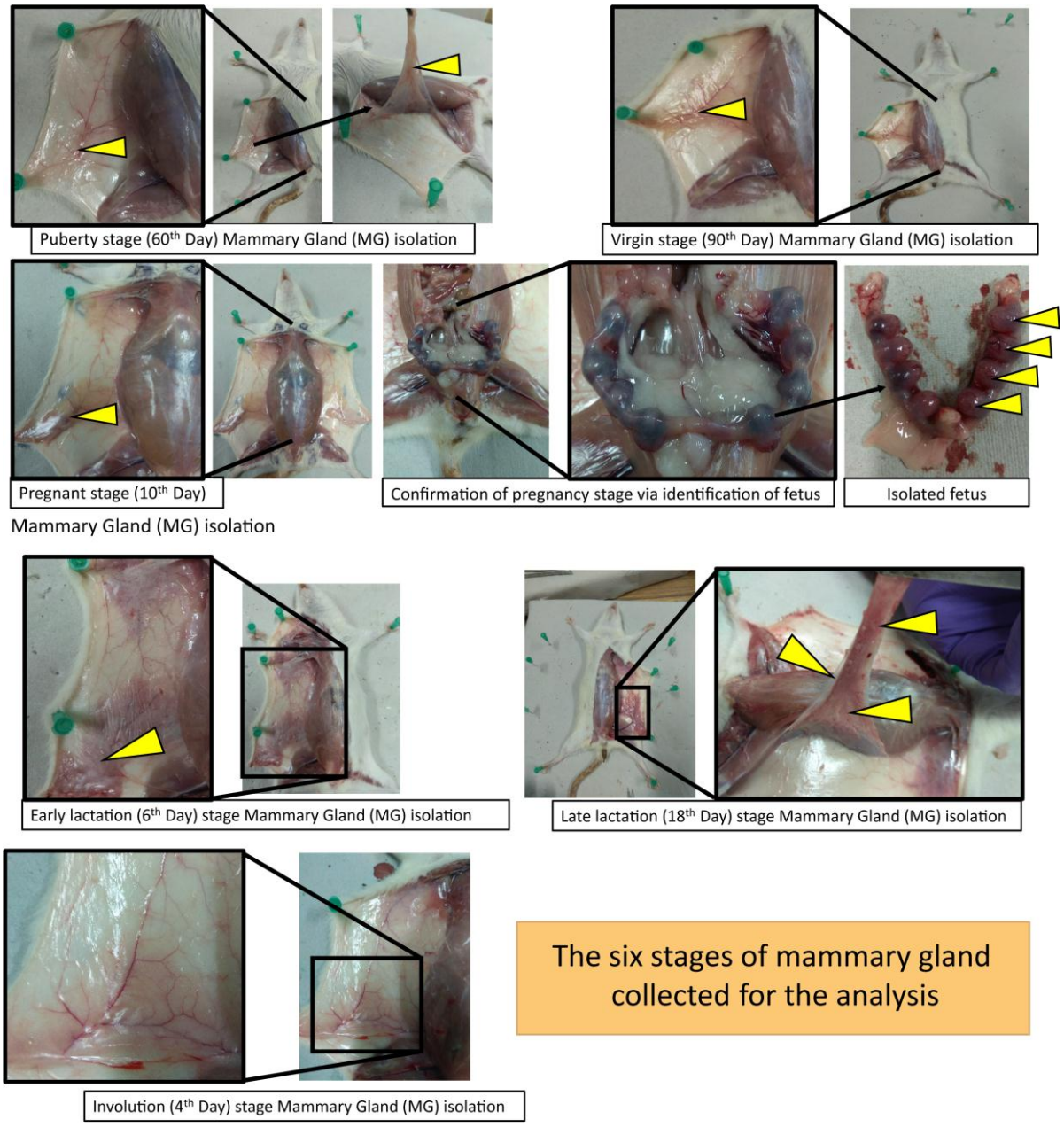

Figure 4.2: **Morphological stage comparison:** Six different stages of Mammary gland isolation and morphological stage comparison.

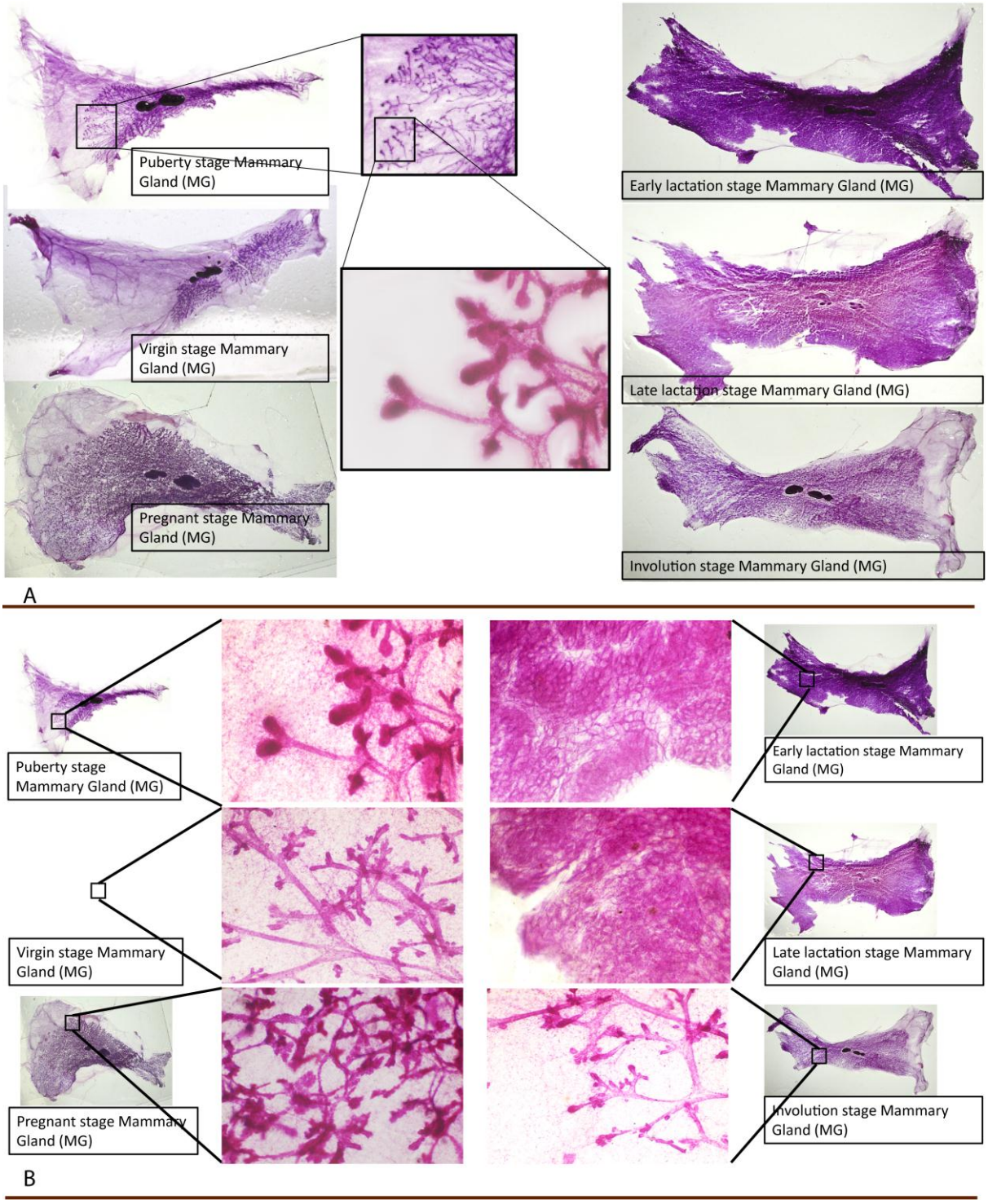

Figure 4.3: **Carmine staining:** Stepwise comparison of ductal growth and alveologenesis in developmental stages of the mammary gland.

4.1.3 Mammary gland phosphoproteome

(Figure 4.2, as indicated with yellow heads). The carmine staining verified the same finding and confirmed the pure isolation of mammary gland from other contaminant tissue like muscle or fibrous tissue in all six stages (Figure 4.3). Subsequently, the magnified carmine staining image showed the branching pattern, ductal growth and alveologenesis in respective stages (Figure 4.3).

We performed the TMT labelled phosphoproteomics analysis with the complete isolation of the mammary gland's respective stage. The detailed illustrative image describes the workflow (Figure 3.3). Briefly, we used IMAC and TiO2 technique to enrich the phosphopeptides, followed with an equal concentration of peptides labelling with six different TMT channels and mass spectrometer acquisition (Figure 3.3, please detailed refer to methodology section). The fractions run in the mass spectrometer instrument resulted in the phosphopeptides' identical elution, as shown by the 2D plot (Figure 4.4). The combined five search engine analysis revealed 6,235 phosphoproteins, 20,328 phosphopeptides and ~25,000 phosphosites in the entire mammary gland. The above mentioned combined analysis also helped to localise the phosphorylation residue with high confident values with least false discovery rate (FDR). Finally, combining all the time-lapse data of six different stages of mammary gland represents the in-depth discovery of proteome and phosphoproteome so far determined.

4.1.3.1 Site localisation of STY amino acids

The site localisation of phospho residue on pSer, pThr, and pTyr (STY amino acids) in individual stages resulted in identifying an average of 10,000 phosphopeptides among the top five stages except for the involution. The last stage involution contains the least 8,350 phosphopeptides identified. The complete ratio average identified for the STY residues for the mammary gland was 10:7:3, respectively (Figure 4.5). The comparative analysis of phosphopeptides and phosphoproteins in different stages through the veen diagram identified the unique values and detailed in figure 8. Interestingly, we found the ubiquitin pathways associated with protein ligase in the unique phosphoproteins hits suggesting the crucial role of the ubiquitination process in the MG remodelling process transition.

4.1.3.2 Clustering of mammary gland Phosphoproteome

The TMT ratio normalised data represent the equal abundance of data points in the phosphoproteomics data (Figure 4.6A). Similarity matrix of Pearson correlation of stages showed the highest correlation of puberty and involution stages with r2 value 0.42. The second maximum correlation was found to be 0.20 with lactation stages (Figure 4.6B).

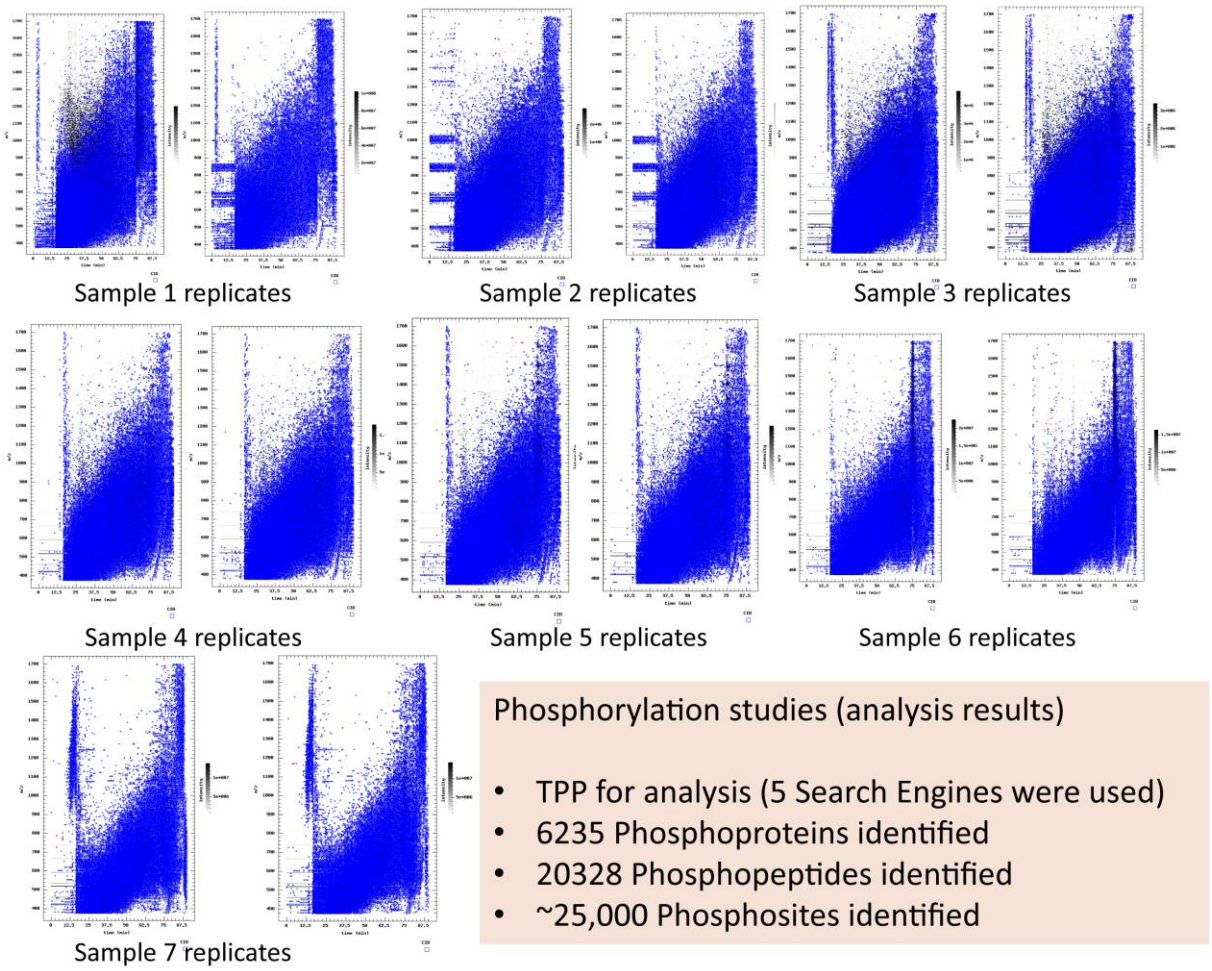

Figure 4.4: **Two Dimensional plot for replicates comparison in LC-MS/MS runs:** 2D plot of MS/MS spectra in the replicate run. Total of seven fractionated samples was analyzed for the identification of phosphopeptides using TMT labelling. The plot shows the replicate runs, and X-axis is the run time of LC while Y-axis is the m/z determined for spectra.

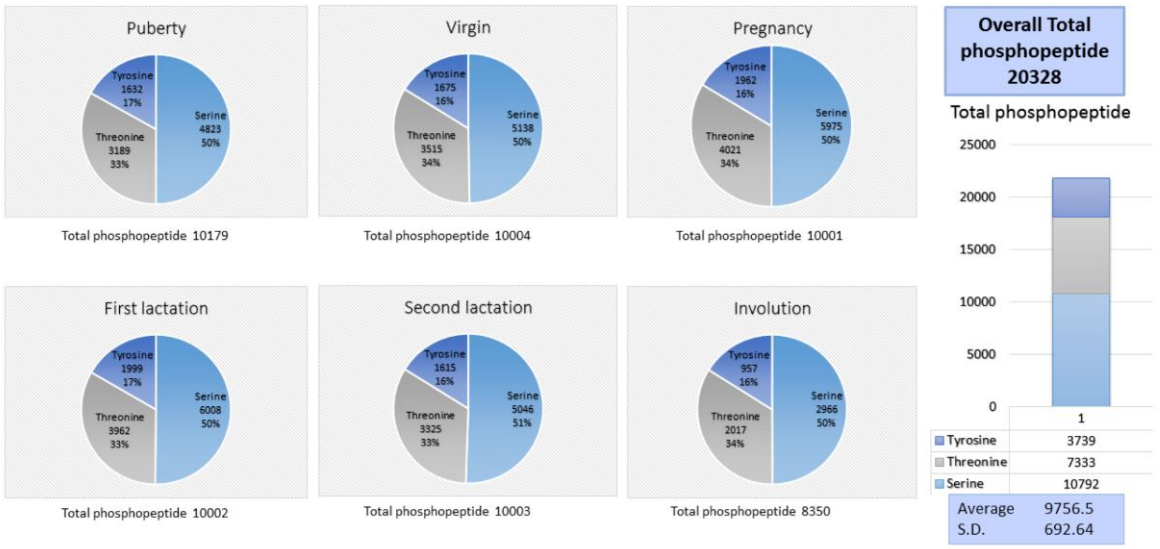

A

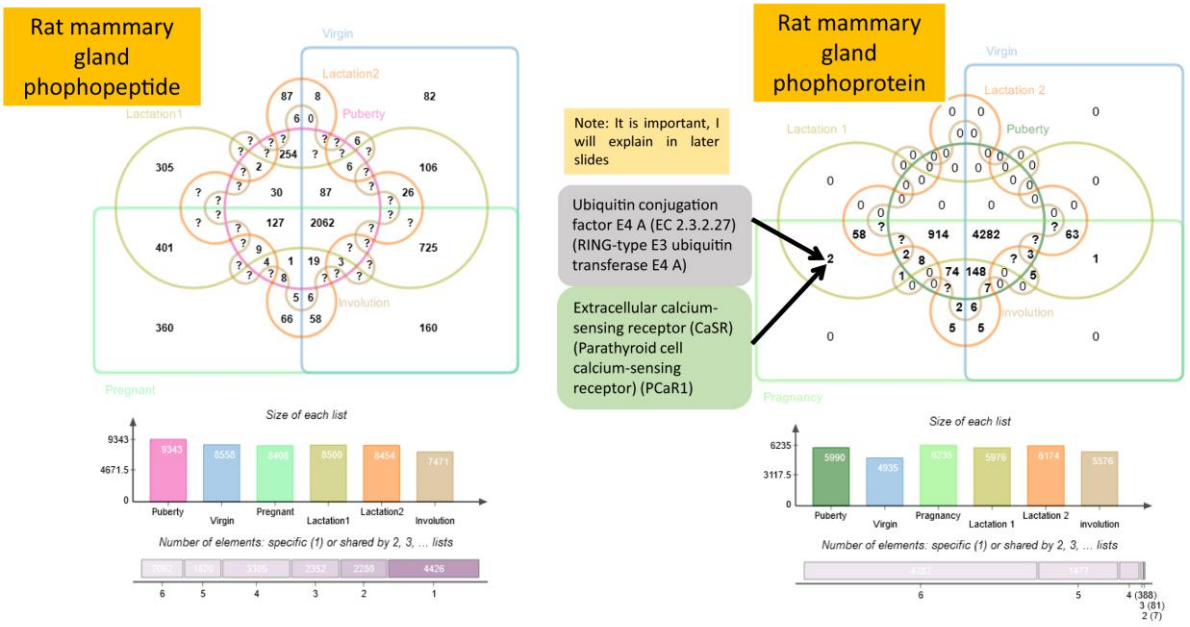

B

Figure 4.5: **Comparison of STY residues among stage:** Total STY phosphorylation of phosphoproteins during different mammary gland stages. Stable phosphorylation status in STY residues of mammary gland developmental stages, including puberty, virgin, pregnancy, Lactation 1 Lactation 2, and involution. Comparative analysis of phosphopeptides and phosphoproteins in six developmental stages of rat mammary gland**.**

The hierarchical clustering analysis (HCA) using Pearson correlation clustering generated the six enriched clusters for the valuable phosphoproteins in all respective six stages (Figure 4.6C, different colour-coded with vertical line). The enriched clusters determined were fetched and mapped for the Kyoto Encyclopedia of Genes and Genomes (KEGG) pathways database. The enriched pathways are as follows puberty, sphingolipid metabolism, glycosaminoglycan degradation; virgin, Pi3K-Akt, Wnt, ABC transporters, calcium signalling; pregnancy, endocytosis, progesterone signalling, regulation of the cytoskeleton, focal adhesion; lactation, ErbB signalling, oxytocin signalling, TGF-beta signalling, phagosome, AMPK signalling; and involution glycosaminoglycan degradation and secretory proteins associated pathways (Figure 4.6D, colour coded histogram with fold enrichment of the pathways).

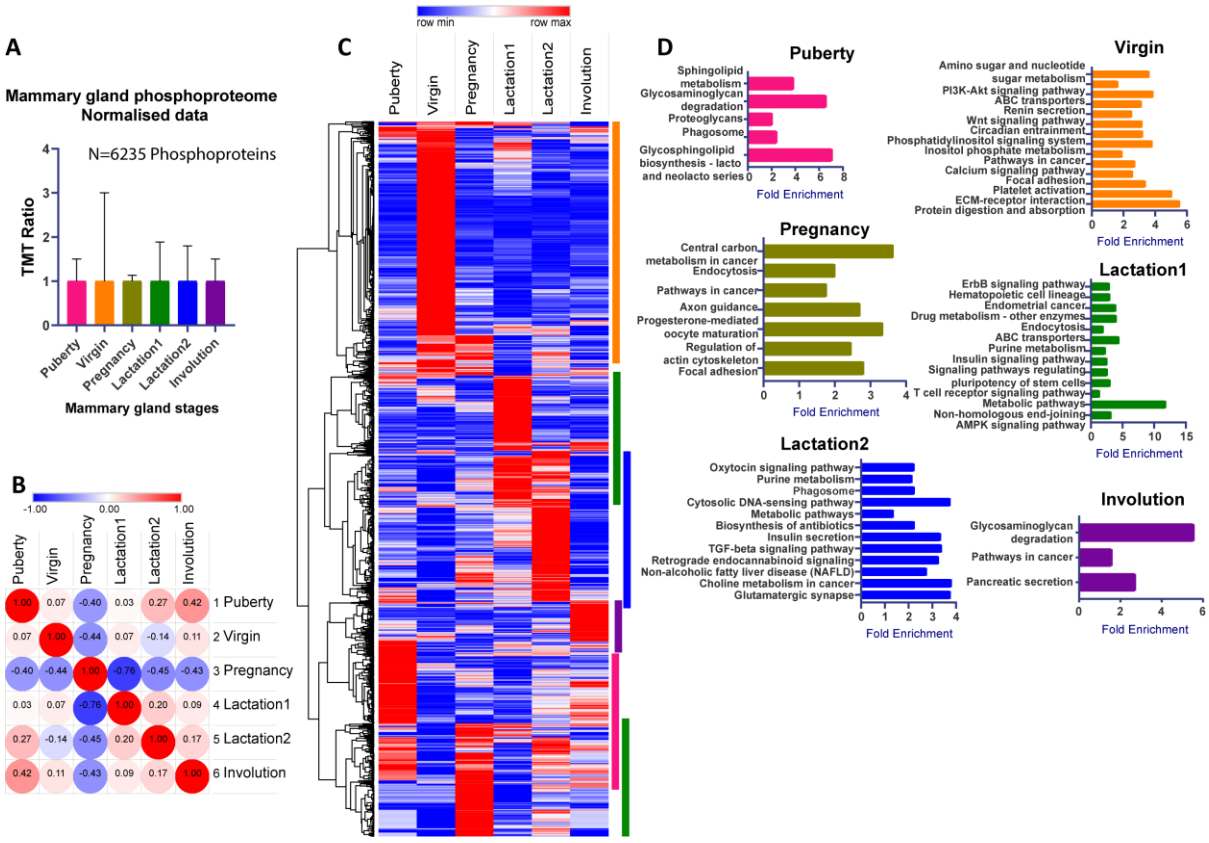

Figure 4.6: **Mammary gland Phosphoproteome: A)** Z-score normalized data **B)** Similarity matrix using Pearson correlation of phosphoproteomics data. **C)** Hierarchical clustering using Pearson correlation clustering. **D)** KEGG Pathways

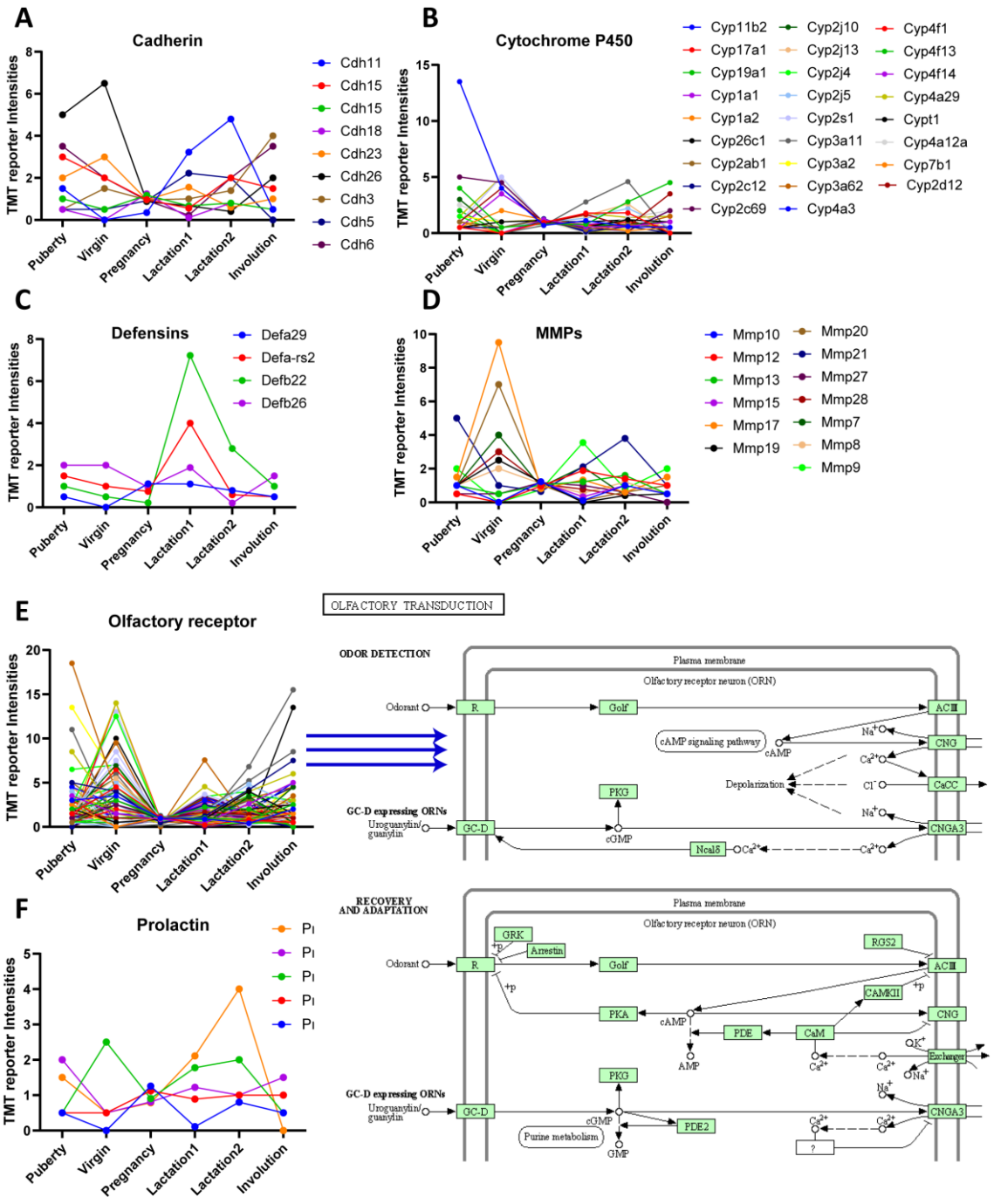

Figure 4.7: **Protein profile analysis:** Protein profile of cadherins, defensins, cytochrome P450 and MMPs (Matrix metalloproteinase) to regulate dynamics of the phosphoproteome incomplete development of mammary gland the during pregnancy-Lactation-Involution cycle. Importance of phosphorylation of the olfactory receptor and Prolactin proteins to regulate phosphoproteome dynamics incomplete development of mammary gland the during pregnancy-Lactation-Involution cycle.

4.1.3.3 Stress-responsive key phosphorylated proteins

Based on the literature search, we have four critically important proteins: cadherin, cytochrome P450, defensins, and MMPs for their significant MG development role. We seek their presence in our phosphoproteomics dataset and found all of them. We perceived cadherin proteins nine isoforms, cytochrome P450 26 isoforms, defensins four isoforms, and MMPs 13 isoforms. It is important to note here that all the identified isoforms are phosphorylated. The profile plot data showed the stable expression of these proteins among all the stages. However, expect few, suggesting their impeccable role in the post-development of the mammary gland. In puberty, Cdh26, Cyp11b2, and MMP21 were essential, whereas, for virgin Cdh26, MMP17 and MMP20 were regulating proteins (Figure 4.7). The normal lactation stage requires the high expression of Cdh11 phosphoprotein. With the help of profile plots, the crucial discovery is identifying the 162 phosphorylated olfactory receptor proteins. The database mapping showed that these proteins were only recognised for odorant signalling. However, our dataset provides new insights for their commanding role in developing mammary gland (Figure 4.7). The prolactin's are the know proteins established of the lactation function. However, we found five isoforms of phosphorylated prolactin in which Prl2a1 is highly upregulated in lactation stage (Figure 4.7).

4.1.3.4 Kinome and Phosphatome cross-talk in lactation

The kinases and phosphatases are the two key enzymes regulating the total phosphorylation of target proteome. We sought to understand the cross-talk between these two classes of enzymes. Remarkably, the protein kinases are accountable for cellular transduction signalling and their hyperactivity, malfunction or overexpression can be found in several pathophysiological conditions. Therefore, total understanding of kinases allows us to learn the proper organ functioning in health and disease conditions. The total kinases in a cell are called kinome while phosphatases are phosphatome, creating the phosphoproteome. The total 6,235 phosphoproteins were comprised of 256 kinases and 80 phosphatases in the developing mammary gland. The analysis of lactation stage-specific top 10% upregulated kinase and phosphatase were 23 and 18, respectively. Likewise, the 10% downregulated kinase and phosphatase were 31 and 14, respectively (Figure 4.8).

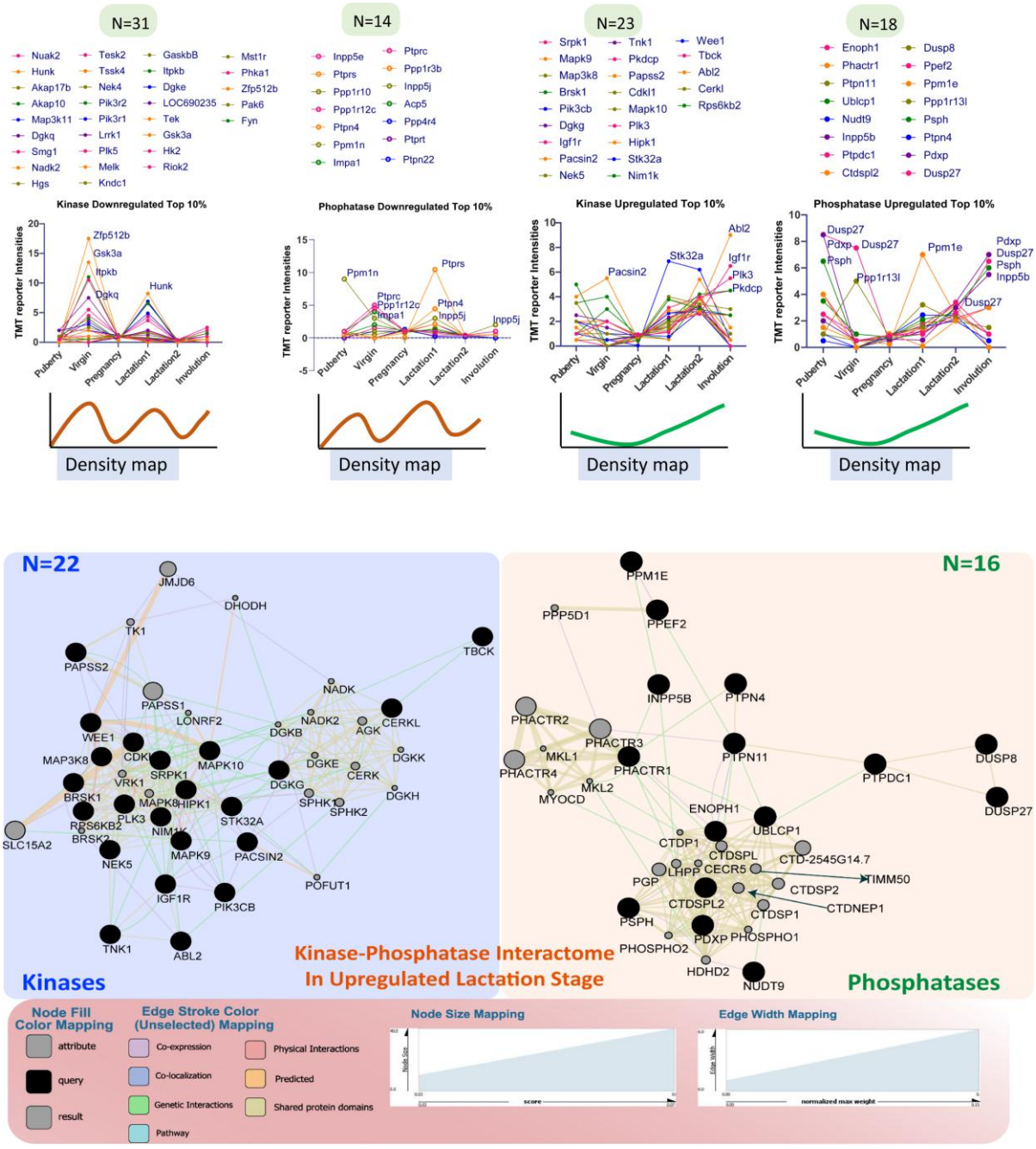

Figure 4.8: **Key kinases and phosphatase enzymes involved in the maintenance of Lactation stage:** Total of 256 protein kinases and 80 phosphatases are responsible for regulating the dynamics of the phosphoproteome incomplete development mammary gland the during pregnancy-Lactation-Involution cycle. **Upregulated Kinases and Phosphatase Interactome:** Total of 22 protein kinases and 16 phosphatases are identified for the regulation of phosphoproteome dynamics in Lactation of mammary gland the during pregnancy-Lactation-Involution cycle.

The density map analysis showed a similar profile plot pattern in both the enzyme category concerning the lactation stage. These results suggest the counter role of kinases and Phosphatases for regulating the lactation stage by maintaining the balance between the phosphorylation and dephosphorylation events. We found the upregulation of four kinases (Abl2, Igf1r, Plk3, and Pkdcp) and phosphatase (Pdxp, Dusp27, Psph, Inpp5b) in involution stage upon considering the top 10% upregulating lactation data. Similarly, the upregulation of three kinases (Zfp522b, Gsk3a, Itpkb) and phosphatase (Ptprc, Ppp1r12c, Impa1) in virgin stage upon considering the top 10% downregulating lactation data (Figure 4.8).

On the same line, we further questioned whether the qualitative data identified in the experiment are linked in terms of physical or any protein-protein interactions (PPIs)? Therefore, we performed the analysis (PPIs) and identified the kinase (N=22) and phosphatase (N=16) interactome in upregulated lactation stage-specific phosphoproteins. The results showed the seven class of interaction among the co-expression proteins, co-localisation, genetic interaction, pathways associated, physical interactions, predicted and shared proteins domains indicated with different edges colours. In the kinase interactome, the predicted and physical interactions had found the weighted while in phosphatase, it is the genetic interaction. We found CERKL ceramide kinase-like; NEK5, NIMA related kinase 5; BRSK1, BR serine/threonine kinase 1; STK32A, serine/threonine kinase 32A; NIM1K, NIM1 serine/threonine-protein kinase; TBCK, TBC1 domain containing kinase; TNK1, tyrosine kinase non receptor 1; PAPSS2, 3'-phosphoadenosine 5'-phosphosulfate synthase 2; DGKG, diacylglycerol kinase gamma; PLK3, polo-like kinase 3; MAP3K8, mitogen-activated protein kinase kinase kinase 8; ABL2, ABL proto-oncogene 2, non-receptor tyrosine kinase; RPS6KB2, ribosomal protein S6 kinase B2; HIPK1, homeodomain interacting protein kinase 1; IGF1R, insulin-like growth factor 1 receptor; MAPK9, mitogen-activated protein kinase 9; PIK3CB, phosphatidylinositol-4,5-bisphosphate 3-kinase catalytic subunit beta; WEE1,WEE1 G2 checkpoint kinase; MAPK10, mitogen-activated protein kinase

10; PACSIN2, protein kinase C and casein kinase substrate in neurons 2; CDKL1, cyclin-dependent kinase-like 1; SRPK1, SRSF protein kinase 1; SLC15A2, solute carrier family 15 member 2; and PAPSS1, 3'-phosphoadenosine 5'-phosphosulfate synthase 1 (Figure 4.8). The ontological classification and the genome and kinase ratio occurrence with q-values are provided in the below table.

Table 4.1: Ontological classification and the occurrence in the genome and kinase ratio with q-values.

GO id	Kinase interactome Description	q-value	Occurrences in Sample	Occurrences in Genome
GO:0004674	protein serine/threonine kinase activity	3.47E-07	11	290
GO:0000287	magnesium ion binding	2.36E-05	7	105
GO:0004707	MAP kinase activity	0.007114	3	10
GO:0046834	lipid phosphorylation	0.021222	3	16
GO:0005524	ATP binding	0.021222	6	217
GO:0030168	platelet activation	0.021222	6	211
GO:0004702	receptor signaling protein serine/threonine kinase activity	0.021372	4	59
GO:0009163	nucleoside biosynthetic process	0.023999	4	67
GO:1901659	glycosyl compound biosynthetic process	0.023999	4	68
GO:0032559	adenyl ribonucleotide binding	0.023999	6	239
GO:0030554	adenyl nucleotide binding	0.023999	6	241
GO:0038095	Fc-epsilon receptor signalling pathway	0.044419	5	166
GO:0035639	purine ribonucleoside triphosphate binding	0.056734	6	296
GO:0005057	receptor signalling protein activity	0.074513	4	98
GO:0004713	protein tyrosine kinase activity	0.074513	4	98

Further for phosphatase, we found PSPH, phosphoserine phosphatase; PPP1R13L, protein phosphatase 1 regulatory subunit 13 like; DUSP27, dual

specificity phosphatase 27; ENOPH1, enolase-phosphatase 1; PHACTR1, phosphatase and actin regulator 1; PDXP, pyridoxal phosphatase; CTDSPL2, CTD small phosphatase like 2; PTPDC1, protein tyrosine phosphatase domain containing 1; DUSP8, dual specificity phosphatase 8; UBLCP1, ubiquitin-like domain-containing CTD phosphatase 1; NUDT9, nudix hydrolase 9; PTPN11, protein tyrosine phosphatase, non-receptor type 11; PPM1E, protein phosphatase, Mg2+/Mn2+ dependent 1E; INPP5B, inositol polyphosphate-5-phosphatase B; PPEF2, protein phosphatase with EF-hand domain 2;PTPN4, protein tyrosine phosphatase non-receptor type 4. The ontological classification and the genome and phosphatase ratio occurrence with q-values is provided in the below table. The results describe the key kinases and phosphatases identified and involved in maintaining the phosphoproteome balance for the pregnancy-lactation-involution cycle.

Table 4.2: Ontological classification and the occurrence in the genome and kinase ratio with q-values.

GO id	Phosphatase interactome Description	q-value	Occurrences in Sample	Occurrences in Genome
GO:0016791	phosphatase activity	2.52E-22	17	168
GO:0016311	dephosphorylation	6.19E-21	18	269
GO:0042578	phosphoric ester hydrolase activity	1.22E-20	17	223
GO:0006470	protein dephosphorylation	1.99E-18	14	132
GO:0004721	phosphoprotein phosphatase activity	3.76E-15	12	118
GO:0004722	protein serine/threonine phosphatase activity	2.59E-09	7	42
GO:0035335	peptidyl-tyrosine dephosphorylation	2.28E-04	5	62
GO:0000287	magnesium ion binding	0.088055	4	105
GO:0004725	protein tyrosine phosphatase activity	0.223533	3	51
GO:0001933	negative regulation of protein phosphorylation	0.682323	4	189

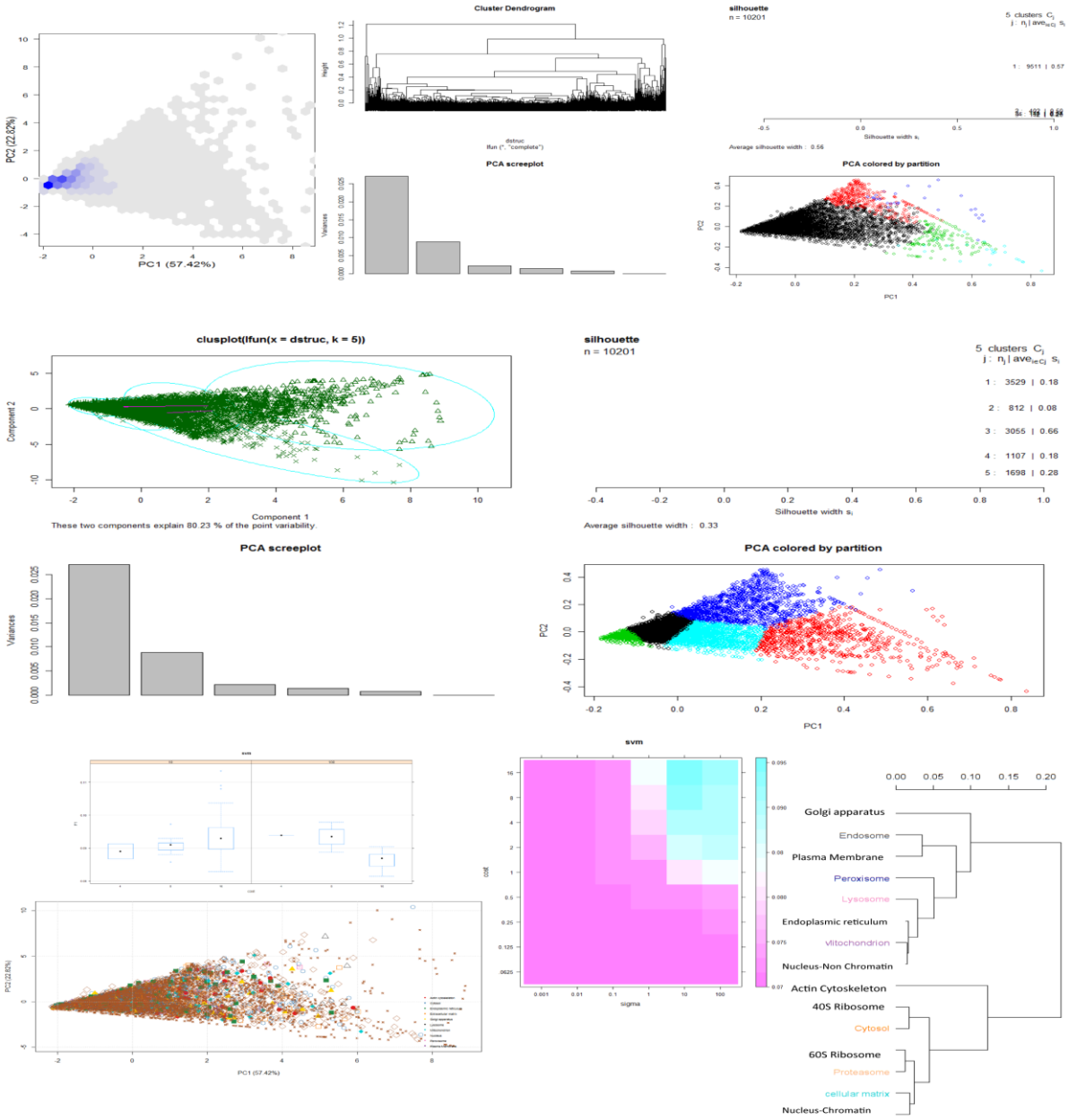

Figure 4.9: **The higher version of Principle Component Analysis (PCA): T-distributed stochastic neighbour embedding (tSNE model) for total organelles classification** in different MG development using machine learning model. **A)** PCA data cut off based on the distance values. **B)** Principle component data to each class. **C)** Clusters classification **D)** Data partitioning **E)** SVM classification of the tSNE data. **F)** Heat map for the SVM and sigma combined score. **G)** Imputation of the organelles attributes on the data for the complete classification of the identified phosphoproteins. **H)** Hierarchical classification of organelles neighbourhood depending on the phosphoproteome TMT reporter ions data values. The graph provides the distance tree too.

4.1.3.5 PCA-tSNE based classification model

We performed dimension reduction using PCA-tSNE calculation. PCA method is a linear dimension reduction that pursues to maximise variance and preserves large pairwise distances. It is like if the variables are dissimilar or diverse, they will end up far separately. Nonetheless, it will lead to poor visualisation, mainly when distributing with non-linear manifold structures; the same is the case in our phosphoproteome data. Therefore, we pursue tSNE over PCA. The t-SNE algorithm estimates a similarity between pairs of occasions in the high dimensional space and the low dimensional space. It then tries to optimise these two similarity measures using a cost function.

To start with our data, we created the PC components in which PC1 contains 57.42%, and PC2 was 22.82%. The PCA scree plot described the set of components on the scale of variance (0.00-0.025) and created the cluster dendrogram for distance comparison (0-1.2). The combination of clusplot function and silhouette (n=10201) on five clusters containing n numbers were 1: 3529, 2:812, 3:3055, 4:1107, 5:1698 formed the point variability plot with a coloured partition (Figure 4.9).

Furthermore, the support vector machine model (SVM) on previously collected cluster allowed the calculation of the sigma factor values. In this way, it was useful to impute the known attribute and collect the results for unknown values. In our case, we use the cellular organelle classification. The created dendrogram showed that Golgi apparatus and actin cytoskeleton are highly distant than all other 13 used organelles in the analysis. Interestingly, the nucleus-non chromatin is closely associated with mitochondrial phosphoproteome. As expected, the peroxisome and lysosome, similarly, endosome and plasma membrane proteins lie in the same clad.

Further, the detailed distant wise clustering represents the organelles' neighbourhood association in the mammary gland based on the determined phosphorylated proteome data (Figure 4.9). The initial PCA plot distribution five iterations of perplexity with the imputed values using organelles data showed the best data reduction at tSNE 50 perplexities. It resulted in organelles classification for unknown values or proteins which was previously not annotated in the database or shallow confidence (Figure 4.10). We found the vital role of nucleus associated phosphoproteins based on the SVM score matrix. The clustering showed Golgi apparatus as evident from the previous dendrogram results (Figure 4.10).

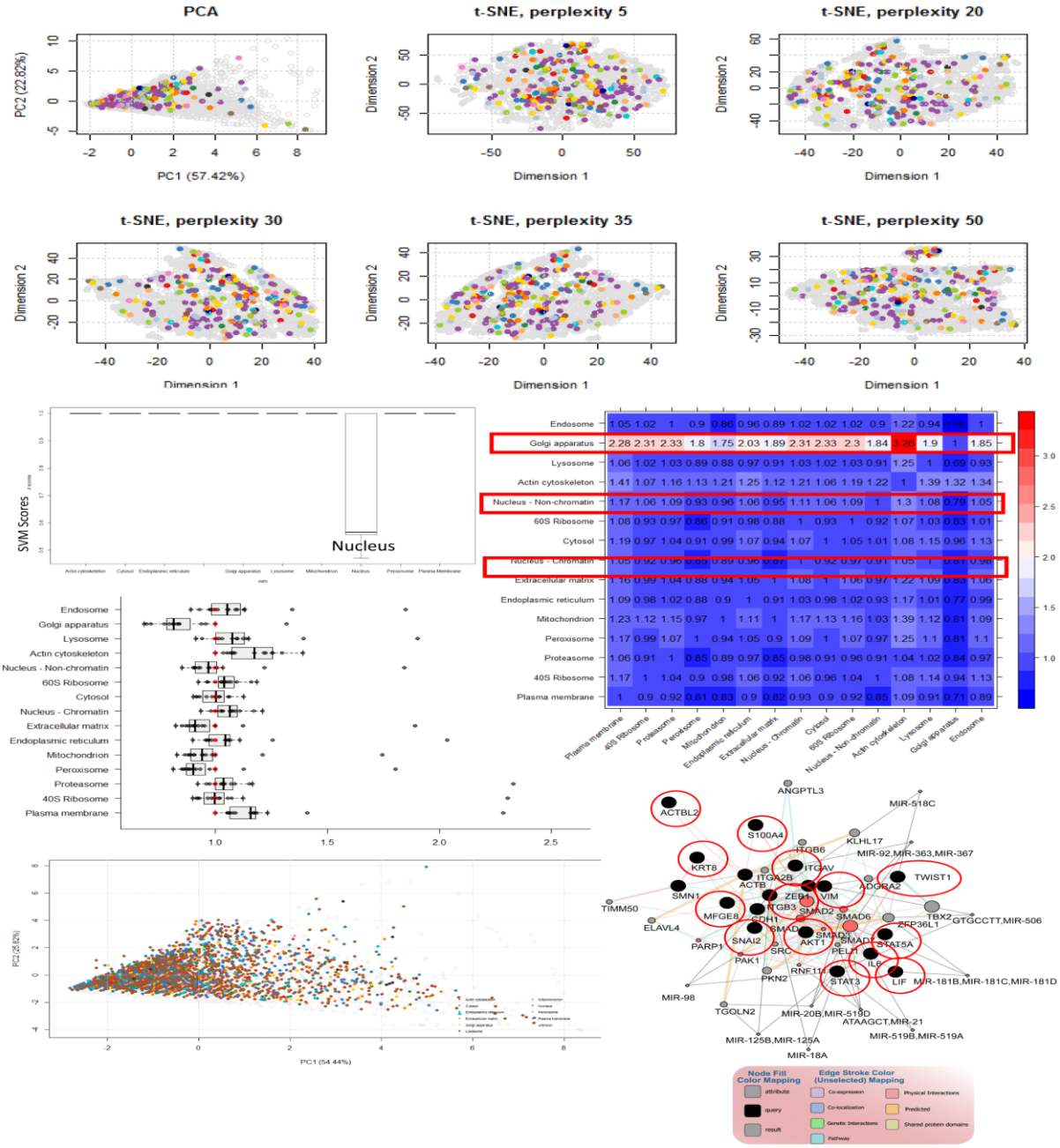

Figure 4.10: **tSNE classified data based on the SVM model: A)** PCA data were plotted with the iteration of perplexity to distribute variables based on the known values of organelles classification. The algorithm takes the iteration of different perplexity to reclassify the matches—distribution of the tSNE classified data based on the SVM model. Nuclear phosphoproteins were found strongly. **B)** Heat map for the combined scoring of the correlation matrix among the organelles predictive proteins. tSNE based imputed organelles classification of the phosphoproteome in different stages of MG tissue. tSNE based classification of identified phosphoproteins. **C)** Protein-protein and protein-miRNA interaction network extracted from the differentially expressed tSNE data.

The tSNE mapping and PPIs network's calculated score resulted in 19 significantly important phosphoproteins in the network. The proteins are Bmi1 polycomb ring finger oncogene; regulatory factor X; cadherin 11; cell division cycle 42; immunoglobulin mu binding protein 2; leukaemia inhibitory factor; milk fat globule-EGF factor 8 protein; thymoma viral proto-oncogene 1; signal transducer and activator of transcription 3; signal transducer and activator of transcription 5A; cadherin 1; vimentin; zinc finger E-box binding homeobox 1; snail family zinc finger 2; SMAD family member 7; S100 calcium-binding protein A4; actin beta; actin beta-like 2; keratin 8; interleukin 6; integrin beta 3; integrin alpha V; twist basic helix-loop-helix transcription factor 1 (Figure 4.10). We choose these proteins for further validation and their respective phosphorylation counterpart role in the mammary gland development.

4.1.4 Mammary gland oil red staining

The oil red O stain is a type of lysochrome diazo dye that showed neutral triglycerides and lipids on frozen sections of six MG development stages. The results showed that pregnant and 18th-day lactation stages contain the maximum lipid contains. Statistical comparison of 18th-day lactation to other stages showed a significant difference (p-value <0.0001) except with pregnant stage (Figure 4.11).

4.1.5 Transmission electron microscopy for six developmental stages

The mammary gland analysis using a transmission electron microscope showed different compartments across the different stages. In the 60th day of puberty, we found mostly the accumulation of lipid droplets. On the 90th day at the virgin state, the lipid droplets reduce while maintaining a similar structure like puberty. As the development starts by introducing the hormones in the 10th-day pregnancy stage, the more clear organelles development was observed. In the case of both the lactation stages analysis, sixth and 18th, we found the aggregation of casein micelles and milk fat globules (MFG) and the presence of lipid droplets and adipocytes. However, the number of adipocytes was negligible on the 18th day of lactation stage. In the case of involution, we found the restoration of the internal structures compared to puberty and virgin stages. Hitherto, we observed many apoptotic bodies forming during this stage, allowing the gland's regeneration to a virgin like condition (Figure 4.11).

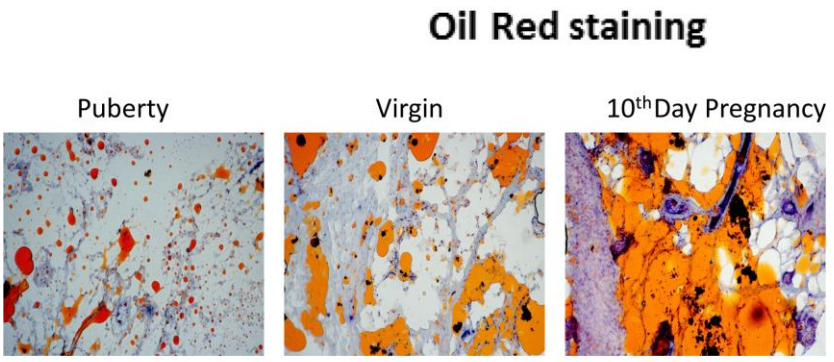

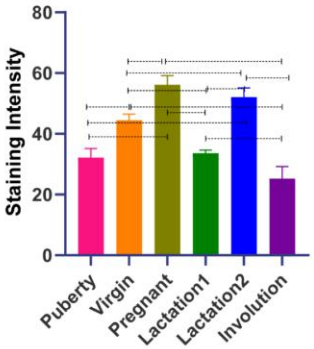

Tukey's test	Summary	P Value
Puberty vs. Virgin	**	0.0031
Puberty vs. Pregnant	****	<0.0001
Puberty vs. Lactation1	ns	>0.9999
Puberty vs. Lactation2	****	<0.0001
Puberty vs. Involution	ns	0.1265
Virgin vs. Pregnant	**	0.0019
Virgin vs. Lactation1	**	0.0044
Virgin vs. Lactation2	*	0.0233
Virgin vs. Involution	****	<0.0001
Pregnant vs. Lactation1	****	<0.0001
Pregnant vs. Lactation2	ns	0.6633
Pregnant vs. Involution	****	<0.0001
Lactation1 vs. Lactation2	****	<0.0001
Lactation1 vs. Involution	ns	0.0915
Lactation2 vs. Involution	****	<0.0001

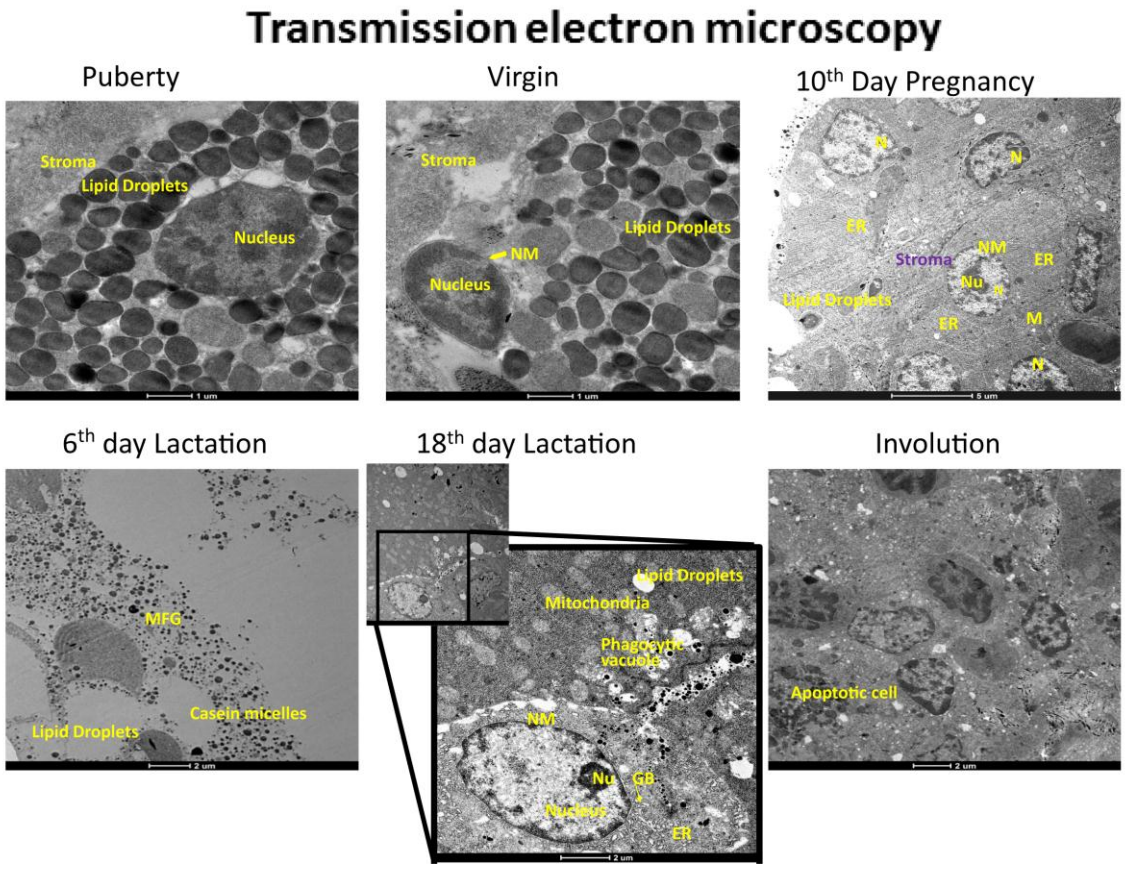

Figure 4.11: **Oil Red staining**: Oil Red O is a lysochrome diazo dye used to staining neutral triglycerides and lipids on frozen sections of different stages of MG development.

4.1.6 Hematoxylin and eosin staining of lobulo-alveolar mammary gland development

The hematoxylin and eosin staining showed the different cellular composition of adipocytes and epithelial cells during the cycle of pregnancy-lactation-involution in mammary gland development. Puberty and virgin stages contain maximum adipocytes, but the adipocytes reduction is visible during the synergic hormonal response. Therefore, we found fewer adipocytes in pregnancy and lactation stage. Amazingly, on the 18th day of lactation, an almost negligible number of adipocytes are present. We found extensive side branching at pregnancy and maximum alveologenesis at lactation. The ducts are viable at the lactation stage. Surprisingly, during the involution stage, all the structures were found degenerated, and at this stage, the gland resembles puberty and virgin stage. The H and E staining corroborate our above findings.

4.1.7 Immunohistochemistry (IHC) of selected proteins from tSNE based network analysis

We performed the immunohisto analysis of 19 proteins identified in our tSNE data. For simplicity purpose, we have discussed the results in line with the lactation stage. The results showed that all nineteen proteins were present in all the six stages validating our proteomics results. Actin is a very abundant protein of the cytoskeleton, and it assists direct roles in cell contraction. To assess the involvement of ACTA2 to mammary cell and related function, we performed the imaging. The smooth muscle actin (SMA) protein found significant to all the stages (p-value <0.05) excluding the cross-comparison of lactation1 and lactation2 (p-value 0.99). The comparison of STAT5 and phosphorylation counterpart showed non-significant difference among all stages. Next, we compared STAT3 and SMAD with respective phosphorylated counterpart. Most of the expression we found in the lactation stage on ductal growth. The image analysis for STAT3 and pSTAT3 showed the significant difference of lactation stage with virgin (p-value 0.284 and 0.0221, respectively). The SMAD staining showed the significant difference with virgin (p-value 0.0018), pregnant (p-value 0.006), and lactation1 vs lactation2 (p-value 0.0157). While for the pSMAD, it showed a significant difference with the puberty stage (0.0031). The results imply the important role of these proteins in the lactation stage (Figure 4.12).

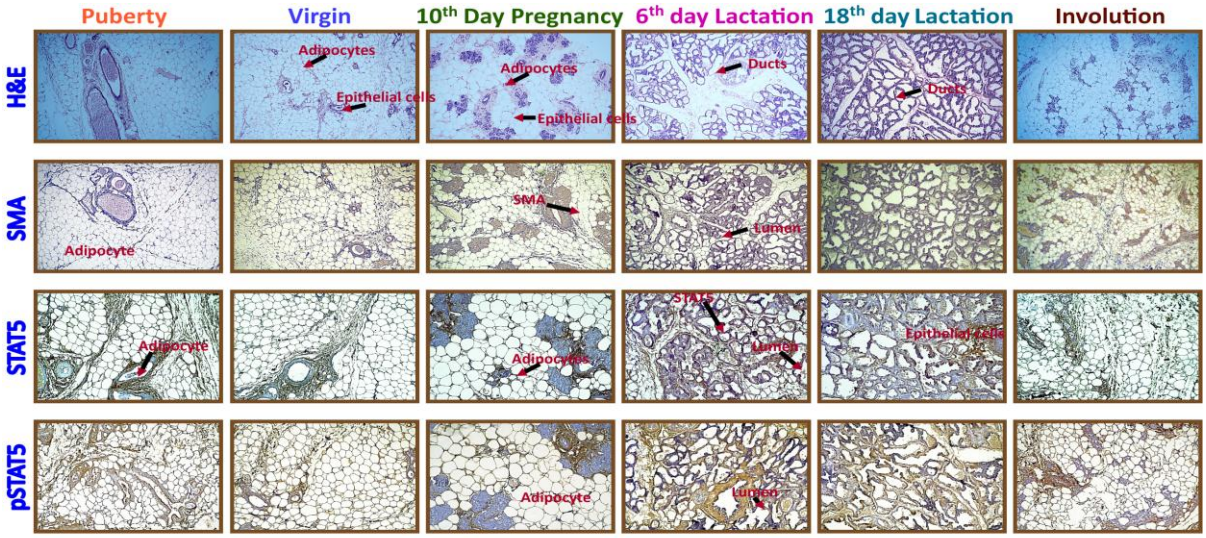

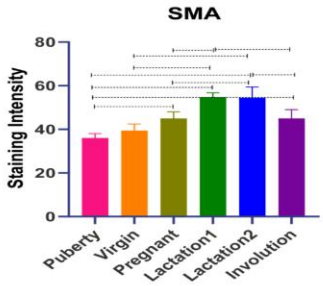

Tukey's multiple comparisons test	Summary	Adjusted P Value
Puberty vs. Virgin	ns	0.5982
Puberty vs. Pregnant	*	0.0325
Puberty vs. Lactation1	****	<0.0001
Puberty vs. Lactation2	****	<0.0001
Puberty vs. Involution	**	0.0096
Virgin vs. Pregnant	ns	0.4016
Virgin vs. Lactation1	***	0.0003
Virgin vs. Lactation2	***	0.0002
Virgin vs. Involution	ns	0.1439
Pregnant vs. Lactation1	**	0.0071
Pregnant vs. Lactation2	**	0.0036
Pregnant vs. Involution	ns	0.9752
Lactation1 vs. Lactation2	ns	0.9980
Lactation1 vs. Involution	*	0.0238
Lactation2 vs. Involution	*	0.0118

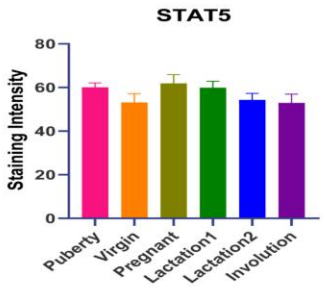

Tukey's multiple comparisons test	Summary	Adjusted P Value
Puberty vs. Virgin	ns	0.3685
Puberty vs. Pregnant	ns	0.9765
Puberty vs. Lactation1	ns	>0.9999
Puberty vs. Lactation2	ns	0.5714
Puberty vs. Involution	ns	0.3427
Virgin vs. Pregnant	ns	0.1310
Virgin vs. Lactation1	ns	0.3498
Virgin vs. Lactation2	ns	0.9986
Virgin vs. Involution	ns	>0.9999
Pregnant vs. Lactation1	ns	0.9817
Pregnant vs. Lactation2	ns	0.2343
Pregnant vs. Involution	ns	0.1198
Lactation1 vs. Lactation2	ns	0.5485
Lactation1 vs. Involution	ns	0.3249
Lactation2 vs. Involution	ns	0.9974

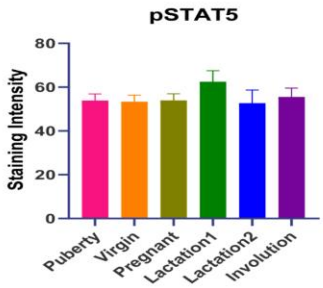

Tukey's multiple comparisons test	Summary	Adjusted P Value
Puberty vs. Virgin	ns	0.9999
Puberty vs. Pregnant	ns	>0.9999
Puberty vs. Lactation1	ns	0.2205
Puberty vs. Lactation2	ns	>0.9999
Puberty vs. Involution	ns	0.9990
Virgin vs. Pregnant	ns	>0.9999
Virgin vs. Lactation1	ns	0.1528
Virgin vs. Lactation2	ns	0.9997
Virgin vs. Involution	ns	0.9887
Pregnant vs. Lactation1	ns	0.1726
Pregnant vs. Lactation2	ns	>0.9999
Pregnant vs. Involution	ns	0.9940
Lactation1 vs. Lactation2	ns	0.2335
Lactation1 vs. Involution	ns	0.3632
Lactation2 vs. Involution	ns	0.9994

Figure 4.12: **Lobulo-alveolar development during different developmental stages of mammary glands:** Representative gross morphological and histological features of hematoxylin and eosin (H&E)-stained paraffin sections of the mammary glands of female Sprague-Dawley rats. Also, differential immunohistochemistry for SMA (Smooth Muscle Actin), STAT5 Signal Transducer And Activator of Transcription 5A), and pSTAT5 (Phospho-STAT5).

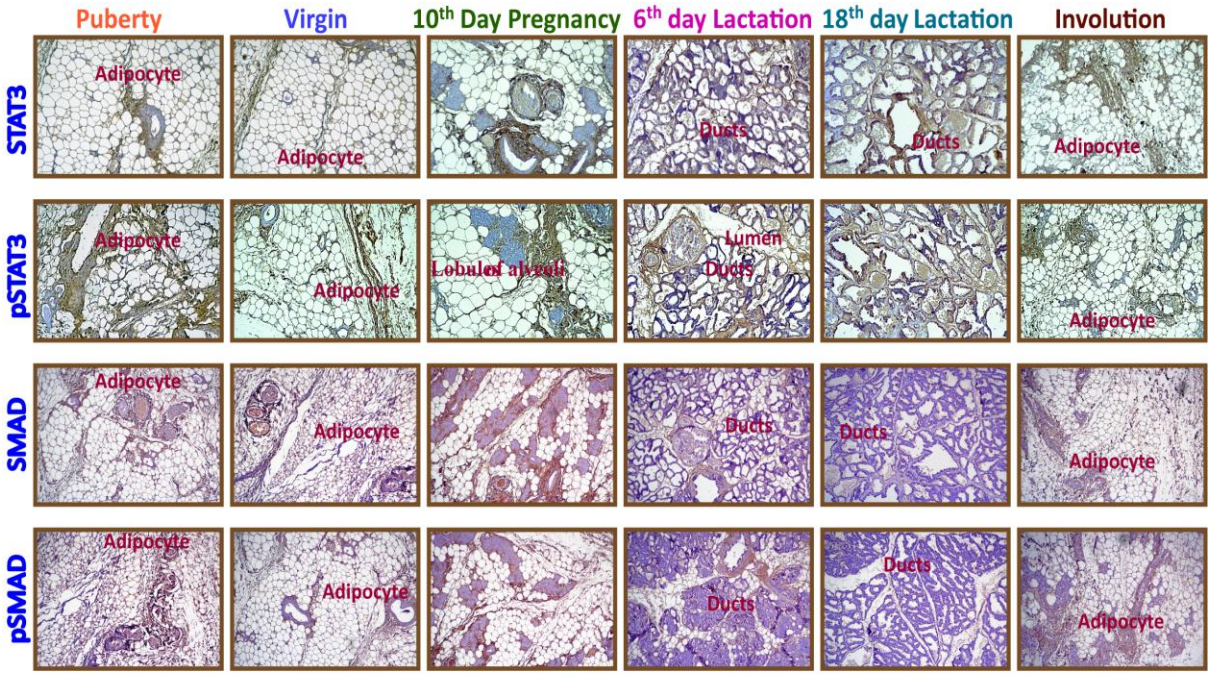

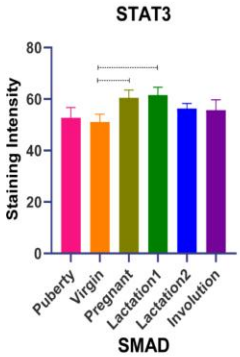

Tukey's test	Summary	Adjusted P Value
Puberty vs. Virgin	ns	0.9524
Puberty vs. Pregnant	ns	0.1160
Puberty vs. Lactation1	ns	0.1155
Puberty vs. Lactation2	ns	0.9492
Puberty vs. Involution	ns	0.8995
Virgin vs. Pregnant	*	0.0285
Virgin vs. Lactation1	*	0.0284
Virgin vs. Lactation2	ns	0.5526
Virgin vs. Involution	ns	0.4598
Pregnant vs. Lactation1	ns	>0.9999
Pregnant vs. Lactation2	ns	0.4021
Pregnant vs. Involution	ns	0.4901
Lactation1 vs. Lactation2	ns	0.4008
Lactation1 vs. Involution	ns	0.4886
Lactation2 vs. Involution	ns	>0.9999

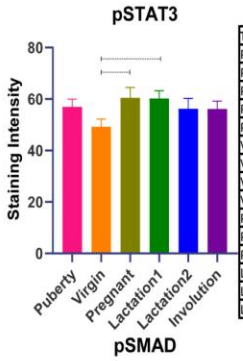

Tukey's test	Summary	Adjusted P Value
Puberty vs. Virgin	ns	0.1409
Puberty vs. Pregnant	ns	0.8308
Puberty vs. Lactation1	ns	0.8644
Puberty vs. Lactation2	ns	>0.9999
Puberty vs. Involution	ns	0.9991
Virgin vs. Pregnant	*	0.0194
Virgin vs. Lactation1	*	0.0221
Virgin vs. Lactation2	ns	0.1478
Virgin vs. Involution	ns	0.2398
Pregnant vs. Lactation1	ns	>0.9999
Pregnant vs. Lactation2	ns	0.8163
Pregnant vs. Involution	ns	0.6431
Lactation1 vs. Lactation2	ns	0.8513
Lactation1 vs. Involution	ns	0.6867
Lactation2 vs. Involution	ns	0.9994

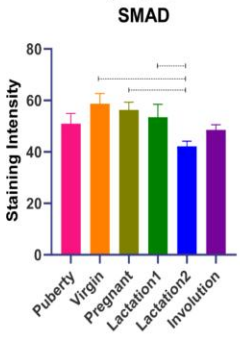

Tukey's test	Summary	Adjusted P Value
Puberty vs. Virgin	ns	0.3768
Puberty vs. Pregnant	ns	0.7940
Puberty vs. Lactation1	ns	0.9782
Puberty vs. Lactation2	ns	0.0511
Puberty vs. Involution	ns	0.9161
Virgin vs. Pregnant	ns	0.9683
Virgin vs. Lactation1	ns	0.7606
Virgin vs. Lactation2	**	0.0018
Virgin vs. Involution	ns	0.0880
Pregnant vs. Lactation1	ns	0.9912
Pregnant vs. Lactation2	**	0.0060
Pregnant vs. Involution	ns	0.2840
Lactation1 vs. Lactation2	*	0.0157
Lactation1 vs. Involution	ns	0.5672
Lactation2 vs. Involution	ns	0.2415

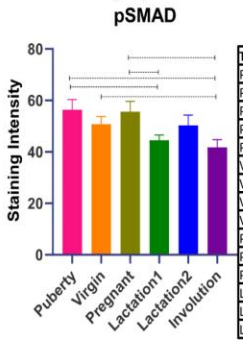

Tukey's test	Summary	Adjusted P Value
Puberty vs. Virgin	ns	0.3077
Puberty vs. Pregnant	ns	0.9929
Puberty vs. Lactation1	**	0.0031
Puberty vs. Lactation2	ns	0.1618
Puberty vs. Involution	***	0.0008
Virgin vs. Pregnant	ns	0.5859
Virgin vs. Lactation1	ns	0.1202
Virgin vs. Lactation2	ns	0.9973
Virgin vs. Involution	*	0.0295
Pregnant vs. Lactation1	**	0.0077
Pregnant vs. Lactation2	ns	0.3529
Pregnant vs. Involution	**	0.0019
Lactation1 vs. Lactation2	ns	0.2359
Lactation1 vs. Involution	ns	0.9519
Lactation2 vs. Involution	ns	0.0619

Figure 4.13: **Lobulo-alveolar development during different developmental stages of mammary glands:** Comparative immunohistochemistry for STAT3 (Signal Transducer and Activator of Transcription 3), and pSTAT3 (Phospho-STAT3) and SMAD (SMA- And MAD-Related Protein), and pSMAD (Phospho-SMAD), during different developmental stages of the mammary gland.

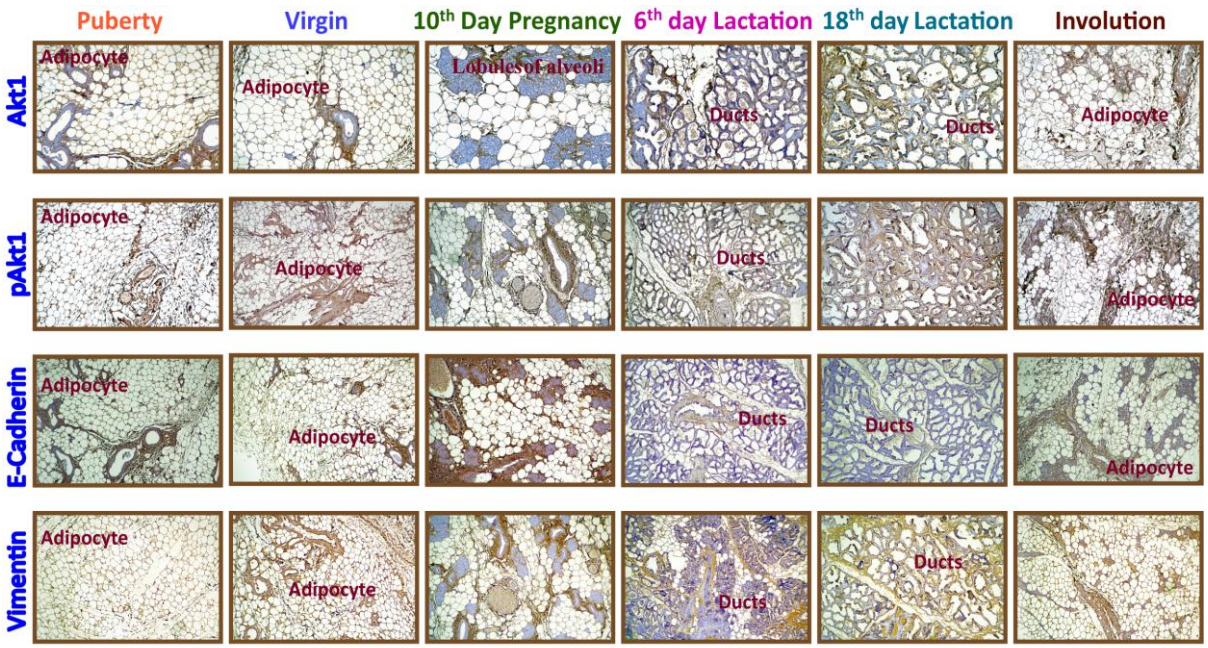

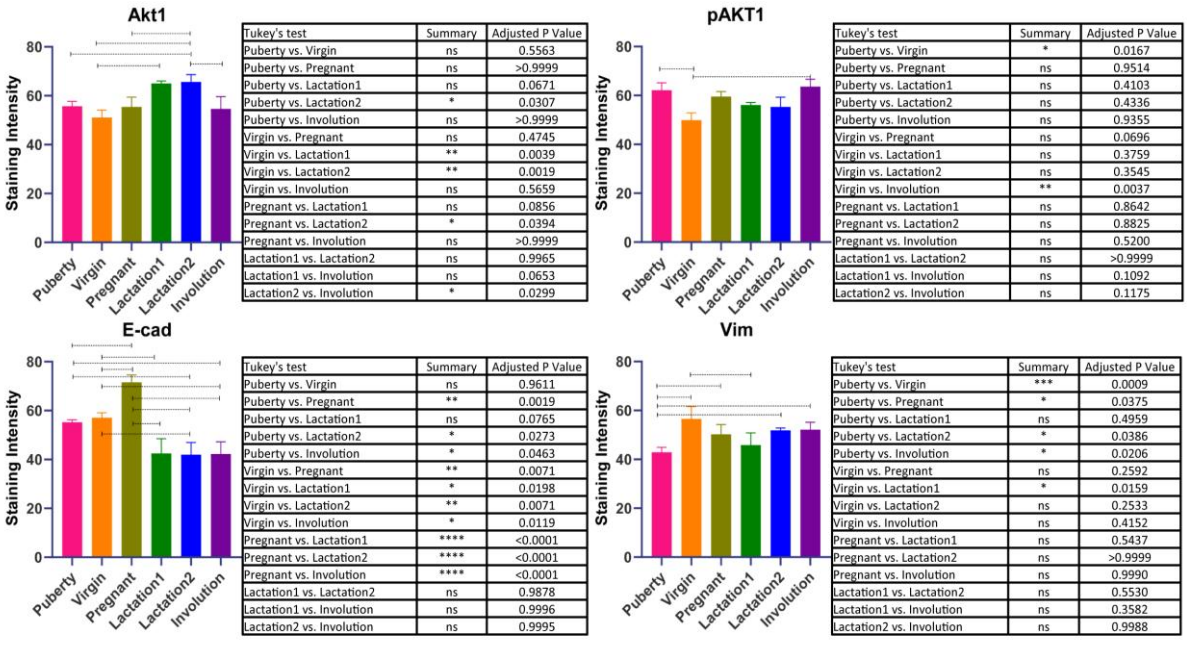

Tukey's test	Summary	Adjusted P Value
Puberty vs. Virgin	ns	0.5563
Puberty vs. Pregnant	ns	>0.9999
Puberty vs. Lactation1	ns	0.0671
Puberty vs. Lactation2	*	0.0307
Puberty vs. Involution	ns	>0.9999
Virgin vs. Pregnant	ns	0.4745
Virgin vs. Lactation1	**	0.0039
Virgin vs. Lactation2	**	0.0019
Virgin vs. Involution	ns	0.5659
Pregnant vs. Lactation1	ns	0.0856
Pregnant vs. Lactation2	*	0.0394
Pregnant vs. Involution	ns	>0.9999
Lactation1 vs. Lactation2	ns	0.9965
Lactation1 vs. Involution	ns	0.0653
Lactation2 vs. Involution	*	0.0299

Tukey's test	Summary	Adjusted P Value
Puberty vs. Virgin	*	0.0167
Puberty vs. Pregnant	ns	0.9514
Puberty vs. Lactation1	ns	0.4103
Puberty vs. Lactation2	ns	0.4336
Puberty vs. Involution	ns	0.9355
Virgin vs. Pregnant	ns	0.0696
Virgin vs. Lactation1	ns	0.3759
Virgin vs. Lactation2	ns	0.3545
Virgin vs. Involution	**	0.0037
Pregnant vs. Lactation1	ns	0.8642
Pregnant vs. Lactation2	ns	0.8825
Pregnant vs. Involution	ns	0.5200
Lactation1 vs. Lactation2	ns	>0.9999
Lactation1 vs. Involution	ns	0.1092
Lactation2 vs. Involution	ns	0.1175

Tukey's test	Summary	Adjusted P Value
Puberty vs. Virgin	ns	0.9611
Puberty vs. Pregnant	**	0.0019
Puberty vs. Lactation1	ns	0.0765
Puberty vs. Lactation2	*	0.0273
Puberty vs. Involution	*	0.0463
Virgin vs. Pregnant	**	0.0071
Virgin vs. Lactation1	*	0.0198
Virgin vs. Lactation2	**	0.0071
Virgin vs. Involution	*	0.0119
Pregnant vs. Lactation1	****	<0.0001
Pregnant vs. Lactation2	****	<0.0001
Pregnant vs. Involution	****	<0.0001
Lactation1 vs. Lactation2	ns	0.9878
Lactation1 vs. Involution	ns	0.9996
Lactation2 vs. Involution	ns	0.9995

Tukey's test	Summary	Adjusted P Value
Puberty vs. Virgin	***	0.0009
Puberty vs. Pregnant	*	0.0375
Puberty vs. Lactation1	ns	0.4959
Puberty vs. Lactation2	*	0.0386
Puberty vs. Involution	*	0.0206
Virgin vs. Pregnant	ns	0.2592
Virgin vs. Lactation1	*	0.0159
Virgin vs. Lactation2	ns	0.2533
Virgin vs. Involution	ns	0.4152
Pregnant vs. Lactation1	ns	0.5437
Pregnant vs. Lactation2	ns	>0.9999
Pregnant vs. Involution	ns	0.9990
Lactation1 vs. Lactation2	ns	0.5530
Lactation1 vs. Involution	ns	0.3582
Lactation2 vs. Involution	ns	0.9988

Figure 4.14: **Lobulo-alveolar development during different developmental stages of mammary glands:** Comparative immunohistochemistry for Akt1, pAkt (Phospho- Akt), E-Cadherin, and Vimentin, during different developmental stages of the mammary gland.

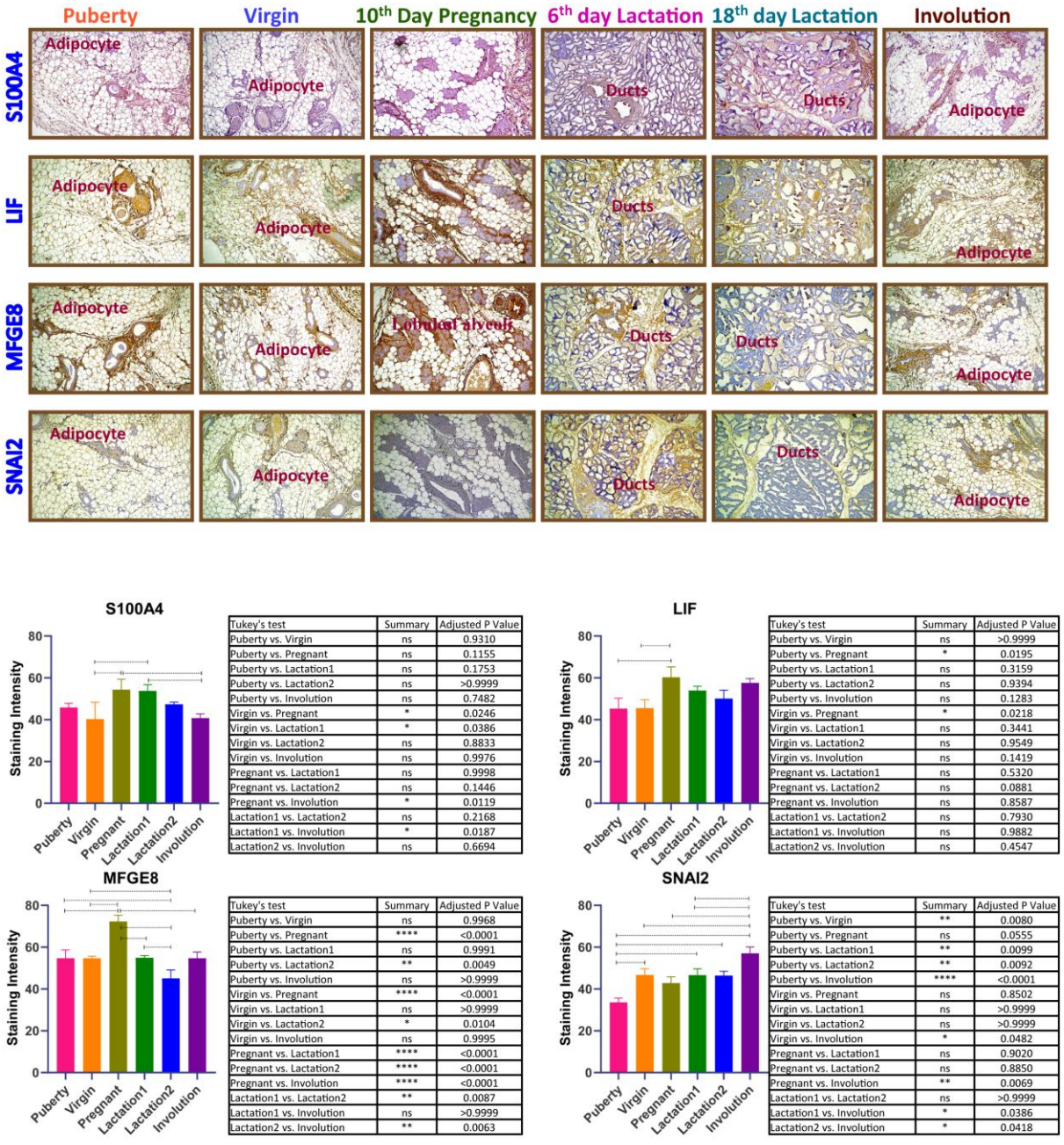

Tukey's test	Summary	Adjusted P Value
Puberty vs. Virgin	ns	0.9310
Puberty vs. Pregnant	ns	0.1155
Puberty vs. Lactation1	ns	0.1753
Puberty vs. Lactation2	ns	>0.9999
Puberty vs. Involution	ns	0.7482
Virgin vs. Pregnant	*	0.0246
Virgin vs. Lactation1	*	0.0386
Virgin vs. Lactation2	ns	0.8833
Virgin vs. Involution	ns	0.9976
Pregnant vs. Lactation1	ns	0.9998
Pregnant vs. Lactation2	ns	0.1446
Pregnant vs. Involution	*	0.0119
Lactation1 vs. Lactation2	ns	0.2168
Lactation1 vs. Involution	*	0.0187
Lactation2 vs. Involution	ns	0.6694

Tukey's test	Summary	Adjusted P Value
Puberty vs. Virgin	ns	>0.9999
Puberty vs. Pregnant	*	0.0195
Puberty vs. Lactation1	ns	0.3159
Puberty vs. Lactation2	ns	0.9394
Puberty vs. Involution	ns	0.1283
Virgin vs. Pregnant	*	0.0218
Virgin vs. Lactation1	ns	0.3441
Virgin vs. Lactation2	ns	0.9549
Virgin vs. Involution	ns	0.1419
Pregnant vs. Lactation1	ns	0.5320
Pregnant vs. Lactation2	ns	0.0881
Pregnant vs. Involution	ns	0.8587
Lactation1 vs. Lactation2	ns	0.7930
Lactation1 vs. Involution	ns	0.9882
Lactation2 vs. Involution	ns	0.4547

Tukey's test	Summary	Adjusted P Value
Puberty vs. Virgin	ns	0.9968
Puberty vs. Pregnant	****	<0.0001
Puberty vs. Lactation1	ns	0.9991
Puberty vs. Lactation2	**	0.0049
Puberty vs. Involution	ns	>0.9999
Virgin vs. Pregnant	****	<0.0001
Virgin vs. Lactation1	ns	>0.9999
Virgin vs. Lactation2	*	0.0104
Virgin vs. Involution	ns	0.9995
Pregnant vs. Lactation1	****	<0.0001
Pregnant vs. Lactation2	****	<0.0001
Pregnant vs. Involution	****	<0.0001
Lactation1 vs. Lactation2	**	0.0087
Lactation1 vs. Involution	ns	>0.9999
Lactation2 vs. Involution	**	0.0063

Tukey's test	Summary	Adjusted P Value
Puberty vs. Virgin	**	0.0080
Puberty vs. Pregnant	ns	0.0555
Puberty vs. Lactation1	**	0.0099
Puberty vs. Lactation2	**	0.0092
Puberty vs. Involution	****	<0.0001
Virgin vs. Pregnant	ns	0.8502
Virgin vs. Lactation1	ns	>0.9999
Virgin vs. Lactation2	ns	>0.9999
Virgin vs. Involution	*	0.0482
Pregnant vs. Lactation1	ns	0.9020
Pregnant vs. Lactation2	ns	0.8850
Pregnant vs. Involution	**	0.0069
Lactation1 vs. Lactation2	ns	>0.9999
Lactation1 vs. Involution	*	0.0386
Lactation2 vs. Involution	*	0.0418

Figure 4.15: **Lobulo-alveolar development during different developmental stages of mammary glands:** Comparative immunohistochemistry for S100A4, LIF (Leukemia Inhibitory Factor), MFGE8 (Milk Fat Globule-EGF Factor 8 Protein), and SNAI2 (Slug Homolog, Zinc Finger Protein), during different developmental stages of the mammary gland.

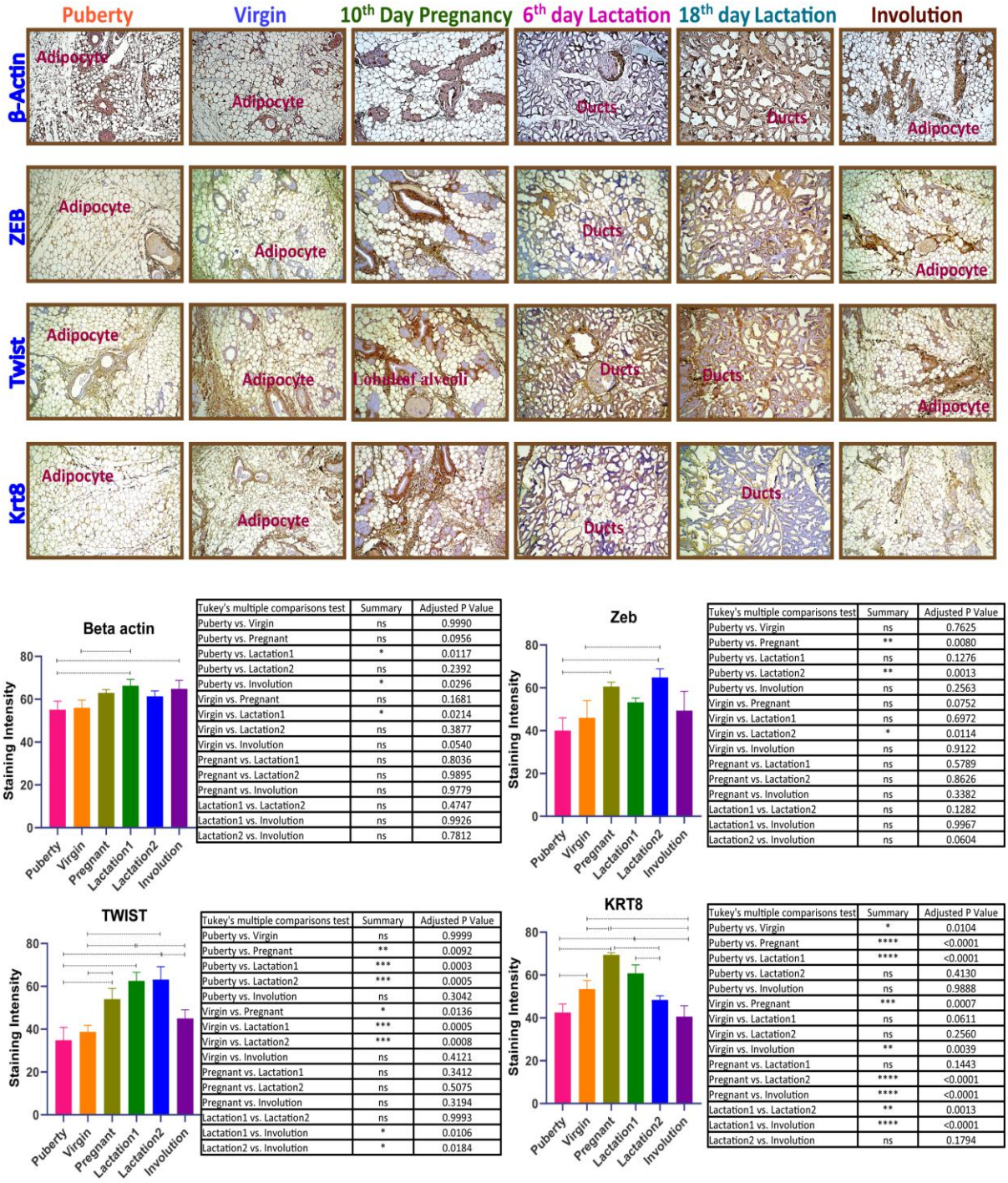

Tukey's multiple comparisons test	Summary	Adjusted P Value
Puberty vs. Virgin	ns	0.9990
Puberty vs. Pregnant	ns	0.0956
Puberty vs. Lactation1	*	0.0117
Puberty vs. Lactation2	ns	0.2392
Puberty vs. Involution	*	0.0296
Virgin vs. Pregnant	ns	0.1681
Virgin vs. Lactation1	*	0.0214
Virgin vs. Lactation2	ns	0.3877
Virgin vs. Involution	ns	0.0540
Pregnant vs. Lactation1	ns	0.8036
Pregnant vs. Lactation2	ns	0.9895
Pregnant vs. Involution	ns	0.9779
Lactation1 vs. Lactation2	ns	0.4747
Lactation1 vs. Involution	ns	0.9926
Lactation2 vs. Involution	ns	0.7812

Tukey's multiple comparisons test	Summary	Adjusted P Value
Puberty vs. Virgin	ns	0.7625
Puberty vs. Pregnant	**	0.0080
Puberty vs. Lactation1	ns	0.1276
Puberty vs. Lactation2	**	0.0013
Puberty vs. Involution	ns	0.2563
Virgin vs. Pregnant	ns	0.0752
Virgin vs. Lactation1	ns	0.6972
Virgin vs. Lactation2	*	0.0114
Virgin vs. Involution	ns	0.9122
Pregnant vs. Lactation1	ns	0.5789
Pregnant vs. Lactation2	ns	0.8626
Pregnant vs. Involution	ns	0.3382
Lactation1 vs. Lactation2	ns	0.1282
Lactation1 vs. Involution	ns	0.9967
Lactation2 vs. Involution	ns	0.0604

Tukey's multiple comparisons test	Summary	Adjusted P Value
Puberty vs. Virgin	ns	0.9999
Puberty vs. Pregnant	**	0.0092
Puberty vs. Lactation1	***	0.0003
Puberty vs. Lactation2	***	0.0005
Puberty vs. Involution	ns	0.3042
Virgin vs. Pregnant	*	0.0136
Virgin vs. Lactation1	***	0.0005
Virgin vs. Lactation2	***	0.0008
Virgin vs. Involution	ns	0.4121
Pregnant vs. Lactation1	ns	0.3412
Pregnant vs. Lactation2	ns	0.5075
Pregnant vs. Involution	ns	0.3194
Lactation1 vs. Lactation2	ns	0.9993
Lactation1 vs. Involution	*	0.0106
Lactation2 vs. Involution	*	0.0184

Tukey's multiple comparisons test	Summary	Adjusted P Value
Puberty vs. Virgin	*	0.0104
Puberty vs. Pregnant	****	<0.0001
Puberty vs. Lactation1	****	<0.0001
Puberty vs. Lactation2	ns	0.4130
Puberty vs. Involution	ns	0.9888
Virgin vs. Pregnant	***	0.0007
Virgin vs. Lactation1	ns	0.0611
Virgin vs. Lactation2	ns	0.2560
Virgin vs. Involution	**	0.0039
Pregnant vs. Lactation1	ns	0.1443
Pregnant vs. Lactation2	****	<0.0001
Pregnant vs. Involution	****	<0.0001
Lactation1 vs. Lactation2	**	0.0013
Lactation1 vs. Involution	****	<0.0001
Lactation2 vs. Involution	ns	0.1794

Figure 4.16: **Lobulo-alveolar development during different developmental stages of mammary glands:** Comparative immunohistochemistry for Beta-actin, ZEB (Zinc Finger E-Box Binding Homeobox 1), Twist, and Krt8, during different developmental stages of the mammary gland.

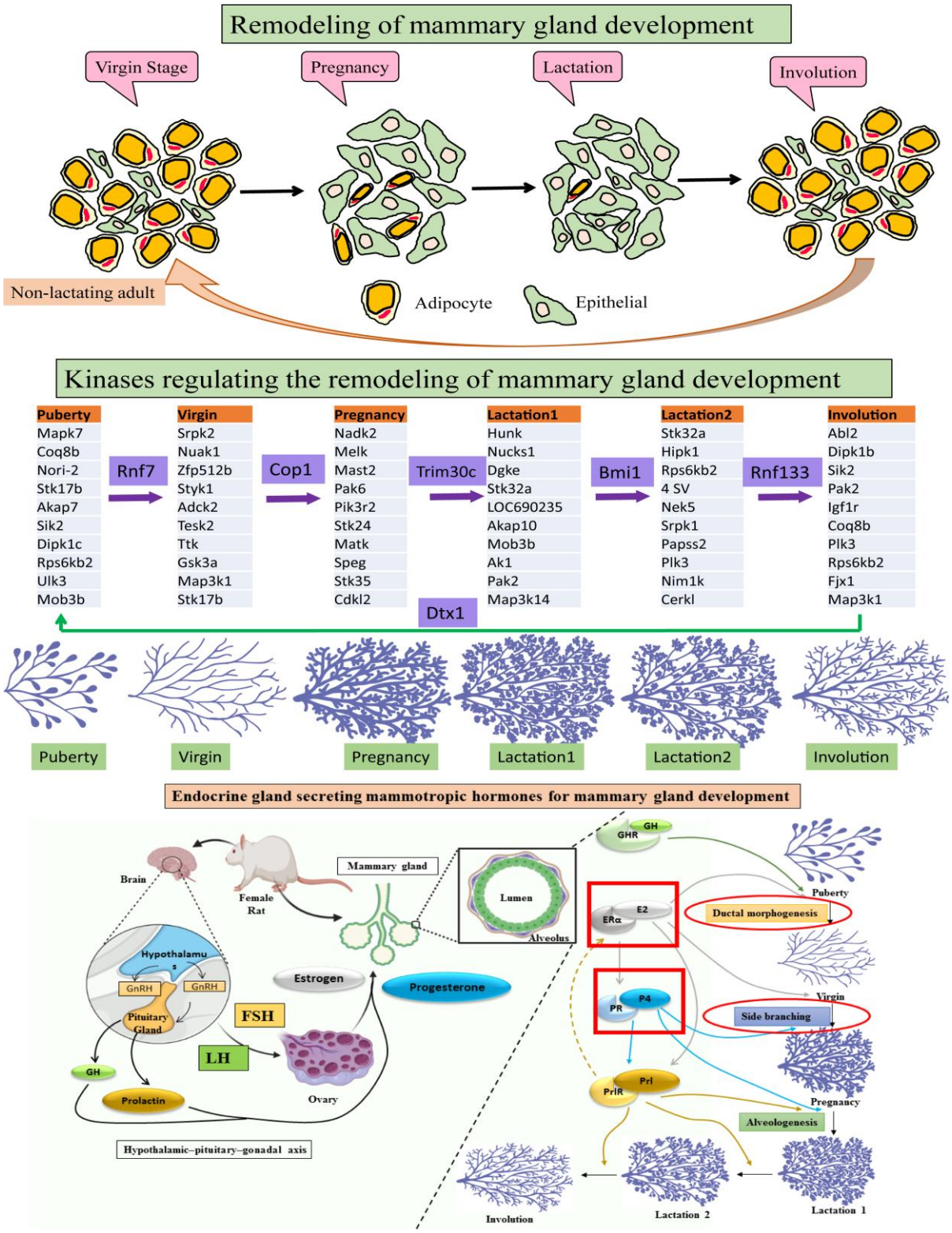

Figure 4.17: **Remodeling of mammary gland development:** Discovery of stage-specific key kinases regulating the phosphoproteome (indicated in light blue colour). Purple colour proteins represent the linking ubiquitinase specific protein for the remodelling of the gland to the subsequent stage in harmony to identified kinases **Endocrine gland secreting mammotropic hormones for mammary gland development.**

Interestingly, in a previous report *Acta2*−/− mice mammary glands encompass less myoepithelial cells expressing keratin 14 and other myoepithelial or smooth muscle markers (such as keratin 5, smooth muscle calponin, GFAP, vimentin, smooth myosin heavy chain, and P-cadherin) (Figure 4.13). Therefore, we mapped keratin, vimentin, E-cadherin and associated kinase importantly, Akt. The results highlight and verify our proteomics, finding that these proteins are essential for the normal development of mammary gland. The mapping of S100A4, LIF, MFGE8, SNAI2, Zeb, Krt8, Twist, and β-actin (p-value <0.05) showed a significant difference in histological sections (Figure 4.14). They were further suggesting their crucial role in lactation function of the mammary gland (Figure 4.15). The overall reported results reveal that these proteins increase in the mammary gland during pregnancy to lactation, suggesting its typical role during the glandular developmental transition. Therefore, all these proteins play an essential role in mammary gland development, mostly, orchestrating lactational mammary gland remodelling (Figure 4.16). Based on the results, we put forth the schematic workflow of mammary gland remodelling and transition of different stages (Figure 4.17). On the same line, we provided an overview of ductal genesis diagram and discovered the critical kinases with a unique ubiquitin associated enzymes in respective stages (Figure 4.17). Detailed information is shown in table 3.

Table 4.3: The presence of top ten Kinases and a ubiquitinase in normal stages of the mammary gland.

Ubiquitinase					
Rnf7	Cop1	Trim30c	Bmi1	Rnf133	Dtx1
Kinases					
Puberty	**Virgin**	**Pregnancy**	**Lactation1**	**Lactation2**	**Involution**
Mapk7	Srpk2	Nadk2	Hunk	Stk32a	Abl2
Coq8b	Nuak1	Melk	Nucks1	Hipk1	Dipk1b
Nori-2	Zfp512b	Mast2	Dgke	Rps6kb2	Sik2
Stk17b	Styk1	Pak6	Stk32a	4 SV	Pak2
Akap7	Adck2	Pik3r2	LOC690235	Nek5	Igf1r

Sik2	Tesk2	Stk24	Akap10	Srpk1	Coq8b
Dipk1c	Ttk	Matk	Mob3b	Papss2	Plk3
Rps6kb2	Gsk3a	Speg	Ak1	Plk3	Rps6kb2
Ulk3	Map3k1	Stk35	Pak2	Nim1k	Fjx1
Mob3b	Stk17b	Cdkl2	Map3k14	Cerkl	Map3k1

4.1.8 Endocrine gland secreting mammotropic hormones for mammary gland development

The role of reproductive hormone signalling is well established. The release of GnRH from the hypothalamus induces the pituitary gland secreted FSH and LH which surge the ovaries to synthesise estrogen and progesterone. The synthesis of two mentioned hormones regulated the reproductive cycle and harmonised mammary gland (Figure 3.4). Based on well know signalling, we sought to ascertain the prominence of estrogen and progesterone mediated phosphorylation. We asked the question, what are the specific kinases exclusively induced by the presence of estrogen or progesterone? To answer, we created the ovariectomy (ovx) model removed the ovaries and treated the rats with two sets of hormones either alone estrogen, progesterone, or estrogen plus progesterone. The similar set of experiment was performed with the normal female without ovariectomy (Figure 4.18). The peeled open image for the mammary gland showed a different concentration of the fat deposition. The carmine staining showed the high adipocyte content in the estrogen-treated ovx mammary gland (Figure 4.18). Before and after the treatment, the body weight was measured. In general, the healthy animal showed an increase in body mass; however, in this case, the results showed a decrease in the total body mass of animal treated with estrogen, especially.

4.1.9 Transcriptomics analysis of the ovariectomy experiment

The combined total analysis resulted in the identification of the ~15,731 transcripts out of which 5,218 were relative and differentially expressed transcripts. We found unique elven transcripts which express on in the presence of ovary. Please find detailed information in table 4.

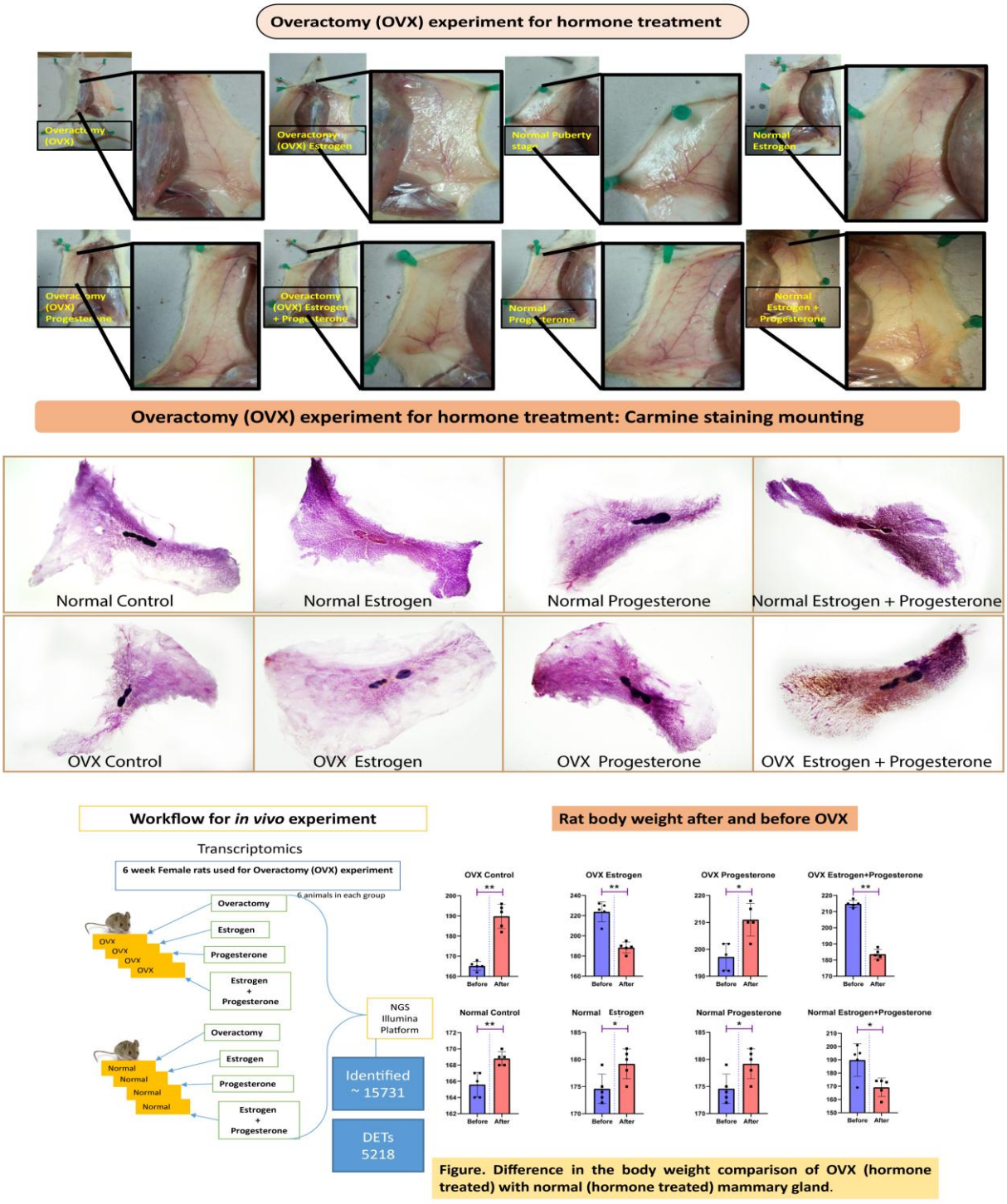

Figure 4.18: **Overactomy (OVX) experiment for hormone treatment**: Overactomy (OVX) experiment for hormone treatment: Carmine staining mounting. **Workflow for *in vivo* experiment.** Rat body weight after and before OVX: **Difference in the bodyweight comparison of OVX (hormone treated) with normal (hormone treated) mammary gland**.

Table 4.4: Exclusive transcripts present in normal females containing ovaries.

Gene Names	OC	OE	OP	OEP	N C	N E	N P	N E P
Rmi2	0	0	0	0	0.935571	0.942057	3.905611	0.218524
Gck	0	0	0	0	0.017654	0.016851	0.016999	0.098302
Hist1h2bo	0	0	0	0	0.466775	0.230562	2.045946	2.85E-05
Nkx1-2	0	0	0	0	0.053213	0.668753	0.104477	0.538403
Rpl30l1	0	0	0	0	0.367483	0.379585	0.401589	0.447857
Chrna10	0	0	0	0	0.018128	0.017311	0.03493	0.020184
Hist1h2ail1	0	0	0	0	0.465102	1.181405	3.939581	0.54973
Eaf2	0	0	0	0	0.370633	0.198217	21.14745	0.18457
Kcnab3	0	0	0	0	0.112257	0.01787	0.333566	0.020834
Fancm	0	0	0	0	0.114703	0.17787	1.169575	0.166651
Rnf222	0	0	0	0	0.057042	0.054399	0.013711	0.031721

4.1.9.1 Hormonal response-dependent kinases regulating the target phosphoproteome

Comparing eight experiments with top ten abundant kinases showed the eight common in ovariectomy and seven common in normal treatment. We found that Dusp3, Cdkn1a and Akt2 expression only in the presence of estrogen. Comparison of common kinases between normal and ovx treatments showed the seven common while one is unique that is Hspb1 Figure 4.19. Next, we compared previously identified top upregulated and downregulated kinases and phosphates from normal mammary gland development. The results showed the presence of 19 upregulated and 21 down-regulated kinases. While 12 upregulated and 10 downregulated phosphatase, common in the ovx-normal hormones treated experiment and phosphoproteomics data. We calculated the Pearson correlation-based HCA analysis and similarity matrix plot. Figure 4.20 details the identification of common expression level of enzymes. It also further reports that enzymes under the induction of either estrogen or progesterone in the normal mammary gland development (Figure 4.21).

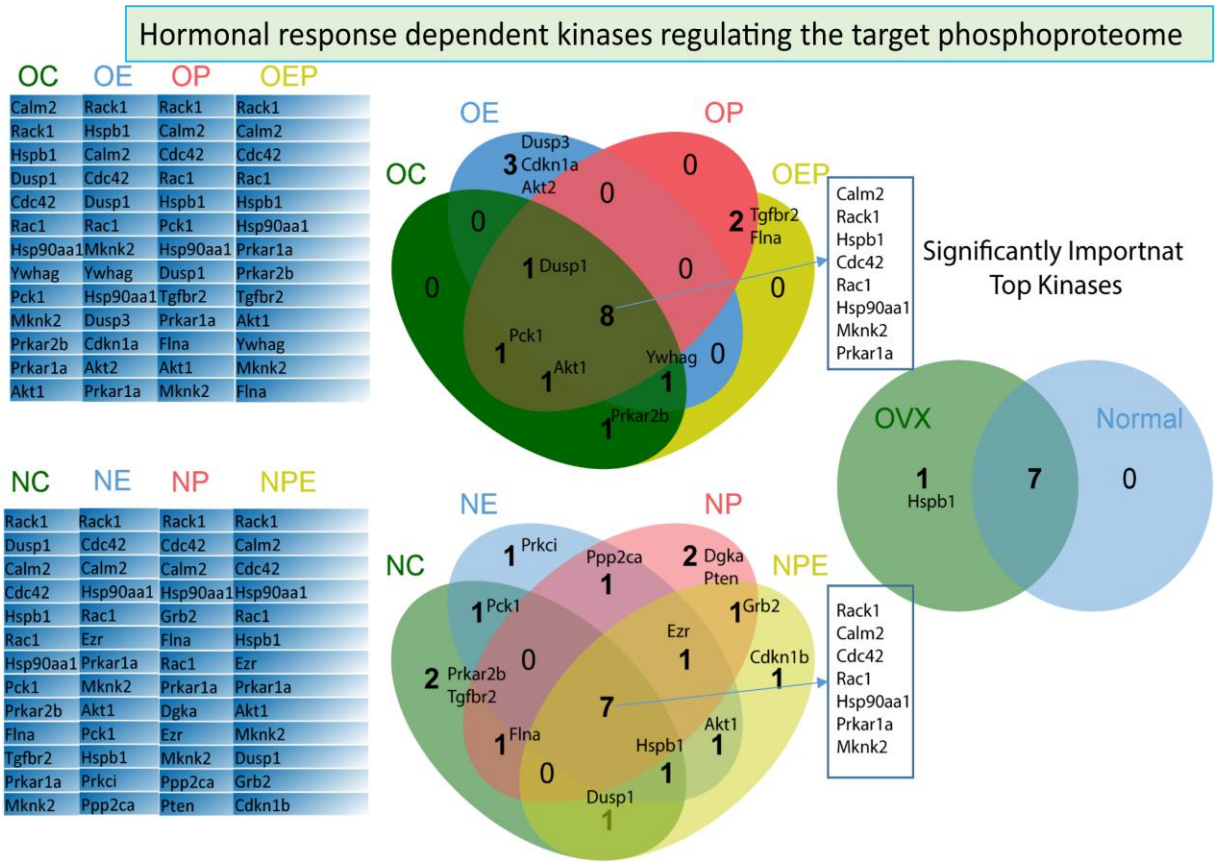

Figure 4.19: Hormonal response-dependent kinases regulating the target phosphoproteome. **Comparison of different kinases in OVX (hormone treated) mammary gland:** Veen diagram depicting the comparison of different kinases involved in downstream hormonal signalling. OC: Ovariectomy control; OE: Ovariectomy estrogen; OP: Ovariectomy progesterone; OEP: Ovariectomy estrogen and progesterone; N: normal with hormones mentioned above.

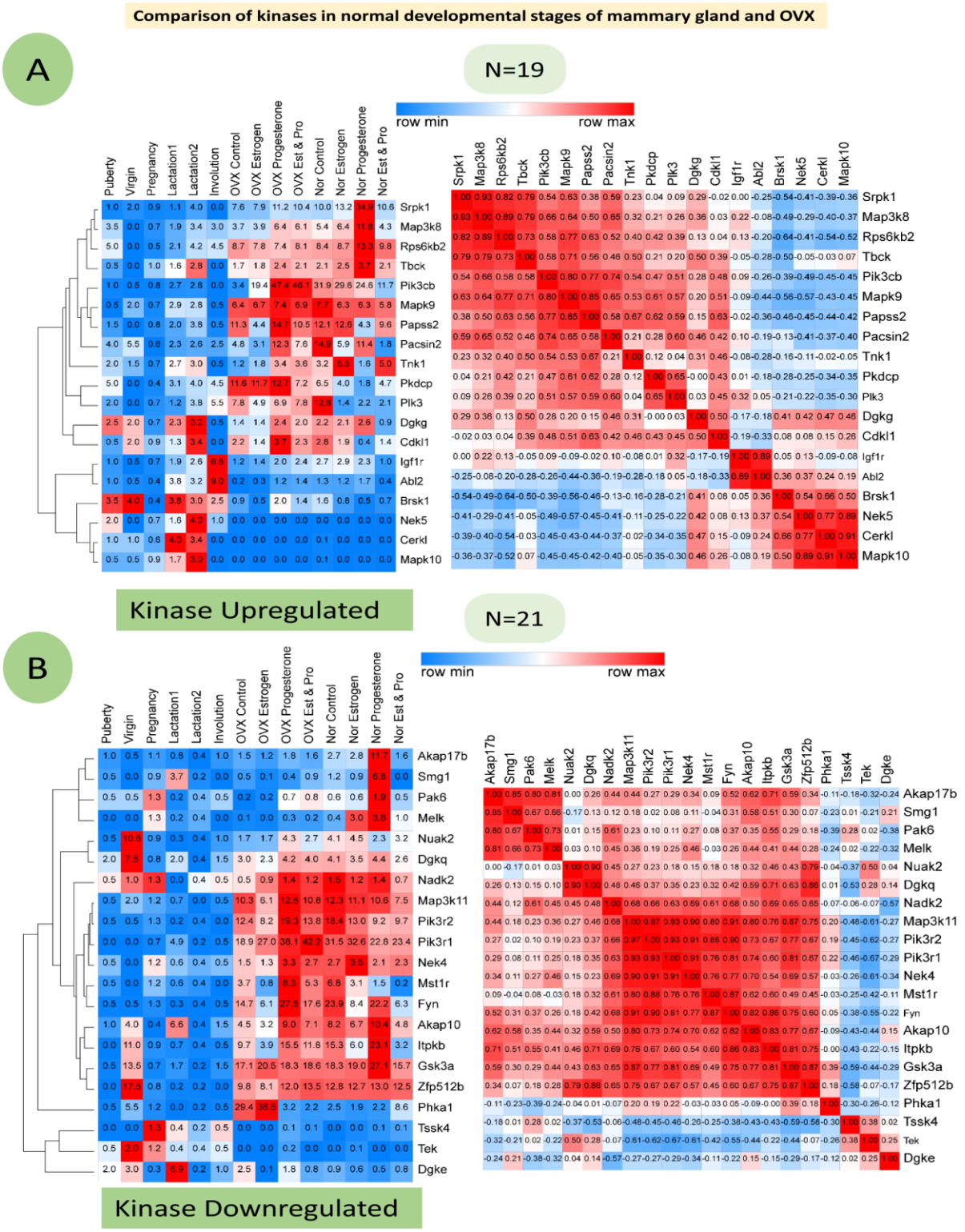

Figure 4.20: **Comparison of normal developmental stages of the mammary gland and OVX (hormone treated) mammary gland:** Hierarchical clustering based comparison of normalized lactation stage-specific identified upregulated and downregulated typical kinases in normal MG development and OVX experiment and similarity matrix using Pearson correlation.

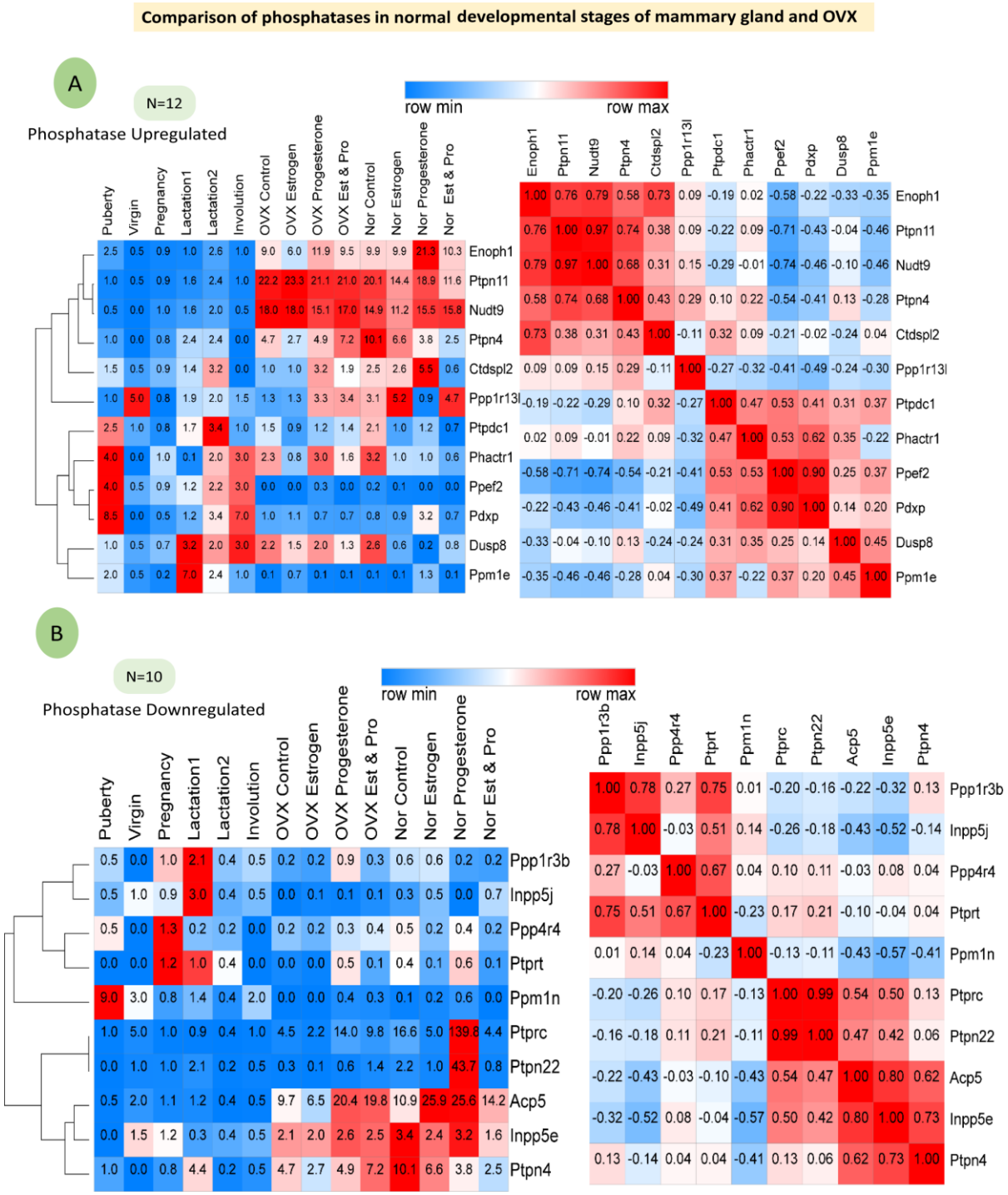

Figure 4.21: **Comparison of normal developmental stages of the mammary gland and OVX (hormone treated) mammary gland:** Hierarchical clustering based comparison of normalized lactation stage-specific identified upregulated and downregulated common phosphatase in normal MG development and OVX experiment and similarity matrix using Pearson correlation.

4.1.10 Ovariectomy experiments: mammary gland oil red staining

The oil red O stain showed neutral triglycerides and lipids on frozen sections of eight different treated MG development. The results showed that the estrogen induces the synthesis of lipids. We compared all the stages together and found that statistically significant difference (p-value <0.0001) NE, NPE, and OPE (Figure 4.22).

4.1.11 Transmission electron microscopy for eight treatment set of ovariectomy experiment

The analysis of the mammary glands ultra-structures using a transmission electron microscope showed the variation of difference compartment presence across the different treatments. In ovx experiments, we found mostly the stocking of lipid droplets. On the treatment of estrogen, we establish the synthesis and accumulation of large adipocytes. However, estrogen and progesterone treatment resulted in the differentiation of structures formation and the aggregation of micelles. In the normal mammary gland, the lipid droplets reduce while maintaining a similar structure like puberty. The treatment extra estrogen and progesterone in the normal mammary gland resulted in the stacking of micelles and more presence of adipocytes (Figure 4.22).

4.1.12 Hematoxylin and eosin staining of lobulo-alveolar for eight treatment set of ovariectomy experiment

The hematoxylin and eosin staining showed the different cellular composition of adipocytes and epithelial cells on the mammary cellular population. Ovx treated with estrogen showed the maximum adipocytes, but the adipocytes reduction is visible during the synergic hormonal response. Therefore, we found comparatively fewer adipocytes in other treatments. Amazingly, estrogen and progesterone showed the morphological similarity in ovx and normal gland. We found extensive side branching and maximum alveologenesis; also, the ducts are viable (Figure 4.23).

4.1.13 Immunohistochemistry (IHC) of selected proteins from tSNE based network analysis

We performed the immunohisto analysis of 19 proteins identified in our tSNE data. For simplicity purpose, we have discussed the results in comparison to normal or ovx control gland. The results showed that all nineteen proteins were present in all the eight treatment validating our transcriptomics analysis. To

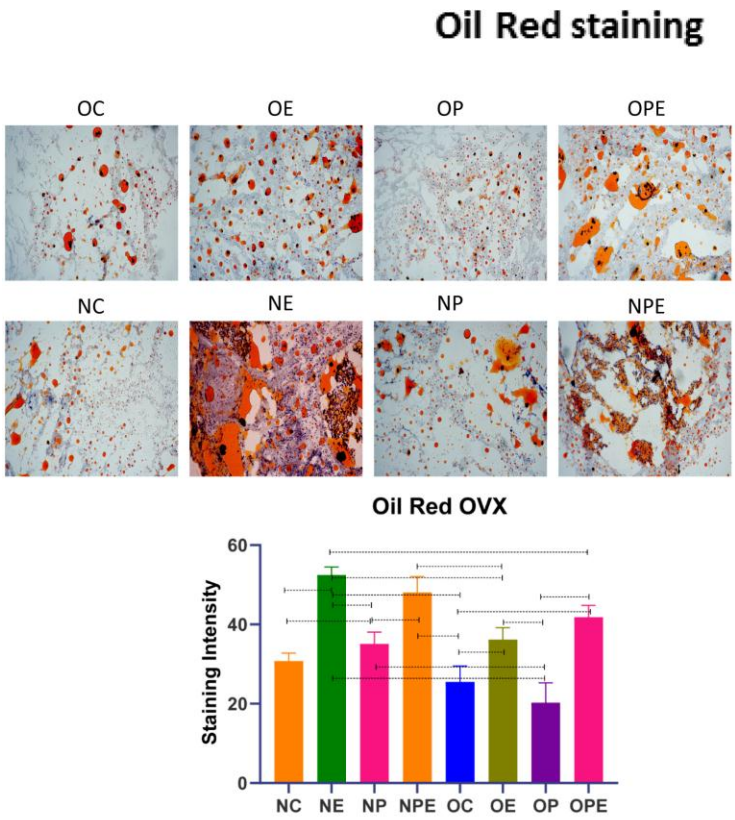

Tukey's multiple comparisons test	Significant?	Summary	Adjusted P Value
OC vs. OE	Yes	*	0.0424
OC vs. OP	No	ns	0.7975
OC vs. OPE	Yes	**	0.0011
OC vs. NC	No	ns	0.8452
OC vs. NE	Yes	****	<0.0001
OC vs. NP	No	ns	0.0866
OC vs. NPE	Yes	****	<0.0001
OE vs. OP	Yes	**	0.0023
OE vs. OPE	No	ns	0.5825
OE vs. NC	No	ns	0.4264
OE vs. NE	Yes	***	0.0007
OE vs. NP	No	ns	>0.9999
OE vs. NPE	Yes	**	0.0058
OP vs. OPE	Yes	****	<0.0001
OP vs. NC	No	ns	0.1380
OP vs. NE	Yes	****	<0.0001
OP vs. NP	Yes	**	0.0049
OP vs. NPE	Yes	****	<0.0001
OPE vs. NC	Yes	*	0.0169
OPE vs. NE	Yes	*	0.0271
OPE vs. NP	No	ns	0.3677
OPE vs. NPE	No	ns	0.1913
NC vs. NE	Yes	****	<0.0001
NC vs. NP	No	ns	0.6499
NC vs. NPE	Yes	***	0.0001
NE vs. NP	Yes	***	0.0004
NE vs. NPE	No	ns	0.9515
NP vs. NPE	Yes	**	0.0027

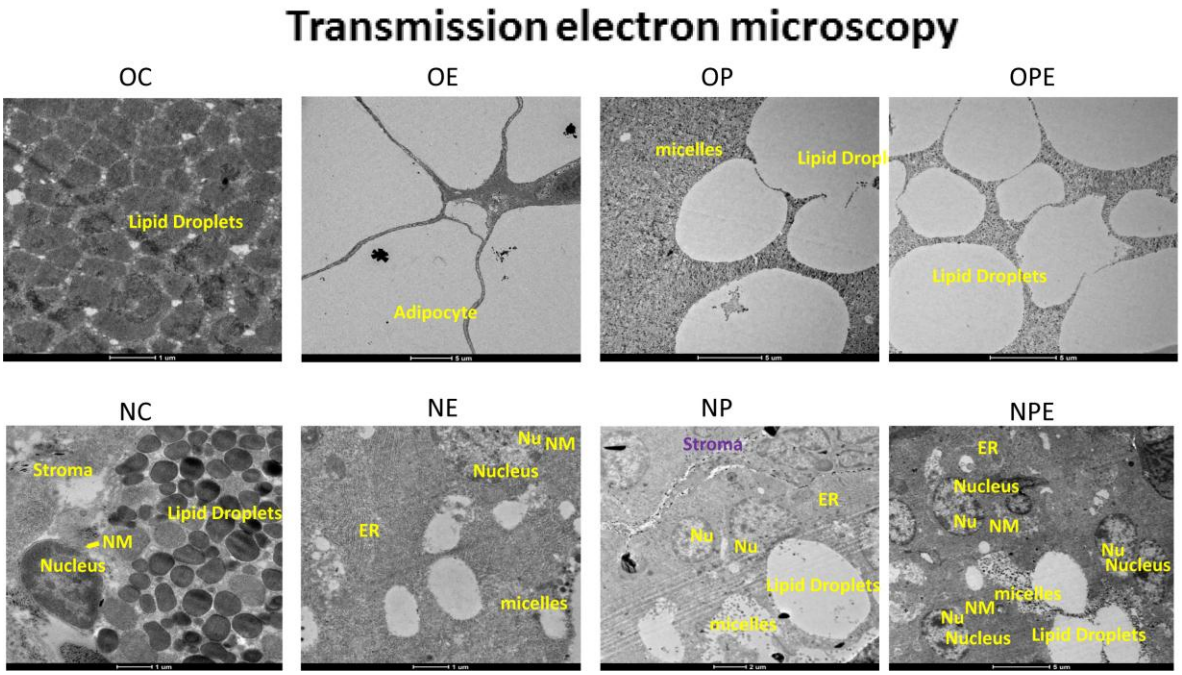

Figure 4.22: **Comparison of OVX (hormone treated) with normal (hormone treated) mammary gland with oil red staining for lipid profile TEM analysis.**

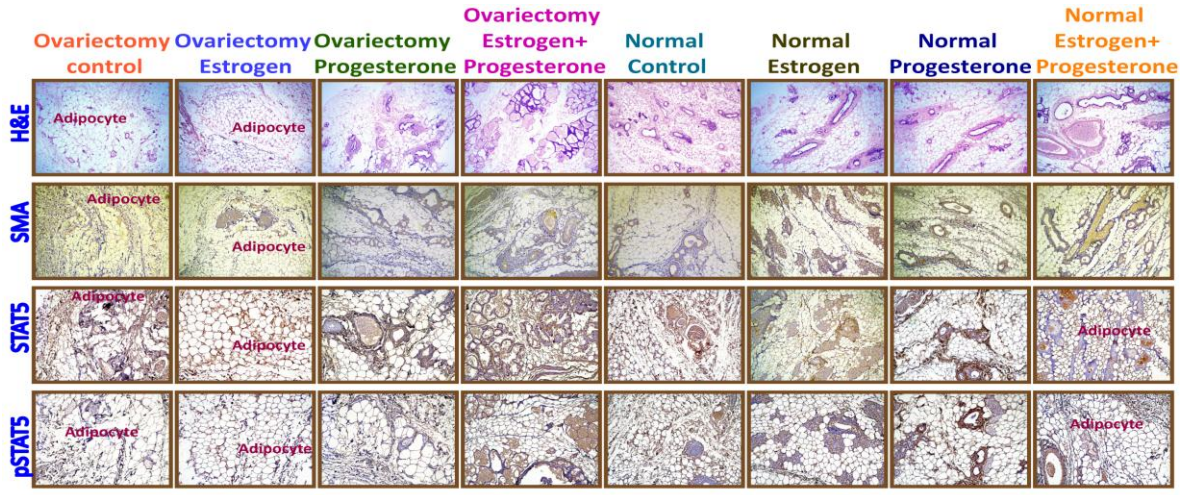

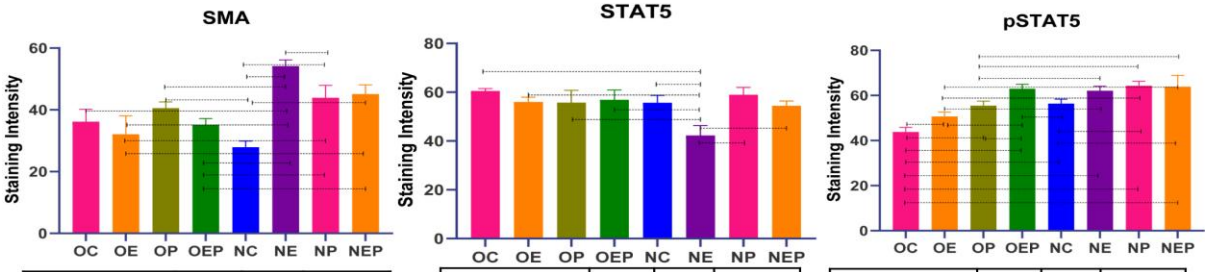

Tukey's multiple comparisons test	Significant?	Summary	Adjusted P Value
OC vs. OE	No	ns	0.9256
OC vs. OP	No	ns	0.6941
OC vs. OEP	No	ns	0.9994
OC vs. NC	No	ns	0.0884
OC vs. NE	Yes	***	0.0001
OC vs. NP	No	ns	0.0987
OC vs. NEP	No	ns	0.0544
OE vs. OP	No	ns	0.1443
OE vs. OEP	No	ns	0.9967
OE vs. NC	No	ns	0.5287
OE vs. NE	Yes	****	<0.0001
OE vs. NP	Yes	*	0.0105
OE vs. NEP	Yes	**	0.0056
OP vs. OEP	No	ns	0.4004
OP vs. NC	Yes	**	0.0035
OP vs. NE	Yes	**	0.0028
OP vs. NP	No	ns	0.8439
OP vs. NEP	No	ns	0.6708
OEP vs. NC	No	ns	0.2109
OEP vs. NE	Yes	****	<0.0001
OEP vs. NP	Yes	*	0.0384
OEP vs. NEP	Yes	*	0.0205
NC vs. NE	Yes	****	<0.0001
NC vs. NP	Yes	***	0.0002
NC vs. NEP	Yes	***	0.0001
NE vs. NP	Yes	*	0.0430
NE vs. NEP	No	ns	0.0788
NP vs. NEP	No	ns	>0.9999

Tukey's multiple comparisons test	Significant?	Summary	Adjusted P Value
OC vs. OE	No	ns	0.7973
OC vs. OP	No	ns	0.9261
OC vs. OEP	No	ns	0.9649
OC vs. NC	No	ns	0.8053
OC vs. NE	Yes	***	0.0001
OC vs. NP	No	ns	>0.9999
OC vs. NEP	No	ns	0.5320
OE vs. OP	No	ns	>0.9999
OE vs. OEP	No	ns	0.9996
OE vs. NC	No	ns	>0.9999
OE vs. NE	Yes	**	0.0020
OE vs. NP	No	ns	0.8377
OE vs. NEP	No	ns	0.9997
OP vs. OEP	No	ns	>0.9999
OP vs. NC	No	ns	>0.9999
OP vs. NE	Yes	**	0.0011
OP vs. NP	No	ns	0.9482
OP vs. NEP	No	ns	0.9918
OEP vs. NC	No	ns	0.9997
OEP vs. NE	Yes	***	0.0008
OEP vs. NP	No	ns	0.9778
OEP vs. NEP	No	ns	0.9759
NC vs. NE	Yes	**	0.0019
NC vs. NP	No	ns	0.8449
NC vs. NEP	No	ns	0.9996
NE vs. NP	Yes	***	0.0001
NE vs. NEP	Yes	**	0.0049
NP vs. NEP	No	ns	0.5815

Tukey's multiple comparisons test	Significant?	Summary	Adjusted P Value
OC vs. OE	Yes	*	0.0176
OC vs. OP	Yes	***	0.0002
OC vs. OEP	Yes	****	<0.0001
OC vs. NC	Yes	****	<0.0001
OC vs. NE	Yes	****	<0.0001
OC vs. NP	Yes	****	<0.0001
OC vs. NEP	Yes	****	<0.0001
OE vs. OP	No	ns	0.3628
OE vs. OEP	Yes	***	0.0002
OE vs. NC	No	ns	0.1343
OE vs. NE	Yes	***	0.0004
OE vs. NP	Yes	****	<0.0001
OE vs. NEP	Yes	****	<0.0001
OP vs. OEP	Yes	*	0.0117
OP vs. NC	No	ns	0.9976
OP vs. NE	Yes	*	0.0300
OP vs. NP	Yes	**	0.0030
OP vs. NEP	Yes	**	0.0012
OEP vs. NC	Yes	*	0.0403
OEP vs. NE	No	ns	0.9996
OEP vs. NP	No	ns	0.9958
OEP vs. NEP	No	ns	0.9213
NC vs. NE	No	ns	0.0985
NC vs. NP	Yes	*	0.0104
NC vs. NEP	Yes	**	0.0040
NE vs. NP	No	ns	0.9246
NE vs. NEP	No	ns	0.6971
NP vs. NEP	No	ns	0.9995

Figure 4.23: **Confinement of mammary gland development under the absence of ovary-dependent hormone in ovariectomized Rat:** Representative of gross morphological and histological features of hematoxylin and eosin (H&E)-stained paraffin sections of the female mammary glands after ovariectomy rat. Protein expression analysis using immunohistochemically; detection of SMA (Smooth Muscle Actin), STAT5 Signal Transducer and Activator of Transcription 5A), and pSTAT5 (Phospho-STAT5).

assess the influence on ACTA2 upon the response of hormones, we performed the imaging. The smooth muscle actin (SMA) protein in normal control found significant to all the treatment (p-value <0.05) excluding the ovx treatments (p-value 0.99). The comparison of STAT5 and phosphorylation counterpart showed non-significant difference among all stages and suggested their ubiquitous expression in all eight treatments. In comparison to previous results, we found these proteins in our analysis, and that is why more prominent to validate the expression in ovx experiment (Figure 4.24).

Next, we compared STAT3 and SMAD with respective phosphorylated counterpart. Most of the expression we found in the lactation stage on ductal growth. The image analysis for STAT3 and pSTAT3 showed the significant difference of lactation stage with virgin (p-value 0.284 and 0.0221, respectively). The SMAD staining showed the significant difference with virgin (p-value 0.0018), pregnant (p-value 0.006), and lactation1 vs lactation2 (p-value 0.0157). While for the pSMAD, it showed a significant difference with the puberty stage (0.0031). The results imply that the important role of these proteins in the lactation stage (Figure 4.25).

Further, the mapping of S100A4, LIF, MFGE8, SNAI2, Zeb, Krt8, Twist, and β-actin (p-value <0.05) significant variation among the stages (Figure 4.26). The overall results reveal that these proteins are induced, and their expression is regulated by the reproductive hormones for the glandular developmental transition (Figure 4.27).

In summary, we conclude that all identified 19 proteins play an indispensable role in mammary gland development in response to reproductive hormones estrogen and progesterone, successful orchestrating mammary gland remodelling (Figure 4.28). We put forth the schematic workflow for adipocyte in mammary gland remodelling and transition of different stages (Figure 4.28).

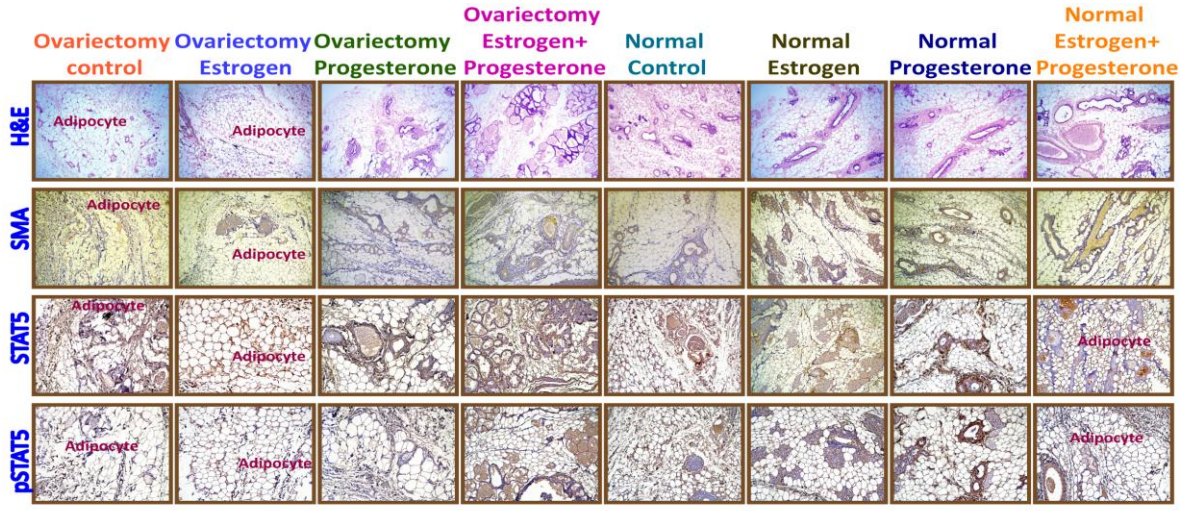

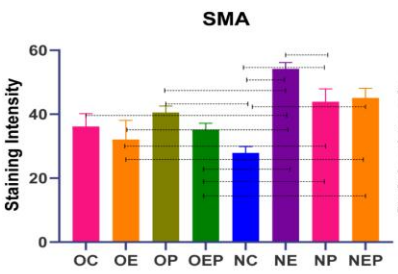

Tukey's multiple comparisons test	Significant?	Summary	Adjusted P Value
OC vs. OE	No	ns	0.9256
OC vs. OP	No	ns	0.6941
OC vs. OEP	No	ns	0.9994
OC vs. NC	No	ns	0.0884
OC vs. NE	Yes	***	0.0001
OC vs. NP	No	ns	0.0987
OC vs. NEP	No	ns	0.0544
OE vs. OP	No	ns	0.1443
OE vs. OEP	No	ns	0.9967
OE vs. NC	No	ns	0.5287
OE vs. NE	Yes	****	<0.0001
OE vs. NP	Yes	*	0.0105
OE vs. NEP	Yes	**	0.0056
OP vs. OEP	No	ns	0.4004
OP vs. NC	Yes	**	0.0035
OP vs. NE	Yes	**	0.0028
OP vs. NP	No	ns	0.8439
OP vs. NEP	No	ns	0.6708
OEP vs. NC	No	ns	0.2109
OEP vs. NE	Yes	****	<0.0001
OEP vs. NP	Yes	*	0.0384
OEP vs. NEP	Yes	*	0.0205
NC vs. NE	Yes	****	<0.0001
NC vs. NP	Yes	***	0.0002
NC vs. NEP	Yes	***	0.0001
NE vs. NP	Yes	*	0.0430
NE vs. NEP	No	ns	0.0788
NP vs. NEP	No	ns	>0.9999

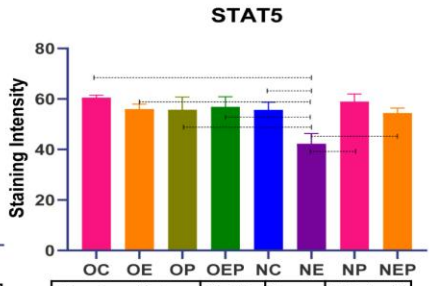

Tukey's multiple comparisons test	Significant?	Summary	Adjusted P Value
OC vs. OE	No	ns	0.7973
OC vs. OP	No	ns	0.9261
OC vs. OEP	No	ns	0.9649
OC vs. NC	No	ns	0.8053
OC vs. NE	Yes	***	0.0001
OC vs. NP	No	ns	>0.9999
OC vs. NEP	No	ns	0.5320
OE vs. OP	No	ns	>0.9999
OE vs. OEP	No	ns	0.9996
OE vs. NC	No	ns	>0.9999
OE vs. NE	Yes	**	0.0020
OE vs. NP	No	ns	0.8377
OE vs. NEP	No	ns	0.9997
OP vs. OEP	No	ns	>0.9999
OP vs. NC	No	ns	>0.9999
OP vs. NE	Yes	**	0.0011
OP vs. NP	No	ns	0.9482
OP vs. NEP	No	ns	0.9918
OEP vs. NC	No	ns	0.9997
OEP vs. NE	Yes	***	0.0008
OEP vs. NP	No	ns	0.9778
OEP vs. NEP	No	ns	0.9759
NC vs. NE	Yes	**	0.0019
NC vs. NP	No	ns	0.8449
NC vs. NEP	No	ns	0.9996
NE vs. NP	Yes	***	0.0001
NE vs. NEP	Yes	**	0.0049
NP vs. NEP	No	ns	0.5815

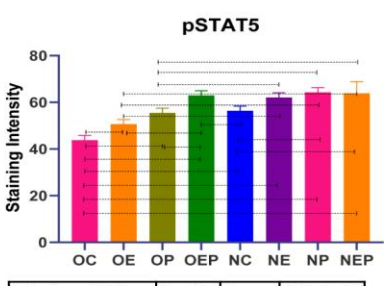

Tukey's multiple comparisons test	Significant?	Summary	Adjusted P Value
OC vs. OE	Yes	*	0.0176
OC vs. OP	Yes	***	0.0002
OC vs. OEP	Yes	****	<0.0001
OC vs. NC	Yes	****	<0.0001
OC vs. NE	Yes	****	<0.0001
OC vs. NP	Yes	****	<0.0001
OC vs. NEP	Yes	****	<0.0001
OE vs. OP	No	ns	0.3628
OE vs. OEP	Yes	***	0.0002
OE vs. NC	No	ns	0.1343
OE vs. NE	Yes	***	0.0004
OE vs. NP	Yes	****	<0.0001
OE vs. NEP	Yes	****	<0.0001
OP vs. OEP	Yes	*	0.0117
OP vs. NC	No	ns	0.9976
OP vs. NE	Yes	*	0.0300
OP vs. NP	Yes	**	0.0030
OP vs. NEP	Yes	**	0.0012
OEP vs. NC	Yes	*	0.0403
OEP vs. NE	No	ns	0.9996
OEP vs. NP	No	ns	0.9958
OEP vs. NEP	No	ns	0.9213
NC vs. NE	No	ns	0.0985
NC vs. NP	Yes	*	0.0104
NC vs. NEP	Yes	**	0.0040
NE vs. NP	No	ns	0.9246
NE vs. NEP	No	ns	0.6971
NP vs. NEP	No	ns	0.9995

Figure 4.24: **Confinement of mammary gland development under the absence of ovary based hormone in ovariectomized Rat:** Comparative immunohistochemistry for STAT3 (Signal Transducer and Activator of Transcription 3), and pSTAT3 (Phospho-STAT3) and SMAD (SMA- And MAD-Related Protein), and pSMAD (Phospho-SMAD), of different developmental stages of the mammary gland under the induction of artificial condition in ovariectomized Rats.

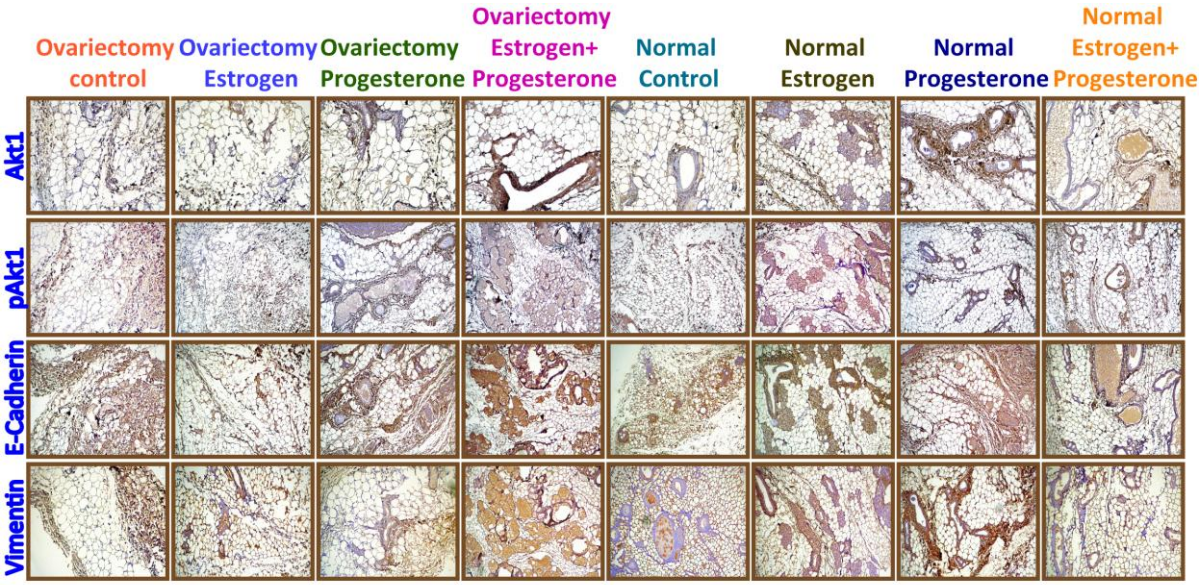

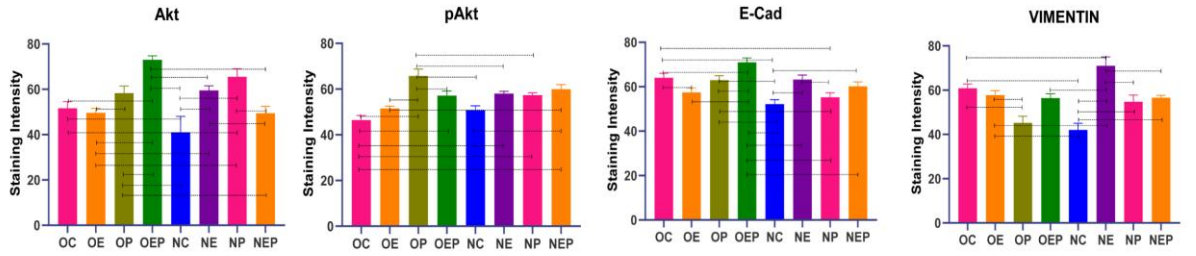

Tukey's multiple comparisons test	Significant?	Summary	Adjusted P Value
OC vs. OE	No	ns	0.9495
OC vs. OP	No	ns	0.1520
OC vs. OEP	Yes	****	<0.0001
OC vs. NC	Yes	**	0.0078
OC vs. NE	No	ns	0.0629
OC vs. NP	Yes	***	0.0001
OC vs. NEP	No	ns	0.9768
OE vs. OP	Yes	*	0.0143
OE vs. OEP	Yes	****	<0.0001
OE vs. NC	No	ns	0.0922
OE vs. NE	Yes	**	0.0050
OE vs. NP	Yes	****	<0.0001
OE vs. NEP	No	ns	>0.9999
OP vs. OEP	Yes	***	0.0004
OP vs. NC	Yes	****	<0.0001
OP vs. NE	No	ns	0.9998
OP vs. NP	No	ns	0.0815
OP vs. NEP	Yes	*	0.0203
OEP vs. NC	Yes	****	<0.0001
OEP vs. NE	Yes	**	0.0012
OEP vs. NP	No	ns	0.3462
OEP vs. NEP	Yes	****	<0.0001
NC vs. NE	Yes	****	<0.0001
NC vs. NP	Yes	****	<0.0001
NC vs. NEP	No	ns	0.0675
NE vs. NP	No	ns	0.1908
NE vs. NEP	Yes	**	0.0072
NP vs. NEP	Yes	****	<0.0001

Tukey's multiple comparisons test	Significant?	Summary	Adjusted P Value
OC vs. OE	No	ns	0.2075
OC vs. OP	Yes	****	<0.0001
OC vs. OEP	Yes	**	0.0012
OC vs. NC	No	ns	0.3173
OC vs. NE	Yes	***	0.0008
OC vs. NP	Yes	**	0.0015
OC vs. NEP	Yes	****	<0.0001
OE vs. OP	Yes	***	0.0001
OE vs. OEP	No	ns	0.1840
OE vs. NC	No	ns	>0.9999
OE vs. NE	No	ns	0.1219
OE vs. NP	No	ns	0.2105
OE vs. NEP	Yes	*	0.0114
OP vs. OEP	Yes	*	0.0185
OP vs. NC	Yes	****	<0.0001
OP vs. NE	Yes	*	0.0296
OP vs. NP	Yes	*	0.0157
OP vs. NEP	No	ns	0.2722
OEP vs. NC	No	ns	0.1144
OEP vs. NE	No	ns	>0.9999
OEP vs. NP	No	ns	>0.9999
OEP vs. NEP	No	ns	0.7930
NC vs. NE	No	ns	0.0739
NC vs. NP	No	ns	0.1323
NC vs. NEP	Yes	**	0.0066
NE vs. NP	No	ns	>0.9999
NE vs. NEP	No	ns	0.8995
NP vs. NEP	No	ns	0.7488

Tukey's multiple comparisons test	Significant?	Summary	Adjusted P Value
OC vs. OE	Yes	*	0.0278
OC vs. OP	No	ns	0.9985
OC vs. OEP	Yes	*	0.0277
OC vs. NC	Yes	****	<0.0001
OC vs. NE	No	ns	0.9980
OC vs. NP	Yes	**	0.0024
OC vs. NEP	No	ns	0.3942
OE vs. OP	No	ns	0.0841
OE vs. OEP	Yes	****	<0.0001
OE vs. NC	No	ns	0.1127
OE vs. NE	No	ns	0.0881
OE vs. NP	No	ns	0.8980
OE vs. NEP	No	ns	0.7655
OP vs. OEP	Yes	**	0.0088
OP vs. NC	Yes	***	0.0003
OP vs. NE	No	ns	>0.9999
OP vs. NP	Yes	**	0.0075
OP vs. NEP	No	ns	0.7336
OEP vs. NC	Yes	****	<0.0001
OEP vs. NE	Yes	**	0.0083
OEP vs. NP	Yes	****	<0.0001
OEP vs. NEP	Yes	***	0.0004
NC vs. NE	Yes	***	0.0003
NC vs. NP	No	ns	0.6600
NC vs. NEP	Yes	**	0.0058
NE vs. NP	Yes	**	0.0079
NE vs. NEP	No	ns	0.7479
NP vs. NEP	No	ns	0.1553

Tukey's multiple comparisons test	Significant?	Summary	Adjusted P Value
OC vs. OE	No	ns	0.9210
OC vs. OP	Yes	***	0.0006
OC vs. OEP	No	ns	0.5815
OC vs. NC	Yes	****	<0.0001
OC vs. NE	Yes	**	0.0034
OC vs. NP	No	ns	0.5847
OC vs. NEP	No	ns	0.7886
OE vs. OP	Yes	**	0.0058
OE vs. OEP	No	ns	0.9964
OE vs. NC	Yes	***	0.0007
OE vs. NE	Yes	***	0.0004
OE vs. NP	No	ns	0.9966
OE vs. NEP	No	ns	>0.9999
OP vs. OEP	Yes	*	0.0220
OP vs. NC	No	ns	0.9380
OP vs. NE	Yes	****	<0.0001
OP vs. NP	Yes	*	0.0217
OP vs. NEP	Yes	*	0.0109
OEP vs. NC	Yes	**	0.0024
OEP vs. NE	Yes	***	0.0001
OEP vs. NP	No	ns	>0.9999
OEP vs. NEP	No	ns	>0.9999
NC vs. NE	Yes	****	<0.0001
NC vs. NP	Yes	**	0.0024
NC vs. NEP	Yes	**	0.0012
NE vs. NP	Yes	***	0.0001
NE vs. NEP	Yes	***	0.0002
NP vs. NEP	No	ns	>0.9999

Figure 4.25: **Confinement of mammary gland development under the absence of ovary-dependent hormone in ovariectomized Rat:** Comparative immunohistochemistry for Akt1, pAkt (Phospho-Akt), E-Cadherin, and Vimentin of different developmental stages of the mammary gland under the induction of artificial condition in ovariectomized Rats.

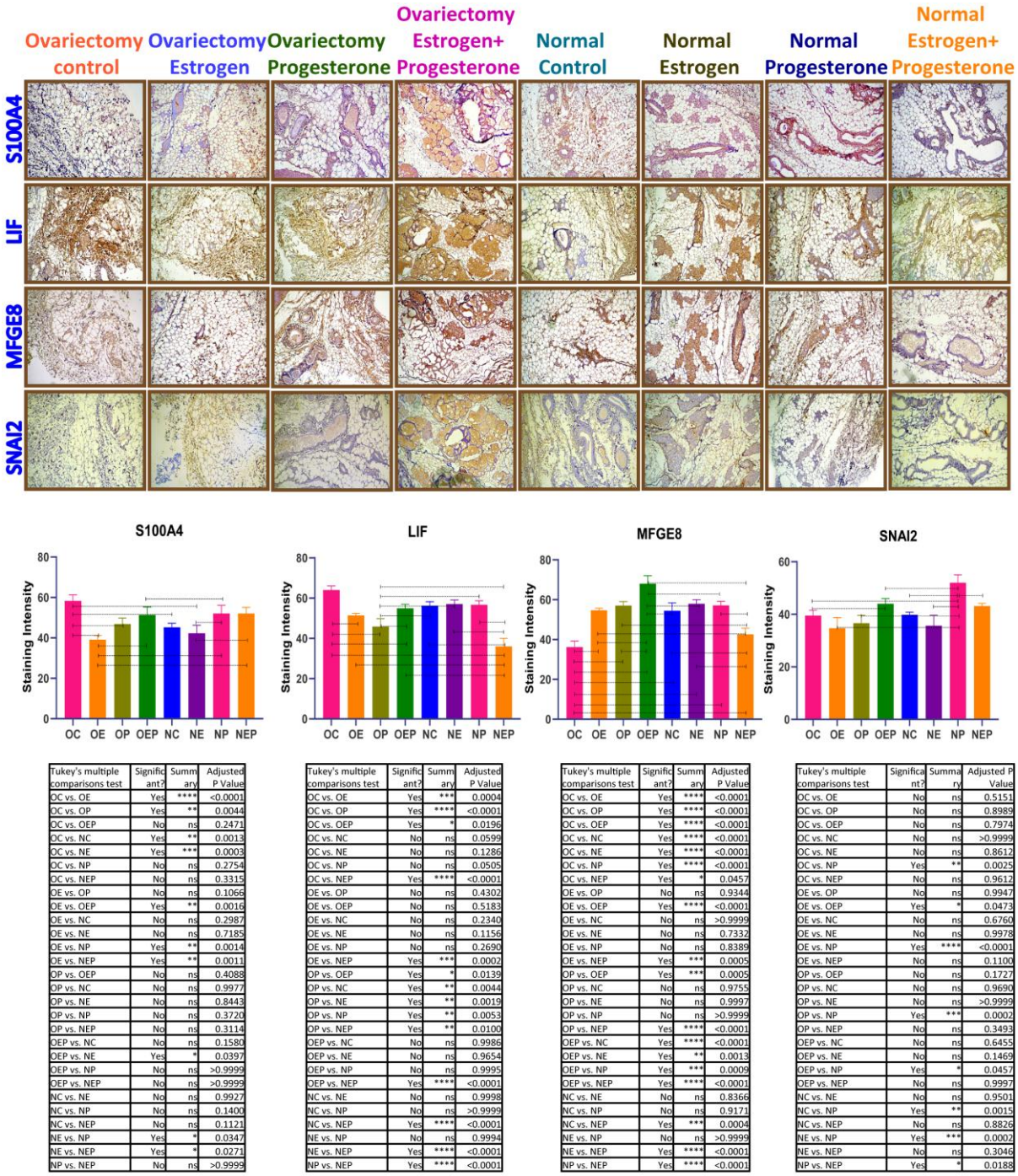

Tukey's multiple comparisons test	Significant?	Summary	Adjusted P Value
OC vs. OE	Yes	****	<0.0001
OC vs. OP	Yes	**	0.0044
OC vs. OEP	No	ns	0.2471
OC vs. NC	Yes	**	0.0013
OC vs. NE	Yes	***	0.0003
OC vs. NP	No	ns	0.2754
OC vs. NEP	No	ns	0.3315
OE vs. OP	No	ns	0.1066
OE vs. OEP	Yes	**	0.0016
OE vs. NC	No	ns	0.2987
OE vs. NE	No	ns	0.7185
OE vs. NP	Yes	**	0.0014
OE vs. NEP	Yes	**	0.0011
OP vs. OEP	No	ns	0.4088
OP vs. NC	No	ns	0.9977
OP vs. NE	No	ns	0.8443
OP vs. NP	No	ns	0.3720
OP vs. NEP	No	ns	0.3114
OEP vs. NC	No	ns	0.1580
OEP vs. NE	Yes	*	0.0397
OEP vs. NP	No	ns	>0.9999
OEP vs. NEP	No	ns	>0.9999
NC vs. NE	No	ns	0.9927
NC vs. NP	No	ns	0.1400
NC vs. NEP	No	ns	0.1121
NE vs. NP	Yes	*	0.0347
NE vs. NEP	Yes	*	0.0271
NP vs. NEP	No	ns	>0.9999

Tukey's multiple comparisons test	Significant?	Summary	Adjusted P Value
OC vs. OE	Yes	***	0.0004
OC vs. OP	Yes	****	<0.0001
OC vs. OEP	Yes	*	0.0196
OC vs. NC	No	ns	0.0599
OC vs. NE	No	ns	0.1286
OC vs. NP	No	ns	0.0505
OC vs. NEP	Yes	****	<0.0001
OE vs. OP	No	ns	0.4302
OE vs. OEP	No	ns	0.5183
OE vs. NC	No	ns	0.2340
OE vs. NE	No	ns	0.1156
OE vs. NP	No	ns	0.2690
OE vs. NEP	Yes	***	0.0002
OP vs. OEP	Yes	*	0.0139
OP vs. NC	Yes	**	0.0044
OP vs. NE	Yes	**	0.0019
OP vs. NP	Yes	**	0.0053
OP vs. NEP	Yes	**	0.0100
OEP vs. NC	No	ns	0.9986
OEP vs. NE	No	ns	0.9654
OEP vs. NP	No	ns	0.9995
OEP vs. NEP	Yes	****	<0.0001
NC vs. NE	No	ns	0.9998
NC vs. NP	No	ns	>0.9999
NC vs. NEP	Yes	****	<0.0001
NE vs. NP	No	ns	0.9994
NE vs. NEP	Yes	****	<0.0001
NP vs. NEP	Yes	****	<0.0001

Tukey's multiple comparisons test	Significant?	Summary	Adjusted P Value
OC vs. OE	Yes	****	<0.0001
OC vs. OP	Yes	****	<0.0001
OC vs. OEP	Yes	****	<0.0001
OC vs. NC	Yes	****	<0.0001
OC vs. NE	Yes	****	<0.0001
OC vs. NP	Yes	****	<0.0001
OC vs. NEP	Yes	*	0.0457
OE vs. OP	No	ns	0.9344
OE vs. OEP	Yes	****	<0.0001
OE vs. NC	No	ns	>0.9999
OE vs. NE	No	ns	0.7332
OE vs. NP	No	ns	0.8389
OE vs. NEP	Yes	***	0.0005
OP vs. OEP	Yes	***	0.0005
OP vs. NC	No	ns	0.9755
OP vs. NE	No	ns	0.9997
OP vs. NP	No	ns	>0.9999
OP vs. NEP	Yes	****	<0.0001
OEP vs. NC	Yes	****	<0.0001
OEP vs. NE	Yes	**	0.0013
OEP vs. NP	Yes	***	0.0009
OEP vs. NEP	Yes	****	<0.0001
NC vs. NE	No	ns	0.8366
NC vs. NP	No	ns	0.9171
NC vs. NEP	Yes	***	0.0004
NE vs. NP	No	ns	>0.9999
NE vs. NEP	Yes	****	<0.0001
NP vs. NEP	Yes	****	<0.0001

Tukey's multiple comparisons test	Significant?	Summary	Adjusted P Value
OC vs. OE	No	ns	0.5151
OC vs. OP	No	ns	0.8989
OC vs. OEP	No	ns	0.7974
OC vs. NC	No	ns	>0.9999
OC vs. NE	No	ns	0.8612
OC vs. NP	Yes	**	0.0025
OC vs. NEP	No	ns	0.9612
OE vs. OP	No	ns	0.9947
OE vs. OEP	Yes	*	0.0473
OE vs. NC	No	ns	0.6760
OE vs. NE	No	ns	0.9978
OE vs. NP	Yes	****	<0.0001
OE vs. NEP	No	ns	0.1100
OP vs. OEP	No	ns	0.1727
OP vs. NC	No	ns	0.9690
OP vs. NE	No	ns	>0.9999
OP vs. NP	Yes	***	0.0002
OP vs. NEP	No	ns	0.3493
OEP vs. NC	No	ns	0.6455
OEP vs. NE	No	ns	0.1469
OEP vs. NP	Yes	*	0.0457
OEP vs. NEP	No	ns	0.9997
NC vs. NE	No	ns	0.9501
NC vs. NP	Yes	**	0.0015
NC vs. NEP	No	ns	0.8826
NE vs. NP	Yes	***	0.0002
NE vs. NEP	No	ns	0.3046
NP vs. NEP	Yes	*	0.0188

Figure 4.26: **Confinement of mammary gland development under the absence of ovary-dependent hormone in ovariectomized Rat:** Comparative immunohistochemistry for S100A4, LIF (Leukemia Inhibitory Factor), MFGE8 (Milk Fat Globule-EGF Factor 8 Protein), and SNAI2 (Slug Homolog, Zinc Finger Protein), during different developmental stages of the mammary gland under artificially mimicking the natural hormonal rhythm condition in ovariectomized rat.

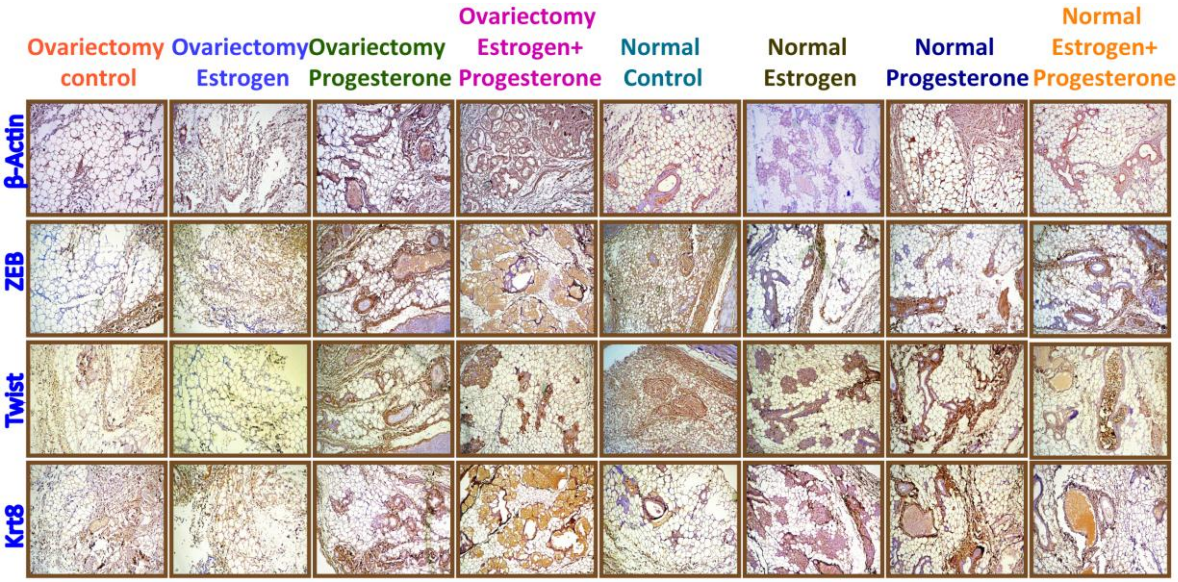

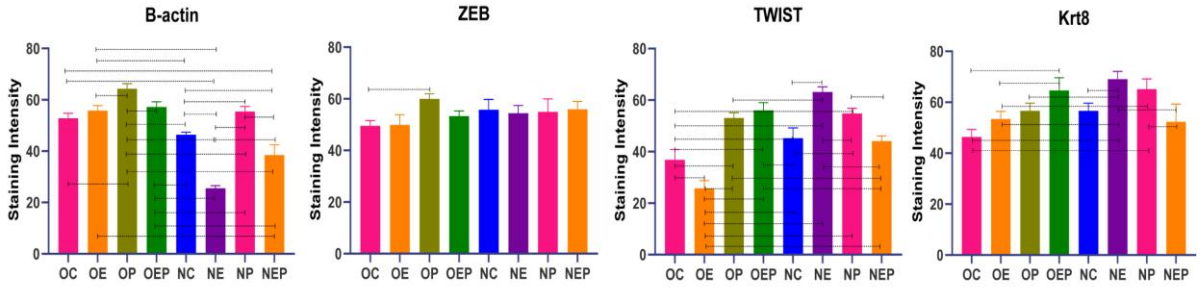

Tukey's multiple comparisons test	Significant?	Summary	Adjusted P Value
OC vs. OE	No	ns	0.8833
OC vs. OP	Yes	***	0.0006
OC vs. OEP	No	ns	0.4721
OC vs. NC	No	ns	0.0797
OC vs. NE	Yes	****	<0.0001
OC vs. NP	No	ns	0.9316
OC vs. NEP	Yes	****	<0.0001
OE vs. OP	Yes	**	0.0070
OE vs. OEP	No	ns	0.9931
OE vs. NC	Yes	**	0.0065
OE vs. NE	Yes	****	<0.0001
OE vs. NP	No	ns	>0.9999
OE vs. NEP	Yes	****	<0.0001
OP vs. OEP	Yes	*	0.0307
OP vs. NC	Yes	****	<0.0001
OP vs. NE	Yes	****	<0.0001
OP vs. NP	Yes	**	0.0053
OP vs. NEP	Yes	****	<0.0001
OEP vs. NC	Yes	**	0.0015
OEP vs. NE	Yes	****	<0.0001
OEP vs. NP	No	ns	0.9812
OEP vs. NEP	Yes	****	<0.0001
NC vs. NE	Yes	****	<0.0001
NC vs. NP	Yes	**	0.0087
NC vs. NEP	Yes	*	0.0375
NE vs. NP	Yes	****	<0.0001
NE vs. NEP	Yes	****	<0.0001
NP vs. NEP	Yes	****	<0.0001

Tukey's multiple comparisons test	Significant?	Summary	Adjusted P Value
OC vs. OE	No	ns	0.9965
OC vs. OP	Yes	*	0.0414
OC vs. OEP	No	ns	0.9336
OC vs. NC	No	ns	0.3868
OC vs. NE	No	ns	0.5059
OC vs. NP	No	ns	0.4049
OC vs. NEP	No	ns	0.4056
OE vs. OP	No	ns	0.1412
OE vs. OEP	No	ns	0.9996
OE vs. NC	No	ns	0.7717
OE vs. NE	No	ns	0.8740
OE vs. NP	No	ns	0.7900
OE vs. NEP	No	ns	0.7907
OP vs. OEP	No	ns	0.3010
OP vs. NC	No	ns	0.8721
OP vs. NE	No	ns	0.7691
OP vs. NP	No	ns	0.8574
OP vs. NEP	No	ns	0.8568
OEP vs. NC	No	ns	0.9542
OEP vs. NE	No	ns	0.9865
OEP vs. NP	No	ns	0.9613
OEP vs. NEP	No	ns	0.9616
NC vs. NE	No	ns	>0.9999
NC vs. NP	No	ns	>0.9999
NC vs. NEP	No	ns	>0.9999
NE vs. NP	No	ns	>0.9999
NE vs. NEP	No	ns	>0.9999
NP vs. NEP	No	ns	>0.9999

Tukey's multiple comparisons test	Significant?	Summary	Adjusted P Value
OC vs. OE	Yes	**	0.0058
OC vs. OP	Yes	****	<0.0001
OC vs. OEP	Yes	****	<0.0001
OC vs. NC	Yes	*	0.0185
OC vs. NE	Yes	****	<0.0001
OC vs. NP	Yes	****	<0.0001
OC vs. NEP	No	ns	0.1346
OE vs. OP	Yes	****	<0.0001
OE vs. OEP	Yes	****	<0.0001
OE vs. NC	Yes	****	<0.0001
OE vs. NE	Yes	****	<0.0001
OE vs. NP	Yes	****	<0.0001
OE vs. NEP	Yes	****	<0.0001
OP vs. OEP	No	ns	0.7562
OP vs. NC	No	ns	0.1098
OP vs. NE	Yes	**	0.0079
OP vs. NP	No	ns	0.9811
OP vs. NEP	Yes	*	0.0148
OEP vs. NC	Yes	**	0.0055
OEP vs. NE	No	ns	0.1513
OEP vs. NP	No	ns	0.9967
OEP vs. NEP	Yes	***	0.0007
NC vs. NE	Yes	****	<0.0001
NC vs. NP	Yes	*	0.0203
NC vs. NEP	No	ns	0.9547
NE vs. NP	Yes	*	0.0452
NE vs. NEP	Yes	****	<0.0001
NP vs. NEP	Yes	**	0.0025

Tukey's multiple comparisons test	Significant?	Summary	Adjusted P Value
OC vs. OE	No	ns	0.3815
OC vs. OP	No	ns	0.0744
OC vs. OEP	Yes	***	0.0006
OC vs. NC	No	ns	0.1051
OC vs. NE	Yes	****	<0.0001
OC vs. NP	Yes	***	0.0003
OC vs. NEP	No	ns	0.3003
OE vs. OP	No	ns	0.9660
OE vs. OEP	Yes	*	0.0414
OE vs. NC	No	ns	0.9893
OE vs. NE	Yes	**	0.0040
OE vs. NP	Yes	*	0.0252
OE vs. NEP	No	ns	>0.9999
OP vs. OEP	No	ns	0.2422
OP vs. NC	No	ns	>0.9999
OP vs. NE	Yes	*	0.0288
OP vs. NP	No	ns	0.1594
OP vs. NEP	No	ns	0.9878
OEP vs. NC	No	ns	0.1784
OEP vs. NE	No	ns	0.9201
OEP vs. NP	No	ns	>0.9999
OEP vs. NEP	No	ns	0.0571
NC vs. NE	Yes	*	0.0199
NC vs. NP	No	ns	0.1148
NC vs. NEP	No	ns	0.9974
NE vs. NP	No	ns	0.9767
NE vs. NEP	Yes	**	0.0056
NP vs. NEP	Yes	*	0.0350

Figure 4.27: **Confinement of mammary gland development under the absence of ovary based hormone in ovariectomized Rat:** Comparative immunohistochemistry for Beta-actin, ZEB (Zinc Finger E-Box Binding Homeobox 1), Twist, and Krt8, during different developmental stages of the mammary gland under artificially mimicking the natural hormonal rhythm condition in ovariectomized rat.

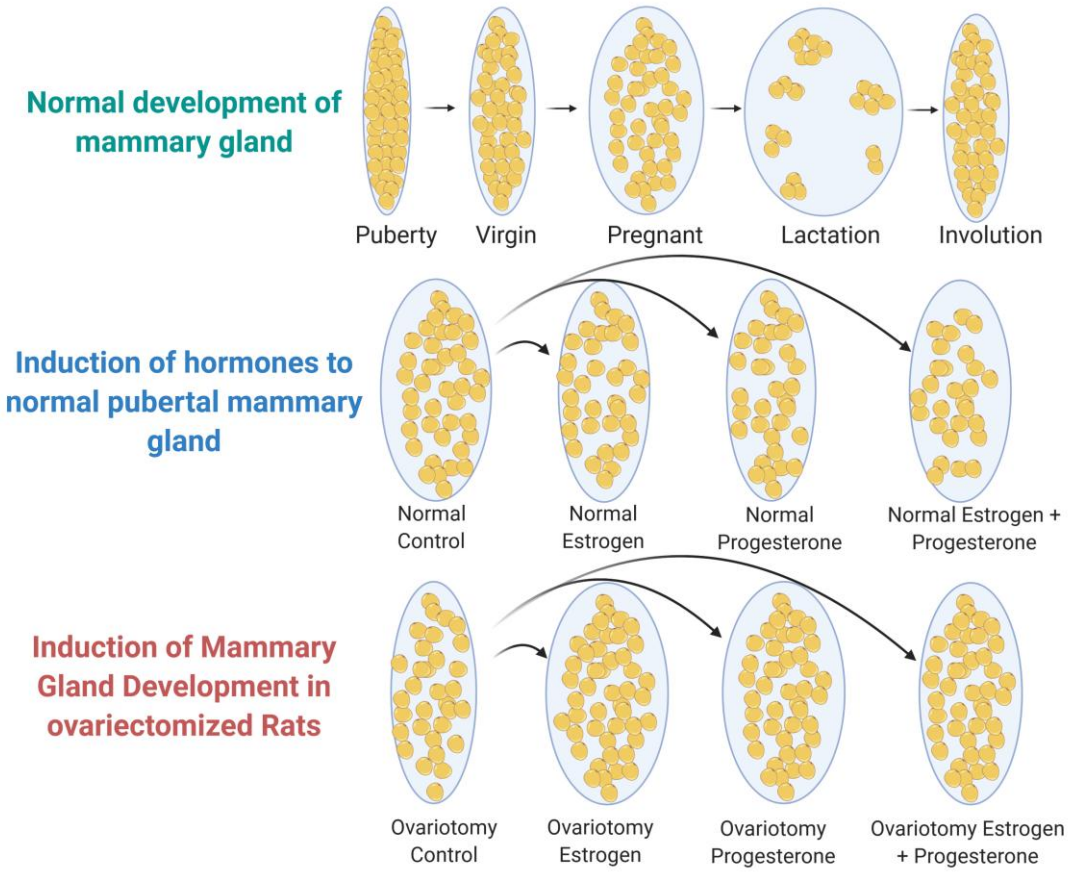

Figure 4.28: **Schematic presentation:** Differential adipogenesis event in the normal development of the mammary gland compared to OVX (hormone treated) with normal (hormone treated) mammary gland.

4.2 Comparative phosphoproteome analysis of mammary epithelial cell line for identification of ubiquitous expression of proteins

4.2.1 Comparison of BuMEC and EpH4 phosphoproteome

Total phosphoproteome comparison between EpH4 and BuMEC cells resulted in the identification of 7036 and 8468 phosphoprotein, respectively (Figure 4.29). The representative unique phosphopeptides mapped were 7060 and 14287 in BuMEC and EpH4, respectively. Albite, we discovered 2552 identical phosphopeptides with identical phosphosites in both the interspecies mammary epithelial cell lines. Interestingly, BuMEC cell lines contain 30% fewer phosphopeptides than EpH4, but the phosphoproteome is almost similar (difference 45-55%). The comparison at the concentration level (in ng for individual proteins) of the phosphoproteome in both the cell lines showed similar patterns except few variant proteins (Figure 4.29).

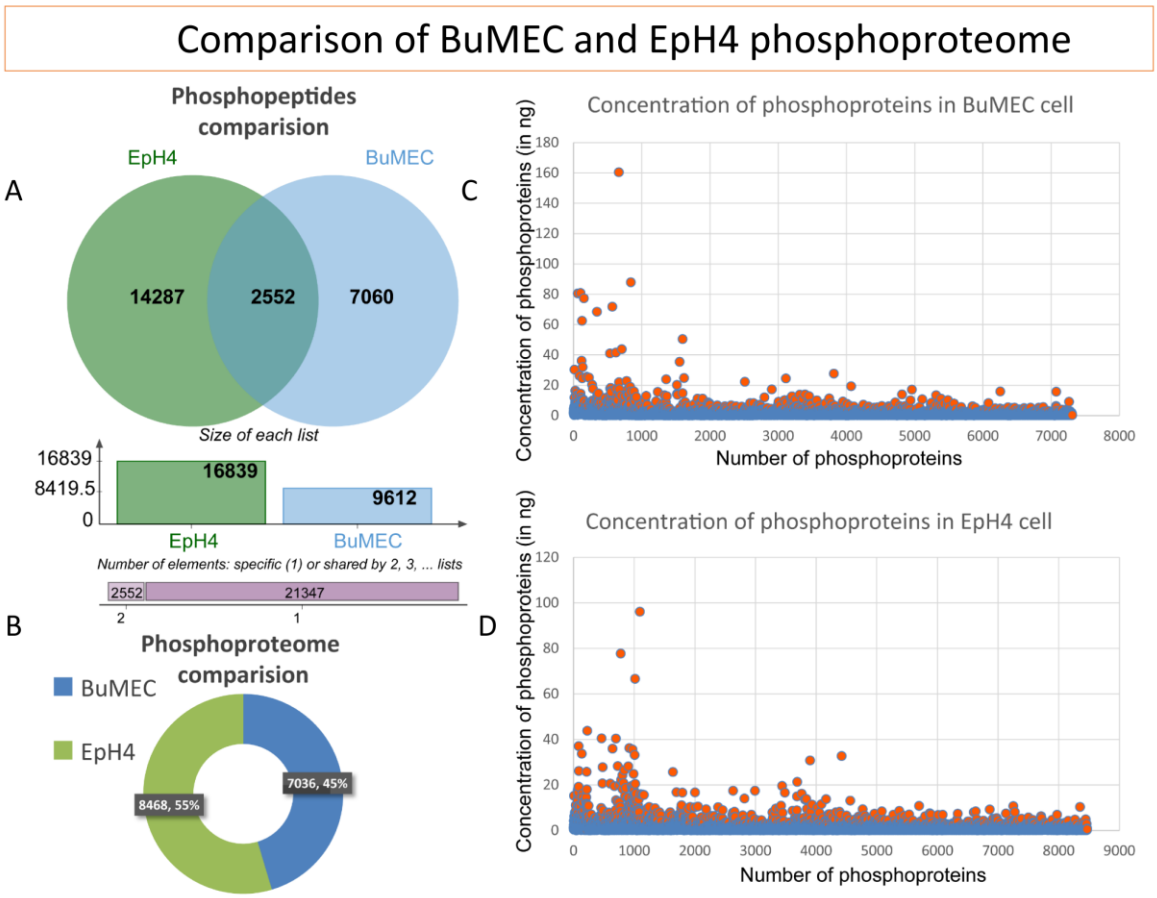

Figure 4.29: **Comparison of BuMEC and EpH4 phosphoproteome: A**. Common and the unique number of phosphopeptides identified. **B**. Total phosphoproteome qualitative difference. **C**. Concentration of phosphoproteins in BuMEC cell line. **D**. Concentration variation in phosphoproteins of EpH4 cell line.

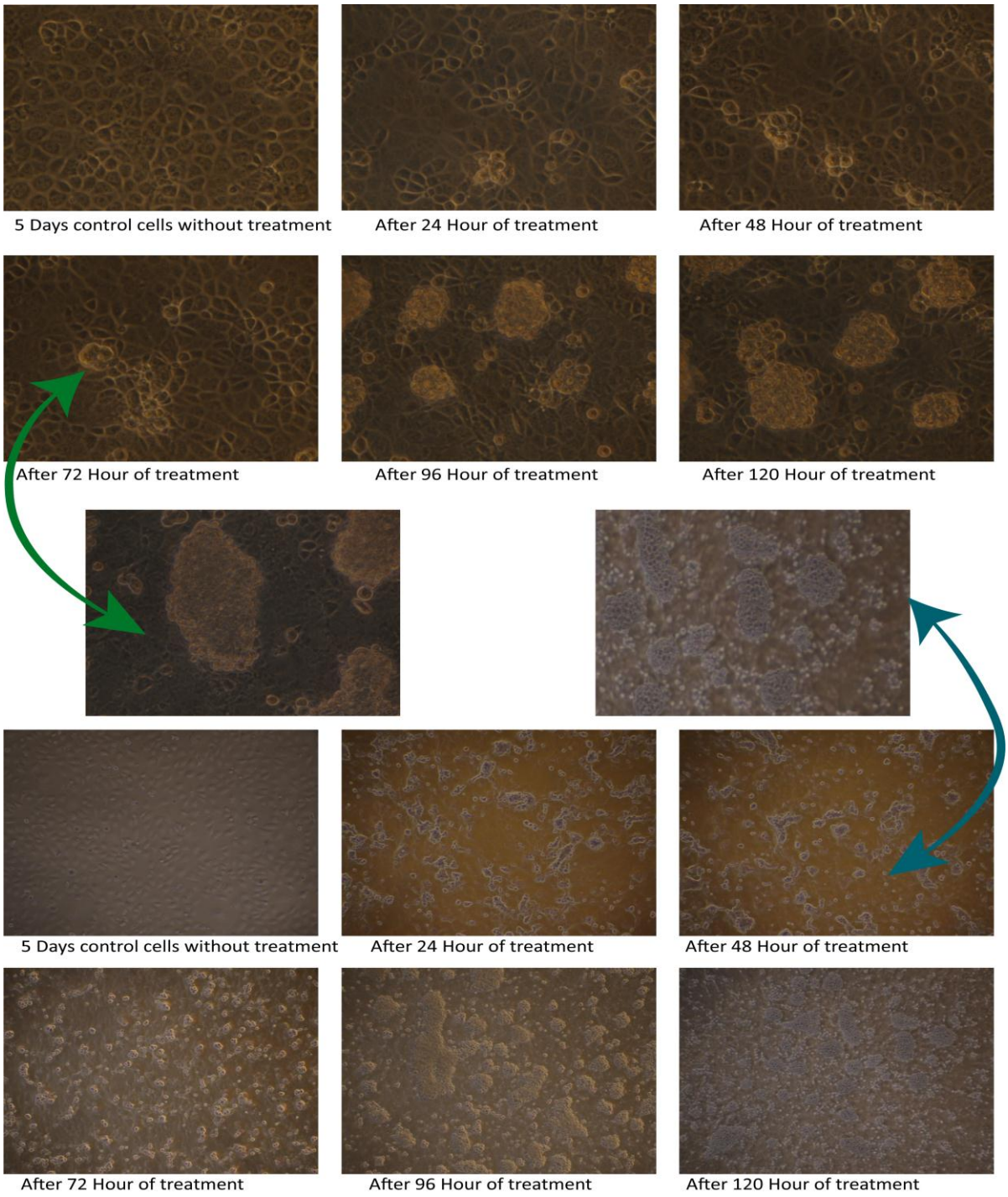

Figure 4.30: **Induction of end terminal differentiation:** BuMEC cells were treated with a hormonal cocktail to induce end terminal differentiation. Hormones used for the treatment are Estrogen, Progesterone, Prolactin and Dexamethasone. The image was taken at 40X objective lens for the final 400 times magnification. EpH4 cells were treated with a hormonal cocktail for the induction of end terminal differentiation. Hormones used for the treatment are Estrogen, Progesterone, Prolactin and Dexamethasone. The image was taken at 10X objective lens for the final 100 times magnification.

4.2.2 Lactogenic differentiation of BuMEC and EpH4 phosphoproteome

We sought to understand the differential expression of phosphoproteome upon lactogenic hormone exposure for six days. For the first day, we take out the control cell at 70% confluency, for the second day acclimatise the cell with estrogen and progesterone with 10 and 100nM, respectively. For the third day onwards, we treated the acclimatize cells with Estrogen = 5 nM, Progesteron = 50 nM, Prolactin= 5 ug/ml, Dexamethasone = 1 um, and BI=5ug/ml for both BuMEC and EpH4 cell lines. The fifth day of the experiment showed absolute alveoli like structures formation, clear from figure 4.30. The morphological analysis showed the end terminal differentiation of both the cell lines. It describes that our cocktail of hormone treatment resulted in lactogenic functional differentiation. These differentiated cells were used to enrich phosphopeptides from individual days of both cell line to study comparative phosphoproteome involvement.

We performed the TMT labelled phosphoproteomics analysis for both the cell lines in all six respective days. The detailed illustrative image describes the workflow (Figure 3.3; 3.7 and 3.8). Briefly, we used IMAC and TiO2 technique to enrich the phosphopeptides, followed with an equal concentration of peptides labelling with six different TMT channels and mass spectrometer acquisition (Figure 3.7 and 3.8, please detailed refer to methodology section). The fractions run in the mass spectrometer instrument resulted in the phosphopeptides' identical elution, as shown by the liquid chromatography chromatogram (Figure 4.31). We used five search engine analyses to localise the phosphorylation residue with high confident values with the least false discovery rate (FDR). Finally, combining all the time-lapse data of six different days represents the in-depth discovery of proteome and phosphoproteome so far determined to intercomparison two cell lines.

The six-plex TMT channels were used for individual day labelling and data were acquired using a high-resolution mass spectrometer (Thermo Orbitrap fusion MS instrument with the combination of HCD and CID). The combined five search engine analysis result revealed 5,451 phosphorylated proteins identified containing 13,855 phosphopeptides with more than 25,000 phosphosites in BuMEC cells. The total proteins identified were 8245. The site localisation occupancy was determined to be 8:6:2 phosphorylation event in STY amino acid

residue, respectively. Interestingly, the average number of phosphopeptide identified per day was 9,500; however, the second day contains only 6000 peptides. The complete spatial-temporal distribution of STY phosphorylation status is shown in figure 4.32. Next, we compare the unique and common phosphopeptide, phosphoprotein among all the days. Figure 4.32 showed a detailed result.

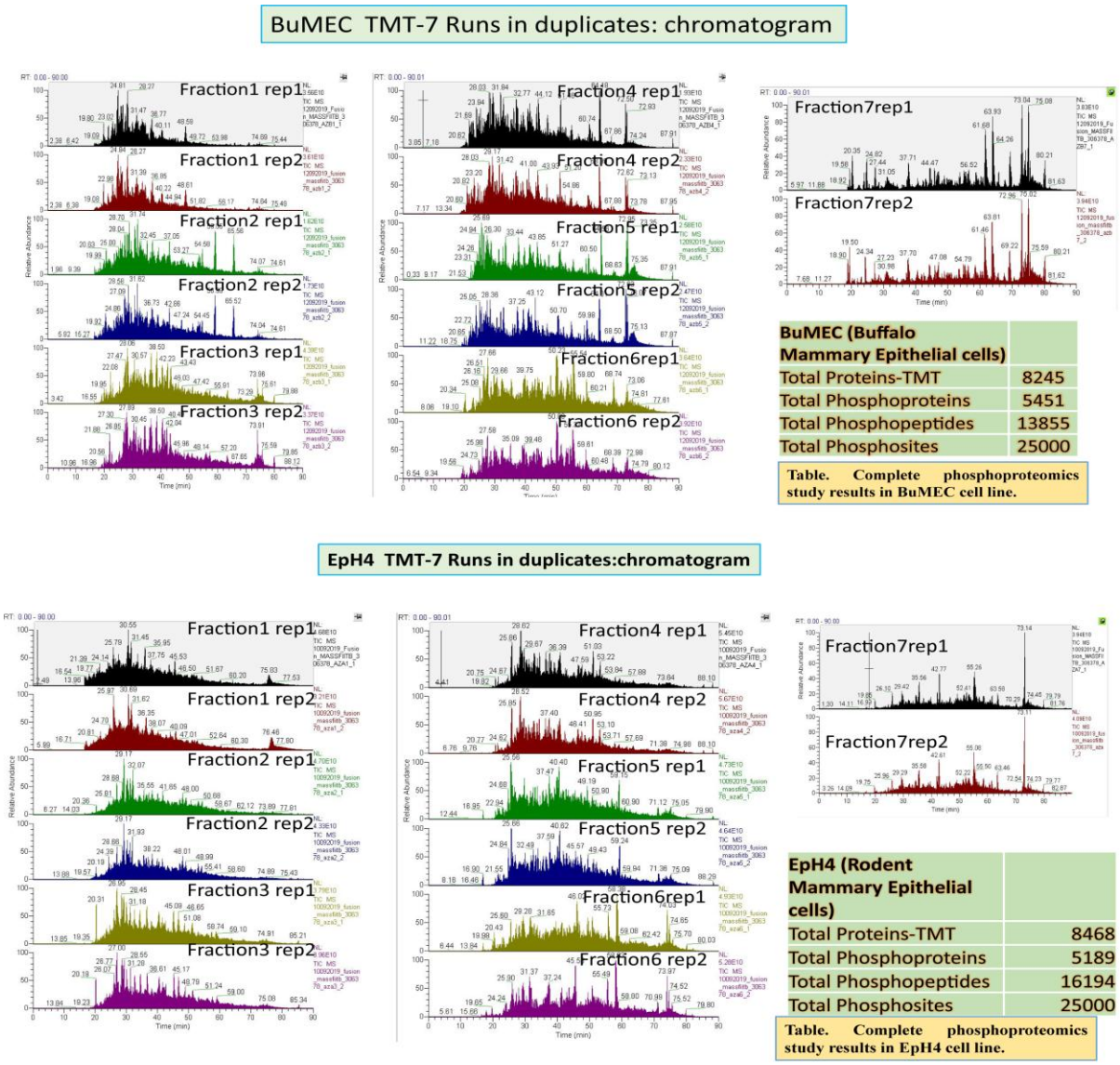

Figure 4.31 **BuMEC TMT-7 Runs in duplicates chromatogram**: LC Chromatogram graphs describing the comparison of peptides elution in complete BuMEC cell line phosphoproteomics study duplicates. **EpH4 TMT-7 Runs in duplicates chromatogram:** LC Chromatogram graphs describing the comparison of peptides elution in complete EpH4 cell line phosphoproteomics study in duplicates.

Similarly, EpH4 based phosphoproteomics study of lactogenic differentiation resulted in the discovery of 5,189 phosphorylated proteins identified containing 16,194 phosphopeptides with more than 25,000 phosphosites. The total proteins identified were 8,468. For EpH4 cell line the site localisation occupancy was determined to be 7:7:5 phosphorylation event in STY amino acid residue, respectively. On average, we found 10,000 phosphopeptides per day of differentiation except day two, where it is 7,798. The detailed STY phosphorylation of spatial-temporal expression profile for each day was presented in figure 4.33. For the same, we check the common and unique phosphopeptides and phosphoprotein identification in all the six days (Figure 4.33).

As we performed the lactogenic differentiation, we sought to identify the milk specific protein in both the cell line. Amazingly, BuMEC showed ten milk specific protein, including alpha, beta, and kappa-casein proteins. These proteins expression levels were high from the third day onwards as estimated based on our experiment. Contrary, we found eight milk specific proteins in EpH4 cell line. However, we were not able to identify kappa-casein but alpha and beta were present. Here, these milk-specific proteins expression level was high from the third day onwards (Figure 4.34).

4.2.3 Comparison of differentiation stages of Eph4 cell line upon hormone treatment

We perform the hierarchical clustering of identified proteins among all the days in both the cell lines. The result showed the common pattern of identification between cells (BuMEC and EpH4) upon hormone treatment. The HCA analysis was performed using the Euclidian clustering, and that is why it resulted in the hard cluster. Therefore, to get the clean differential cluster, we choose the fuzzy CMean clustering algorithm for our TMT labelled phosphoproteome data sets. For both the cell lines, we performed the membership plot and distributed in six clusters. In the case of BuMEC cluster one contains 2091, cluster two 825, cluster three 512, cluster four 750, cluster five 401, and cluster six 872 accomplishing phosphoproteins. Similarly, in case EpH4 cluster one contains 544, cluster two 1025, cluster three 636, cluster four 1185, cluster five 642, and cluster six 1156 containing phosphoproteins (Figure 4.35).

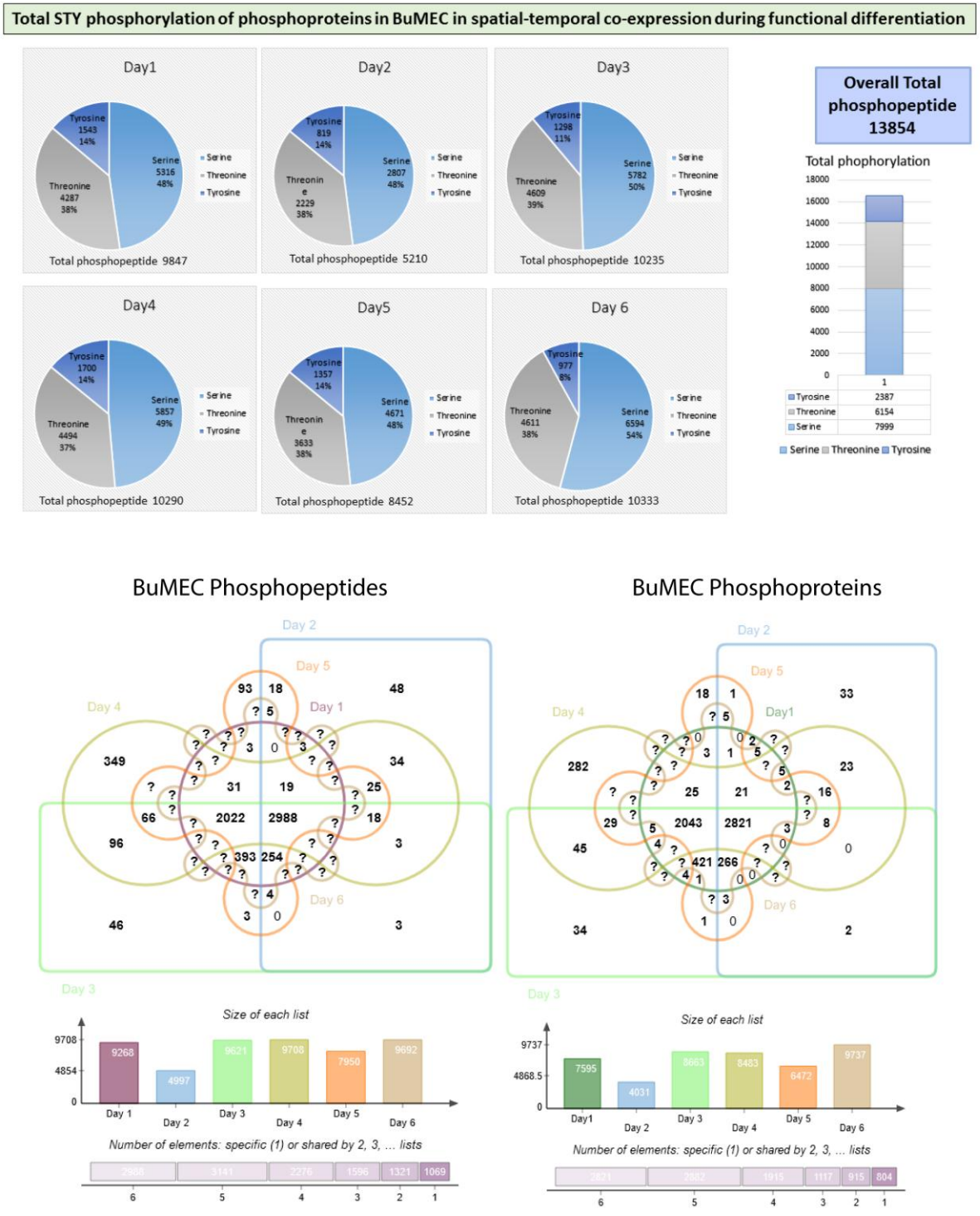

Figure 4.32: **Phosphoproteome comparison BuMEC**: Analyzed phosphorylation in BuMEC mammary cells line while mimicking the natural lactogenic condition through hormones **A**. Common and the unique number phosphopeptides identified. **B**. Common and the unique number of phosphoproteins identified.

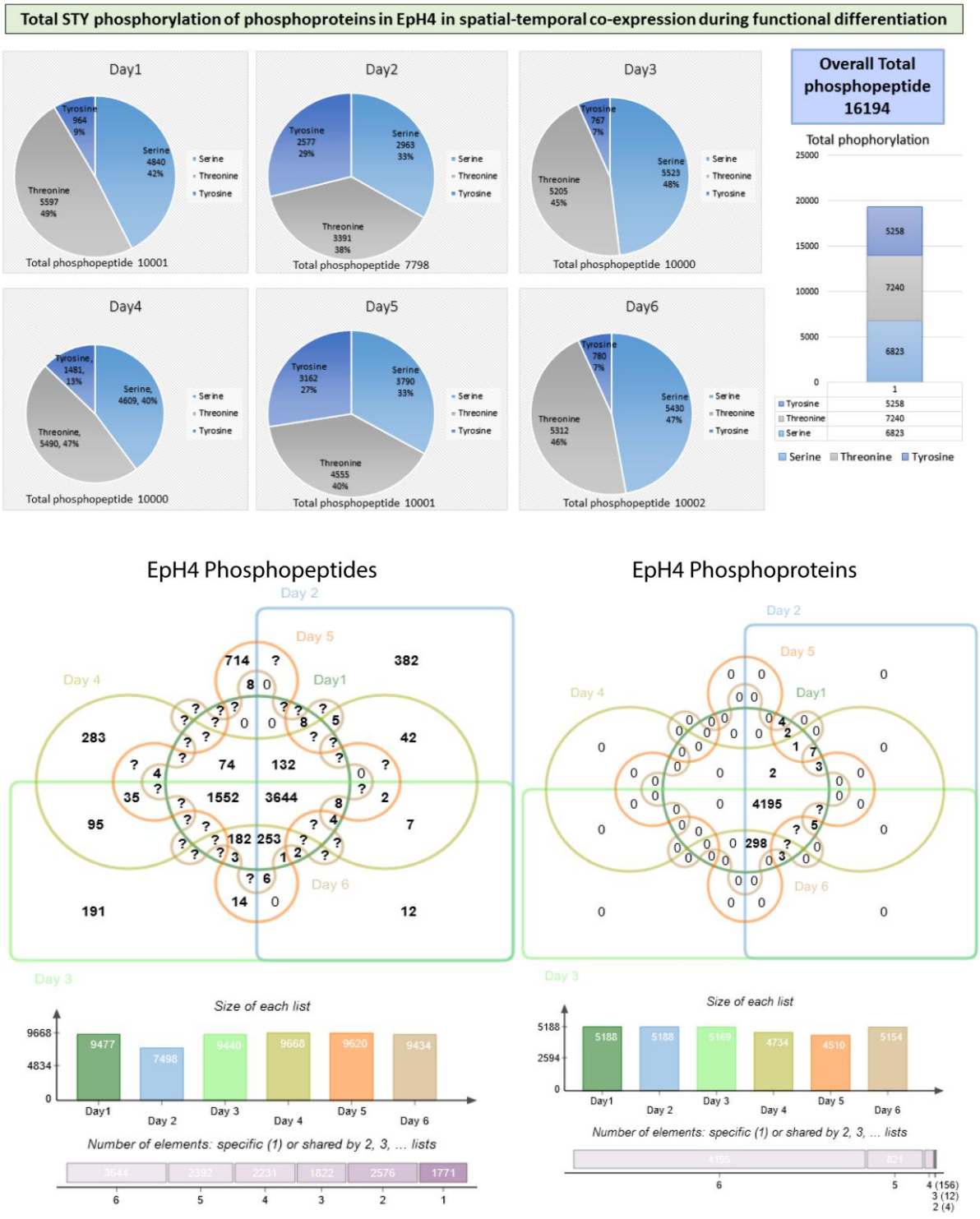

Figure 4.33: **Phosphoproteome comparison EpH4**: Analyzed phosphorylation status in EpH4 mammary cells line while mimicking the natural lactogenic condition through hormones. **A**. Common and the unique number of phosphopeptides identified. **B**. Common and the unique number of phosphoproteins identified.

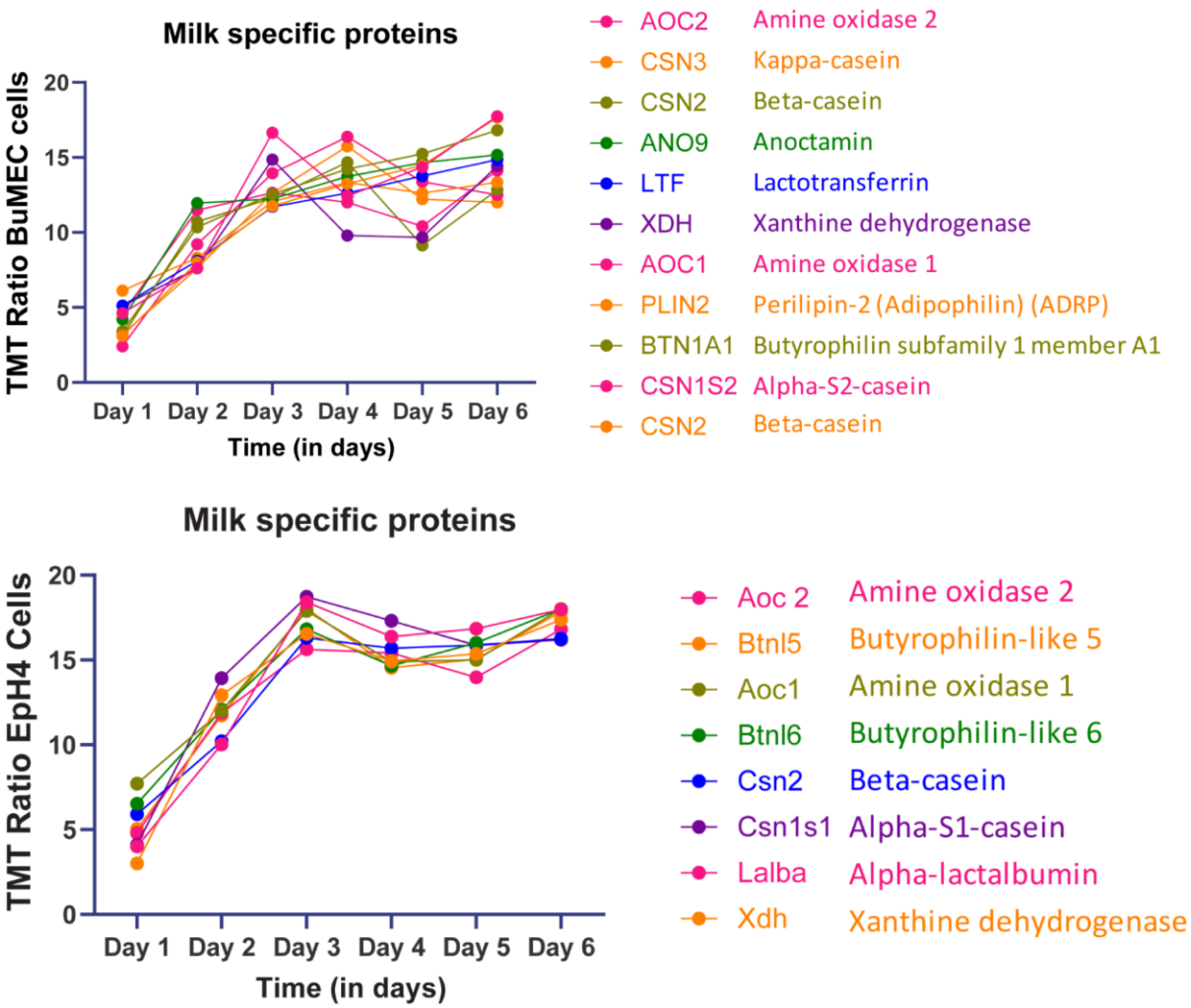

Figure 4.34: **Quantitative comparisons of milk specific proteins in BuMEC and EpH4 cell line:** Quantitative comparisons of ten milk specific proteins identified in BuMEC and EpH4 cell line during six days of differentiation. X-axis describes the number of days while Y-axis is the total concentration of TMT reporter ions quantified in each day of differentiation.

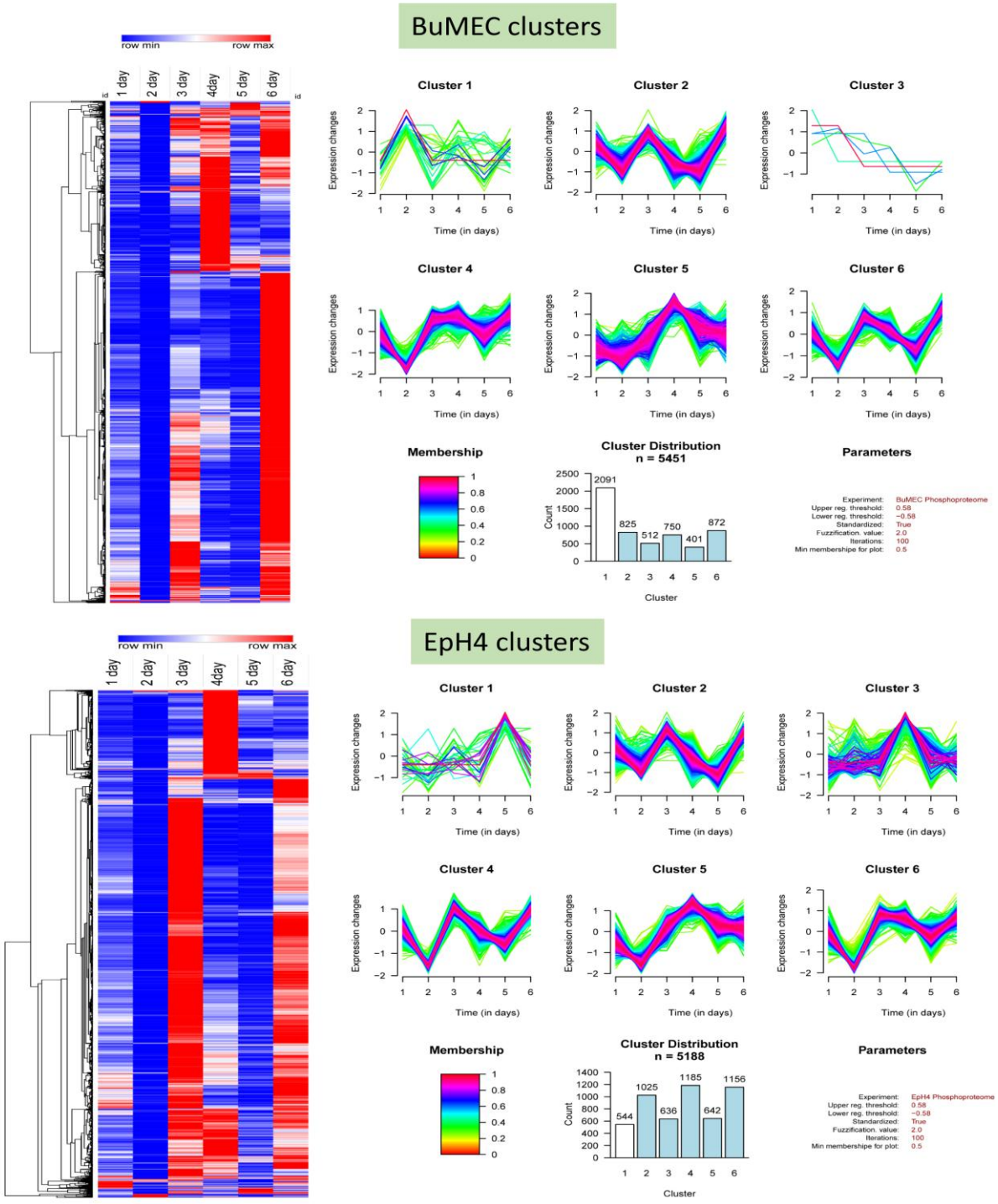

Figure 4.35: **Comparison of differentiation stages of BuMEC and EpH4 cell line upon hormone treatment:** Hierarchical clustering based comparison of normalized data. Membership plot for cluster formation in TMT phosphoproteome data.

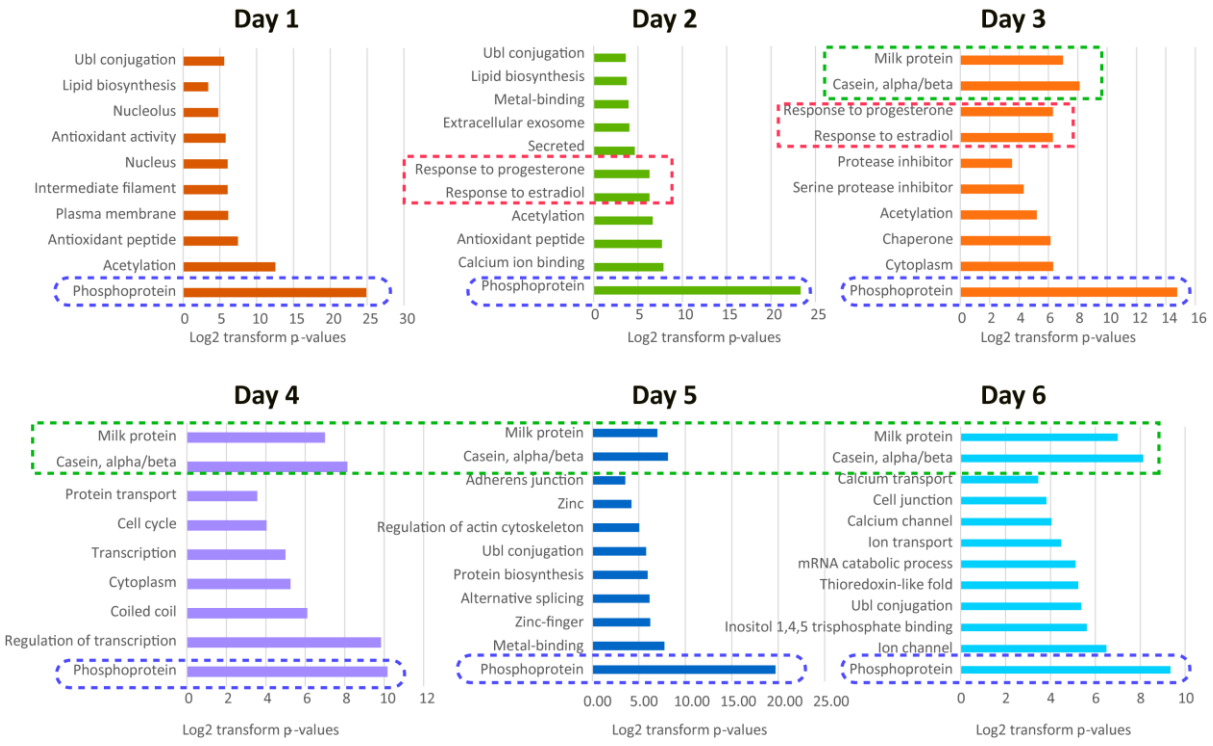

Figure 4.36: **Comparison of terms identified for BuMEC and EpH4 Lactogenic differentiation:** Day-wise comparison of shared terms identified in both cell line (BuMEC and EpH4) upon stimulation with hormones Lactogenic differentiation.

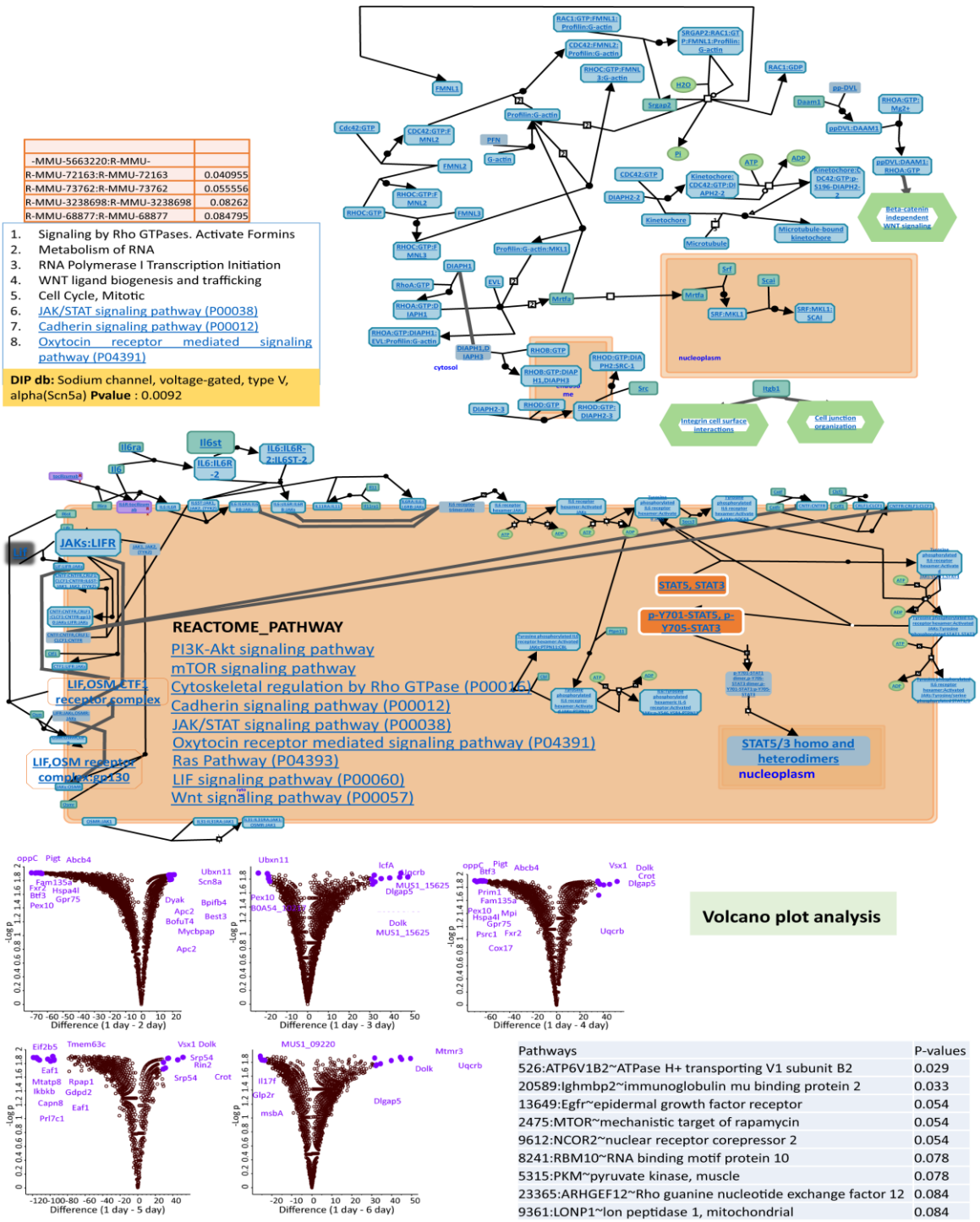

Figure 4.37: **Clustered isolated and enriched pathways: Volcano plot analysis:** Day-wise comparison of shared phosphoproteins identified in both cell line (BuMEC and EpH4) upon stimulation with hormones for Lactogenic differentiation.

4.2.4 Comparison of the shared term between BuMEC and EpH4 phosphoproteome

The complete differentially expressed identified phosphoprotein were used for mapping the common terms in both the cell lines. The histogram showed detailed information of top enriched critical terms for all six days (Figure 4.36). It is important to report here that all the days contains phosphoprotein as the highest enriched key term. This analysis also verifies our experimental design of lactogenic differentiation. Reporting the identification of protein-specific to respond progesterone and estrogen on day two and three. In a similar manner, the data showed continuous expression of milk protein (casein alpha-beta) on the third, fourth, fifth and sixth day. The following result also highlights the cross talk of acetylation and phosphorylation for early lactogenic differentiation in day one, two and three. However, adherens junction and cell junction phosphoproteins were seen in day fifth and sixth of differentiation. Suggesting the restructuring of the cellular organisation for creating the functional state. In summary, the comparative phosphoproteome result identified and verified that our hormonal induction on these cell lines is successful.

4.2.5 Comparative cluster 5 analysis

Based on the fuzzy c mean clustering results, we selected cluster five and six from both cell line. Both clusters showed the spiked increase in proteins expression from the third day till the sixth day of differentiation. The collective mapping of proteins related to pathways from cluster five showed the significant enrichment pathways that are signalling by Rho GTPases, activate formins; metabolism of RNA; RNA Polymerase I transcription initiation; WNT ligand biogenesis and trafficking; cell cycle, mitotic; JAK/STAT signalling pathway (P00038); cadherin signalling pathway (P00012); and oxytocin receptor-mediated signalling pathway (P04391). The results validate the previous finding in vivo studies and describe the significance of redundantly identifying pathways. The detailed description of the pathway was fetched from KEGG and REACTOME database and plotted the connection (Figure 4.37).

We created PPI interaction using 642 phosphoproteins from cluster five. We found the interaction of proteins-nodes: 358, among them connection-number of edges: 403, average node degree: 2.25, average local clustering coefficient: 0.378, expected number of edges: 377 finally the PPI enrichment p-value: 0.0952. The mapping of an identified interactome for biological process showed the cluster's relevance for the cellular functioning. The detailed description of the biological findings as detailed in table 5 below.

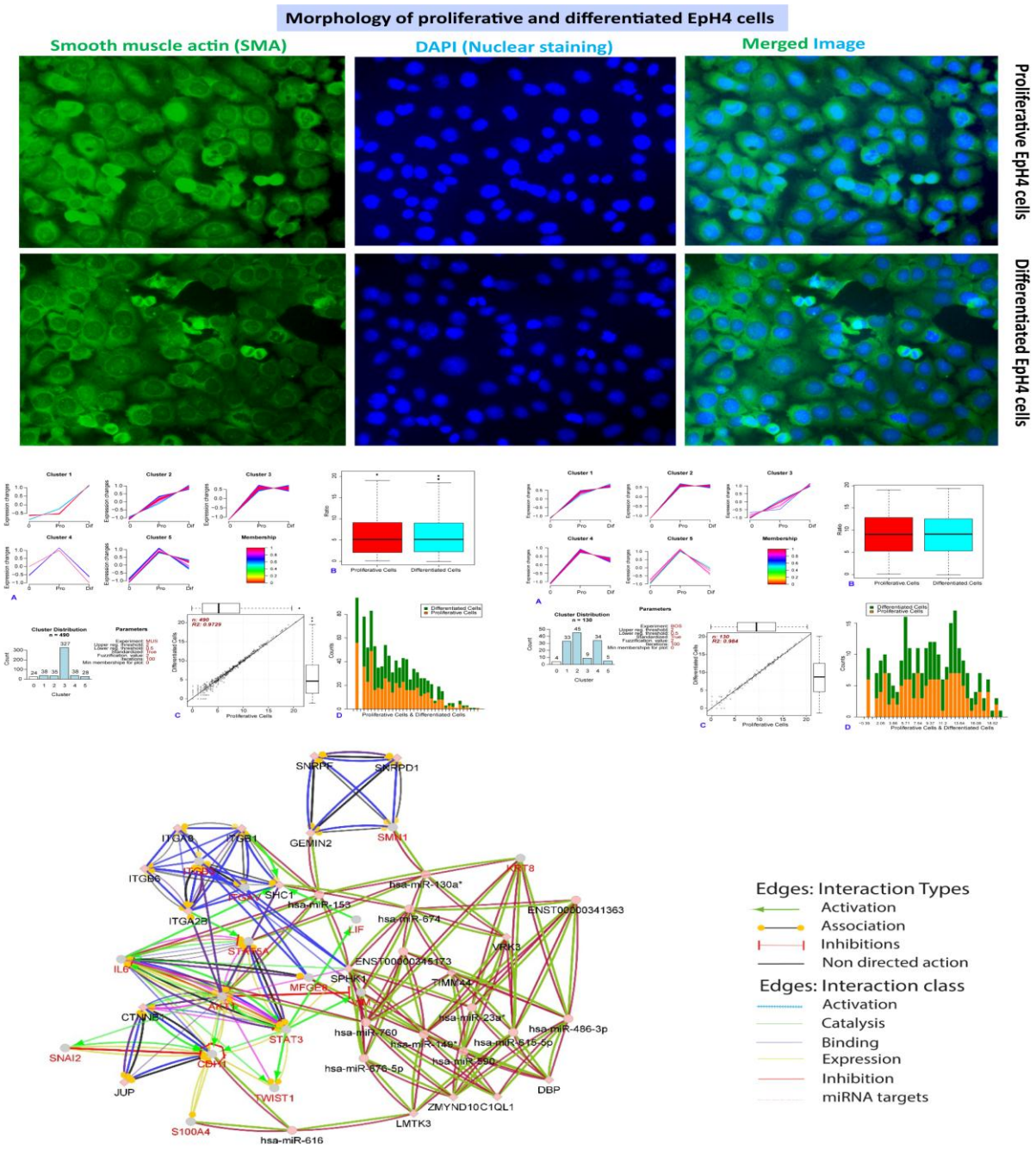

Figure 4.38: **Immunofluorescence staining:** Smooth muscle actin (SMA) protein with DAPI staining A. Membership plot of cluster formation in EpH4 cell line dataset. B. Boxplot comparison. C. Scatter plot D. Histogram comparison. Membership plot of cluster formation in BuMEC cell line dataset. B. Boxplot comparison. C. Scatter plot D. Histogram comparison. Important identified miRNAs are **miRNA-335p and miRNA-146a. The directed network of phosphoproteome-miRNA interactome:** A directed network of combined data interactome. The network analysis of directly interacted miRNAs and their associated phosphoproteins partners were identified as significantly ($p<0.001$) differentially expressed combined analysis.

Table 4.5: Biological processes associated with the classified cluster 5 phosphoproteins.

Biological process	term description	observed gene count	strength	false discovery rate
GO:0009987	cellular process	249	0.09	0.0012
GO:0050794	regulation of cellular process	193	0.12	0.0013
GO:0050789	regulation of biological process	201	0.11	0.0016
GO:0065007	biological regulation	210	0.1	0.0016
GO:0007017	microtubule-based process	26	0.43	0.0064
GO:0000226	microtubule cytoskeleton organization	20	0.49	0.0087
GO:0007275	multicellular organism development	109	0.16	0.0087
GO:0031109	microtubule polymerization or depolymerization	7	0.97	0.0087
GO:0032502	developmental process	120	0.15	0.0087
GO:0060255	regulation of macromolecule metabolic process	121	0.15	0.0087
GO:0006996	organelle organization	73	0.2	0.0122
GO:0048856	anatomical structure development	113	0.15	0.0122
GO:0016043	cellular component organization	105	0.15	0.0218
GO:0071840	cellular component organization or biogenesis	108	0.15	0.0218
GO:0019222	regulation of metabolic process	123	0.13	0.0292
GO:0032501	multicellular organismal process	128	0.13	0.0292
GO:0051171	regulation of nitrogen compound metabolic process	113	0.14	0.0292
GO:0006139	nucleobase-containing compound metabolic process	87	0.16	0.0402
GO:0048731	system development	94	0.15	0.0402
GO:0080090	regulation of primary metabolic process	114	0.13	0.0412
GO:0010468	regulation of gene expression	87	0.16	0.0424
GO:0048522	positive regulation of cellular process	107	0.14	0.0479

4.2.6 Comparative cluster 6 analysis

Based on the profile plot we choose cluster also. The pathways enrichment analysis resulted in identifying nine key pathways that are PI3K-Akt; mTOR; Cadherin; JAK/STAT; Oxytocin receptor-mediated; LIF; and Wnt signalling pathways. The results validate the previous finding in vivo studies and describe the significance of redundantly identifying pathways. The detailed description of the pathway was fetched from KEGG and REACTOME database and plotted the connection (Figure 4.37).

We created PPI interaction using 1,156 phosphoproteins from cluster six. We found the interaction of proteins-number of nodes: 653; the number of edges: 1456; average node degree: 4.46; avg. local clustering coefficient: 0.352; expected number of edges: 1290; and PPI enrichment p-value: 2.93e-06. The mapping of an identified interactome for biological process showed the cluster's relevance for the cellular functioning. The detailed description of the biological findings as detailed in Table 6 below.

Table 4.6: Biological processes associated with the classified cluster 6 phosphoproteins.

Biological process	term description	observed gene count	strength	false discovery rate
GO:0009987	cellular process	460	0.1	1.77E-09
GO:0065007	biological regulation	394	0.12	1.77E-09
GO:0050789	regulation of biological process	368	0.11	9.78E-08
GO:0050794	regulation of cellular process	351	0.12	9.78E-08
GO:0008152	metabolic process	314	0.11	7.44E-06
GO:0071704	organic substance metabolic process	301	0.12	7.44E-06
GO:0044237	cellular metabolic process	286	0.12	1.99E-05
GO:0022607	cellular component assembly	103	0.24	4.82E-05
GO:0048522	positive regulation of cellular process	202	0.15	4.82E-05
GO:0006807	nitrogen compound metabolic process	271	0.12	6.33E-05
GO:0016043	cellular component organization	192	0.15	6.33E-05
GO:0071840	cellular component organization	197	0.15	7.89E-05

	or biogenesis			
GO:0006793	phosphorus metabolic process	92	0.24	9.22E-05
GO:0006796	phosphate-containing compound metabolic process	91	0.24	9.29E-05
GO:0044238	primary metabolic process	282	0.11	0.00012
GO:0034329	cell junction assembly	15	0.7	0.00029
GO:0034330	cell junction organization	17	0.59	0.0013
GO:0032501	multicellular organismal process	225	0.11	0.0022
GO:0038127	ERBB signaling pathway	10	0.81	0.0022
GO:0044260	cellular macromolecule metabolic process	204	0.12	0.0022
GO:0019222	regulation of metabolic process	216	0.11	0.0023
GO:0007275	multicellular organism development	182	0.13	0.0033
GO:0048856	anatomical structure development	192	0.12	0.0033
GO:0006996	organelle organization	121	0.16	0.0036
GO:0007049	cell cycle	58	0.26	0.0036
GO:0043933	protein-containing complex subunit organization	72	0.22	0.0037
GO:0060255	regulation of macromolecule metabolic process	202	0.11	0.0039
GO:0007173	epidermal growth factor receptor signaling pathway	9	0.81	0.0043
GO:0019538	protein metabolic process	146	0.14	0.0056
GO:0044267	cellular protein metabolic process	126	0.15	0.0058
GO:0032502	developmental process	199	0.11	0.0069
GO:0080090	regulation of primary metabolic process	198	0.11	0.0069
GO:0051171	regulation of nitrogen compound metabolic process	193	0.11	0.0087
GO:0016310	phosphorylation	54	0.25	0.0091
GO:0030183	cell differentiation	12	0.62	0.0091
GO:0006464	cellular protein modification process	106	0.16	0.0111
GO:0045216	cell-cell junction organization	14	0.55	0.0111
GO:0048731	system development	160	0.12	0.0111

GO:0031325	positive regulation of cellular metabolic process	124	0.14	0.0117
GO:0007043	cell-cell junction assembly	9	0.72	0.0134
GO:0043412	macromolecule modification	111	0.15	0.0134
GO:0051056	regulation of small GTPase mediated signal transduction	19	0.44	0.0134
GO:0035023	regulation of Rho protein signal transduction	13	0.56	0.0146
GO:0051641	cellular localization	81	0.18	0.0146
GO:0065003	protein-containing complex assembly	62	0.21	0.0202
GO:0051726	regulation of cell cycle	49	0.24	0.0214
GO:0007041	lysosomal transport	10	0.63	0.0241
GO:0071902	positive regulation of protein serine/threonine kinase activity	22	0.38	0.0241
GO:0032147	activation of protein kinase activity	21	0.39	0.0258
GO:0002520	immune system development	38	0.27	0.0265
GO:0023051	regulation of signaling	126	0.13	0.0284
GO:0006468	protein phosphorylation	42	0.25	0.0297
GO:0009893	positive regulation of metabolic process	128	0.13	0.0297
GO:0048869	cellular developmental process	139	0.12	0.0297
GO:0030154	cell differentiation	136	0.12	0.0309
GO:0030097	hemopoiesis	34	0.28	0.0329
GO:0007229	integrin-mediated signaling pathway	9	0.64	0.0338
GO:0034641	cellular nitrogen compound metabolic process	161	0.11	0.0377
GO:0002376	immune system process	75	0.17	0.0399
GO:0048534	hematopoietic or lymphoid organ development	36	0.27	0.0399
GO:0048646	anatomical structure formation involved in morphogenesis	45	0.23	0.0406
GO:0008333	endosome to lysosome transport	7	0.73	0.0438
GO:0051347	positive regulation of transferase activity	32	0.28	0.0476
GO:0007044	cell-substrate junction assembly	6	0.8	0.0482

GO:0010647	positive regulation of cell communication	71	0.17	0.0482
GO:0051639	actin filament network formation	4	1.09	0.0483
GO:0033674	positive regulation of kinase activity	29	0.29	0.049
GO:0010646	regulation of cell communication	123	0.12	0.05
GO:1903727	positive regulation of phospholipid metabolic process	7	0.71	0.05

Further, we analyse the volcano plot to show the significance of unique proteins in lactogenic differentiation days. The data were detailed in figure 4.37 of volcano plots.

4.2.7 NGS based miRNA Profiling and quantification

For the same cell lines and treatment, we performed the miRNA seq analysis using advance NGS platform. Except for miRNA analysis, we only used two conditions which are proliferative and differentiated cells. The detailed workflow is provided in figure 4.38. The SMA staining showed the cellular population morphology differences for EpH4 cell line (Figure 4.38). It showed the presence of queen cells or dome-like structures upon hormonal treatment. The fuzzy c means clustering of both the cell lines was performed to identify the similar clusters. For EpH4 cells, the total number of miRNAs identified were n=490 and r2=0.97 while for the BuMEC the miRNAs identified were n=130 and r2=0.98. The difference in identified miRNAs between the cell lines is due to the annotation data's difference. Figure 34 details the box plot, scatter plot and histogram for both cell lines. We found the miRNA-335p and miRNA-146a as essential molecules in both cases using fuzzy membership values.

4.2.7.1 Directed network-based topological analysis of phosphoproteome-miRNA interactome

Previously identified phosphoproteins in all the datasets and miRNA from NGS analysis were used to identify the standard directed interaction network with multiple database annotation (Figure 4.39). The network determines the same 19 phosphoproteins, that we redundantly identified in the tSNE data (in vivo mammary gland dataset), RNAseq data (OVX experiment), BuMEC end terminal differentiation (lactogenic hormones induction), EpH4 end terminal differentiation (lactogenic hormones induction). Interestingly, we classified the association of interaction among each other with activation, inhibition, and non-directed. Further, the interaction class were established with a significant p-value <0.001 (Figure 4.39).

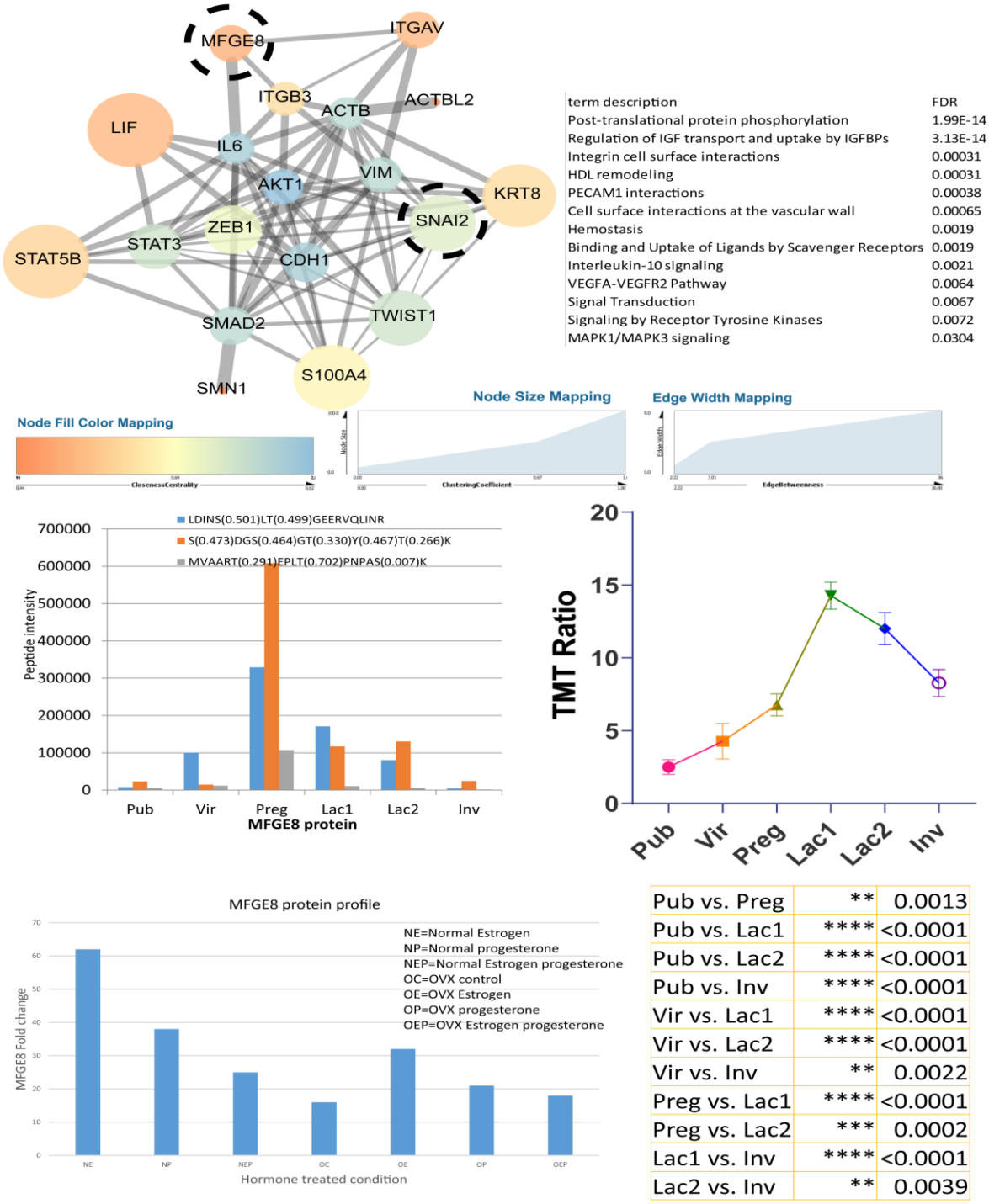

Pub vs. Preg	**	0.0013
Pub vs. Lac1	****	<0.0001
Pub vs. Lac2	****	<0.0001
Pub vs. Inv	****	<0.0001
Vir vs. Lac1	****	<0.0001
Vir vs. Lac2	****	<0.0001
Vir vs. Inv	**	0.0022
Preg vs. Lac1	****	<0.0001
Preg vs. Lac2	***	0.0002
Lac1 vs. Inv	****	<0.0001
Lac2 vs. Inv	**	0.0039

Figure 4.39: **Network-based topological analysis of phosphoproteome:** A directed network of combined data interactome. The network analysis of directly interacted miRNAs and their associated phosphoproteins partners were identified as significantly ($p<0.001$) differentially expressed combined analysis. **MFGE8 protein comparison in phosphoproteome and RNA seq data.**

From the above-described network, we fetched information classify the interaction based on the topological classification. The criteria used was closeness centrality, clustering coefficient, and edge betweenness values. The interaction network describes the identification of significant hit of post-translation modification protein phosphorylation as the top hit with FDR 1.99E-14. Further, the same contains the annotation of signal transduction (FDR 0.0067), and kinase activity (FDR 0.0072) (Figure 4.39). The network identified the two key proteins MFGE8 and SNAI2. We seek these proteins relevance in previously analysed datasets.

4.2.7.2 MFGE8 protein and phosphoprotein profile

We found the MFGE8 protein in our phosphoproteomics datasets and perform the profile analysis for protein and phosphoprotein level. The phosphoprotein contains the three phosphorylated peptides. All three peptides were multi phosphorylated and contained a total of 10 phosphosites (Figure 4.39). Amazingly, the phosphoprotein of MFGE8 expression was high at the pregnancy stage; however, its protein counterpart showed the highest expression in lactation and involution stage, making it the strong candidate for further analysis. In NGS based RNAseq analysis, we found the high upregulation of MFGE8 in normal mammary gland treated with estrogen than in comparison to other treatments (Figure 4.39).

In summary, MFGE8 phosphorylation expression is decreased in the lactataion2 while its protein level increases. We found that the kinase and MFGE8 expression has an inverse relationship while phosphatase and MFGE8 expression directly correlate. Lately, we also identified in our Difference Gel Electrophoresis (DiGE) based proteomics dataset that MFG-E8 is upregulated in MECs isolated from the high milk yielding cows (Janjanam et al., 2014). Despite the several reports emphasising the association between this molecule and various cellular physiologies, the exact mechanism, its intracellular targets, and downstream signalling circuits in MECs are unknown. The interpretation of MFG-E8 mediated regulatory control on homeostasis in healthy and diseased conditions remains poorly understood.

4.3 Targeted validation of an important phosphoprotein in cell line involved in lactation

4.3.1 Analysis of MFG-E8 protein sequence and evolutionary relationship

The mammary gland remodelling is a highly programmed, genetically controlled process involving cell death during involution that is spectacular in scope and well-organised in execution. As shown in multiple reports that MFG-E8 is an essential protein for accomplishing the involution process (Stubbs *et al.,* 1990; Lonnerdal, 2003, Atabai et al., 2005, Hanayama, R. & Nagata). This study aims to determine the associated regulatory proteins and signalling pathways linked with MFG-E8 protein through its knock-down in buffalo MECs. As the information on the role of MFG-E-8 in bovine is scanty, we examined the sequence and its domain organisation for evolutionary conservation (accession number NP_001277850.1). The MSA of MFG-E8 from 35 organisms showed the absolute conservation of the RGD motif involved in cellular interactions with cell-surface integrins (Taylor et al., 1997). However, we argued that its presence may be fortuitous and may imply another cellular process. Likewise, we determined another NPC novel conserved motif among the organisms, not discussed in the previous literature. Nonetheless, the deletion of 42 amino acid residues was observed (28th to 70th aa) in the MFG-E8 sequence of a human, baboon, Ghana monkey, and Bolivian monkey its role in evolutionary selection. Interestingly, in the same region in remaining all organisms, a conserved GGTC sequence was observed. The result implies that the later got diverged during evolution and lost 42 aa length peptide (Figure 4.40A).

Further using full-length protein MSA and different databases, we determined the five conserved domains namely: 1 signal peptide, 2 EGF domains (respective e-values are 0.000197 and 0.00000435), and 2 FA58C domains (respective e-values are 6.56e-41 and 2.01e-36) in the protein sequence which were found consistent among all 12 databases and algorithm searched; (Figure 4.40B). The conservation, quality, and consensus among protein sequences revealed that the residues from 115th to the 185th amino acid at the N-terminal is non-conserved. The results were consistent, validated by the four independent algorithms for calculating protein disorderliness (Figure 4.40C). The secondary structure prediction identified eight α-helix and twenty-two β-sheets. These results were consistent among three secondary structure programs (jnetpred, JNETPSSM, and JNETHMM) (Figure 4.40D).

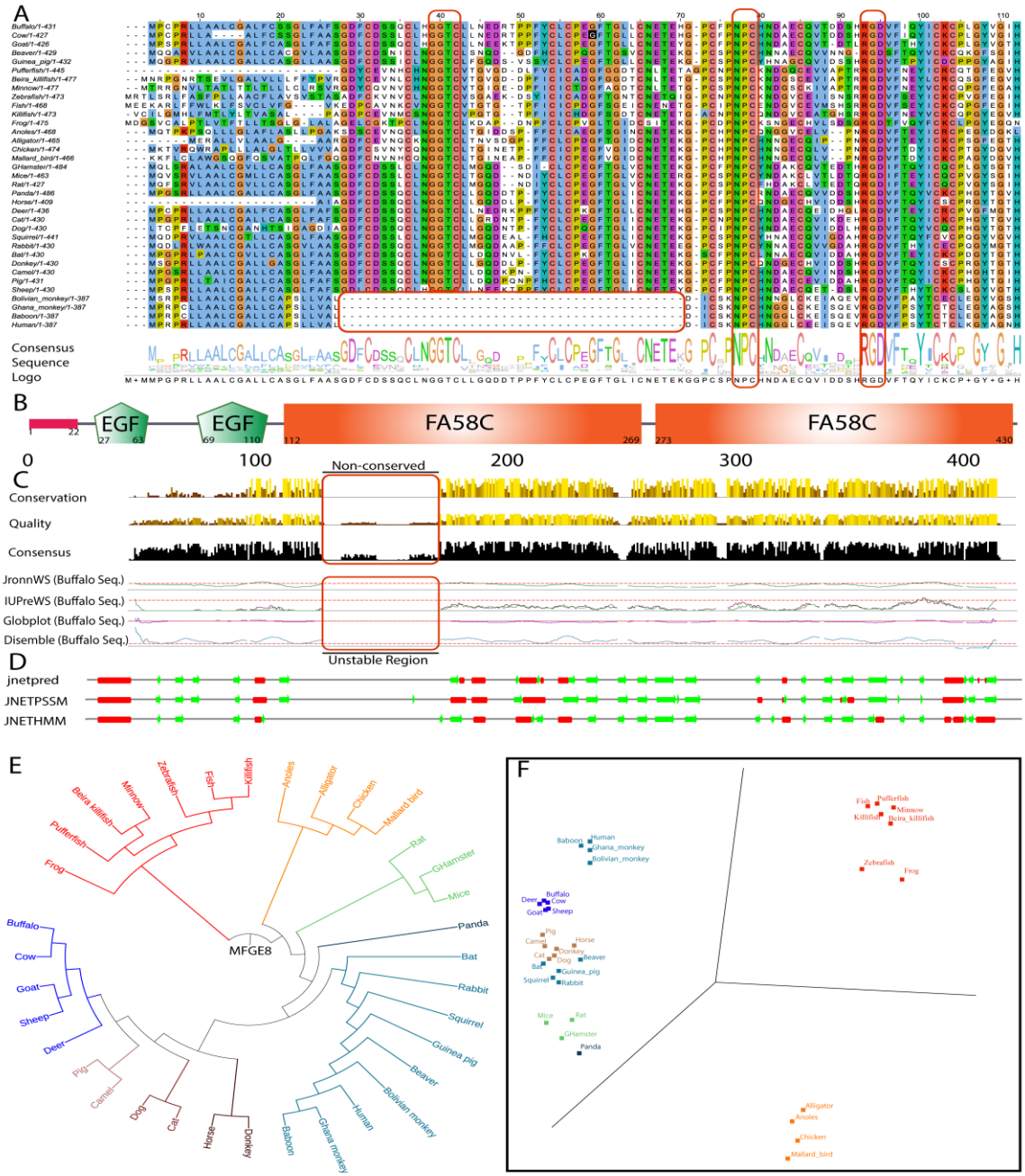

Figure 4.40: **In silico based MFGE8 protein sequence characterization. A)** Multiple sequence alignment (MSA) of 35 organisms used from UniProt non-redundant and reviewed database. **B)** The structure of the MFGE8 protein containing the complete common domains observed in all programs. **C)** The full-length sequence quality, conservation, and consensus nature of MSA are shown compared to 35 organism-specific MFGE8 protein. **D)** The secondary structure was predicted for a full-length MFGE8 sequence **E)** Phylogenetic tree analysis of all 35 organisms used using distance tree **F)** Principle component analysis of MSA for all 35 organisms using BLOSUM 62 algorithm.

The phylogenetic analysis of MFG-E8 from 35 organisms showed that buffalo is highly close to bovine, goat, sheep, and deer and comes in one cluster out of 8 classified groups. The results were validated with principal component analysis (PCA) analysis using the MSA BLOSUM62 model. In the PCA plot, a similar sequence lies close to each other. We identified the highly divergent nature of MFG-E8 in alligator, anoles, chicken, and mallard birds, which were grouped into a separate cluster. (Figure 4.40E and F). Altogether, these results suggest that intradomain regions are conserved among the organisms. However, many differences were observed in the interdomain areas.

4.3.2 Impact of MFG-E8 repression on the morphology and phagocytic activity of MEC

Phosphatidylserine-MFG-E8 axis mediated cell death modality is evolutionarily conserved, recently explained (Birge et al., 2016). In support, we identified the conserved MFG-E8 domains in all the species, signifying for the necessary cellular proliferation process and involvement in phagocytosis. The qRT-PCR analysis showed 90 fold down-regulation in the expression of MFG-E8 transcripts (Figure 4.41i). The same results were validated by western blot analysis. The dense expression of GFP shows the expression of a scramble and MFG-E8 specific shRNAs (Figure 4.42ii A and B).

Interestingly, the low expression level of inherent MFG-E8 protein resulted in globule-shaped structures that are not seen in the healthy or scrambled shRNA transfected cells (Figure 4.42ii C and D). However, these structures' formation was prominent at 72 h in KD BuMEC cells (Figure 4.42ii E and F). To exclude the possibility that GFP is stimulating these globules aggregation, we transfected non-target scramble shRNA GFP vector to BuMEC cells as a negative control, and no such structures were observed (Figure 4.42ii C and D). To understand and discover the MFG-E8 associated interconnection of pathways in the regulation of MEC proliferation, apoptosis, and transformation, we performed iTRAQ based comprehensive quantitative proteomic analysis between KD_MEC and WT_MEC and validated the findings through multiple *in vitro* assays as discussed later.

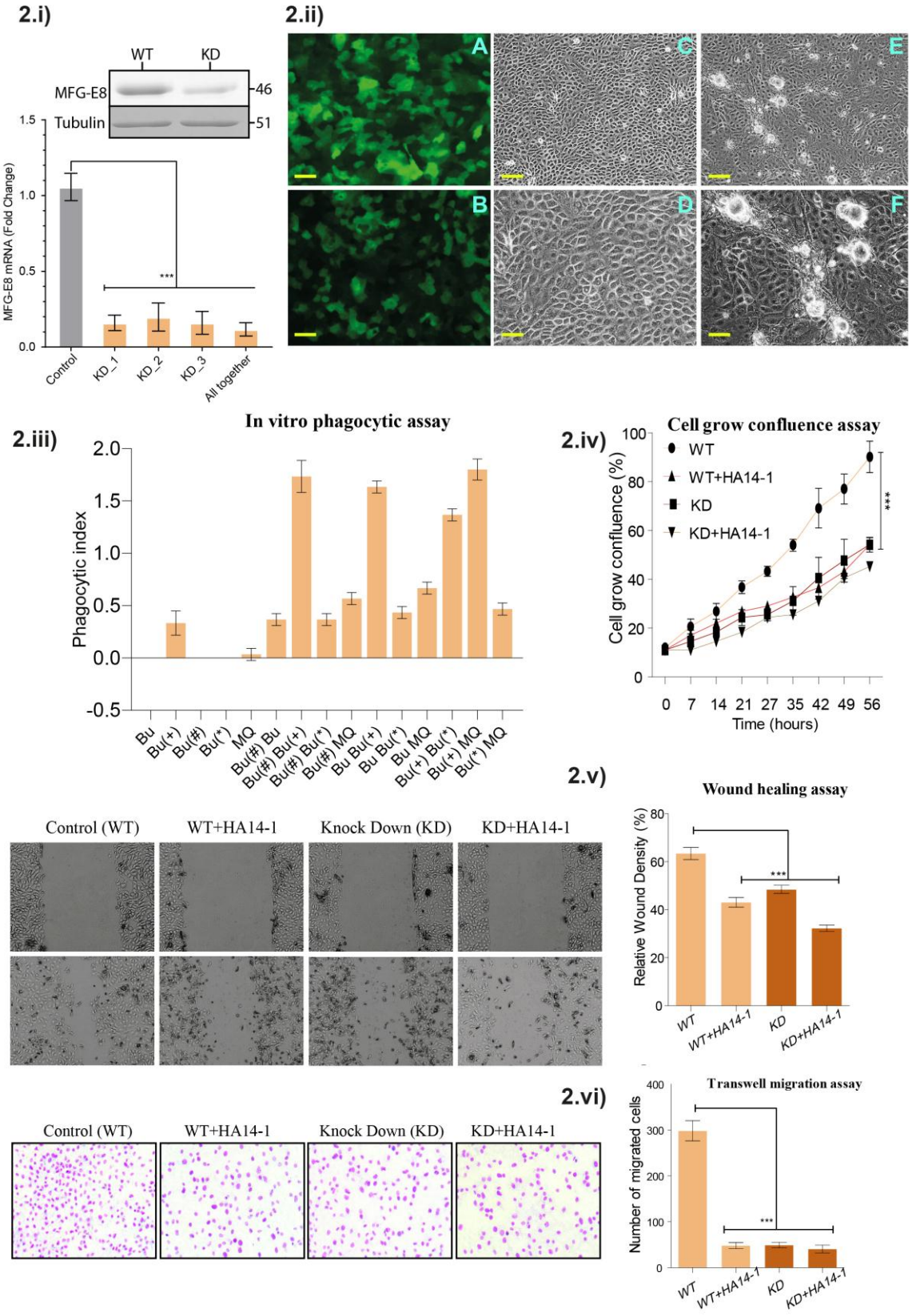

Figure 4.41: **i) Quantitative real-time PCR assay: ii) Stable transfection of Buffalo mammary epithelial cells (BuMECs) cells: A)** Transfected BuMEC cells over-expressing non-target scramble shRNA pLKO.1-

puro-CMV-tGFP vector. **B)** Transfected BuMEC cells with MFGE-8 specific shRNA containing pLKO.1-puro-CMV-tGFP vector, respectively. **C)** Transfected BuMEC cells over-expressing non-target scramble shRNA pLKO.1-puro-CMV-tGFP vector at 72 hours of growth, magnification 200X. **D)** The same **panel-C** cells at higher magnification 600X. **E)** Transfected BuMEC cells with MFGE-8 specific shRNA containing pLKO.1-puro-CMV-tGFP vector at 72 hours of growth, magnification 200X. **F)** The same **panel-E** cells at higher magnification 600X. Scale bar is 100 µm, **iii) In vitro phagocytic assay.** The co-culture phagocytic assay was performed to determine the phagocytosis ability in the absence of mfg-e8 and the induction of apoptotic inducer (HA 14-1). The graph axis is denoted with Bu (Normal or wild type BuMEC cells), Bu(+) (Apoptotic induced BuMEC), Bu(#) (scrambled shRNA-MFG-E8 BuMEC cells), Bu(*) (MFG-E8 Knockdown BuMEC cells), and MQ (BOMAC). **iv) Cell grown confluence assay. v) Wound healing assay. vi) Transwell migration assay**.

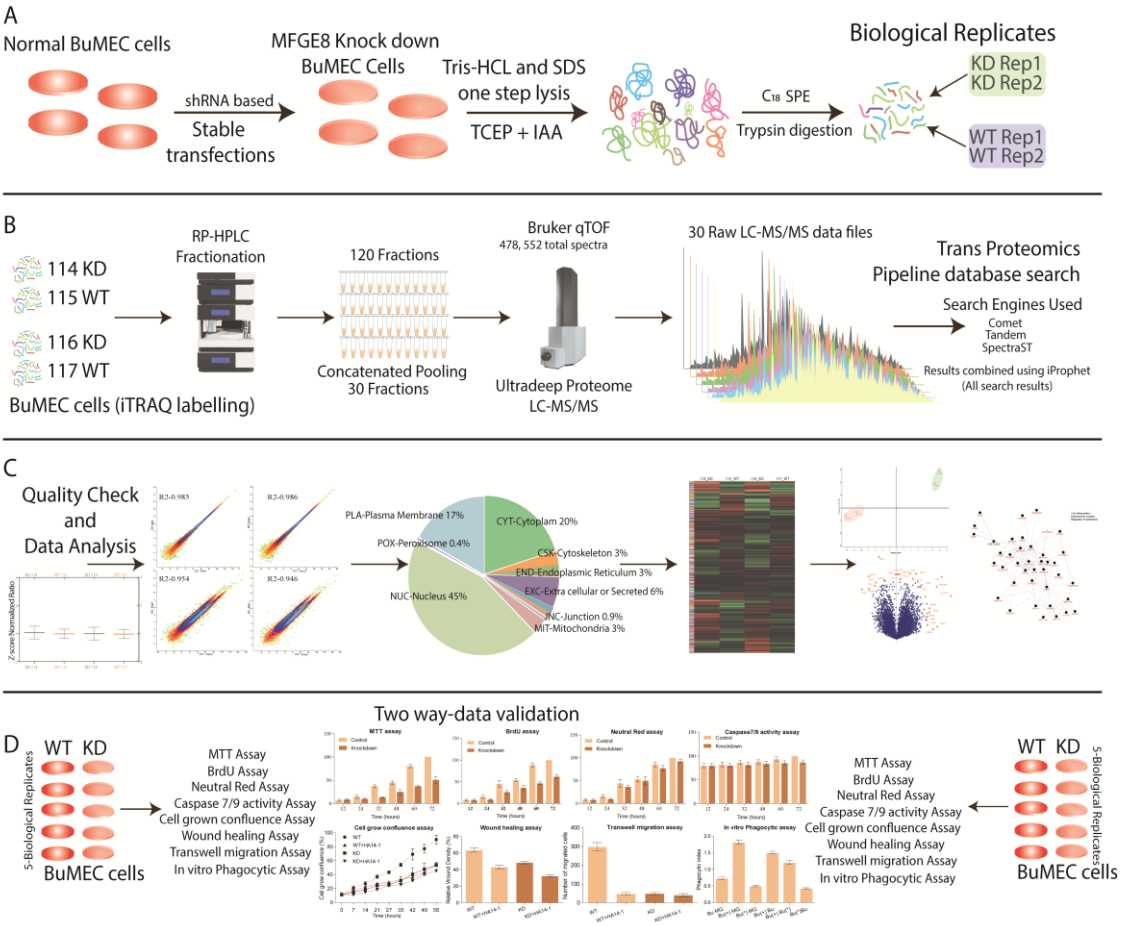

Figure 4.42: **Experimental design and quantitative proteomics workflow allow a comprehensive analysis of MFGE8 affected proteome.**

As MFG-E8 was previously described as a bridging molecule between macrophages (MQ) and apoptotic cells (Oshima et al., 2002), we determined the phagocytic index of MFG-E8 knocked down MEC cells. For the control, we performed the assay alone for Bu (Normal or wild type BuMEC cells), Bu(+) (Apoptotic induced BuMEC), Bu(#) (scrambled shRNA-MFG-E8 BuMEC cells), Bu(*) (MFG-E8 Knockdown BuMEC cells), and MQ (BOMAC) cell. Surprisingly, apoptotic induced BuMEC cells showed phagocytosis behaviour but not others. We tested two separate control for the assay, one with scrambled shRNA and other with WT cells. The results showed the minimal phagocytic index in Bu Bu(*) and Bu Bu(#) (0.42) than Bu(*) MQ (0.49) and lastly to Bu(#) MQ and Bu MQ (0.73) (Figure 4.42iii). The suggested reasons for low phagocytosis index in MFG-E8 knock-down Bu(*) cells may be the low expression of MFG-E8 or the decreased level of its associated receptors. Later the same results got confirmed in the proteomics data.

On the other hand, the maximal phagocytosis index was seen in the apoptosis induced Bu(+) MQ (1.81), which was used as a positive control. Unexpectedly, we observed the higher index in apoptosis caused Bu(+) Bu(*) and Bu(#) Bu(*), co-cultured (1.50) and in apoptotic induced Bu Bu(+) and Bu(#) Bu(+) (1.21). The phagocytosis assay results support previous findings that the healthy epithelial cells act as amateur phagocytes and are involved in the clearance of apoptotic cells through the expression of MFG-E8 (Monks et al., 2005, Monks et al., 2008).

Further, we examined the cell growth percentage in KD and WT cells up to 56 h; the results confirmed the significant high growth disparity in WT cells $p<0.001$ at 56 h to MFG-E8 KD. Subsequently, we tested the growth rate in the presence of the apoptotic inducer HA14-1, it resulted in the reduction of the KD cell population at 56 h to 52% growth, and WT treated with HA14-1 at 56 h to 55% growth compared to control with significant difference p-value <0.001. Compared to wild type, the initial significant difference for all three conditions was observed from 21 h of the cell growth assay (Figure 4.42iv). Next, we performed the wound healing assay using the same four conditions. The analysis of variance showed that in the first comparison of WT versus WT+HA14-1 mean difference-20.33 (P<value 0.0001), in second comparison WT versus KD, mean difference-15.00(P<value 0.0001), and in the third

comparison WT versus KD+HA14-1 mean difference-31.17(P<value 0.0001) (Figure 4.42v). The results describe that KD or treatment with the HA 14-1 inhibitor showed a remarkable reduction in the proliferation ability during would healing assay. Comparable results were perceived in the transwell migration assay with a significant difference with WT cells for cellular migration (Figure 4.42vi).

4.3.3 Widespread proteome changes triggered by ablation of MFG-E8

We employed the loss of function strategy and optimised the iTRAQ based global quantitative proteomics workflow to unravel the regulators of MFG-E8 mediated signalling pathways cross-talk. The protein samples were prepared from 5 days grown MFG-E8 deficient and wild type epithelial cells, followed by digestion, iTRAQ labelling, fractionation, and LC-MS/MS-based identification quantitation. The combined workflow trans proteomics pipeline analysis enabled the identification of 4,78,552 total spectra using three search engines, which represented 12,649 proteins having an iProphet probability of > =0.999 and error rate <0.00001 (Figure 4.43A-B). The Libra based relative quantification of non-redundant protein entries resulted in 8858 differentially expressed proteins (DEPs) (p-value< 0.01). Only those proteins were selected for analysis, which qualified the inclusion criteria of ≥ 2 peptides, minimum cutoff MS/MS count 2, minimum of seven amino acid residues, and iProphet probability ≥ 0.95 per peptide. (Figure 4.43C). Subsequently, the data acquisition precision was determined using statistical correlation among technical and biological replicates, shown as multiple densities scatter plots. The Pearson correlation R^2 value of 0.985 and 0.986 was observed between KD and WT cells' biological replicates, respectively. The plots show the precision in acquired MS/MS spectral intensities used for the quantification. A list of identified proteins, iProphet protein probability, sequence coverage, peptide sequence, Libra quantification values, and fold change values between MFG-E8_KD and Wild type control cells. Proteomics findings were verified with results obtained from various cellular assays (Figure 4.43D).

The profiled ultra-deep MEC proteome was catalogued, and individual proteins were predicted for its localisation in the cellular compartments based on the consensus motifs available in the full-length protein sequences. Remarkably, we identified 45% of the whole proteome associated with the nucleus, while 20%

of proteins were from the cytoplasm. With the help of our optimised proteomics workflow, including the microwave energy pretreatment of the proteins before digestion for optimal cell lysis, it allowed us to identify 17% of plasma membrane protein without any additional enrichment step. The remaining 18% were distributed in the other cellular compartment including peroxisome 0.4%, cytoskeleton 3%, endoplasmic reticulum 3%, Golgi 1%, lysosome 1%, junction proteins 0.9 %, mitochondrial 3%, and extracellular or secreted proteins 6% (Figure 4.43A). The downstream statistical analysis in the R- environment using a two-sample *t*-test based modified SAM-test showed significant proteins in the volcano plot (Figure 4B). For all DE proteins corrected p-values were calculated assuming the equal variance in biological replicates while keeping the *fudge factor* s0 = 1 and FDR = 0.01, as the constant parameters to locate out the "t-test Significance," "-Log t-test p-value," "t-test Difference" and "test statistic" for all entries. The volcano plot provided an estimate for both sided significance values of proteins. Our statistically defined data portrayed that the knock-down of MFG-E8 changes proteome expression dynamics in MECs, indicating its crucial role in basic cell proliferation.

The majority of highly down-regulated proteins in KD_MEC cells included RFX8, SIX6, ELP3, ZMYM3, EIF4, ENIF1, MYH14, DNAH11, TSBP, CBLN4, CNP, OR14C36, and CD2BP. They belong to protein classes of cytoskeletal protein (PC00085), transferase (PC00220), and transcription factor (PC00218), hydrolase (PC00121), an enzyme modulator (PC00095). The upregulated proteins in KD_MEC cells included LYVE1, FOLH1, PRKCSH, TRPV3, RING1, DOCK1, PLTP, SLC16A13, LENG1, and DMTN which are involved in the functions of transporter activity (GO:0005215), receptor activity (GO:0004872), signal transducer activity (GO:0004871), catalytic activity (GO:0003824). The proteins perturbed by the suppression of MFG-E8 expression in the epithelial cell showed the significant rearrangement of 572 membrane trafficking, 220 ion channel-specific, and 202 cytoskeleton proteins KEGG annotation. The variety of ion channels include calcium-activated potassium channel, potassium voltage-gated channel, potassium channel regulatory protein, epithelial chloride channel, sodium channel protein, amiloride-sensitive sodium channel, transmembrane channel-like protein, short transient receptor potential channel 1, transient receptor potential cation channel, voltage-dependent anion-selective channel, and ATP-sensitive inward rectifier potassium channel.

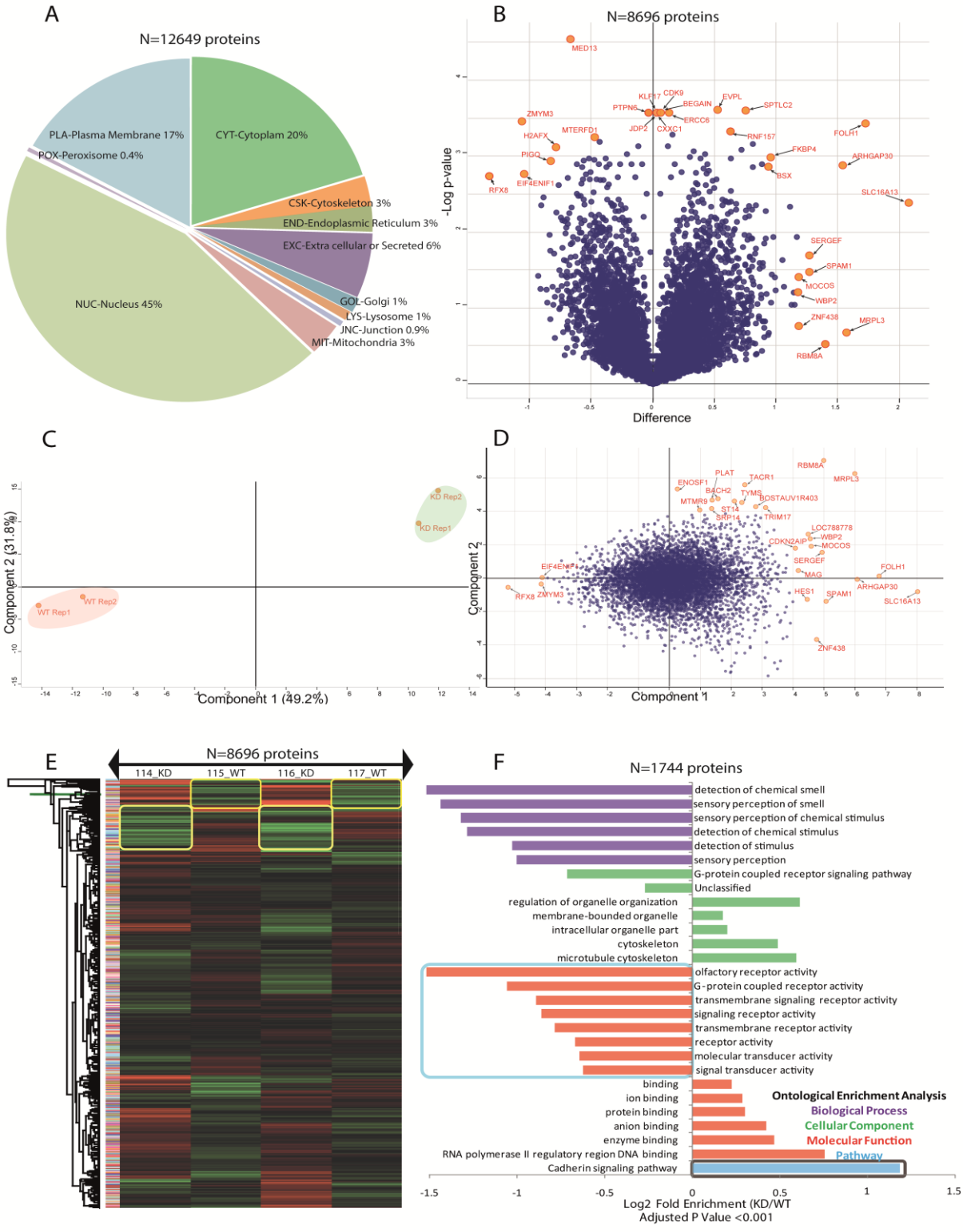

Figure 4.43: **BuMEC in-depth proteome analysis: A)** A pie chart shows the different percentage of occupancy of the identified proteome in compartmental based localization of epithelial cells. **B)** Volcano plot shows that significantly differentially expressed proteins, and extremely affected proteins were labelled with the orange colour circle named in red colour. **C)** Principle component analysis shows

the proteome data isolation of different iTRAQ labels components for biological duplicates samples. **D)** The biplot of PCA shows proteome data for comparison of component 1 (X-axis) to component 2 (Y-axis) for WT and KD cells in differentially identified proteins. **F)** Protein ontologies enrichment analysis is shown in the form of a bar graph. Biological process (BP), Cellular Component (CC), Molecular Functions (MF), and Pathways were colour-coded with bars.

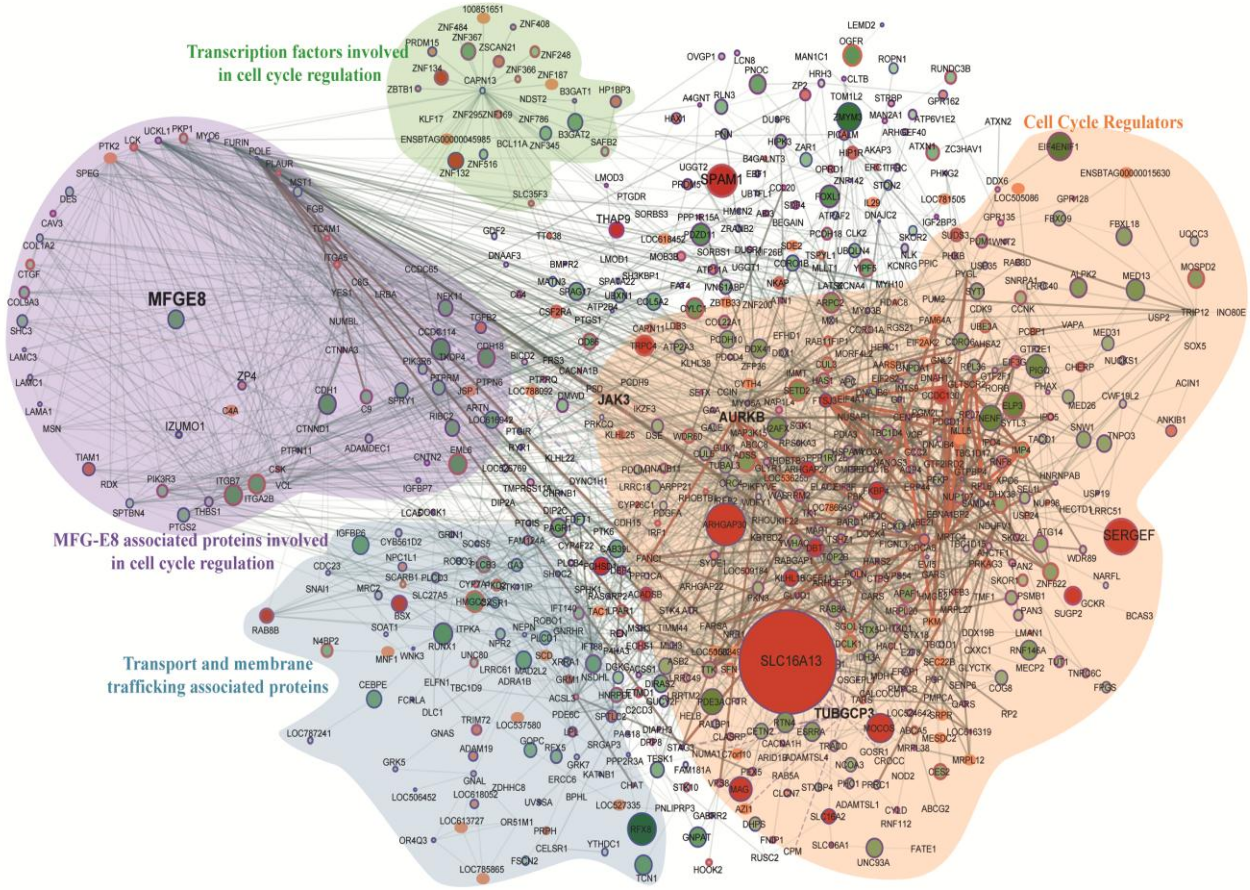

Figure 4.44: **Protein-protein interaction map for top significantly (p-value <0.001) expressed proteins:** The total number of nodes is 682 with 2140 interacting edges, node colour and size both show the up/downregulation, specifically, darker colour and more significant size node defines the high value of the fold change. The smaller size node defines no observed fold change in proteomics data. The nodes border shows the significance of the lesser p-values<0.001**;** thicker the border lowest is the assigned p-values. The thickness of the edges describes the experimentally identified co-expressed proteins in the database.

Another interesting observation is the up-regulation of cytokinesis protein isoforms; DOCK1, DOCK2, DOCK3, DOCK4, DOCK6, DOCK8, DOCK9, DOCK10, and DOCK11. The cytoskeletal changes and dramatic upregulation of transporter activity proteins together probably contribute to the distortion in the shape of KD_MEC cells on the 5th day of the culture, as seen in Figure 4.42ii. The size of the MFG-E8 knocked down cells as measured in terms of area and perimeter over the different points of observation, i.e., 12, 72, and 120h of cell growth showed significant expansion (*p-value* ≤0.001). It may be associated with ionic imbalance inside MECs due to perturbation in many membrane channel proteins.

We assessed all DEPs using the PCA plot to gain insight for its distribution in component 1 (49.2%) and component 2 (31.8%) with the identification of orthogonally transformed of essential proteins, indicated in the red label (Fig 4.43C and D). The majority of the proteins identified as PCA outliers showed their involvement in the cell cycle regulation in consonance with GO analysis and KEGG annotation. The comparison using hierarchical cluster analysis with Euclidean distance and average linkage with K-mean 300 clusters revealed significant changes in the expression level of all 8858 proteins (Figure 4.43E) which is same as shown in the volcano plot (Figure 4.43B; 4,025 upregulated genes, 4,833 down-regulated genes, false-discovery rate-adjusted P < 0.05). Thus, our result strongly suggests that knock-down of MFG-E8 protein directs overall cellular response reflected by the changes in the whole proteome profile of MEC, requiring additional investigation into prominent cellular pathways and linked proteins can distinguish the assault control mechanism from the direct downstream effects of MFG-E8 knock-down.

We observed that the suppression of MFG-E8 expression increased the G0-G1 phase transition duration by 32.62% compared to WT_MEC 18.4%. However, the S-phase duration is shortened in KD_MEC from 65.85% to 47.20%. We looked at the Gene Ontology classification of DEPs by GO analysis (See M and M section) to explain this effect. The investigation revealed significant enrichment of 530 GO terms with adjusted P-value < 0.05, including BP (321), CC (94), MF (86), Reactome/pathways, (11), and protein class (18) terms respectively. We further scrutinised the main GO terms simultaneously using fold change cut off (2.0 fold up and 0.5 fold down-regulated) and highly

significant P-value <0.01 in each category to visualise the pervasive impact of low MFG-E8 level in cells (Figure 4.43F). Surprisingly, we found the over-enrichment of the process for the negative regulation of intracellular signal transduction (GO: 1902532) and negative control of the cell cycle (GO: 0045786). It supports our observation of an increase in the cell cycle, doubling the time of KD_MEC cells. It is important to note here that the over-representation of key GO terms significantly enriched in the biological process showed posttranscriptional gene silencing (GO: 0016441) and gene silencing by RNA (GO: 0031047) which proves the shRNA mediated MFG-E8 silencing in our experiment. Further exploration of results showed that MFG-E8 knocked down disturbs the regulation of Ras protein signal transduction (GO: 0046578), cell-substrate adhesion (GO: 0031589), extracellular matrix organisation (GO: 0030198), DNA repair (GO: 0006281), protein auto phosphorylation (GO: 0046777). The under-representation analysis indicated the predominant effect on nucleosome assembly (GO: 0006334), G-protein coupled receptor signalling pathway (GO: 0007186), natural killer cell activation involved in immune response (GO: 0002323), detection of the stimulus (GO: 0051606), Fc gamma R-mediated phagocytosis (bta04666) providing the evidence for a low phagocytic index of KD cells.

We mapped DE proteome ($P < 0.05$) using genemania, reactome, and string database in a single platform on Cytoscape into different cellular processes to illustrate interdependent proteins regulation under the signalling of MFG-E8 (Figure 4.44). Overall, with these results, we understand that the repression of the MFG-E8 affects a wide variety of proteins in MEC, leading to a severe breach in cellular homeostasis.

4.3.3.1 MFG-E8 associated proteome regulates MEC homeostasis through cytoskeleton rearrangement

To understand the process of homeostasis in the absence of MFG-E8, we executed four powerful databases; Gene Ontology Enrichment Analysis Software Toolkit (GOEAST), ClueGO, DAVID, and KEEG (Figure 4.45). The over-enrichment of the prominent cellular component containing terms included GO:0005737 cytoplasms (12.35), GO:0016020 membrane (10.86), GO:0005654 nucleoplasm (9.06), GO:0005871 kinesin complex (7.77), GO:0005622 intracellular (6.72), GO:0005813 centrosomes (6.51), GO:0005925 focal

adhesion (5.64), GO:0005829 cytosols (5.44), and GO:0008270 Ion channels (6.21). This analysis highlighted the negative regulation of cytoskeleton organisation (GO: 0051494), microtubule cytoskeleton organisation (GO: 0000226), which was in parallel to the finding of morphological changes in KD_MEC cells (Figure 4.42ii). The globular structure formation resulting from cytoskeletal perturbances has been reported in other studies as well, where stat3 mediated Na-K+ channels are the key players (Ali et al., 2017). To gain insight on various pathways and their interconnections, we identified bta04510:Focal adhesion (10.19), bta04512:ECM-receptor interaction (10.18), bta04810:Regulation of actin cytoskeleton (10.18), bta02010:ABC transporters (5.90), bta04110:Cell cycle (5.18), bta04390:Hippo signaling pathway (4.67), bta00562:Inositol phosphate metabolism (4.31), bta04070:Phosphatidylinositol signaling system (4.15), bta04010:MAPK signaling pathway (3.97), bta04150:mTOR signaling pathway (3.72). The down-regulation of MFG-E8 thus proves that it is a central molecule in the maintenance of cellular homeostasis. A large number of cellular processes are interconnected through MFG-E8, among which structural components involved in focal adhesion, ECM receptor interaction, and actin cytoskeleton regulation are worst affected in its absence (Figure 4.45 A and B).

4.3.3.2 Immunoregulatory effects of MFG-E8 downregulation in BuMECs

We next set forth to determine the MFG-E8 associated protein's immunological behaviour, we mapped the proteome against the immune pathways and identified the B cells/T cells activation, lymphocytes activation, NK cell-mediated immunity, and leukocytes differentiation (Figure 4.45C). In correspondence with the multiple previous reports where MFG-E8 has been shown to elicit the immune response in terms of phagocytic activity in the mammary epithelial cells (Watson, 2006; Stein et al., 2007; Watson and Kreuzaler, 2011; Monks et al., 2002; Abrahams et al., 2004).

Although MFG-E8 associated genome-wide studies were previously performed but only at the transcriptomics level (Sugano et al., 2011) and as per our knowledge, no MFG-E8 associated proteome-wide global ultra-deep proteomics study has been so far done. Moreover, looking into the importance of hundreds of genes target previously recognised (Sugano et al., 2011), and

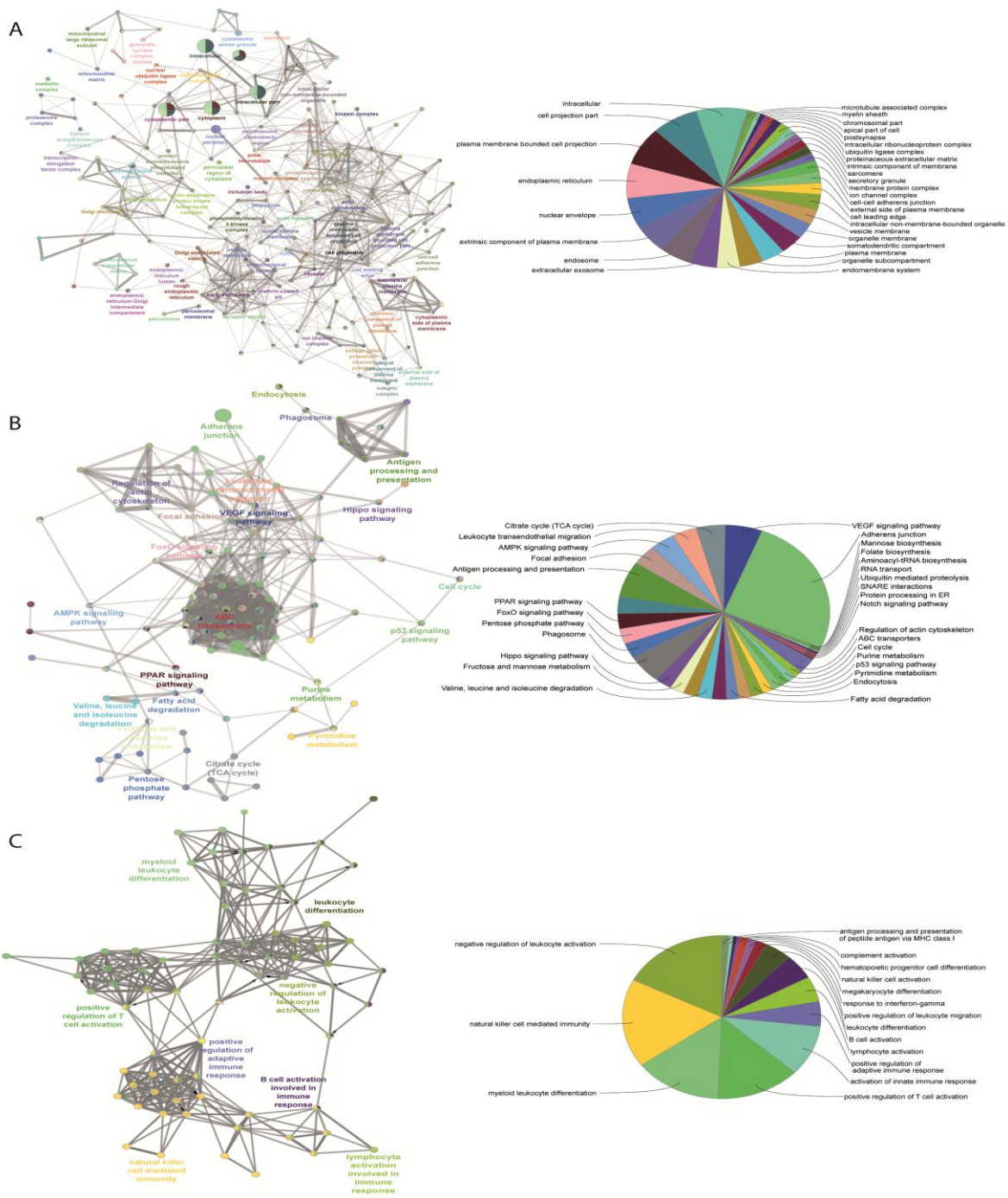

Figure 4.45: **Pathway-Pathway interaction analysis:** A functionally grouped network of enriched categories was generated for the target genes. GO terms are represented as nodes, and the node size represents the term enrichment significance. Functionally related groups partially overlap. **A)** Representative molecular function interactions among targets. **B)** Representative Reactome analysis interactions among predicted targets. **C)** Representative immune system processes interactions among targets.

protein targets identified in our current study (Figure 4.44b), point out several questions regarding its diverse downstream associated signalling which remain unresolved. The critical prerequisite of MFG-E8 in basic organ developmental biology; such as mammary gland (Hu et al., 2009; Sugano et al., 2011), intestinal epithelium (Zhao et al., 2012), and lungs remodelling process (Aziz et al., 2015) further enforced to accomplish the comprehensive proteome analysis.

Interestingly, recent findings described that MFG-E8 derived short peptide, known as MSP68, showed immunomodulatory function in sepsis-injured tissue. These studies indicate the unique therapeutic property of MFG-E8 and its derived peptide for regulating the inhibition of the infiltrating neutrophils migration, especially in lungs sepsis (Hirano et al., 2017; Hendricks et al., 2017). Our proteomics data proves that the MFG-E8 mediated signals towards neutrophils activation and migration are severely compromised in correspondence to these previous results. The under enrichment of the immune-related proteins upon MFG-E8 knock-down and provide mechanistic insight into its downstream pathway.

4.3.3.3 MFG-E8 affects signature transcription factors (TFs)

Around 45% of the total profiled proteins belonged to the nucleus (Figure 4A). We determined the MFG-E8-dependent signature transcription factors (TFs) with a cutoff of 1.5 fold up/down-regulated differentially expressed MEC proteome (n=938 proteins) with significant p-value <0.001) using a computational regulatory analysis with iRegulon (Janky et al., 2014). The analysis resulted in the identification of 12 TFs, which regulated 806 DEPs out of 938 identified proteins in the nucleus, as shown in the interaction map (Figure 7A). The identified TFs and their targets includes ZNF652 (232), CHD2 (222), MEF2A (243), GATA2 (256), FOXF2 (73), HDAC2 (77), FOXA1 (112), JUN (60), TFDP3 (140), POU2F1 (221), NFYA (68), and SNAI2 (23). We identified a common motif of C/ACAATXXXXGCG on the target genome for binding with these TFs, as revealed by the JASPAR database analysis for transcription regulatory region DNA binding (GO: 0044212p-value-0.0022).

The affected proteins with these TFs further narrowed down to control cell cycle regulation and maintenance (GO: 0007050, cell cycle arrest, p-value 0.004; GO: 0051301, cell division, p-value 0.021). Secondly, we discover all the targets were identified to be directly connected with the individual TF; instead, a

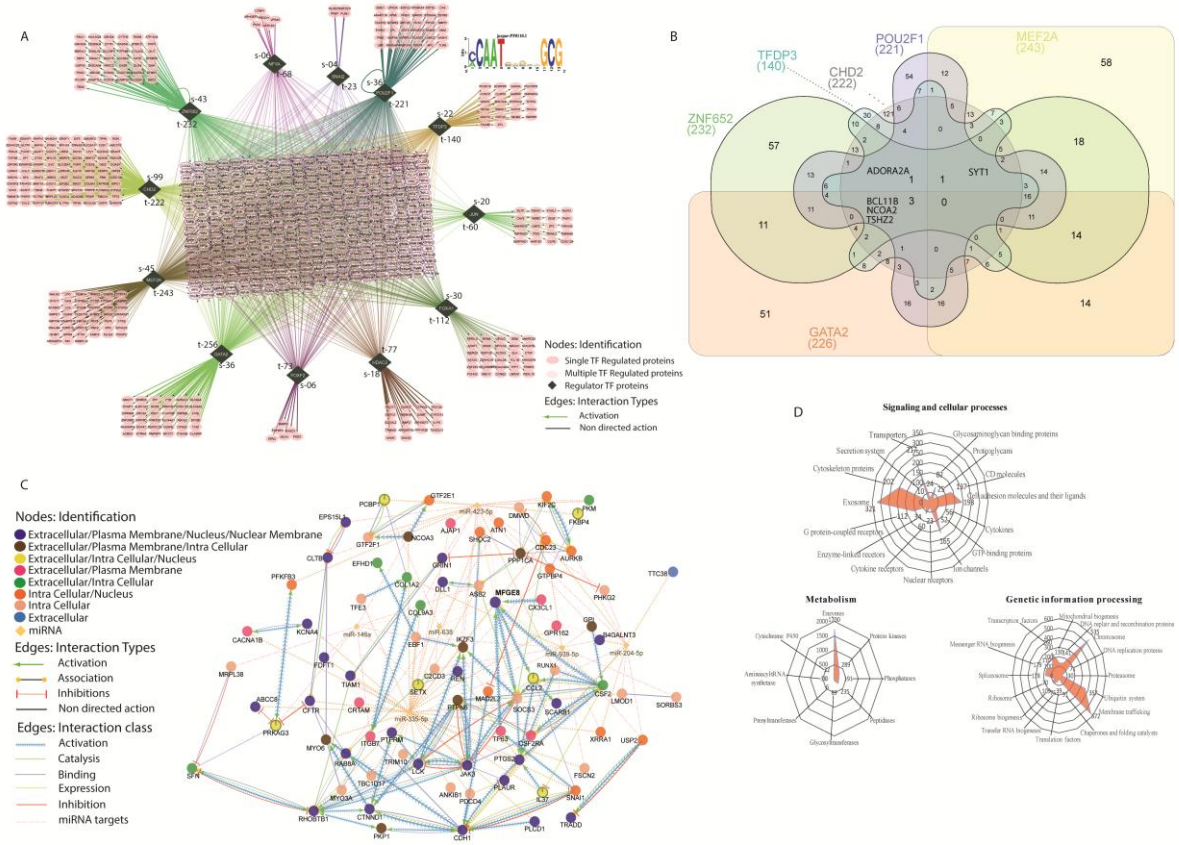

Figure 4.46: **Transcription factor associated with regulome: A)** All the identified significantly ($p<0.001$) differentially expressed proteins with 1.5 fold change up and down were used, n=938 proteins for identifying associated transcription factors involved in the cell cycle regulation. B) Venn Diagram. C) A directed network of MFGE8-miRNA interactome. D) Radar Plot.

large portion was synergistically regulated, and extensive overlap resulted in the formation of the large regulon in the centre of the interactome (Figure 4.46A). Particularly, among the 226 targets proteins activated downstream to GATA2, we found a combination of multiple TFs controlled 77.5% of the total targets. Interestingly, only three proteins (BCL11B, NCOA2 TSHZ2) were associated with all the TFs, and 51 proteins were associated with the only GATA2, as shown in the logic diagram (Figure 4.46A). The same is the case with MEF2A (243 total, 76.2% commonly regulated, 58 unique targets), POU2F1 (221 total, 75.6% commonly regulated, 54 unique targets), CHD2 (222 total, 45.5% commonly regulated, 121 unique targets), TFDP3 (140 total, 78.6% commonly regulated, 30 unique targets), and ZNF652 (232 total, 75.5% commonly regulated, 57 unique targets). These secondary regulons present the extensive overlap with the primary TFs regulon, intimating that these combinational functions of TFs are the leading contributors in gene regulation downstream to MFG-E8 (Figure 4.46B). The sharing of collective targets (more than 70% of each regulon) with the MFG-E8 regulon symbolises the prevailing co-factorship among these TFs, something that has been described previously for individual TF, although not on such a lengthened order for the cell cycle proliferation. In extension, all of the TFs shown are implicated in cell cycle progression that is bona fide regulators of cell growth progression (Koga et al., 2007; Kumar et al., 2006; Wang et al., 2018; Tang et al., 2018; Semba et al., 2017; Qiao et al., 2007).

4.3.3.4 Exploration of the mechanism of MFG-E8 for downstream signalling

Next, we sought to determine the impact of MFG-E8 mediated signalling on cellular outcomes. For that, we also considered the possibility of a critical confounding variable of miRNA for the regulation and downstream signalling of MFG-E8 (Figure 4.46B). The combination of databases such as GeneMANIA, Reactome, CluePedia showed the activation of MFG-E8 through CX3CL1, TP63, and CSF2 in identified differentially expressed proteins. The inferred directed network also indicates that MFG-E8 leads to activation of two proteins SOCS3 and CCL2, along with six miRNAs (miR-423-5p, miR-638, miR-939-5p, miR-204-5p, miR146a, and miR-335-5p) in the direct connection. The miR-423-5p and miR-638 were identified for autophagy promotion, while miR-204p and miR 335-

5p were previously reported in invasion and metastasis suppression. The interaction is expanded by finding associated proteins from DEPs with miRNAs and MFG-E8 collectively and dividing it into four underlying strata: extracellular, plasma membrane, intracellular, and nucleus associated. However, the network is described with a particular interaction type for all diverse associations such as activation, association, inhibition, catalysis, binding, and expression indicated with an individual variety of edges (Figure 4.46B). It helped us identify the specific molecules regulating cellular growth via down-regulated MFG-E8 such as AURKB, TRADD, SNAI1, USP2, and KIF2C. Figure 5 describes the illustrated signalling.

4.3.4 Determination of cell proliferation and caspase activity in MFG-E8 KD_MEC cells

The downregulation of MFG-E8 protein resulted in the cells' slow growth in MFG-E8 KD_MEC cells (Figure 4.47A-C). MTT assay results indicated that there was a decline in the MTT reductive capacity in MFG-E8 KD_MEC cells over different time points in culture (12, 24, 32, 48, 60, and 72 h) (Figure 8A), which was also validated by BrdU assay (Figure 8B). The cell growth rate was relatively equal for 12 and 24 h (non-significant $p>0.05$). In comparison, it continuously declined from 32 to 72 h onwards to nearly half with significant $p>0.001$ (Figure 4.47B). Interestingly, these cellular proliferation assay showed a high growth rate of control cells compared to the MFG-E8 KD_MEC cells, especially at 72 h of cell incubation. To check whether MFG-E8 knock-down leads to apoptosis in MEC cells, we performed the caspase 3/7 activity assay for all the same 6-time intervals (Figure 4.47C). Caspase 3/7 activity results were identified as non-significant changes for nearly all time points, suggesting that the decrease in the proliferation shown in cell growth is because of knock-down of MFG-E8 and not due to the induction of apoptosis. The results point out that MFG-E8 knock-down does not lead to caspases mediated apoptotic pathway. Similarly, MFG-E8 downregulation remarkably repressed wound healing and cell migration which is also highlighted in the enrichment analysis GO: 0016477, GO: 0043536, cell migration (p-value 0.000104) were validated by the migration assay (P<value 0.0001) WT versus WT+HA14-1/KD /KD+HA14-1 proves our finding of proteomics-based pathway analysis data.

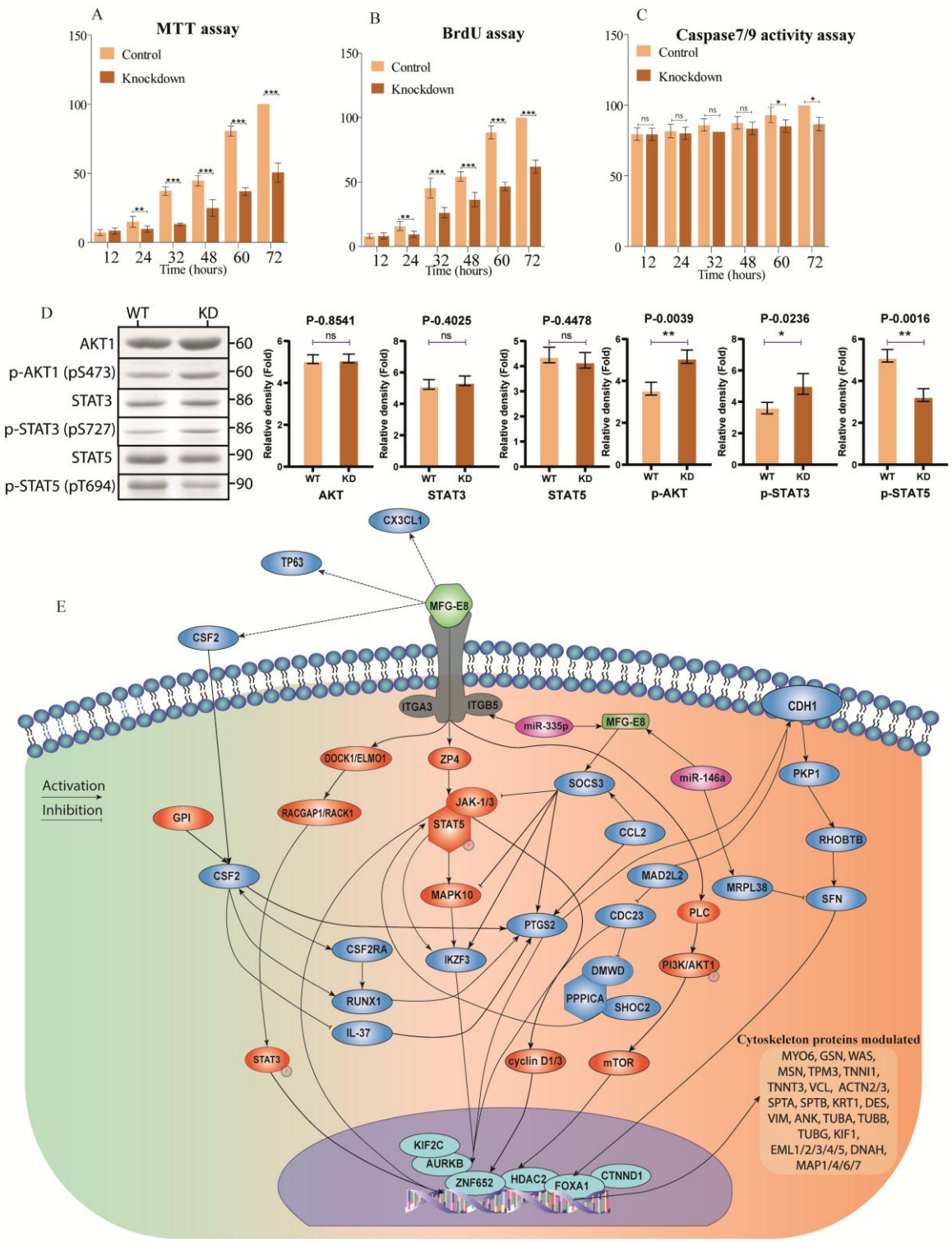

Figure 4.47: **Multiple assays for validation:** A) MTT assay. B) BrdU assay. C) Caspase-3/7 assay. D) Western blot analysis. E) Schematic representation for the signalling regulated through MFGE8 protein in mammary epithelial cells.

Dynamics of the phosphorylation of proteins majorly regulate the cellular signalling inside the cell. Therefore, based on the network analysis, we selected three key proteins (AKT1, STAT3, and STAT5) and counterpart phosphoproteins for western blot analysis. We found the non-significant change in the non-phosphorylated AKT but upregulation of p-AKT (p-S473) in KD cells. Similarly, STAT3 and STAT5 proteins were observed downregulated in KD cells. The results are in correspondence to the proteomics data. However, p-STAT3 (pS727) shown the high abundance in KD, but surprisingly, p-STAT5 (p-T694) was decreased in KD cells in comparison to WT cells (Figure 4.47D). Collectively, these data support that the dynamic phosphorylation event is more critical for the regulation of downstream signalling.

CHAPTER –5

Discussion

DISCUSSION

The presence of mammary gland discriminates mammals from other animals. It is a unique and complex secretory organ, whose primary function is to secret milk to new-borns for nourishment. Mammary glands are composed of distinct cell types, for example, epithelial cells for ductal network embedded into the fat bedding, variety of adipocytes, stroma including fibroblast, immune cells, and endothelial cells. Majority of the mammary gland development occurs postnatally under the influence of hormones through different stages. These hormones trigger the changes in both epithelium and the surrounding mesenchyme/stroma during development. Subsequent stages of mammary gland development are pubertal growth, pregnancy, lactation, and involution.

The distinctive development of mammary gland undergoes extensive tissue remodelling episodes regulated by several hormonal signals during adulthood and pregnancy. Whole epithelial cell hierarchy consists of distinct stages of cell types such as lineage-committed progenitor cells, multipotent stem cell lineages, and mature differentiated cell types which contribute to the complex morphological changes in the mammary gland. These cells flux is moderated by hormones using transcription factors and paracrine signals to activate related signalling pathways. Interestingly, the hormones, paracrine signals and transcription factors which control the normal growth and development of mammary gland also contribute to the breast carcinogenesis. Thus it is essential to understand the normal mammary gland development to further dissect breast cancer development and progression for better patient care and potential treatments.

In addition to several factors, three essential hormones such as oestrogen, progesterone (Pg), and prolactin (PRL) have been recognised as the principal regulators of mammary gland development and regulation. This thesis aims to examine the salient interactions among these hormones and draw implications for lactation and additionally, useful for breast cancer biology. These experiments significant findings are the discovery of 284 kinases and 80 phosphatases specific to mammary gland development. Post translation modification, such as phosphorylation, plays an essential role in the epigenetic

during lineage commitment processes during normal mammary development (Rijnkels et al., 2010). However, scarce information is available to examine the influence of inappropriate phosphorylation-dependent epigenetic remodelling on epithelial hierarchy during normal mammary glands development. In 2008, Bloushtain-Qimron et al. described the pattern and expression of methylation in specific cell type during normal mammary gland development (Bloushtain-Qimron et al., 2008). They have shown the influence of epigenetic modifiers, Pygo2 (Gu et al., 2009) and Bmi-1 (Pietersen et al., 2008) on epithelial hierarchy. There is no literature describing the phosphorylation-dependent epigenetic control of transcription factors known to regulate mammary gland development.

Reproductive hormones are known as an essential regulator of lactation and use the post-translation modification phosphorylation for signalling. My thesis's first objective is to investigate and discover the type of phosphoproteins involved in the normal mammary gland development signalling. In 2003, Leung et al. depicted PRL signalling inhibition in a transfected cell model inconsistent with oestrogens effects on GH signalling. The oestrogen treatment of breast cancer cells was induced by CIS, SOCS protein which showed no oestrogen role in PRL signalling inhibition. Also, oestrogen exhibit no effect on PRL-induced milk expression in a mouse mammary cell line. The findings argue that mammary gland cells SOCS expression might induce the interaction between oestrogen and PRL signalling.

Both exogenous and endogenous oestrogen have different roles, i.e. exogenous oestrogen is administered to suppress lactation in women who considered not to breastfeed, while endogenous oestrogen stimulates mammary gland development during puberty. During pregnancy, mammary gland development is regulated by many hormonal signalling factors, and Elf5 is one of the well-established moderators of PRL reported in the literature. Several experiments have been performed to explore between Pg and Elf5 during mammary gland development, including Pg induction of Elf5 in cell lines and comparison in mammary glands null for PR and Elf5.

Puberty instigates branching morphogenesis or terminal end buds formation, to build a ductal tree that is embedded into the fat pad, under the influence of growth hormones (GH), estrogen (ER), and insulin-like growth factor

1 (IGF1). Further combine progesterone and prolactin's action stimulate extensive and rapid proliferation of the ductal epithelium to form mammary alveolar structures responsible for milk synthesis and secretion at the time of lactation. Lastly, in a single round of cycle mammary gland demolition occurs during involution, which remodels and brings back to the pre-pregnancy stage (Macias and Hinck, 2012; Watson et al., 2008). We compiled the high-resolution mass spectrometry-based phosphoproteomics data and determined the critical kinases and phosphatase for remodelling. The combined analysis of phosphoproteins showed the identification of nineteen fundamental phosphoproteins.

Actin is an extensively found structural protein of cytoskeleton found in eukaryotes that play a myriad of functions like muscle contraction and cell motility. Among the six different isoforms of actin (Vandekerckhove and Weber, 1978), (Herman, 1993, Miwa et al., 1991, Rubenstein, 1990), four are muscle actins, including ACTA2, smooth muscle γ-actin, skeletal muscle α-actin, and cardiac muscle α-actin and other two are ubiquitous cytoplasmic actins, known as β- and γ-actin which found in all epithelial and mesenchymal cells. Since mammary myoepithelial cells of the mammary gland are specialised smooth muscle-like epithelial cells, they express smooth muscle actin isoform known as smooth muscle alpha-actin (ACTA2) were prominently found in our results. The primary function of actin protein is to accelerate the contraction force in response to oxytocin for milk ejection during lactation (Franke et al., 1980). However, our results emphasised that its post-translation modification, phosphorylation plays a significantly central role in the mammary gland's normal lactation function. Previously, a study was performed to evaluate the contribution of ACTA2 to mammary myoepithelial cell contraction using knockout *Acta2* null mice. In correspondence to our results, they also found that lactating mammary glands from Acta2−/− mice showed the signs of advanced involution and apoptosis compared to the number of apoptotic cells at lactation from Acta2+/+ mice. Moreover, in Acta2+/+ mice, branched hollow ducts of epithelial cells in the mammary gland are surrounded by smooth muscle α-actin and keratin 14 positive myoepithelial cells. Interestingly, they have shown that Acta2−/− mice's mammary glands appeared to reside with fewer myoepithelial cells that expressing keratin 14 as well as other myoepithelial or smooth muscle markers

(such as Vimentin, keratin 5, GFAP, smooth muscle calponin, P-cadherin, and smooth myosin heavy chain) (Weymouth et al., 2012).

Another study demonstrated that the Acta2$^{-/-}$ dams are impotent to nurse their offspring productively. The defect is due to the less contractile force is generated than wild type in response to oxytocin other than structural defects that are the same as wild type. Therefore present literature suggests the importance of ACTA2 in myoepithelial cells especially for its active contraction in response to oxytocin required for milk ejection and successful lactation, and not require to myoepithelial cell and mammary gland development (Carol et al., 2011). Contrary to the previously reported information, our results suggest its essential role in the cellular development and differentiation of mammary epithelial cells.

Vimentin is a type III intermediate filament (IF) protein that expresses particularly in mesenchymal cells (Coulombe and Wong, 2004). Therefore knockout of Vim$^{-/-}$ causes defects in endothelial functioning (Nieminen et al., 2006; Antfolk et al., 2017), motor coordination (Colucci-Guyon et al., 1999), and wound healing (Cheng et al., 2016; Eckes et al., 2000). In correspondence to our results, other studies also demonstrated that the Vimentin are the critical regulator of normal mammary gland development. As Vim$^{-/-}$ mice showed the significantly delayed outgrowth of mice mammary ducts *in vivo.* Therefore Vim$^{-/-}$ mammary gland, characterised by the lesser basal epithelial cells. Also, Vimentin is essential proteins of cellular signalling in the mammary gland and demonstrated as a breast cancer promoter, indicating its function in regulating cancer stem cell capacity.

Furthermore, some study has been reported its role in basal mammary epithelium. It has been demonstrated that proliferation of basal mouse mammary epithelial cells (bMMECs) of Vim$^{-/-}$ decreases in vitro, and a significant reduction in the number of basal epithelial in Vim$^{-/-}$ mammary epithelium. This phenotype indicates that Vimentin could be a signal-integrating hub key player through interacting with phosphorylated kinases and even transcription factors (Eriksson et al., 2009; Ivaska et al., 2007; Virtakoivu et al., 2015). As evident from protein-protein interaction network analysis results. Predominantly, Vimentin assumes to be a central node in the cell signalling cascade set off in normal stem cells, regulates the rate of mammary ductal outgrowth and breast cancer. Therefore it

is vital for the understanding of how Vimentin contributes to mammary stem cell regulation. Moreover, it can be crucial in developing therapeutic strategies against breast cancer (Virtakoivu et al., 2015; Peuhu et al., 2017).

In 2010, Hilton et al. described the long-term treatment of Pg in vivo induced the expression of Elf5, and our results were consistent with initial findings from human breast cancer cell lines with rat ovx model (Hilton et al., 2010). A microarray data published in 2008 indicated loss of Elf5 which does not affect PR expression (Oakes et al., 2008a) however, reduction of Elf5 expression in PR null mouse mammary gland was reported confirming the role of Elf5 lies downstream of Pg signalling. Similar microarray experiments were performed in vitro using normal human breast epithelium (Graham et al., 2009) showing the downregulation of Elf5 expression after the Pg treatment for 6 hours.

An earlier study revealed that over-expression of Elf5 saved the unsuccessful development of PRLR null mammary gland transplants (Harris et al., 2006) demonstrates the role of Elf5 as a primary mediator of PRL action. Some studies reported the active state of PR promoters and MMTV in steroid-responsive cells (Vicent et al., 2009; Mukherjee et al., 2010) which tells us that Elf5 is usually expressed in steroid receptor-negative cells (Oakes et al., 2008a). Furthermore, an attempt can be made using a retroviral approach to drive higher expression of Elf5 under the control of promoter such as CMV promoter, which can help rescue PR null phenotype. Interestingly, in virgin mice, the expression of Elf5 was different from Pg treatment which proves the idea of Elf5 is not the principal modulator of Pg action during pregnancy.

Elf5 and Pg's potential role in mammary gland development was identified, the expression profile of Elf5 was measured in the presence and absence of exogenous Pg. Co-immunoflurosece of PR and Elf5 was performed to dissect the mechanism of Pg induced Elf5 expression. Oakes et al., 2008a suggested Elf5 and PR in different mammary gland cells, which resulted in findings of induction of Elf5 by Pg via a paracrine mechanism. Given the similarities between MMTV-RANKL and Pg treated Elf5tg mammary glands, probability of paracrine mechanism regulated RANKL mediates Pg induction of Elf5 expression was investigated (Fernandez-Valdivia et al., 2009). They reported no effect of Elf5 on RANKL expression in HC11 cells or mouse mammary glands which were consistent with the earlier interpretation of

microarray analysis (Oakes et al., 2008a). Whereas breast cancer cell lines were treated with RANKL showed the forced expression of RANKL induced the Elf5 in the mammary gland, which validated the fact that Elf5 lies downstream of RANKL in the development of mammary glands. In future, extensive work is needed to understand the intracellular signalling pathways which mediate RANKL induction of Elf5 expression. In addition, studies require to investigate the paracrine factors such as Wnt proteins responsible for Pg mediated induction of Elf5 expression. In the mammary gland, Efl5 is a well-known mediator of PRL action; however, the mean of PRL induces Elf5 expression largely a question. Therefore future studies should consider the investigation of parallel paracrine mechanisms responsible for PRL induced Elf5 expression.

We found the ER based regulation of transcription factors expression such as FOXA1, STAT5, GATA3, and Sox6 are might be involved. GATA3 and FOXA1 were found expressed in steroid receptor-positive cells (Kouros-Mehr et al., 2006; Bernardo et al., 2010). According to Choi et al., binding of Elf5 to STAT5 promoter is vital for STAT5 expression (Choi et al., 2009). However, other studies show the expression of STAT5 in ER+ mammary cells (Santos et al., 2008). On the other hand, transcription factor Sox6 has been shown as expressed only in ER- cells (Kendrick et al., 2008), however lack of proper evidence can predict the linking of Sox6 with cross-regulation of Elf5, ER, GATA3 or FOXA1.

Another exciting target of the study is E-Cadherins. Cadherins are transmembrane receptor proteins, present at the adherens junctions in the mammary gland, a large superfamily consisting of six groups including fat and daschous, classical, flamingo, 7-pass transmembrane, protocadherins, and desmosomal cadherins (Peinado et al., 2004). Cadherin is calcium-dependent, works in both heterophilic and homophilic interactions that mediate cell-cell contact and communication in various organ systems. In the normal mammary gland, few members of the cadherins family have been characterised. For instance, E-cadherin is exclusively expressed in all of the mammary epithelial cells, whereas P-cadherin, expressed in mammary epithelial cells of the alveoli and ducts, also in the myoepithelial cells.

On the other hand, N-cadherin expressed in mesenchymal cells of the mammary stroma. The cadherin superfamily requires cell-cell contact and

communication in various organ systems. This interaction allows cells to not only interact with neighbouring cells but also assist in cell signalling. Our finding of the IHC imaging proves the critical role of E-Cadherins in mammary gland signalling. It was also reported that during breast cancer, alteration in E-cadherin regulation, which consequently down-regulate E-cadherin expression, facilitating an epithelial-mesenchymal transition (EMT) process.

We found the nine isoforms of cadherins in our dataset. In which Cdh26 were highly expressed in puberty and virgin stage. We also found that E-cadherin interaction with members of the Wnt, EGF, and FGF families. The previous report describes that these interactions form a delicate balance among signals via several intracellular pathways such as glycogen synthase kinase (GSKβ), β-catenin, and AKT. However, various molecular mechanisms govern the downregulation of E-cadherin. We found the significant differential regulation of E-cadherin in mammary gland signalling in puberty (p-values 0.0019), pregnancy (p-values 0.001), lactation (p-values 0.0071) and involution (p-values 0.0463). At the time of EMT, Snail1 and Slug (Snail family of suppressor transcription factors) and Zeb1 and Zeb2 (E-box-binding zinc finger transcription factors) coordinate the decrease of E-cadherin expression whereas enhancing N-cadherin, which further contribute to the EMT (Schmalhofer et al., 2009). These transcriptional suppressors majorly include the basic helix-loop-helix (bHLH) family members such as E12/47 (the *e2A* gene product) and Twist, Snail1 and Snail2 (Slug), the Snail family, and members of the zinc finger homeobox family of repressors, for instance, ZEB1 (TCF8 or δEF1) and ZEB2 (ZFXH1B or SIP1).

We found the direct inaction of slug protein with MFGE8. Both the protein Snail and Slug can lower the E-cadherin expression in numerous breast cancer cell lines, suggesting that Slug is extensively correlated with E-cadherin's down-regulation in breast carcinomas *in vivo (*Hajra et al., 2002*).* However, the GSKβ has been demonstrated as an inhibitor of Snail and Slug's activity to activate Zeb. The transcription factor, ZEB1, could govern the cell fate determination and development of mesodermally derived tissue. It has been reported that ZEB1, can bind to DNA through its E-box consensus motif and played as a transcriptional activator, which interacts with acetyltransferase p300/pCAF and further activated SMADs (Nishimura et al., 2006; Postigo et al., 2003; Postigo et

al., 2003; Liu et al., 2008; Graham et al., 2008). Any mutations in the *ZEB1* gene can cause mesenchymal to epithelial transition (METs) with elevated ectopic expression of E-cadherin. Moreover TGF- β (Transforming growth factor-β), TNF-α (tumour necrosis factor-α), and IGF-1 (insulin-like growth factor-1) signalling can trigger the activation of ZEB1 and induce EMT in breast cancer, whereas reducing E-cadherin expression. It concludes that various transcriptional repressors, including Snail1, Snail2, Zeb1, and Zeb2, are potentiated to down-regulate E-cadherin, which consequently inhibiting the cell's ability to establish correct adhesion properties and leaving the cell endangered to enhance invasiveness and metastasis in breast cancer (Schmalhofer et al., 2009).

Twist, bHLH protein, participates in the differentiation of numerous cellular lineages, such as myogenesis, neurogenesis, and osteogenesis (Jiang et al., 1996; Hamamori et al., 1997). Additionally, Twist potentiates to activate EMT by down-regulated E-cadherin expression and elevates the N-cadherin expression in the fruit fly (Maestro et al., 1999; Castanon et al., 2001). On the other hand, in the mice model, the increase of Twist expression is correlated with the downregulation of E-cadherin, the activation of mesenchymal markers, and the promotion of metastasis (Yang et al., 2004; Howe et al., 2003). Contrarily, in the mice mammary tumour model, Wnt 1 signalling regulates Twist expression through β-catenin, and also both could subdue the mammary differentiation, allow further cell growth and even tumorigenesis to continue. It has been demonstrated that SNAIL protein expression can be trigger by cells exposed to high levels of hypoxia, which consequent in SNAIL is localising to the nucleus, where it stabilised by an SCP (small carboxyterminal domain phosphatase). There SNAIL could then bind to the promoter of ZEB1 and cause ZEB1 to inhibit the E-cadherin gene. Phosphorylation of SNAIL by GSKβ further divulge NLS (nuclear localisation signal) that allow the SNAIL to exit the nucleus (Zhou et al., 2004; de Herreros et al., 2010). It further enables the re-expression of the *CDH1* and the other genes which previously repressed by SNAIL. Interestingly, SNAIL does not directly change the expression of mesenchymal proteins such as N-cadherin; and Vimentin, instead TWIST could trigger activation via HIF1 to elevate Vimentin N-cadherin expression (Yang et al., 2008; Andrews et al., 2012).

On an exciting note, it has been found that the absence of E-cadherin cause sequesters the activated form of Stat5a, even though at normal prolactin levels which is not explore in detail yet. It suggests that prolactin can no longer signal to its receptor to establish the activated form of Stat5, which indicates that E-cadherin is essential for the correct localisation of the prolactin receptor over the epithelial cell membrane. Also, inactivation of E-cadherin induces apoptosis, together with the decreased expression of milk protein genes which initiate the involution. Further studies are needed to elucidate whether a fully coordinated apoptotic program at the onset of involution, i.e. cell-cycle control genes and others, upregulation of cell-death factors, can be observed in the mutant mammary glands (Boussadia et al., 2002).

S100 calcium-binding protein S100A4 is also called fibroblast specific protein 1 (FSP1). S100A4 acts as a stromal factor, play a significant role during the mammary gland developmental process, S100A4 accelerates branching morphogenesis through an extensive and rapid proliferation of the ductal epithelium invasion into fat bedding, via influence the expression of branching morphogen through induction of MMP-2. Furthermore, S100A4 expression reached a peak at the time of ductal expansion, specifically in stromal cells. (Andersen et al., 2011) .

Milk Fat Globule-EGF-factor (MFG-E8), a phosphatidylserine binding protein, is also known by many other names such as lactadherin, PAS 6/7, SED1, BA46, p47, rags, and HMFG. It is a 72-kDa secreted glycoprotein initially recognised in milk fat globules membrane (MFGM) released into milk by mammary epithelial cells. MFG-E8 is a multifunctional molecule shown to be released by a variety of cell types such as macrophages, immature dendrocytes, myoepithelial, endothelial, retinal, intestinal epithelial cells (Ceriani et al., 1993; Stubbs et al., 1990; Raymond et al., 2009) and it is also expressed at high levels in many tumour types (Neutzner et al., 2007; Carmon et al., 2002). Multiple studies have shown that MFG-E8 plays an essential role in mammary gland development, mostly, orchestrating post-lactational mammary gland remodelling (Stubbs et al., 1990; Lonnerdal, 2003; Atabai et al., 2005; Hanayama and Nagata, 2005). This protein shares structural domain homology with Del-1 (developmental endothelial locus 1), constituting a two-gene family of $\alpha_v\beta_3$ integrin ligands (Hidai et al., 1998). It was also reported that MFG-E8 transcripts

increase in the mammary gland during pregnancy to lactation, suggesting its typical role during the glandular developmental transition (Oshima et al., 1999). Lately, we also identified in our Difference Gel Electrophoresis (DiGE) based proteomics dataset that MFG-E8 is up-regulated in MECs isolated from the high milk yielding cows (Janjanam et al., 2014). Despite the several reports emphasising the association between this molecule and various cellular physiologies, the exact mechanism, its intracellular targets, and downstream signalling circuits in MECs are unknown. The interpretation of MFG-E8 mediated regulatory control on homeostasis in healthy and diseased conditions remains poorly understood.

Furthermore, it has been shown that LIF known as leukaemia inhibitory factor, triggers the epithelium apoptosis via Stat3 activation at the time of mice mammary gland involution. In the normal mice mammary gland, Stat3 is a pro-apoptotic protein and an essential mediator of post-lactational regression. During involution, the mammary gland's local factors trigger the phosphorylation of Stat3 (Li et al., 1997). Furthermore, conditional knockout of Stat3 in mice mammary glands demonstrated as a suppressor of epithelial apoptosis that engendered a significant delay in mammary gland involution (Chapman et al., 1999). Furthermore, LIF has been reported to establish the physiological activator of Stat3 during mammary gland involution and prime regulator of the apoptotic process (Schere-Levy et al., 2003; Kritikou et al., 2003).

Moreover, it has been shown that LIF is also potentiated to trigger the phosphorylation of stat3 in various studies (Quaglino et al., 2007). LIF is a multifunctional glycoprotein expressed at a low but detectable level in post-pubertal, adult virgin, and pregnant mice mammary glands. However, LIF levels go down even undetectable after parturition and during lactation (Schere-Levy et al., 2002).

Whereas, STAT5 performed an essential function in the development and differentiation of the mammary gland regarding lactation proficiency (Santos et al., 2010). STAT5 is essential that gives rise to luminal progenitor cells which further differentiate into alveolar cells. Hence STAT5 is a highly expressed isoform of the STAT family in the mammary gland. During the pubertal stage, the absence of STAT5 results in defect of secondary ductal and side branching and delay in the differentiation of TEBs. Moreover, during the pregnancy stage, this

protein is required to develop the mammary gland for harbouring the lactation and its differentiation and formation of milk protein (Furth et al., 2011; Barash I, et al., 2006).

Interestingly, the absence of STAT5 is substituted by the STAT5A and increases the expression of SATA5B, especially during serial pregnancies. Activation of STAT5 is downregulated as the late lactation or during the onset of involution. Hence STAT5 is necessary to differentiate luminal progenitor cells further into alveolar cells in the mammary gland. STAT5 is a key player mediator for alveolar cell fate commitment and proliferation, which leads to lactational differentiation.

Since protein-protein interaction between STAT5 and other cellular proteins in the mammary gland activates STAT5, hence STAT5 and other nuclear hormone receptors such as ERα, PR, and glucocorticoid receptor are expressed in mammary epithelial cells. Cellular protein which has been demonstrated as the impact the SATA5 activity, for instance, such as serine/threonine-protein kinase Akt (AKT), PI 3-kinase enhancer A (PIKE-A), p21-activated kinase 1 (Pak1), breast tumour kinase (Brk), the transcription factor protooncogene v-Myb myeloblastosis viral oncogene homolog (avian) (c-Myb) and caveolin.

It is essential to maintain the rigid balance between cell death and clearance of its cadaver, avoid any inflammation, and support the tissue homeostasis. In distinction to other organs, most of the mammary gland development occurs postnatally, which is hormonally regulated during pregnancy (Hovey and Trott, 2004), allowing it to be a superlative structure understanding of the systemic molecular mechanisms of organ development. At the end of the lactation, the accumulation of milk in the glands triggers excessive epithelial cells death. Majorly, these cells are promptly removed by neighbouring epithelial cells and also by infiltrating phagocytes to ensure that the gland returns to its pre-pregnant state (Watson and Kreuzaler 2011; Monks et al., 2008; Sumbal et al., 2020; Ensslin et al., 2007; Watson, 2009). Multiple proteins regulate the apoptotic death and clearance of dying epithelial cells. One such widely known protein is MFG-E8 (Clarkson et al., 2004; Stein et al., 2004). This third objective-based study aims to determine the pathways associated with MFG-E8 protein in

mammary gland development, especially in the lactation to involution transition, phagocytosis, and oncogenesis process.

In the third objective, we asked whether the loss of function of MFG-E8 may promote MEC transformation and its involvement in the regulation of essential cellular homeostasis for cell proliferation. Our quantitative differential proteome analysis and phagocytosis results, along with reported findings, illustrated that the lower expression of MFG-E8 is significantly detrimental to cell health. It is also associated with vesicle trafficking and membrane-associated ion channels, which functions for intracellular transportation (Peng and Elkon, 2011). In contrast, MFG-E8 overexpression in MEC showed aggressive tumour growth in vivo (34). However, we found that the downregulation of MFG-E8 in vitro resulted in the impaired epithelial morphology and decreased cell growth. The lower expression of MFG-E8 is associated with a high level of cyclin-dependent kinase five activator protein (CDK5R2, FC-2). In contrast, all the remaining identified 19 cyclin proteins, including cyclin D1 were either not changed or down-regulated. A similar observation could be seen in the findings where MFG-E8 silencing in 4T1 cells reduces the cyclin protein expression level (Carrascosa et al., 2012).

Specifically, cyclin D1 regulates cell cycle progression during the G1/S transition, and its expression is mostly increased at the activation of oncogenes such as Ras or Neu and found to be up-regulated in breast cancer (Lee and Yang, 2003; Roy and Thompson, 2006). The transgenic mice overexpressing the cyclin D1 protein in the mammary gland resulted in hyperplasia and further led to neoplastic transformation (Wang et al., 1994). However, knockout in transgenic mice producing oncogenic protein Ras prevents mammary tumour development (Yu et al., 2001). Our finding of down-regulation of MFG-E8 resulting in low expression of cyclin D1 in MEC suggests that it is a valuable player involved in the initiation of MEC transformation, pushing it towards slowing down the cell growth; that is an essential requirement during the involution process.

In the iTRAQ based quantitative proteomic dataset, the network analysis reveals direct molecular linkage between knocked down state MFG-E8 activating ZP4 and STAT3/5 proteins. The STAT family proteins are orchestrators of mammary gland remodelling via cell proliferation and breast cells involution (Resemann et al., 2014). These transcription factors are present in the

downstream signalling through various receptors, including cytokines receptors, growth factor receptors, and G-protein-coupled receptors. Here, we found that the ZP4 is physically interacting with JAK1/3-STAT5 and ITGA3/ITGB5 complex. Previously, the immunoprecipitation followed by mass spectrometric and Western blot results validated our findings, where zona pellucida-like domain-containing protein 1 (CUZD1) similar protein like ZP4 in mammary epithelial cells was found physically associated JAK-STAT5 complex (Mapes et al., 2017). The CUZD1/ZP4 expression's amplification is associated with increased JAK1/JAK2/STAT5 signalling, which translocates the STAT5 into the nucleus the mechanism is poorly understood (Mapes et al., 2017). We determined that ZP4 potentiates JAK/STAT signalling downstream of MFG-E8 by mediating ITGA3/ITGB5 receptor activation by our bioinformatics data bridging an adaptor that assists in the recruitment of STAT5 to the stabilising JAK1/3-STAT5 complex. The available literature about the effector proteins roles is the primary precedence of this hypothesis that alters signalling through this complex (Rawlings et al., 2004; Seif et al., 2017). An interesting example is a c-Src protein, which has been shown to propagate PRL initiated JAK/STAT signalling in healthy mammary tissue (García-Martínez et al., 2010). Likewise, STAT5 signalling is inhibited by caveolin-1 (Cav-1) pathway by competitively binding to the domain of JAK2 tyrosine kinase, preventing subsequent activation of STAT5 (Park et al., 2002).

Another molecule regulated by MFG-E8 downstream signalling is DOCK1 resulted into the activation of RACGAP1 (FC-0.8)/RACK1 (FC-0.54) complex by STAT3 phosphorylation on Y705 (Tonozuka et al., 2004) and further transfer to the nucleus to act as a nuclear chaperone (Kawashima et al., 2009). The activation of Rac1 signalling supports the expression level of IL-6 production (Arulanandam et al., 2009) which is complementary to our results were down-regulation of this pathway results in the decreased expression of interleukins (with respective FCs; IL-6, IL-9, IL-16 0.52, IL-18 0.47 and IL-21). Previously, it was observed that the absence of DOCK1 in small mammary gland neoplasia reduced the STAT3 activation (Laurin et al., 2013). Here, we showed that the expression of STAT3 is diminished in the absence of MFG-E8 along with RAC1 and DOCK1. These results suggest that DOCK1 is a key Guanine nucleotide exchange factor (GEF) activating Rac1 complex and initiates the STAT3

activation mutually in mammary gland involution and breast cancer. It will be interesting to investigate the molecular intermediates of the RACGAP1/RACK1 complex in vivo to connect to STAT3 signalling pathway mammary gland developmental physiology as the down-regulation of this signalling resulted into the delays of the proliferation of MEC growth.

On the other hand, we revealed that MFG-E8 mediated DOCK1/Rac1 signalling is essential for nonprofessional epithelial phagocytes to endorse apoptotic cells' engulfment. This work is the first demonstration to address possible global conservation of the function of MFG-E8 mediated DOCK1/RAC1 signalling in mammals' clearance. The DOCK1- binding partner ELMO1 was formerly revealed to operate downstream to the PtdSer receptor BAIAP3 (a form of Bai1) to support dead cells removal. An in vivo study of ELMO1 mutant had shown a defect in removing apoptotic germ cells in the testis (Park et al., 2007; Elliott et al., 2010). Based on these results, we further confirm that BAIAP3 is necessarily required by epithelial cells to promote activation of the MFG-E8/DOCK1/ELMO1/RAC1 component to stimulate the elimination of dead mammary epithelial cells in respect to mammary gland involution. Simultaneously, the other phagocytic receptors, for example, ITGA3/ITGB5 or Tyro3, Axl, or MerTK, are equally vital to clear dying cells through DOCK1/RAC1 signalling. We reason that MFG-E8 mediated signalling is responsible for the activation of the DOCK1/RAC pathway, mainly required for the clearance of dying MECs.

The importance of the PI3K/AKT pathway is typically indispensable, and it plays a crucial role in the process of cell proliferation, survival, motility, secretion, apoptosis, and metabolism (Freudlsperger et al., 2011; Kamal, 2016). The activation of AKT pathway supports cell proliferation and avoids apoptosis in several cell types, consequently delaying cell death, but only limited reports have clearly explained the relationship between MFG-E8 and PI3K/Akt signalling (Jinushi et al., 2008; Neutzner et al., 2007). Our results indicate that downregulation of MFG-E8 leads to decreased expression of multiple PLC proteoforms (with respective Fold change; PLCB1 0.84, PLCB3 0.63, PLCH1 0.91, PLCL1 0.86, PLCG1 0.77, PLCD1 0.67, PLCL2 0.88, PLCD3 0.74, PLCB4 0.86, PLCE1 0.91, PLCG2 0.97, and PLCH2 0.8) mediated PI3K/AKT (FC 0.70) signaling via mTOR modulating the expression of transcription factors which

resulted in the slow proliferation of the MEC cells. The results from the MTT, BrdU, and cell growth confluence assay suggested that the down-regulation of MFG-E8 reduces the cell proliferation rate and does not induce the apoptosis as confirmed by the caspase 3/7 activity assay. Our results of shRNA based knockdown of the MFG-E8 in MECs cells is an excellent reference for future clinical trials as it was previously shown that preventing MFG-E8 signalling via anti- MFG-E8 antibodies caused the regression of experimental breast cancers (Ceriani et al., 1987). Concomitantly, using this approach, synergistically and traditional chemotherapy showed reduced experimental colon carcinomas, melanomas, and lymphomas (Jinushi et al., 2009). In triple-negative breast cancer cells when MFG-E8 expression was silenced, the cells showed high sensitivity to cisplatin treatment (Yang et al., 2011). We collectively present results and published evidence, promoting the notion that MFGE-8 is a constitutive molecule essential for cellular homeostasis. Its expression pattern changes during mammary gland development to restore the molecular balance. The study highlights that combinatorial therapies combined with the blocking of MFG-E8 may prove sufficiently effective outcomes in breast cancer treatment.

Akt1 is a PKB/Akt gene family member, a serine-threonine protein kinase that plays essential critical roles in regulating a myriad of cellular processes, in lactation and breast cancer development. Three Akt isoforms (Akt1, Akt2, and Akt3) are present in mammals. We found all of three in our dataset, especially the expression of Akt2 on the induction of estrogen surge proved by our ovariectomy experiments. In the mammary epithelial cell, consistent activation of Akt triggers the accumulation of the intracellular lipid droplets during pregnancy and delays involution by inhibiting apoptosis after weaning. Our study also found that combining Akt1 and Akt2 is essential for activation of STAT5 during pregnancy and lactation for the mammary epithelial differentiation. Also, Akt is the critical player and central regulator of epithelial cell differentiation and metabolism during lactation. Therefore, Akt seems to be the prevalent downstream connecting link of various signalling pathways mediated through tyrosine kinases receptor. Likewise, Akt and Stat5 signalling pathways were found to be functionally interconnected. Akt1 is required for both the proper mammary gland during postnatal growth and then during functional adult development. Furthermore, regarding postnatal growth, Akt1 showed as the

essential candidate for ductal outgrowth via the fat pad along with for the bifurcation of TEBs, and formation of alveolar buds and terminal ducts (LaRocca et al., 2011; Chen et al., 2010).

During mammary gland development, cell fate decisions are controlled via a transcriptional regulatory network, such as an increase in the methylation or phosphorylation of basal cells compared to luminal cells. In addition, several other epigenetic marks must be involved in controlling the epithelial hierarchy during mammary gland development. Future studies can use whole-genome approaches to understand the pattern of gene expression and epigenetic modifications, hormonal signalling which regulate the development of mammary glands.

CHAPTER –6

Summary and Conclusions

SUMMARY AND CONCLUSION

Mammary gland development occurs in three distinct and differentially regulated stages: embryonic, pubertal and adult. The mature mammary gland consists of ducts which contains an outer layer of myoepithelial cells and an inner layer of luminal epithelial cells that surround a hollow lumen and differentiate into milk-producing alveoli. Massive apoptosis in post lactation stage removes up to 80% of the epithelium during involution. Remarkably, the mammary gland maintains its ability to perform this dramatic remodelling during the pregnancy–lactation–involution cycle for several decades in animals.

Post translation modification (PTM) in the form of protein phosphorylation is an essential cellular machinery, as numerous enzymes and receptors are activated/deactivated by phosphorylation and dephosphorylation events, employing kinases and phosphatases. It is one of the PTM that plays a fundamental role in signal transduction and is a crucial regulator of essential cellular processes including metabolism, growth, cell cycle progression, migration and apoptosis. Here, we focus on development stages during puberty to involution, paying close attention to phosphoproteins mechanisms that establish the mammary epithelial tree's pattern. Some of the elegant mechanisms that drive mammary patterning might be conserved across branched epithelia, and others will pave the way for new paradigms in the study of morphogenesis. We also showed proteins and collective cellular phosphoproteome roles in branching and how they are involved in signalling networks, specifically lactation (Milk Production). The principles that will emerge should help us build comprehensive models for mammary development and important foreplay of phosphoproteomics, particularly milk production and organogenesis in general. Here, in current project work, I studied how these fundamental processes contour the gland's composition and function at different development point using proteomics, phosphoproteomics, transcriptomics, and miRNAomics techniques.

6.1 Time resolved identification of phosphoproteome in mammary gland at six stages of development

- The phosphoproteomics study resulted in the discovery of 6,235 phosphorylated proteins containing 20,328 phosphopetides with more than 25,000 phospho sites.
- The site localization occupancy was determined to be 10:7:3 phosphorylation event in STY amino acid residue, respectively.
- Upon hormonal changes remodeling of mammary gland occurs with the presence of six unique phosphorylated ubiquitin pathway associated proteins in each different stages are Rnf7; Cop1; Trim30c; Bmi1; Rnf133; and Dtx1.
- Phosphorylated olfactory receptors (N=162) found to play significant role in lactation process of mammary gland.
- We discovered kinase (N=256) and phosphate (N=80) cross talk for lactation function in mammary gland.
- tSNE based phosphoproteme classification identified the 19 regulator proteins and an important role of MFGE8 and associated downstream signaling for lactation function in mammary gland.
- We found the upregulation of four kinases (Abl2, Igf1r, Plk3, and Pkdcp) and phosphatase (Pdxp, Dusp27, Psph, Inpp5b) in involution stage upon considering the top 10% upregulating lactation data. Similarly, the upregulation of three kinases (Zfp522b, Gsk3a, Itpkb) and phosphatase (Ptprc, Ppp1r12c, Impa1) in virgin stage upon considering the top 10% downregulating lactation data
- Metabolic activity of mammary gland is regulated by adipogenesis and epithelial cells trans-differentaiation through shifting the phosphorylation event in different stages.

6.2 Transcriptomics analysis of hormone treated female rats with and without ovariectomy

- The combined transcriptomics analysis resulted in the identification of the ~15,731 transcripts out of which 5,218 were relative and differentially expressed transcripts in all eight conditions.
- The carmine staining showed the high adipocyte content in the estrogen-treated ovariectomy mammary gland.
- Comparing eight experiments with top ten abundant kinases showed the eight common in ovariectomy and seven common in normal treatment. We found that Dusp3, Cdkn1a and Akt2 expression only in the presence of estrogen.
- The comparison of identified top upregulated and downregulated kinases and phosphates from normal mammary gland development showed the presence of 19 upregulated and 21 down-regulated kinases in ovx treatment. While 12 upregulated and 10 downregulated phosphatase, common in the normal hormones treated experiment and phosphoproteomics data.
- The transmission electron microscopy showed that the treatment extra estrogen and progesterone in the normal mammary gland resulted in the stacking of micelles and more presence of adipocytes.

6.3 Comparative phosphoproteome analysis of mammary epithelial cell line for identification of ubiquitous expression of proteins

- Combined phosphopeptide analysis between EpH4 and BuMEC identified 2552 common phosphopeptides while 14287 and 7060 in EpH4 and BuMEC, respectively.
- The total identification of phosphoproteome in EpH4 8,468 and BuMEC 7,036 phosphoproteins.

- BuMEC based phosphoproteomics study of lactogenic differentiation resulted in the discovery of 5,451 phosphorylated proteins identified containing 13,855 phosphopetides with more than 25,000 phospho sites.
- The site localization occupancy was determined to be 8:6:2 phosphorylation event in STY amino acid residue, respectively.
- EpH4 based phosphoproteomics study of lactogenic differentiation resulted in the discovery of 5,189 phosphorylated proteins identified containing 16,194 phosphopetides with more than 25,000 phospho sites.
- The site localization occupancy was determined to be 7:7:5 phosphorylation event in STY amino acid residue, respectively.
- Upon hormonal differentiation ten and eight milk associated phosphoproteins are identified in BuMEC and EpH4 cell line, respectively.
- PI3K-Akt; mTOR; Cadherin; JAK/STAT; Oxytocin receptor mediated; LIF; and Wnt signaling pathways were discovered to be commonly regulated between *in-vivo* and *in-vitro* studies.
- Two key miRNA that are miRNA-335p and miRNA-146a in both the EpH4 and BUMEC cell lines was identified upon functional differentiation.
- MFGE8 is one of the highlighted important common connecting phosphoprotein identified among these studies.

6.4 Targeted validation of an important phosphoprotein in cell line involved in lactation

- MFG-E8 suppression results in reduced growth of mammary epithelial cells by an autocrine/paracrine mechanism
- Results in the induction of transcription factors such as cyclins D1, FOXA1, ZNF652, AURKB and many others for modulating the cytoskeleton-associated proteins and cell cycle regulators.

- The significance of MFG-E8 signalling concerning mammary gland developmental remodelling and disease is indisputable, and this study through proteomic examination has underscored its importance in cellular homeostasis.

Conclusion

We conclude that the metabolic activity of mammary gland remodeling is regulated by adipogenesis and epithelial cells trans-differentiation through shifting the phosphorylation event in different stages. The phosphoproteomics data provide new insight into the cell polarization linked to the PI3K-Akt; mTOR; Cadherin; JAK/STAT; Oxytocin receptor mediated; LIF; and Wnt signaling pathways. Our findings brighten up the concept regarding the importance of MFGE8 protein in overall mammary gland development.

We finally anticipate that our comprehensive datasets will serve as a valuable foundation for further validation and mechanistic exposition of many novel proteins involved in the mammary gland (breast) development signalling.

Bibliography

BIBLIOGRAPHY

Abell, K., Bilancio, A., Clarkson, R.W., Tiffen, P.G., Altaparmakov, A.I., Burdon, T.G., Asano, T., Vanhaesebroeck, B. and Watson, C.J., 2005. Stat3-induced apoptosis requires a molecular switch in PI (3) K subunit composition. *Nature cell biology*, ***7*****(4),** pp.392-398.

Adams, J.C. and Watt, F.M., 1993. Regulation of development and differentiation by the extracellular matrix. *Development*, ***117*****(4),** pp.1183-1198.

Aebersold, R. and Mann, M., 2003. Mass spectrometry-based proteomics. *Nature*, ***422*****(6928),** pp.198-207.

Affolter, M., Zeller, R. and Caussinus, E., 2009. Tissue remodelling through branching morphogenesis. *Nature reviews Molecular cell biology*, ***10*****(12),** pp.831-842.

Ali, S.A., Kaur, G., Kaushik, J.K., Malakar, D., Mohanty, A.K. and Kumar, S., 2017. Examination of pathways involved in leukemia inhibitory factor (LIF)-induced cell growth arrest using label-free proteomics approach. *Journal of proteomics*, ***168*****,** pp.37-52.

Andersen, K., Mori, H., Fata, J., Bascom, J., Øyjord, T., Mælandsmo, G.M. and Bissell, M., 2011. The metastasis-promoting protein S100A4 regulates mammary branching morphogenesis. *Developmental biology*, **352(2)**, pp.181-190.

Andres, A.C. and Strange, R., 1999. Apoptosis in the estrous and menstrual cycles. *Journal of mammary gland biology and neoplasia*, ***4*****(2),** pp.221-228.

Andrews, J.L., Kim, A.C. and Hens, J.R., 2012. The role and function of cadherins in the mammary gland. *Breast cancer research*, **14(1),** pp.1-10.

Antfolk, D., Sjöqvist, M., Cheng, F., Isoniemi, K., Duran, C.L., Rivero-Muller, A., Antila, C., Niemi, R., Landor, S., Bouten, C.V. and Bayless, K.J., 2017. Selective regulation of Notch ligands during angiogenesis is mediated

by vimentin. Proceedings of the National Academy of Sciences, **114(23)**, pp.E4574-E4581.

Arendt, L.M. and Rugowski, D., Grafwallner-Huseth, E., Garcia-Barchino, MJ, Rui, H., and Schuler, LA (2011) Prolactin-induced mouse mammary carcinomas model estrogen resistant luminal breast cancer. *Breast Cancer Res*, **13**, p.R11.

Arendt, L.M., Evans, L.C., Rugowski, D.E., Garcia-Barchino, M.J., Rui, H. and Schuler, L.A., 2009. Ovarian hormones are not required for PRL-induced mammary tumorigenesis, but estrogen enhances neoplastic processes. *The Journal of endocrinology*, **203(1)**, p.99.

Arulanandam, R., Vultur, A., Cao, J., Carefoot, E., Elliott, B.E., Truesdell, P.F., Larue, L., Feracci, H. and Raptis, L., 2009. Cadherin-cadherin engagement promotes cell survival via Rac1/Cdc42 and signal transducer and activator of transcription-3. *Molecular Cancer Research*, **7(8)**, pp.1310-1327.

Asch, H.L. and Asch, B.B., 1985. Expression of keratins and other cytoskeletal proteins in mouse mammary epithelium during the normal developmental cycle and primary culture. *Developmental biology*, ***107*(2),** pp.470-482.

Atabai, K., Fernandez, R., Huang, X., Ueki, I., Kline, A., Li, Y., Sadatmansoori, S., Smith-Steinhart, C., Zhu, W., Pytela, R. and Werb, Z., 2005. Mfge8 is critical for mammary gland remodeling during involution. *Molecular biology of the cell*, ***16*(12)**, pp.5528-5537.

Atwood, C.S., Hovey, R.C., Glover, J.P., Chepko, G., Ginsburg, E., Robison, W.C. and Vonderhaar, B.K., 2000. Progesterone induces side-branching of the ductal epithelium in the mammary glands of peripubertal mice. *Journal of Endocrinology*, ***167*(1)**, pp.39-52.

Aziz, M., Yang, W.L., Corbo, L.M., Chaung, W.W., Matsuo, S. and Wang, P., 2015. MFG-E8 inhibits neutrophil migration through αvβ3-integrin-dependent MAP kinase activation. *International journal of molecular medicine*, ***36*(1)**, pp.18-28.

Balinsky, B.I., 1950. On the prenatal growth of the mammary gland rudiment in the mouse. *Journal of anatomy*, ***84*****(Pt 3)**, p.227.

Bantscheff, M., Schirle, M., Sweetman, G., Rick, J. and Kuster, B., 2007. Quantitative mass spectrometry in proteomics: a critical review. *Analytical and bioanalytical chemistry*, ***389*****(4)**, pp.1017-1031.

Barash, I., 2006. Stat5 in the mammary gland: controlling normal development and cancer. *Journal of cellular physiology*, **209(2)**, pp.305-313.

Bernichtein, S., Touraine, P. and Goffin, V., 2010. New concepts in prolactin biology. *The Journal of endocrinology*, **206(1)**, p.1.

Bertucci, P.Y., Quaglino, A., Pozzi, A.G., Kordon, E.C. and Pecci, A., 2010. Glucocorticoid-induced impairment of mammary gland involution is associated with STAT5 and STAT3 signaling modulation. *Endocrinology*, **151(12)**, pp.5730-5740.

Birge, R.B., Boeltz, S., Kumar, S., Carlson, J., Wanderley, J., Calianese, D., Barcinski, M., Brekken, R.A., Huang, X., Hutchins, J.T. and Freimark, B., 2016. Phosphatidylserine is a global immunosuppressive signal in efferocytosis, infectious disease, and cancer. *Cell Death & Differentiation*, ***23*****(6)**, pp.962-978.

Bjornstrom, L., Kilic, E., Norman, M., Parker, M.G. and Sjoberg, M., 2001. Cross-talk between Stat5b and estrogen receptor-alpha and-beta in mammary epithelial cells. *Journal of molecular endocrinology*, **27(1)**, pp.93-106.

Bloushtain-Qimron, N., Yao, J., Snyder, E.L., Shipitsin, M., Campbell, L.L., Mani, S.A., Hu, M., Chen, H., Ustyansky, V., Antosiewicz, J.E. and Argani, P., 2008. Cell type-specific DNA methylation patterns in the human breast. *Proceedings of the National Academy of Sciences,* **105(37)**, pp.14076-14081.

Bocchinfuso, W.P. and Korach, K.S., 1997. Mammary gland development and tumorigenesis in estrogen receptor knockout mice. *Journal of mammary gland biology and neoplasia*, ***2*****(4)**, pp.323-334.

Boerner, J.L., Gibson, M.A., Fox, E.M., Posner, E.D., Parsons, S.J., Silva, C.M. and Shupnik, M.A., 2005. Estrogen negatively regulates epidermal growth factor (EGF)-mediated signal transducer and activator of transcription 5 signaling in human EGF family receptor-overexpressing breast cancer cells. *Molecular endocrinology*, **19(11),** pp.2660-2670.

Boeuf, H., Hauss, C., Graeve, F.D., Baran, N. and Kedinger, C., 1997. Leukemia inhibitory factor–dependent transcriptional activation in embryonic stem cells. *The Journal of cell biology*, **138(6),** pp.1207-1217.

Bolander Jr, F.F., 1990. Differential characteristics of the thoracic and abdominal mammary glands from mice. *Experimental cell research*, ***189*(1)**, pp.142-144.

Bonaldi, T., Straub, T., Cox, J., Kumar, C., Becker, P.B. and Mann, M., 2008. Combined use of RNAi and quantitative proteomics to study gene function in Drosophila. *Molecular cell*, ***31*(5)**, pp.762-772.

Boussadia, O., Kutsch, S., Hierholzer, A., Delmas, V. and Kemler, R., 2002. E-cadherin is a survival factor for the lactating mouse mammary gland. *Mechanisms of development*, **115(1-2),** pp.53-62.

Bradbury, J.M., Edwards, P.A., Niemeyer, C.C. and Dale, T.C., 1995. Wnt-4 expression induces a pregnancy-like growth pattern in reconstituted mammary glands in virgin mice. *Developmental biology*, ***170*(2)**, pp.553-563.

Brisken, C. and Duss, S., 2007. Stem cells and the stem cell niche in the breast: an integrated hormonal and developmental perspective. *Stem cell reviews*, ***3*(2)**, pp.147-156.

Brisken, C., 1999. Kaur S, Chavarria TE, Binart N, Sutherland RL, Weinberg RA, Kelly PA, and Ormandy CJ. *Prolactin controls mammary gland development via direct and indirect mechanisms. Dev Biol*, ***210***, pp.96-106.

Brisken, C., Ayyannan, A., Nguyen, C., Heineman, A., Reinhardt, F., Jan, T., Dey, S.K., Dotto, G.P. and Weinberg, R.A., 2002. IGF-2 is a mediator

of prolactin-induced morphogenesis in the breast. *Developmental cell*, ***3*(6)**, pp.877-887.

Brisken, C., Heineman, A., Chavarria, T., Elenbaas, B., Tan, J., Dey, S.K., McMahon, J.A., McMahon, A.P. and Weinberg, R.A., 2000. Essential function of Wnt-4 in mammary gland development downstream of progesterone signaling. *Genes & development*, ***14*(6)**, pp.650-654.

Brisken, C., Kaur, S., Chavarria, T.E., Binart, N., Sutherland, R.L., Weinberg, R.A., Kelly, P.A. and Ormandy, C.J., 1999. Prolactin controls mammary gland development via direct and indirect mechanisms. *Developmental biology*, ***210*(1)**, pp.96-106.

Brisken, C., Park, S., Vass, T., Lydon, J.P., O'Malley, B.W. and Weinberg, R.A., 1998. A paracrine role for the epithelial progesterone receptor in mammary gland development. *Proceedings of the National Academy of Sciences*, ***95*(9)**, pp.5076-5081.

Britt, K., Ashworth, A. and Smalley, M., 2007. Pregnancy and the risk of breast cancer. *Endocrine-related cancer*, *14*(4), pp.907-933.

Buser, A.C., Gass-Handel, E.K., Wyszomierski, S.L., Doppler, W., Leonhardt, S.A., Schaack, J., Rosen, J.M., Watkin, H., Anderson, S.M. and Edwards, D.P., 2007. Progesterone receptor repression of prolactin/signal transducer and activator of transcription 5-mediated transcription of the β-casein gene in mammary epithelial cells. *Molecular Endocrinology*, **21(1)**, pp.106-125.

Butter, F., Kappei, D., Buchholz, F., Vermeulen, M. and Mann, M., 2010. A domesticated transposon mediates the effects of a single-nucleotide polymorphism responsible for enhanced muscle growth. *EMBO reports*, ***11*(4)**, pp.305-311.

Carmon, L., Bobilev-Priel, I., Brenner, B., Bobilev, D., Paz, A., Bar-Haim, E., Tirosh, B., Klein, T., Fridkin, M., Lemonnier, F. and Tzehoval, E., 2002. Characterization of novel breast carcinoma–associated BA46-derived peptides in HLA-A2. 1/D b-β2mtransgenic mice. The *Journal of clinical investigation*, **110(4)**, pp.453-462.

Carrascosa, C., Obula, R.G., Missiaglia, E., Lehr, H.A., Delorenzi, M., Frattini, M., Rüegg, C. and Mariotti, A., 2012. MFG-E8/lactadherin regulates cyclins D1/D3 expression and enhances the tumorigenic potential of mammary epithelial cells. *Oncogene*, **31(12)**, pp.1521-1532.

Castanon, I., Von Stetina, S., Kass, J. and Baylies, M.K., 2001. Dimerization partners determine the activity of the Twist bHLH protein during Drosophila mesoderm development. *Development*, **128(16)**, pp.3145-3159.

Cella, N., Groner, B. and Hynes, N.E., 1998. Characterization of Stat5a and Stat5b homodimers and heterodimers and their association with the glucocortiocoid receptor in mammary cells. *Molecular and Cellular Biology*, **18(4)**, pp.1783-1792.

Ceriani, R.L., Blank, E.W. and Peterson, J.A., 1987. Experimental immunotherapy of human breast carcinomas implanted in nude mice with a mixture of monoclonal antibodies against human milk fat globule components. *Cancer research*, **47(2)**, pp.532-540.

Ceriani, R.L., Peterson, J.A., Lee, J.Y., Moncada, R. and Blank, E.W., 1983. Characterization of cell surface antigens of human mammary epithelial cells with monoclonal antibodies prepared against human milk fat globule. *Somatic cell genetics*, **9(4)**, pp.415-427.

Chan, C.B., Liu, X., Ensslin, M.A., Dillehay, D.L., Ormandy, C.J., Sohn, P., Serra, R. and Ye, K., 2010. PIKE-A is required for prolactin-mediated STAT5a activation in mammary gland development. *The EMBO journal*, **29(5)**, pp.956-968.

Chapman, R.S., Lourenco, P.C., Tonner, E., Flint, D.J., Selbert, S., Takeda, K., Akira, S., Clarke, A.R. and Watson, C.J., 1999. Suppression of epithelial apoptosis and delayed mammary gland involution in mice with a conditional knockout of Stat3. *Genes & development,* **13(19)**, pp.2604-2616.

Chen, C.C., Boxer, R.B., Stairs, D.B., Portocarrero, C.P., Horton, R.H., Alvarez, J.V., Birnbaum, M.J. and Chodosh, L.A., 2010. Akt is required for

Stat5 activation and mammary differentiation. *Breast Cancer Research*, **12(5)**, p.R72.

Chen, C.C., Stairs, D.B., Boxer, R.B., Belka, G.K., Horseman, N.D., Alvarez, J.V. and Chodosh, L.A., 2012. Autocrine prolactin induced by the Pten–Akt pathway is required for lactation initiation and provides a direct link between the Akt and Stat5 pathways. *Genes & development*, ***26*(19)**, pp.2154-2168.

Chiquet-Ehrismann, R., Mackie, E.J., Pearson, C.A. and Sakakura, T., 1986. Tenascin: an extracellular matrix protein involved in tissue interactions during fetal development and oncogenesis. *Cell*, ***47*(1)**, pp.131-139.

Choi, Y.S., Chakrabarti, R., Escamilla-Hernandez, R. and Sinha, S., 2009. Elf5 conditional knockout mice reveal its role as a master regulator in mammary alveolar development: failure of Stat5 activation and functional differentiation in the absence of Elf5. *Developmental biology*, **329(2)**, pp.227-241.

Choudhary, C. and Mann, M., 2010. Decoding signalling networks by mass spectrometry-based proteomics. *Nature reviews Molecular cell biology*, ***11*(6)**, pp.427-439.

Choudhary, C., Kumar, C., Gnad, F., Nielsen, M.L., Rehman, M., Walther, T.C., Olsen, J.V. and Mann, M., 2009. Lysine acetylation targets protein complexes and co-regulates major cellular functions. *Science*, ***325*(5942)**, pp.834-840.

Clarkson, R.W., Wayland, M.T., Lee, J., Freeman, T. and Watson, C.J., 2004. Gene expression profiling of mammary gland development reveals putative roles for death receptors and immune mediators in post-lactational regression. *Breast Cancer Research*, ***6*(2)**, p.R92.

Clarkson, R.W., Wayland, M.T., Lee, J., Freeman, T. and Watson, C.J., 2004. Gene expression profiling of mammary gland development reveals putative roles for death receptors and immune mediators in post-lactational regression. *Breast Cancer Research*, **6(2)**, p.R92.

Cohen, P., 2001. The role of protein phosphorylation in human health and disease. *FEBS Journal*, ***268*****(19)**, pp.5001-5010.

Colucci-Guyon, E., Portier, M.M., Dunia, I., Paulin, D., Pournin, S. and Babinet, C., 1994. Mice lacking vimentin develop and reproduce without an obvious phenotype. *Cell*, **79(4)**, pp.679-694.

Conneely, O.M., Mulac-Jericevic, B. and Lydon, J.P., 2003. Progesterone-dependent regulation of female reproductive activity by two distinct progesterone receptor isoforms. *Steroids*, ***68*****(10-13)**, pp.771-778.

Corthals, G.L., Wasinger, V.C., Hochstrasser, D.F. and Sanchez, J.C., 2000. The dynamic range of protein expression: a challenge for proteomic research. *Electrophoresis: An International Journal*, ***21*****(6)**, pp.1104-1115.

Coulombe, P.A. and Wong, P., 2004. Cytoplasmic intermediate filaments revealed as dynamic and multipurpose scaffolds. *Nature cell biology*, **6(8)**, pp.699-706.

Couse, J.F. and Korach, K.S., 1999. Estrogen receptor null mice: what have we learned and where will they lead us?. *Endocrine reviews*, ***20*****(3)**, pp.358-417.

Cunha, G.R., Chung, L.W., Shannon, J.M. and Reese, B.A., 1980. Stromal-epithelial interactions in sex differentiation. *Biology of reproduction*, ***22*****(1)**, pp.19-42.

Cutillas, P.R. and Jørgensen, C., 2011. Biological signalling activity measurements using mass spectrometry. *Biochemical Journal*, ***434*****(2)**, pp.189-199.

Daniel, C.W. and Smith, G.H., 1999. The mammary gland: a model for development. *Journal of mammary gland biology and neoplasia*, ***4*****(1)**, p.3.

Daniel, C.W., Silberstein, G.B. and Strickland, P., 1987. Direct action of 17β-estradiol on mouse mammary ducts analyzed by sustained release implants and steroid autoradiography. *Cancer research*, ***47*****(22)**, pp.6052-6057.

Davies, J.A., 2002. Do different branching epithelia use a conserved developmental mechanism?. *Bioessays*, ***24*****(10)**, pp.937-948.

De Godoy, L.M., Olsen, J.V., Cox, J., Nielsen, M.L., Hubner, N.C., Fröhlich, F., Walther, T.C. and Mann, M., 2008. Comprehensive mass-spectrometry-based proteome quantification of haploid versus diploid yeast. *Nature*, ***455*****(7217)**, pp.1251-1254.

De Herreros, A.G., Peiró, S., Nassour, M. and Savagner, P., 2010. Snail family regulation and epithelial mesenchymal transitions in breast cancer progression. *Journal of mammary gland biology and neoplasia*, **15(2)**, pp.135-147.

Deane, C.M., Salwiński, Ł., Xenarios, I. and Eisenberg, D., 2002. Protein interactions: two methods for assessment of the reliability of high throughput observations. *Molecular & Cellular Proteomics*, ***1*****(5)**, pp.349-356.

Deroo, B.J., Hewitt, S.C., Collins, J.B., Grissom, S.F., Hamilton, K.J. and Korach, K.S., 2009. Profile of estrogen-responsive genes in an estrogen-specific mammary gland outgrowth model. *Molecular reproduction and development*, ***76*****(8)**, pp.733-750.

Deutsch, E.W., Mendoza, L., Shteynberg, D., Farrah, T., Lam, H., Tasman, N., Sun, Z., Nilsson, E., Pratt, B., Prazen, B. and Eng, J.K., 2010. A guided tour of the Trans-Proteomic Pipeline. *Proteomics*, ***10*****(6)**, pp.1150-1159.

Dhouailly, D., Rogers, G.E. and Sengel, P., 1978. The specification of feather and scale protein synthesis in epidermal-dermal recombinations. *Developmental biology*, ***65*****(1)**, pp.58-68.

Domon, B. and Aebersold, R., 2006. Mass spectrometry and protein analysis. *science*, ***312*****(5771)**, pp.212-217.

Ekblom, P., 1984. Basement membrane proteins and growth factors in kidney differentiation. *The role of extracellular matrix in development*, pp.173-206.

Elliott, M.R., Zheng, S., Park, D., Woodson, R.I., Reardon, M.A., Juncadella, I.J., Kinchen, J.M., Zhang, J., Lysiak, J.J. and Ravichandran, K.S., 2010. Unexpected requirement for ELMO1 in clearance of apoptotic germ cells in vivo. *Nature*, **467(7313)**, pp.333-337.

Ensslin, M.A. and Shur, B.D., 2007. The EGF repeat and discoidin domain protein, SED1/MFG-E8, is required for mammary gland branching morphogenesis. *Proceedings of the National Academy of Sciences*, **104(8)**, pp.2715-2720.

Eriksson, J.E., Dechat, T., Grin, B., Helfand, B., Mendez, M., Pallari, H.M. and Goldman, R.D., 2009. Introducing intermediate filaments: from discovery to disease. *The Journal of clinical investigation*, **119(7)**, pp.1763-1771.

Fang, F., Rycyzyn, M.A. and Clevenger, C.V., 2009. Role of c-Myb during prolactin-induced signal transducer and activator of transcription 5a signaling in breast cancer cells. *Endocrinology*, **150(4)**, pp.1597-1606.

Fata, J.E., Kong, Y.Y., Li, J., Sasaki, T., Irie-Sasaki, J., Moorehead, R.A., Elliott, R., Scully, S., Voura, E.B., Lacey, D.L. and Boyle, W.J., 2000. The osteoclast differentiation factor osteoprotegerin-ligand is essential for mammary gland development. *Cell*, ***103*(1)**, pp.41-50.

Fata, J.E., Werb, Z. and Bissell, M.J., 2003. Regulation of mammary gland branching morphogenesis by the extracellular matrix and its remodeling enzymes. *Breast cancer research*, ***6*(1)**, p.1.

Feng, Z., Marti, A., Jehn, B., Altermatt, H.J., Chicaiza, G. and Jaggi, R., 1995. Glucocorticoid and progesterone inhibit involution and programmed cell death in the mouse mammary gland. *The Journal of Cell Biology*, ***131*(4)**, pp.1095-1103.

Fernandez-Valdivia, R., Mukherjee, A., Ying, Y., Li, J., Paquet, M., DeMayo, F.J. and Lydon, J.P., 2009. The RANKL signaling axis is sufficient to elicit ductal side-branching and alveologenesis in the mammary gland of the virgin mouse. *Developmental biology*, ***328*(1)**, pp.127-139.

Fernandez-Valdivia, R., Mukherjee, A., Ying, Y., Li, J., Paquet, M., DeMayo, F.J. and Lydon, J.P., 2009. The RANKL signaling axis is sufficient to elicit ductal side-branching and alveologenesis in the mammary gland of the virgin mouse. *Developmental biology*, **328(1)**, pp.127-139.

Foley, J., Dann, P., Hong, J., Cosgrove, J., Dreyer, B., Rimm, D., Dunbar, M., Philbrick, W. and Wysolmerski, J., 2001. Parathyroid hormone-related protein maintains mammary epithelial fate and triggers nipple skin differentiation during embryonic breast development. *Development*, ***128*(4)**, pp.513-525.

Forsyth, I.A. and Neville, M.C., 2009. Introduction: the myoepithelial cell and milk letdown; entrance to the multifunctional role of oxytocin. *Journal of mammary gland biology and neoplasia*, ***14*(3)**, pp.221-222.

Fox, E.M., Andrade, J. and Shupnik, M.A., 2009. Novel actions of estrogen to promote proliferation: integration of cytoplasmic and nuclear pathways. *Steroids*, **74(7)**, pp.622-627.

Franke, W.W., Schmid, E., Freudenstein, C., Appelhans, B., Osborn, M., Weber, K. and Keenan, T.W., 1980. Intermediate-sized filaments of the prekeratin type in myoepithelial cells. *The Journal of cell biology*, **84(3)**, pp.633-654.

Freischmajer R., and Billingham R., 1968. Epithelial–mesenchymal interactions; 18th Hahnemann symposium. Baltimore: *Williams & Wilkins*; 326 pp.

Freudlsperger, C., Burnett, J.R., Friedman, J.A., Kannabiran, V.R., Chen, Z. and Van Waes, C., 2011. EGFR–PI3K–AKT–mTOR signaling in head and neck squamous cell carcinomas: attractive targets for molecular-oriented therapy. *Expert opinion on therapeutic targets*, **15(1)**, pp.63-74.

Fukamachi, H., Mizuno, T. and Takayama, S., 1979. Epithelial-mesenchymal interactions in differentiation of stomach epithelium in fetal mice. *Anatomy and embryology*, ***157*(2)**, pp.151-160.

Furth, P.A., Nakles, R.E., Millman, S., Diaz-Cruz, E.S. and Cabrera, M.C., 2011. Signal transducer and activator of transcription 5 as a key signaling

pathway in normal mammary gland developmental biology and breast cancer. *Breast Cancer Research*, **13(5)**, pp.1-14.

García-Martínez, J.M., Calcabrini, A., González, L., Martín-Forero, E., Agulló-Ortuño, M.T., Simon, V., Watkin, H., Anderson, S.M., Roche, S. and Martín-Pérez, J., 2010. A non-catalytic function of the Src family tyrosine kinases controls prolactin-induced Jak2 signaling. *Cellular signalling*, **22(3)**, pp.415-426.

Geiger, T., Cox, J., Ostasiewicz, P., Wisniewski, J.R. and Mann, M., 2010. Super-SILAC mix for quantitative proteomics of human tumor tissue. *Nature methods*, ***7*(5)**, pp.383-385.

Gossage, L. and Eisen, T., 2010. Targeting multiple kinase pathways: a change in paradigm. *Clinical Cancer Research*, ***16*(7)**, pp.1973-1978.

Graham, J.D., Mote, P.A., Salagame, U., van Dijk, J.H., Balleine, R.L., Huschtscha, L.I., Reddel, R.R. and Clarke, C.L., 2009. DNA replication licensing and progenitor numbers are increased by progesterone in normal human breast. *Endocrinology*, **150(7)**, pp.3318-3326.

Graham, T.R., Zhau, H.E., Odero-Marah, V.A., Osunkoya, A.O., Kimbro, K.S., Tighiouart, M., Liu, T., Simons, J.W. and O'Regan, R.M., 2008. Insulin-like growth factor-I–dependent up-regulation of ZEB1 drives epithelial-to-mesenchymal transition in human prostate cancer cells. *Cancer research*, **68(7),** pp.2479-2488.

Grobstein, C., 1953. Morphogenetic interaction between embryonic mouse tissues separated by a membrane filter. *Nature*, ***172*(4384)**, pp.869-871.

Grobstein, C., 1967. Mechanisms of organogenetic tissue interaction. *Natl cancer inst monogr*, ***26***, pp.279-299.

Gstaiger, M. and Aebersold, R., 2009. Applying mass spectrometry-based proteomics to genetics, genomics and network biology. *Nature Reviews Genetics*, ***10*(9)**, pp.617-627.

Gu, B., Sun, P., Yuan, Y., Moraes, R.C., Li, A., Teng, A., Agrawal, A., Rhéaume, C., Bilanchone, V., Veltmaat, J.M. and Takemaru, K.I., 2009. Pygo2

expands mammary progenitor cells by facilitating histone H3 K4 methylation. *Journal of Cell Biology*, **185(5)**, pp.811-826.

Gygi, S.P., Rist, B., Gerber, S.A., Turecek, F., Gelb, M.H. and Aebersold, R., 1999. Quantitative analysis of complex protein mixtures using isotope-coded affinity tags. *Nature biotechnology*, ***17*(10)**, pp.994-999.

Haaksma, C.J., Schwartz, R.J. and Tomasek, J.J., 2011. Myoepithelial cell contraction and milk ejection are impaired in mammary glands of mice lacking smooth muscle alpha-actin. *Biology of reproduction*, **85(1)**, pp.13-21.

Hajra, K.M., Chen, D.Y. and Fearon, E.R., 2002. The SLUG zinc-finger protein represses E-cadherin in breast cancer. *Cancer research*, **62(6)**, pp.1613-1618.

Hamamori, Y., Wu, H.Y., Sartorelli, V. and Kedes, L., 1997. The basic domain of myogenic basic helix-loop-helix (bHLH) proteins is the novel target for direct inhibition by another bHLH protein, Twist. *Molecular and cellular biology*, **17(11)**, pp.6563-6573.

Hanayama, R. and Nagata, S., 2005. Impaired involution of mammary glands in the absence of milk fat globule EGF factor 8. *Proceedings of the National Academy of Sciences*, ***102*(46)**, pp.16886-16891.

Hanayama, R., Tanaka, M., Miwa, K., Shinohara, A., Iwamatsu, A. and Nagata, S., 2002. Identification of a factor that links apoptotic cells to phagocytes. *Nature*, ***417*(6885)**, pp.182-187.

Hanayama, R., Tanaka, M., Miyasaka, K., Aozasa, K., Koike, M., Uchiyama, Y. and Nagata, S., 2004. Autoimmune disease and impaired uptake of apoptotic cells in MFG-E8-deficient mice. *Science*, **304(5674)**, pp.1147-1150.

Harris, J., Stanford, P.M., Sutherland, K., Oakes, S.R., Naylor, M.J., Robertson, F.G., Blazek, K.D., Kazlauskas, M., Hilton, H.N., Wittlin, S. and Alexander, W.S., 2006. Socs2 and elf5 mediate prolactin-induced mammary gland development. *Molecular endocrinology*, ***20*(5)**, pp.1177-1187.

Hazan, R.B., Kang, L., Whooley, B.P. and Borgen, P.I., 1997. N-cadherin promotes adhesion between invasive breast cancer cells and the stroma. *Cell adhesion and communication*, **4(6)**, pp.399-411.

Hendricks, L., Aziz, M., Yang, W.L., Nicastro, J., Coppa, G.F., Symons, M. and Wang, P., 2017. Milk fat globule-epidermal growth factor-factor VIII–derived peptide MSP68 is a cytoskeletal immunomodulator of neutrophils that inhibits Rac1. *Journal of Surgical Research*, ***208***, pp.10-19.

Hennighausen, L. and Robinson, G.W., 2001. Signaling pathways in mammary gland development. *Developmental cell*, ***1*(4)**, pp.467-475.

Hens, J.R. and Wysolmerski, J.J., 2005. Key stages of mammary gland development: molecular mechanisms involved in the formation of the embryonic mammary gland. *Breast Cancer Research*, ***7*(5)**, p.220.

Hens, J.R., Dann, P., Zhang, J.P., Harris, S., Robinson, G.W. and Wysolmerski, J., 2007. BMP4 and PTHrP interact to stimulate ductal outgrowth during embryonic mammary development and to inhibit hair follicle induction. *Development*, ***134*(6)**, pp.1221-1230.

Herman, I.M., 1993. Actin isoforms. *Current opinion in cell biology*, **5(1)**, pp.48-55.

Hidai, C., Zupancic, T., Penta, K., Mikhail, A., Kawana, M., Quertermous, E.E., Aoka, Y., Fukagawa, M., Matsui, Y., Platika, D. and Auerbach, R., 1998. Cloning and characterization of developmental endothelial locus-1: an embryonic endothelial cell protein that binds the αvβ3 integrin receptor. *Genes & development*, **12(1)**, pp.21-33.

Hilton, H.N., Kalyuga, M., Cowley, M.J., Alles, M.C., Lee, H.J., Caldon, C.E., Blazek, K., Kaplan, W., Musgrove, E.A., Daly, R.J. and Naylor, M.J., 2010. The antiproliferative effects of progestins in T47D breast cancer cells are tempered by progestin induction of the ETS transcription factor Elf5. *Molecular Endocrinology*, **24(7)**, pp.1380-1392.

Hinck, L. and Silberstein, G.B., 2005. Key stages in mammary gland development: the mammary end bud as a motile organ. *Breast Cancer Research*, ***7*(6)**, p.245.

Hirano, Y., Yang, W.L., Aziz, M., Zhang, F., Sherry, B. and Wang, P., 2017. MFG-E8-derived peptide attenuates adhesion and migration of immune cells to endothelial cells. *Journal of leukocyte biology*, ***101*(5)**, pp.1201-1209.

Hovey, R.C. and Trott, J.F., 2004. Morphogenesis of mammary gland development. In Protecting Infants through Human Milk (pp. 219-228). Springer, Boston, MA.

Howard, B.A. and Gusterson, B.A., 2000. Human breast development. *Journal of mammary gland biology and neoplasia*, ***5*(2)**, pp.119-137.

Howe, L.R., Watanabe, O., Leonard, J. and Brown, A.M., 2003. Twist is up-regulated in response to Wnt1 and inhibits mouse mammary cell differentiation. *Cancer research*, **63(8)**, pp.1906-1913.

Howlett, A.R. and Bissell, M.J., 1993. The influence of tissue microenvironment (stroma and extracellular matrix) on the development and function of mammary epithelium. *Epithelial cell biology*, ***2*(2)**, p.79.

Hsu, J.L., Huang, S.Y., Chow, N.H. and Chen, S.H., 2003. Stable-isotope dimethyl labeling for quantitative proteomics. *Analytical chemistry*, ***75*(24)**, pp.6843-6852.

Hu, C.Y., Wu, C.S., Tsai, H.F., Chang, S.K., Tsai, W.I. and Hsu, P.N., 2009. Genetic polymorphism in milk fat globule-EGF factor 8 (MFG-E8) is associated with systemic lupus erythematosus in human. *Lupus*, **18(8)**, pp.676-681.

Hu, Q., Noll, R.J., Li, H., Makarov, A., Hardman, M. and Graham Cooks, R., 2005. The Orbitrap: a new mass spectrometer. *Journal of mass spectrometry*, ***40*(4)**, pp.430-443.

Hubner, N.C., Bird, A.W., Cox, J., Splettstoesser, B., Bandilla, P., Poser, I., Hyman, A. and Mann, M., 2010. Quantitative proteomics combined

with BAC TransgeneOmics reveals in vivo protein interactions. *Journal of Cell Biology*, ***189*****(4)**, pp.739-754.

Humphreys, R.C., Krajewska, M., Krnacik, S., Jæger, R., Weiher, H., Krajewski, S., Reed, J.C. and Rosen, J.M., 1996. Apoptosis in the terminal endbud of the murine mammary gland: a mechanism of ductal morphogenesis. *Development*, ***122*****(12)**, pp.4013-4022.

Humphreys, R.C., Lydon, J., O'Malley, B.W. and Rosen, J.M., 1997. Mammary gland development is mediated by both stromal and epithelial progesterone receptors. *Molecular endocrinology*, ***11*****(6)**, pp.801-811.

Hutson, S.W., Cowen, P.N. and Bird, C.C., 1985. Morphometric studies of age related changes in normal human breast and their significance for evolution of mammary cancer. *Journal of clinical pathology*, ***38*****(3)**, pp.281-287.

Inaguma, Y., Kusakabe, M., Mackie, E.J., Pearson, C.A., Chiquet-Ehrismann, R. and Sakakura, T., 1988. Epithelial induction of stromal tenascin in the mouse mammary gland: from embryogenesis to carcinogenesis. *Developmental biology*, ***128*****(2)**, pp.245-255.

Inaguma, Y., Kusakabe, M., Mackie, E.J., Pearson, C.A., Chiquet-Ehrismann, R. and Sakakura, T., 1988. Epithelial induction of stromal tenascin in the mouse mammary gland: from embryogenesis to carcinogenesis. *Developmental biology*, ***128*****(2)**, pp.245-255.

Ingman, W.V. and Robertson, S.A., 2008. Mammary gland development in transforming growth factor beta1 null mutant mice: systemic and epithelial effects. *Biology of reproduction*, ***79*****(4)**, pp.711-717.

Janjanam, J., Singh, S., Jena, M.K., Varshney, N., Kola, S., Kumar, S., Kaushik, J.K., Grover, S., Dang, A.K., Mukesh, M. and Prakash, B.S., 2014. Comparative 2D-DIGE proteomic analysis of bovine mammary epithelial cells during lactation reveals protein signatures for lactation persistency and milk yield. *PLoS One*, **9(8)**, p.e102515.

Jenab, S. and Morris, P.L., 1998. Testicular leukemia inhibitory factor (LIF) and LIF receptor mediate phosphorylation of signal transducers and

activators of transcription (STAT)-3 and STAT-1 and induce c-fos transcription and activator protein-1 activation in rat Sertoli but not germ cells. *Endocrinology*, **139(4)**, pp.1883-1890.

Jiang, W.G., 1996. E-cadherin and its associated protein catenins, cancer invasion and metastasis. *British journal of surgery*, **83(4)**, pp.437-446.

Jinushi, M., Draganov, D., Carrascco, D., Mihm, M., Tahara, H. and Dranoff, G., 2008. MFG-E8 derived from tumor-infiltrating myeloid cells plays a critical role in promoting tumor growth and metastasis.

Jinushi, M., Nakazaki, Y., Dougan, M., Carrasco, D.R., Mihm, M. and Dranoff, G., 2007. MFG-E8–mediated uptake of apoptotic cells by APCs links the pro-and antiinflammatory activities of GM-CSF. *The Journal of clinical investigation*, **117(7)**, pp.1902-1913.

Jinushi, M., Sato, M., Kanamoto, A., Itoh, A., Nagai, S., Koyasu, S., Dranoff, G. and Tahara, H., 2009. Milk fat globule epidermal growth factor–8 blockade triggers tumor destruction through coordinated cell-autonomous and immune-mediated mechanisms. *Journal of Experimental Medicine*, **206(6)**, pp.1317-1326.

Johnston, S.R., 2006. Clinical efforts to combine endocrine agents with targeted therapies against epidermal growth factor receptor/human epidermal growth factor receptor 2 and mammalian target of rapamycin in breast cancer. *Clinical Cancer Research*, ***12*(3)**, pp.1061s-1068s.

Kamal, A., Nayak, V.L., Nagesh, N., Vishnuvardhan, M.V.P.S. and Reddy, N.S., 2016. Benzo [b] furan derivatives induces apoptosis by targeting the PI3K/Akt/mTOR signaling pathway in human breast cancer cells. *Bioorganic Chemistry*, **66**, pp.124-131.

Kamal, A., Nayak, V.L., Nagesh, N., Vishnuvardhan, M.V.P.S. and Reddy, N.S., 2016. Benzo [b] furan derivatives induces apoptosis by targeting the PI3K/Akt/mTOR signaling pathway in human breast cancer cells. *Bioorganic Chemistry*, **66**, pp.124-131.

Kaur, G., Ali, S.A., Pachauri, S., Malakar, D., Kaushik, J.K., Mohanty, A.K. and Kumar, S., 2017. Buffalo leukemia inhibitory factor induces

differentiation and dome-like secondary structures in COS-1 cells. *Cytogenetic and genome research*, ***151*****(3)**, pp.119-130.

Kawashima, T., Bao, Y.C., Minoshima, Y., Nomura, Y., Hatori, T., Hori, T., Fukagawa, T., Fukada, T., Takahashi, N., Nosaka, T. and Inoue, M., 2009. A Rac GTPase-activating protein, MgcRacGAP, is a nuclear localizing signal-containing nuclear chaperone in the activation of STAT transcription factors. *Molecular and cellular biology*, **29(7)**, pp.1796-1813.

Kelly, P.A., 2002. Bachelot A, Kedzia C, Hennighausen L, Ormandy CJ, Kopchick JJ, Binart N. The role of prolactin and growth hormone in mammary gland development. *Mol Cell Endocrinol*, **197**, pp.127-131.

Kendrick, H., Regan, J.L., Magnay, F.A., Grigoriadis, A., Mitsopoulos, C., Zvelebil, M. and Smalley, M.J., 2008. Transcriptome analysis of mammary epithelial subpopulations identifies novel determinants of lineage commitment and cell fate. *BMC genomics*, **9(1)**, p.591.

Kimata, K., Sakakura, T., Inaguma, Y., Kato, M. and Nishizuka, Y., 1985. Participation of two different mesenchymes in the developing mouse mammary gland: synthesis of basement membrane components by fat pad precursor cells. *Development*, ***89*****(1)**, pp.243-257.

Köcher, T. and Superti-Furga, G., 2007. Mass spectrometry–based functional proteomics: from molecular machines to protein networks. *Nature methods*, ***4*****(10)**, pp.807-815.

Kodama, H., Fukuda, K., Pan, J., Makino, S., Baba, A., Hori, S. and Ogawa, S., 1997. Leukemia inhibitory factor, a potent cardiac hypertrophic cytokine, activates the JAK/STAT pathway in rat cardiomyocytes. *Circulation research*, **81(5)**, pp.656-663.

Koga, S., Yamaguchi, N., Abe, T., Minegishi, M., Tsuchiya, S., Yamamoto, M. and Minegishi, N., 2007. Cell-cycle–dependent oscillation of GATA2 expression in hematopoietic cells. *Blood*, ***109*****(10)**, pp.4200-4208.

Kollar, E.J. and Fisher, C., 1980. Tooth induction in chick epithelium: expression of quiescent genes for enamel synthesis. *Science*, ***207*****(4434)**, pp.993-995.

Kratochwil, K. and Schwartz, P., 1976. Tissue interaction in androgen response of embryonic mammary rudiment of mouse: identification of target tissue for testosterone. *Proceedings of the National Academy of Sciences*, ***73*****(11)**, pp.4041-4044.

Kratochwil, K., 1969. Organ specificity in mesenchymal induction demonstrated in the embryonic development of the mammary gland of the mouse. *Developmental biology*, ***20*****(1)**, pp.46-71.

Kratochwil, K., 1971. In vitro analysis of the hormonal basis for the sexual dimorphism in the embryonic development of the mouse mammary gland. *Development*, ***25*****(1)**, pp.141-153.

Kreft, H. and Jetz, W., 2007. Global patterns and determinants of vascular plant diversity. *Proceedings of the National Academy of Sciences*, **104(14)**, pp.5925-5930.

Kreuzaler, P.A., Staniszewska, A.D., Li, W., Omidvar, N., Kedjouar, B., Turkson, J., Poli, V., Flavell, R.A., Clarkson, R.W. and Watson, C.J., 2011. Stat3 controls lysosomal-mediated cell death in vivo. *Nature cell biology*, ***13*****(3)**, pp.303-309.

Kritikou, E.A., Sharkey, A., Abell, K., Came, P.J., Anderson, E., Clarkson, R.W. and Watson, C.J., 2003. A dual, non-redundant, role for LIF as a regulator of development and STAT3-mediated cell death in mammary gland*. Development*, **130(15),** pp.3459-3468.

Kumar, R., Manning, J., Spendlove, H.E., Kremmidiotis, G., McKirdy, R., Lee, J., Millband, D.N., Cheney, K.M., Stampfer, M.R., Dwivedi, P.P. and Morris, H.A., 2006. ZNF652, a novel zinc finger protein, interacts with the putative breast tumor suppressor CBFA2T3 to repress transcription. *Molecular cancer research*, ***4*****(9)**, pp.655-665.

Kusakabe, M., Sakakura, T., Sano, M. and Nishizuka, Y., 1985. A pituitary-salivary mixed gland induced by tissue recombination of embryonic

pituitary epithelium and embryonic submandibular gland mesenchyme in mice. *Developmental biology*, ***110*(2)**, pp.382-391.

Kwak, P.B., Iwasaki, S. and Tomari, Y., 2010. The microRNA pathway and cancer. *Cancer science*, **101(11),** pp.2309-2315.

Lahm, H.W. and Langen, H., 2000. Mass spectrometry: a tool for the identification of proteins separated by gels. *ELECTROPHORESIS: An International Journal*, ***21*(11)**, pp.2105-2114.

LaMarca, H.L. and Rosen, J.M., 2007. Estrogen regulation of mammary gland development and breast cancer: amphiregulin takes center stage. *Breast Cancer Research*, ***9*(4)**, p.304.

LaMarca, H.L. and Rosen, J.M., 2008. Hormones and Mammary Cell Fate—What Will I Become When I Grow Up?. *Endocrinology*, ***149*(9)**, pp.4317-4321.

LaRocca, J., Pietruska, J. and Hixon, M., 2011. Akt1 is essential for postnatal mammary gland development, function, and the expression of Btn1a1. *PloS one*, **6(9)**, p.e24432.

Laurin, M., Huber, J., Pelletier, A., Houalla, T., Park, M., Fukui, Y., Haibe-Kains, B., Muller, W.J. and Côté, J.F., 2013. Rac-specific guanine nucleotide exchange factor DOCK1 is a critical regulator of HER2-mediated breast cancer metastasis. *Proceedings of the National Academy of Sciences*, **110(18)**, pp.7434-7439.

Lee, M.H. and Yang, H.Y., 2003. Regulators of G1 cyclin–dependent kinases and cancers. *Cancer and Metastasis Reviews*, **22(4)**, pp.435-449.

Lee, S., Medina, D., Tsimelzon, A., Mohsin, S.K., Mao, S., Wu, Y. and Allred, D.C., 2007. Alterations of gene expression in the development of early hyperplastic precursors of breast cancer. *The American journal of pathology*, ***171*(1)**, pp.252-262.

Leung, K.C., Doyle, N., Ballesteros, M., Sjogren, K., Watts, C.K.W., Low, T.H., Leong, G.M., Ross, R.J.M. and Ho, K.K.Y., 2003. Estrogen inhibits GH signaling by suppressing GH-induced JAK2 phosphorylation, an effect

mediated by SOCS-2. *Proceedings of the National Academy of Sciences*, 1**00(3)**, pp.1016-1021.

Li, M., Liu, X., Robinson, G., Bar-Peled, U., Wagner, K.U., Young, W.S., Hennighausen, L. and Furth, P.A., 1997. Mammary-derived signals activate programmed cell death during the first stage of mammary gland involution. *Proceedings of the National Academy of Sciences*, ***94*(7)**, pp.3425-3430.

Litterst, C.M., Kliem, S., Marilley, D. and Pfitzner, E., 2003. NCoA-1/SRC-1 is an essential coactivator of STAT5 that binds to the FDL motif in the α-helical region of the STAT5 transactivation domain. *Journal of Biological Chemistry*, **278(46)**, pp.45340-45351.

Liu, T., Dong, X.G., Wang, Y., Yan, Y. and Zhang, J.J., 2008. The mechanism of twist gene regulation during the retina angiogenesis. [Zhonghua yan ke za zhi] *Chinese journal of ophthalmology*, **44(7)**, pp.634-639.

Lönnerdal, B., 2003. Nutritional and physiologic significance of human milk proteins. *The American journal of clinical nutrition*, ***77*(6)**, pp.1537S-1543S.

Lu, P. and Werb, Z., 2008. Patterning mechanisms of branched organs. *Science*, ***322*(5907)**, pp.1506-1509.

Luban, J. and Goff, S.P., 1995. The yeast two-hybrid system for studying protein—protein interactions. *Current opinion in biotechnology*, ***6*(1)**, pp.59-64.

Luber, C.A., Cox, J., Lauterbach, H., Fancke, B., Selbach, M., Tschopp, J., Akira, S., Wiegand, M., Hochrein, H., O'Keeffe, M. and Mann, M., 2010. Quantitative proteomics reveals subset-specific viral recognition in dendritic cells. *Immunity*, ***32*(2)**, pp.279-289.

Lund, L.R., Romer, J., Thomasset, N., Solberg, H., Pyke, C., Bissell, M.J., Dano, K. and Werb, Z., 1996. Two distinct phases of apoptosis in mammary gland involution: proteinase-independent and-dependent pathways. *Development*, ***122*(1)**, pp.181-193.

Macias, H. and Hinck, L., 2012. Mammary gland development. *Wiley Interdisciplinary Reviews: Developmental Biology*, **1(4)**, pp.533-557.

MacLean, B., Eng, J.K., Beavis, R.C. and McIntosh, M., 2006. General framework for developing and evaluating database scoring algorithms using the TANDEM search engine. *Bioinformatics*, ***22*(22)**, pp.2830-2832.

Maestro, R., Dei Tos, A.P., Hamamori, Y., Krasnokutsky, S., Sartorelli, V., Kedes, L., Doglioni, C., Beach, D.H. and Hannon, G.J., 1999. Twist is a potential oncogene that inhibits apoptosis. *Genes & development*, **13(17)**, pp.2207-2217.

Mailleux, A.A., Spencer-Dene, B., Dillon, C., Ndiaye, D., Savona-Baron, C., Itoh, N., Kato, S., Dickson, C., Thiery, J.P. and Bellusci, S., 2002. Role of FGF10/FGFR2b signaling during mammary gland development in the mouse embryo. *Development*, ***129*(1)**, pp.53-60.

Makarov, A. and Denisov, E., 2009. Dynamics of ions of intact proteins in the Orbitrap mass analyzer. *Journal of the American Society for Mass Spectrometry*, ***20*(8)**, pp.1486-1495.

Makarov, A. and Scigelova, M., 2010. Coupling liquid chromatography to Orbitrap mass spectrometry. *Journal of Chromatography A*, ***1217*(25)**, pp.3938-3945.

Makarov, A., Denisov, E., Kholomeev, A., Balschun, W., Lange, O., Strupat, K. and Horning, S., 2006. Performance evaluation of a hybrid linear ion trap/orbitrap mass spectrometer. *Analytical chemistry*, ***78*(7)**, pp.2113-2120.

Makarov, A., Denisov, E., Lange, O. and Horning, S., 2006. Dynamic range of mass accuracy in LTQ Orbitrap hybrid mass spectrometer. *Journal of the American Society for Mass Spectrometry*, ***17*(7)**, pp.977-982.

Mallepell, S., Krust, A., Chambon, P. and Brisken, C., 2006. Paracrine signaling through the epithelial estrogen receptor α is required for proliferation and morphogenesis in the mammary gland. *Proceedings of the National Academy of Sciences*, ***103*(7)**, pp.2196-2201.

Mann, M., 2006. Functional and quantitative proteomics using SILAC. *Nature reviews Molecular cell biology*, ***7*****(12)**, pp.952-958.

Manning, G., Whyte, D.B., Martinez, R., Hunter, T. and Sudarsanam, S., 2002. The protein kinase complement of the human genome. *Science*, ***298*****(5600)**, pp.1912-1934.

Mapes, J., Li, Q., Kannan, A., Anandan, L., Laws, M., Lydon, J.P., Bagchi, I.C. and Bagchi, M.K., 2017. CUZD1 is a critical mediator of the JAK/STAT5 signaling pathway that controls mammary gland development during pregnancy. *PLoS genetics*, **13(3)**, p.e1006654.

Marshall, A.G., Hendrickson, C.L. and Jackson, G.S., 1998. Fourier transform ion cyclotron resonance mass spectrometry: a primer. *Mass spectrometry reviews*, ***17*****(1)**, pp.1-35.

Marti, A., Jehn, B., Costello, E., Keon, N., Ke, G., Martin, F. and Jaggi, R., 1994. Protein kinase A and AP-1 (c-Fos/JunD) are induced during apoptosis of mouse mammary epithelial cells. *Oncogene*, ***9*****(4)**, pp.1213-1223.

Marti, A., Lazar, H., Ritter, P. and Jaggi, R., 1999. Transcription factor activities and gene expression during mouse mammary gland involution. *Journal of mammary gland biology and neoplasia*, ***4*****(2)**, pp.145-152.

Mather, I.H. and Keenan, T.W., 1998. Origin and secretion of milk lipids. *Journal of mammary gland biology and neoplasia*, ***3*****(3)**, pp.259-273.

Mayer, J.A., Foley, J., De La Cruz, D., Chuong, C.M. and Widelitz, R., 2008. Conversion of the nipple to hair-bearing epithelia by lowering bone morphogenetic protein pathway activity at the dermal-epidermal interface. *The American journal of pathology*, ***173*****(5)**, pp.1339-1348.

McNally, S. and Martin, F., 2011. Molecular regulators of pubertal mammary gland development. *Annals of medicine*, ***43*****(3)**, pp.212-234.

Miermont, A.M., Parrish, A.R. and Furth, P.A., 2010. Role of ERα in the differential response of Stat5a loss in susceptibility to mammary preneoplasia and DMBA-induced carcinogenesis. *Carcinogenesis*, **31(6)**, pp.1124-1131.

Milanese, T.R., Hartmann, L.C., Sellers, T.A., Frost, M.H., Vierkant, R.A., Maloney, S.D., Pankratz, V.S., Degnim, A.C., Vachon, C.M., Reynolds, C.A. and Thompson, R.A., 2006. Age-related lobular involution and risk of breast cancer. *Journal of the National Cancer Institute*, ***98*(22)**, pp.1600-1607.

Minami, M., Inoue, M., Wei, S., Takeda, K., Matsumoto, M., Kishimoto, T. and Akira, S., 1996. STAT3 activation is a critical step in gp130-mediated terminal differentiation and growth arrest of a myeloid cell line. *Proceedings of the National Academy of Sciences*, **93(9)**, pp.3963-3966.

Miwa, T., Manabe, Y., Kurokawa, K., Kamada, S., Kanda, N., Bruns, G., Ueyama, H. and Kakunaga, T., 1991. Structure, chromosome location, and expression of the human smooth muscle (enteric type) gamma-actin gene: evolution of six human actin genes. *Molecular and cellular biology*, **11(6)**, pp.3296-3306.

Moll, R., Franke, W.W., Schiller, D.L., Geiger, B. and Krepler, R., 1982. The catalog of human cytokeratins: patterns of expression in normal epithelia, tumors and cultured cells. *Cell*, ***31*(1)**, pp.11-24.

Monks, J., Rosner, D., Geske, F.J., Lehman, L., Hanson, L., Neville, M.C. and Fadok, V.A., 2005. Epithelial cells as phagocytes: apoptotic epithelial cells are engulfed by mammary alveolar epithelial cells and repress inflammatory mediator release. *Cell Death & Differentiation*, ***12*(2)**, pp.107-114.

Monks, J., Smith-Steinhart, C., Kruk, E.R., Fadok, V.A. and Henson, P.M., 2008. Epithelial cells remove apoptotic epithelial cells during post-lactation involution of the mouse mammary gland. *Biology of reproduction*, ***78*(4)**, pp.586-594.

Monks, J., Smith-Steinhart, C., Kruk, E.R., Fadok, V.A. and Henson, P.M., 2008. Epithelial cells remove apoptotic epithelial cells during post-lactation involution of the mouse mammary gland. *Biology of reproduction*, **78(4)**, pp.586-594.

Mukherjee, A., Soyal, S.M., Li, J., Ying, Y., He, B., DeMayo, F.J. and Lydon, J.P., 2010. Targeting RANKL to a specific subset of murine mammary epithelial cells induces ordered branching morphogenesis and alveologenesis in the absence of progesterone receptor expression. *The FASEB Journal*, **24(11)**, pp.4408-4419.

Mulac-Jericevic, B., Lydon, J.P., DeMayo, F.J. and Conneely, O.M., 2003. Defective mammary gland morphogenesis in mice lacking the progesterone receptor B isoform. *Proceedings of the National Academy of Sciences*, *100*(17), pp.9744-9749.

Mustacchi, P. and Shimkin, M.B., 1957. Occurrence of cancer in acromegaly and in hypopituitarism. *Cancer*, ***10*(1)**, pp.100-104.

Myers, J.A., 1917. Studies on the mammary gland. II. The fetal development of the mammary gland in the female albino rat. *American Journal of Anatomy*, *22*(2), pp.195-223.

Nandi, S., 1958. Endocrine control of mammary-gland development and function in the C3H/He Crgl mouse. *Journal of the National Cancer Institute*, ***21*(6)**, pp.1039-1063.

Neilson, L.M., Zhu, J., Xie, J., Malabarba, M.G., Sakamoto, K., Wagner, K.U., Kirken, R.A. and Rui, H., 2007. Coactivation of janus tyrosine kinase (Jak) 1 positively modulates prolactin-Jak2 signaling in breast cancer: recruitment of ERK and signal transducer and activator of transcription (Stat) 3 and enhancement of Akt and Stat5a/b pathways. *Molecular endocrinology*, **21(9)**, pp.2218-2232.

Nelson, C.M., VanDuijn, M.M., Inman, J.L., Fletcher, D.A. and Bissell, M.J., 2006. Tissue geometry determines sites of mammary branching morphogenesis in organotypic cultures. *Science*, ***314*(5797)**, pp.298-300.

Nesvizhskii, A.I., Keller, A., Kolker, E. and Aebersold, R., 2003. A statistical model for identifying proteins by tandem mass spectrometry. *Analytical chemistry*, ***75*(17)**, pp.4646-4658.

Neubauer, B.L., Chung, L.W., McCormick, K.A., Taguchi, O., Thompson, T.C. and Cunha, G.R., 1983. Epithelial-mesenchymal interactions in prostatic development. II. Biochemical observations of prostatic induction by urogenital sinus mesenchyme in epithelium of the adult rodent urinary bladder. *Journal of Cell Biology*, ***96*****(6)**, pp.1671-1676.

Neutzner, M., Lopez, T., Feng, X., Bergmann-Leitner, E.S., Leitner, W.W. and Udey, M.C., 2007. MFG-E8/lactadherin promotes tumor growth in an angiogenesis-dependent transgenic mouse model of multistage carcinogenesis. *Cancer research*, **67(14)**, pp.6777-6785.

Neville, M.C., 1999. Physiology of lactation. *Clinics in perinatology*, ***26*****(2)**, pp.251-279.

Neville, M.C., McFadden, T.B. and Forsyth, I., 2002. Hormonal regulation of mammary differentiation and milk secretion. *Journal of mammary gland biology and neoplasia*, ***7*****(1)**, pp.49-66.

Nguyen, D.A., Parlow, A.F. and Neville, M.C., 2001. Hormonal regulation of tight junction closure in the mouse mammary epithelium during the transition from pregnancy to lactation. *Journal of Endocrinology*, ***170*****(2)**, pp.347-356.

Nishimura, Y., Yoshioka, K., Bernard, O., Bereczky, B. and Itoh, K., 2006. A role of LIM kinase 1/cofilin pathway in regulating endocytic trafficking of EGF receptor in human breast cancer cells. *Histochemistry and cell biology*, **126(5)**, p.627.

O'Brien, J., Martinson, H., Durand-Rougely, C. and Schedin, P., 2012. Macrophages are crucial for epithelial cell death and adipocyte repopulation during mammary gland involution. *Development*, ***139*****(2)**, pp.269-275.

Oda, Y., Huang, K., Cross, F.R., Cowburn, D. and Chait, B.T., 1999. Accurate quantitation of protein expression and site-specific phosphorylation. *Proceedings of the National Academy of Sciences*, ***96*****(12)**, pp.6591-6596.

Oftedal, O.T., 2002. The mammary gland and its origin during synapsid evolution. *Journal of mammary gland biology and neoplasia*, ***7*(3)**, pp.225-252.

Olijnyk, D., Ibrahim, A.M., Ferrier, R.K., Tsuda, T., Chu, M.L., Gusterson, B.A., Stein, T. and Morris, J.S., 2014. Fibulin-2 is involved in early extracellular matrix development of the outgrowing mouse mammary epithelium. *Cellular and molecular life sciences*, ***71*(19)**, pp.3811-3828.

Olsen, J.V., Andersen, J.R., Nielsen, P.A., Nielsen, M.L., Figeys, D., Mann, M. and Wiśniewski, J.R., 2004. HysTag—a novel proteomic quantification tool applied to differential display analysis of membrane proteins from distinct areas of mouse brain. *Molecular & Cellular Proteomics*, ***3*(1)**, pp.82-92.

Olsen, J.V., Blagoev, B., Gnad, F., Macek, B., Kumar, C., Mortensen, P. and Mann, M., 2006. Global, in vivo, and site-specific phosphorylation dynamics in signaling networks. *Cell*, ***127*(3)**, pp.635-648.

Olsen, J.V., de Godoy, L.M., Li, G., Macek, B., Mortensen, P., Pesch, R., Makarov, A., Lange, O., Horning, S. and Mann, M., 2005. Parts per million mass accuracy on an Orbitrap mass spectrometer via lock mass injection into a C-trap. *Molecular & Cellular Proteomics*, ***4*(12)**, pp.2010-2021.

Olsen, J.V., Vermeulen, M., Santamaria, A., Kumar, C., Miller, M.L., Jensen, L.J., Gnad, F., Cox, J., Jensen, T.S., Nigg, E.A. and Brunak, S., 2010. Quantitative phosphoproteomics reveals widespread full phosphorylation site occupancy during mitosis. *Science signaling*, ***3*(104)**, pp.ra3-ra3.

Ong, S.E. and Mann, M., 2005. Mass spectrometry–based proteomics turns quantitative. *Nature chemical biology*, ***1*(5)**, pp.252-262.

Ong, S.E., Blagoev, B., Kratchmarova, I., Kristensen, D.B., Steen, H., Pandey, A. and Mann, M., 2002. Stable isotope labeling by amino acids in cell culture, SILAC, as a simple and accurate approach to expression proteomics. *Molecular & cellular proteomics*, ***1*(5)**, pp.376-386.

Ong, S.E., Foster, L.J. and Mann, M., 2003. Mass spectrometric-based approaches in quantitative proteomics. *Methods*, ***29*****(2)**, pp.124-130.

Ormandy, C.J., Naylor, M., Harris, J., Robertson, F., Horseman, N.D., Lindeman, G.J., Visvader, J.A.N.E. and Kelly, P.A., 2003. Investigation of the transcriptional changes underlying functional defects in the mammary glands of prolactin receptor knockout mice. *Recent progress in hormone research*, ***58***, pp.297-324.

Oshima, K., Aoki, N., Kato, T., Kitajima, K. and Matsuda, T., 2002. Secretion of a peripheral membrane protein, MFG-E8, as a complex with membrane vesicles: A possible role in membrane secretion. *European Journal of Biochemistry*, ***269*****(4)**, pp.1209-1218.

Oshima, K., Aoki, N., Negi, M., Kishi, M., Kitajima, K. and Matsuda, T., 1999. Lactation-Dependent Expression of an mRNA Splice Variant with an Exon for a MultiplyO-Glycosylated Domain of Mouse Milk Fat Globule Glycoprotein MFG-E8. *Biochemical and biophysical research communications***, 254(3),** pp.522-528.

Paredes, J., Milanezi, F., Reis-Filho, J.S., Leitão, D., Athanazio, D. and Schmitt, F., 2002. Aberrant P-cadherin expression: is it associated with estrogen-independent growth in breast cancer? *Pathology-Research and Practice*, **198(12)**, pp.795-801.

Paredes, J., Milanezi, F., Viegas, L., Amendoeira, I. and Schmitt, F., 2002. P-cadherin expression is associated with high-grade ductal carcinoma in situ of the breast. *Virchows Archiv***, 440(1)**, pp.16-21.

Park, D., Tosello-Trampont, A.C., Elliott, M.R., Lu, M., Haney, L.B., Ma, Z., Klibanov, A.L., Mandell, J.W. and Ravichandran, K.S., 2007. BAI1 is an engulfment receptor for apoptotic cells upstream of the ELMO/Dock180/Rac module. *Nature*, **450(7168)**, pp.430-434.

Park, D.S., Lee, H., Frank, P.G., Razani, B., Nguyen, A.V., Parlow, A.F., Russell, R.G., Hulit, J., Pestell, R.G. and Lisanti, M.P., 2002. Caveolin-1-deficient mice show accelerated mammary gland development during pregnancy, premature lactation, and hyperactivation of the Jak-

2/STAT5a signaling cascade. *Molecular biology of the cell*, **13(10)**, pp.3416-3430.

Parmar, H. and Cunha, G.R., 2004. Epithelial–stromal interactions in the mouse and human mammary gland in vivo. *Endocrine-related cancer*, ***11*(3)**, pp.437-458.

Peaker, M., 2002. The mammary gland in mammalian evolution: a brief commentary on some of the concepts. *Journal of mammary gland biology and neoplasia*, ***7*(3)**, pp.347-353.

Peinado, H., Portillo, F. and Cano, A., 2004. Transcriptional regulation of cadherins during development and carcinogenesis. *International Journal of Developmental Biology*, **48(5-6)**, pp.365-375.

Peng, Y. and Elkon, K.B., 2011. Autoimmunity in MFG-E8–deficient mice is associated with altered trafficking and enhanced cross-presentation of apoptotic cell antigens. *The Journal of clinical investigation*, **121(6)**, pp.2221-2241.

Perry, R.H., Cooks, R.G. and Noll, R.J., 2008. Orbitrap mass spectrometry: instrumentation, ion motion and applications. *Mass spectrometry reviews*, ***27*(6)**, pp.661-699.

Peuhu, E., Virtakoivu, R., Mai, A., Wärri, A. and Ivaska, J., 2017. Epithelial vimentin plays a functional role in mammary gland development. *Development*, **144(22)**, pp.4103-4113.

Pietersen, A.M., Evers, B., Prasad, A.A., Tanger, E., Cornelissen-Steijger, P., Jonkers, J. and van Lohuizen, M., 2008. Bmi1 regulates stem cells and proliferation and differentiation of committed cells in mammary epithelium. *Current biology*, **18(14)**, pp.1094-1099.

Polyak, K. and Kalluri, R., 2010. The role of the microenvironment in mammary gland development and cancer. *Cold Spring Harbor perspectives in biology*, ***2*(11)**, p.a003244.

Postigo, A.A., 2003. Opposing functions of ZEB proteins in the regulation of the TGFβ/BMP signaling pathway. *The EMBO journal*, **22(10)**, pp.2443-2452.

Postigo, A.A., Depp, J.L., Taylor, J.J. and Kroll, K.L., 2003. Regulation of Smad signaling through a differential recruitment of coactivators and corepressors by ZEB proteins. *The EMBO journal*, **22(10)**, pp.2453-2462.

Prilusky, J. and Deis, R.P., 1975. Effect of L-DOPA on milk ejection and prolactin release in lactating rats. *Journal of Endocrinology*, ***67*(3)**, pp.397-401.

Propper, A. and Gomot, L., 1967. Tissue interactions during organogenesis of the mammary gland in the rabbit embryo. *Comptes rendus hebdomadaires des seances de l'Academie des sciences. Serie D: Sciences naturelles*, ***264*(22)**, p.2573.

Propper, A.Y., 1978. Wandering epithelial cells in the rabbit embryo milk line: a preliminary scanning electron microscope study. *Developmental biology*, ***67*(1)**, pp.225-231.

Qiao, H., Di Stefano, L., Tian, C., Li, Y.Y., Yin, Y.H., Qian, X.P., Pang, X.W., Li, Y., McNutt, M.A., Helin, K. and Zhang, Y., 2007. Human TFDP3, a novel DP protein, inhibits DNA binding and transactivation by E2F. *Journal of Biological Chemistry*, ***282*(1)**, pp.454-466.

Quaglino, A., Schere-Levy, C., Romorini, L., Meiss, R.P. and Kordon, E.C., 2007. Mouse mammary tumors display Stat3 activation dependent on leukemia inhibitory factor signaling. *Breast cancer research*, **9(5),** p.R69.

Radice, G.L., Ferreira-Cornwell, M.C., Robinson, S.D., Rayburn, H., Chodosh, L.A., Takeichi, M. and Hynes, R.O., 1997. Precocious mammary gland development in P-cadherin–deficient mice. *The Journal of cell biology*, ***139*(4)**, pp.1025-1032.

Radice, G.L., Sauer, C.L., Kostetskii, I., Soler, A.P. and Knudsen, K.A., 2003. Inappropriate P-cadherin expression in the mouse mammary epithelium is compatible with normal mammary gland function. *Differentiation*, **71(6)**, pp.361-373.

Rawlings, J.S., Rosler, K.M. and Harrison, D.A., 2004. The JAK/STAT signaling pathway. *Journal of cell science*, **117(8)**, pp.1281-1283.

Raymond, A., Ensslin, M.A. and Shur, B.D., 2009. SED1/MFG-E8: a bi-motif protein that orchestrates diverse cellular interactions. *Journal of cellular biochemistry*, **106(6)**, pp.957-966.

Raynaud A., 1961. Morphogenesis of the mammary gland. In: Kon SK, Cowie AT, editors. Milk: the mammary gland and its secretion, vol. 1. *New York: Academic*; p.3–46.

Resemann, H.K., Watson, C.J. and Lloyd-Lewis, B., 2014. The Stat3 paradox: a killer and an oncogene. *Molecular and cellular endocrinology*, **382(1)**, pp.603-611.

Richert, M.M., Schwertfeger, K.L., Ryder, J.W. and Anderson, S.M., 2000. An atlas of mouse mammary gland development. *Journal of mammary gland biology and neoplasia*, ***5*(2)**, pp.227-241.

Rijnkels, M., Kabotyanski, E., Montazer-Torbati, M.B., Beauvais, C.H., Vassetzky, Y., Rosen, J.M. and Devinoy, E., 2010. The epigenetic landscape of mammary gland development and functional differentiation. *Journal of mammary gland biology and neoplasia*, **15(1)**, pp.85-100.

Robinson, G.W., 2007. Cooperation of signalling pathways in embryonic mammary gland development. *Nature Reviews Genetics*, ***8*(12)**, pp.963-972.

Rocha-Viegas, L., Vicent, G.P., Barañao, J.L., Beato, M. and Pecci, A., 2006. Glucocorticoids repress bcl-X expression in lymphoid cells by recruiting STAT5B to the P4 promoter. *Journal of Biological Chemistry*, **281(45),** pp.33959-33970.

Ross, P.L., Huang, Y.N., Marchese, J.N., Williamson, B., Parker, K., Hattan, S., Khainovski, N., Pillai, S., Dey, S., Daniels, S. and Purkayastha, S., 2004. Multiplexed protein quantitation in Saccharomyces cerevisiae using amine-reactive isobaric tagging reagents. *Molecular & cellular proteomics*, ***3*(12)**, pp.1154-1169.

Roy, P.G. and Thompson, A.M., 2006. Cyclin D1 and breast cancer. *The Breast*, **15(6)**, pp.718-727.

Rubenstein, P.A., 1990. The functional importance of multiple actin isoforms. *Bioessays*, **12(7),** pp.309-315.

Russo, I.H. and Russo, J., 1996. Mammary gland neoplasia in long-term rodent studies. *Environmental health perspectives*, ***104*(9)**, pp.938-967.

Russo, I.H. and Russo, J., 2011. Pregnancy-induced changes in breast cancer risk. *Journal of mammary gland biology and neoplasia*, ***16*(3)**, p.221.

Russo, J. and Russo, I.H., 2004. Development of the human breast. *Maturitas*, ***49*(1)**, pp.2-15.

Russo, J., Russo, IH., 1987. The mammary gland: development, regulation and function. Plenum, *New York*, NY.

Sakakura T., 1987. Mammary embryogenesis. In: Neville MC, Daniel CW, editors. The mammary gland. *New York: Plenum Pub Corp*; p. 37–66.

Sakakura, T., Kusano, I., Kusakabe, M., Inaguma, Y. and Nishizuka, Y., 1987. Biology of mammary fat pad in fetal mouse: capacity to support development of various fetal epithelia in vivo. *Development*, ***100*(3)**, pp.421-430.

Sakakura, T., Nishizuka, Y. and Dawe, C.J., 1976. Mesenchyme-dependent morphogenesis and epithelium-specific cytodifferentiation in mouse mammary gland. *Science*, ***194*(4272)**, pp.1439-1441.

Sakakura, T., Sakagami, Y. and Nishizuka, Y., 1982. Dual origin of mesenchymal tissues participating in mouse mammary gland embryogenesis. *Developmental biology*, ***91*(1)**, pp.202-207.

Santos, S.J., Haslam, S.Z. and Conrad, S.E., 2008. Estrogen and progesterone are critical regulators of Stat5a expression in the mouse mammary gland. *Endocrinology*, **149(1)**, pp.329-338.

Santos, S.J., Haslam, S.Z. and Conrad, S.E., 2010. Signal transducer and activator of transcription 5a mediates mammary ductal branching and proliferation in the nulliparous mouse. *Endocrinology*, **151(6)**, pp.2876-2885.

Saxen, L., 1970. Failure to demonstrate tubule induction in a heterologous mesenchyme. *Developmental biology*, ***23*****(4)**, pp.511-523.

Schere-Levy, C., Buggiano, V., Quaglino, A., Gattelli, A., Cirio, M.C., Piazzon, I., Vanzulli, S. and Kordon, E.C., 2003. Leukemia inhibitory factor induces apoptosis of the mammary epithelial cells and participates in mouse mammary gland involution. *Experimental cell research*, **282(1)**, pp.35-47.

Schmalhofer, O., Brabletz, S. and Brabletz, T., 2009. E-cadherin, β-catenin, and ZEB1 in malignant progression of cancer. *Cancer and Metastasis Reviews*, **28(1-2)**, pp.151-166.

Schulze, W.X. and Usadel, B., 2010. Quantitation in mass-spectrometry-based proteomics. *Annual review of plant biology*, ***61***, pp.491-516.

Schwertfeger, K.L., Richert, M.M. and Anderson, S.M., 2001. Mammary gland involution is delayed by activated Akt in transgenic mice. *Molecular endocrinology*, ***15*****(6)**, pp.867-881.

Seif, F., Khoshmirsafa, M., Aazami, H., Mohsenzadegan, M., Sedighi, G. and Bahar, M., 2017. The role of JAK-STAT signaling pathway and its regulators in the fate of T helper cells. *Cell communication and signaling*, **15(1)**, pp.1-13.

Semba, Y., Harada, A., Maehara, K., Oki, S., Meno, C., Ueda, J., Yamagata, K., Suzuki, A., Onimaru, M., Nogami, J. and Okada, S., 2017. Chd2 regulates chromatin for proper gene expression toward differentiation in mouse embryonic stem cells. *Nucleic acids research*, ***45*****(15)**, pp.8758-8772.

Silberstein, G.B., Van Horn, K.A.T.H.A.R.I.N.E., Shyamala, G. and Daniel, C.W., 1994. Essential role of endogenous estrogen in directly stimulating mammary growth demonstrated by implants containing pure antiestrogens. *Endocrinology*, ***134*****(1)**, pp.84-90.

Silvestre, J.S., Théry, C., Hamard, G., Boddaert, J., Aguilar, B., Delcayre, A., Houbron, C., Tamarat, R., Blanc-Brude, O., Heeneman, S. and

Clergue, M., 2005. Lactadherin promotes VEGF-dependent neovascularization. Nature medicine, **11(5)**, pp.499-506.

Simon-Assmann, P., Bouziges, F., Arnold, C., Haffen, K. and Kedinger, M., 1988. Epithelial-mesenchymal interactions in the production of basement membrane components in the gut. *Development*, ***102*(2)**, pp.339-347.

Slavkin, H.C., Zeichner-David, M. and Siddiqui, M.A.Q., 1981. Molecular aspects of tooth morphogenesis and differentiation. *Molecular Aspects of Medicine*, ***4*(2)**, pp.125-188.

Smith, G.P., 1985. Filamentous fusion phage: novel expression vectors that display cloned antigens on the virion surface. *Science*, ***228*(4705)**, pp.1315-1317.

Soady, K.J., Kendrick, H., Gao, Q., Tutt, A., Zvelebil, M., Ordonez, L.D., Quist, J., Tan, D.W.M., Isacke, C.M., Grigoriadis, A. and Smalley, M.J., 2015. Mouse mammary stem cells express prognostic markers for triple-negative breast cancer. *Breast Cancer Research*, **17(1)**, p.31.

Sommers, C.L., 1996. The role of cadherin-mediated adhesion in breast cancer. *Journal of mammary gland biology and neoplasia*, **1(2)**, pp.219-229.

Soriano, J.V., Pepper, M.S., Orci, L. and Montesano, R., 1998. Roles of hepatocyte growth factor/scatter factor and transforming growth factor-β1 in mammary gland ductal morphogenesis. *Journal of mammary gland biology and neoplasia*, ***3*(2)**, pp.133-150.

Sotgia, F., Williams, T.M., Schubert, W., Medina, F., Minetti, C., Pestell, R.G. and Lisanti, M.P., 2006. Caveolin-1 deficiency (−/−) conveys premalignant alterations in mammary epithelia, with abnormal lumen formation, growth factor independence, and cell invasiveness. *The American journal of pathology*, **168(1)**, pp.292-309.

Spemann, H. and Mangold, H., 2003. Induction of embryonic primordia by implantation of organizers from a different species. 1923. *International Journal of Developmental Biology*, ***45*(1)**, pp.13-38.

Steen, H. and Pandey, A., 2002. Proteomics goes quantitative: measuring protein abundance. *Trends in biotechnology*, ***20*****(9)**, pp.361-364.

Stein, T., Morris, J.S., Davies, C.R., Weber-Hall, S.J., Duffy, M.A., Heath, V.J., Bell, A.K., Ferrier, R.K., Sandilands, G.P. and Gusterson, B.A., 2004. Involution of the mouse mammary gland is associated with an immune cascade and an acute-phase response, involving LBP, CD14 and STAT3. *Breast Cancer Research*, **6(2)**, p.R75.

Sternlicht, M.D., Kouros-Mehr, H., Lu, P. and Werb, Z., 2006. Hormonal and local control of mammary branching morphogenesis. *Differentiation*, ***74*****(7)**, pp.365-381.

Strange, R., Li, F., Saurer, S., Burkhardt, A. and Friis, R.R., 1992. Apoptotic cell death and tissue remodelling during mouse mammary gland involution. *Development*, ***115*****(1)**, pp.49-58.

Stubbs, J.D., Lekutis, C., Singer, K.L., Bui, A., Yuzuki, D., Srinivasan, U. and Parry, G., 1990. cDNA cloning of a mouse mammary epithelial cell surface protein reveals the existence of epidermal growth factor-like domains linked to factor VIII-like sequences. *Proceedings of the National Academy of Sciences*, **87(21)**, pp.8417-8421.

Sugano, G., Bernard-Pierrot, I., Lae, M., Battail, C., Allory, Y., Stransky, N., Krumeich, S., Lepage, M.L., Maille, P., Donnadieu, M.H. and Abbou, C.C., 2011. Milk fat globule—epidermal growth factor—factor VIII (MFGE8)/lactadherin promotes bladder tumor development. *Oncogene*, ***30*****(6)**, pp.642-653.

Tang, X., Zhao, Y., Buchon, N. and Engström, Y., 2018. The POU/Oct Transcription factor nubbin controls the balance of intestinal stem cell maintenance and differentiation by isoform-specific regulation. *Stem cell reports*, ***10*****(5)**, pp.1565-1578.

Taniguchi, C.M., Emanuelli, B. and Kahn, C.R., 2006. Critical nodes in signalling pathways: insights into insulin action. *Nature reviews Molecular cell biology*, ***7*****(2)**, pp.85-96.

Taylor, M.R., Couto, J.R., Scallan, C.D., Ceriani, R.L. and Peterson, J.A., 1997. Lactadherin (formerly BA46), a membrane-associated glycoprotein expressed in human milk and breast carcinomas, promotes Arg-Gly-Asp (RGD)-dependent cell adhesion. *DNA and cell biology*, ***16*(7)**, pp.861-869.

Tonozuka, Y., Minoshima, Y., Bao, Y.C., Moon, Y., Tsubono, Y., Hatori, T., Nakajima, H., Nosaka, T., Kawashima, T. and Kitamura, T., 2004. A GTPase-activating protein binds STAT3 and is required for IL-6–induced STAT3 activation and for differentiation of a leukemic cell line. *Blood*, **104(12)**, pp.3550-3557.

Topper, Y.J. and Freeman, C.S., 1980. Multiple hormone interactions in the developmental biology of the mammary gland. *Physiological reviews*, ***60*(4)**, pp.1049-1106.

Traurig, H.H., 1967. A radioautographic study of cell proliferation in the mammary gland of the pregnant mouse. *The Anatomical Record*, ***159*(2)**, pp.239-247.

Turner, C.W. and Gomez, E.T., 1933. *The normal development of the mammary gland of the male and female albino mouse*. University of Missouri, College of Agriculture, Agricultural Experiment Station.

Ubersax, J.A. and Ferrell Jr, J.E., 2007. Mechanisms of specificity in protein phosphorylation. *Nature reviews Molecular cell biology*, ***8*(7)**, pp.530-541.

Vafaizadeh, V., Klemmt, P., Brendel, C., Weber, K., Doebele, C., Britt, K., Grez, M., Fehse, B., Desriviéres, S. and Groner, B., 2010. Mammary epithelial reconstitution with gene-modified stem cells assigns roles to Stat5 in luminal alveolar cell fate decisions, differentiation, involution, and mammary tumor formation. *Stem cells*, **28(5)**, pp.928-938.

Vandekerckhove, J. and Weber, K., 1978. At least six different actins are expressed in a higher mammal: an analysis based on the amino acid sequence of the amino-terminal tryptic peptide. *Journal of molecular biology*, **126(4)**, pp.783-802.

Veltmaat, J.M., Mailleux, A.A., Thiery, J.P. and Bellusci, S., 2003. Mouse embryonic mammogenesis as a model for the molecular regulation of pattern formation. *Differentiation*, ***71*****(1)**, pp.1-17.

Veltmaat, J.M., Relaix, F., Le, L.T., Kratochwil, K., Sala, F.G., van Veelen, W., Rice, R., Spencer-Dene, B., Mailleux, A.A., Rice, D.P. and Thiery, J.P., 2006. Gli3-mediated somitic Fgf10 expression gradients are required for the induction and patterning of mammary epithelium along the embryonic axes. *Development*, ***133*****(12)**, pp.2325-2335.

Verfaillie, A., Imrichová, H., Van de Sande, B., Standaert, L., Christiaens, V., Hulselmans, G., Herten, K., Sanchez, M.N., Potier, D., Svetlichnyy, D. and Atak, Z.K., 2014. iRegulon: from a gene list to a gene regulatory network using large motif and track collections. *PLoS Comput Biol*, ***10*****(7)**, p.e1003731.

Verma, R., Oania, R., Graumann, J. and Deshaies, R.J., 2004. Multiubiquitin chain receptors define a layer of substrate selectivity in the ubiquitin-proteasome system. *Cell*, **118(1)**, pp.99-110.

Vermeulen, M., Hubner, N.C. and Mann, M., 2008. High confidence determination of specific protein–protein interactions using quantitative mass spectrometry. *Current opinion in biotechnology*, ***19*****(4)**, pp.331-337.

Vicent, G.P., Zaurin, R., Ballaré, C., Nacht, A.S. and Beato, M., 2009. Erk signaling and chromatin remodeling in MMTV promoter activation by progestins. *Nuclear receptor signaling*, **7(1)**, pp.nrs-07008.

Vickers, N.J., 2017. Animal communication: when i'm calling you, will you answer too?. *Current biology*, ***27*****(14)**, pp.R713-R715.

Virtakoivu, R., Mai, A., Mattila, E., De Franceschi, N., Imanishi, S.Y., Corthals, G., Kaukonen, R., Saari, M., Cheng, F., Torvaldson, E. and Kosma, V.M., 2015. Vimentin–ERK Signaling Uncouples Slug Gene Regulatory Function. *Cancer research*, **75(11)**, pp.2349-2362.

Virtakoivu, R., Peuhu, E., Mai, A., Wärri, A. and Ivaska, J., 2017. Vimentin plays a functional role in mammary gland regeneration. *bioRxiv*, p.134544.

Visvader, J.E., 2009. Keeping abreast of the mammary epithelial hierarchy and breast tumorigenesis. *Genes & development*, ***23*****(22)**, pp.2563-2577.

Wagner, K.U. and Rui, H., 2008. Jak2/Stat5 signaling in mammogenesis, breast cancer initiation and progression. *Journal of mammary gland biology and neoplasia*, **13(1)**, pp.93-103.

Wagner, K.U., Krempler, A., Triplett, A.A., Qi, Y., George, N.M., Zhu, J. and Rui, H., 2004. Impaired alveologenesis and maintenance of secretory mammary epithelial cells in Jak2 conditional knockout mice. *Molecular and cellular biology*, ***24*****(12)**, pp.5510-5520.

Wang, T.C., Cardiff, R.D., Zukerberg, L., Lees, E., Arnold, A. and Schmidt, E.V., 1994. Mammary hyperplasia and carcinoma in MMTV-cyclin D1 transgenic mice. *Nature*, **369(6482)**, pp.669-671.

Wang, Y.N., Yang, W.C., Li, P.W., Wang, H.B., Zhang, Y.Y. and Zan, L.S., 2018. Myocyte enhancer factor 2A promotes proliferation and its inhibition attenuates myogenic differentiation via myozenin 2 in bovine skeletal muscle myoblast. *PLoS One*, ***13*****(4)**, p.e0196255.

Watkin, H., Richert, M.M., Lewis, A., Terrell, K., McManaman, J.P. and Anderson, S.M., 2008. Lactation failure in Src knockout mice is due to impaired secretory activation. *BMC developmental biology*, **8(1)**, pp.1-22.

Watson, C.J. and Khaled, W.T., 2008. Mammary development in the embryo and adult: a journey of morphogenesis and commitment. *Development*, **135(6)**, pp.995-1003.

Watson, C.J. and Kreuzaler, P.A., 2011. Remodeling mechanisms of the mammary gland during involution. *International Journal of Developmental Biology*, **55(7-8-9)**, pp.757-762.

Watson, C.J., 2006. Key stages in mammary gland development-Involution: apoptosis and tissue remodelling that convert the mammary gland from milk factory to a quiescent organ. *Breast Cancer Research*, **8(2)**, pp.1-5.

Wessells, N.K. and Cohen, J.H., 1967. Early pancreas organogenesis: morphogenesis, tissue interactions, and mass effects. *Developmental biology*, ***15*****(3)**, pp.237-270.

Weymouth, N., Shi, Z. and Rockey, D.C., 2012. Smooth muscle α actin is specifically required for the maintenance of lactation. *Developmental biology*, **363(1)**, pp.1-14.

Wilkins, M.R., Pasquali, C., Appel, R.D., Ou, K., Golaz, O., Sanchez, J.C., Yan, J.X., Gooley, A.A., Hughes, G., Humphery-Smith, I. and Williams, K.L., 1996. From proteins to proteomes: large scale protein identification by two-dimensional electrophoresis and arnino acid analysis. *Bio/technology*, ***14*****(1)**, pp.61-65.

Williams, J.M. and Daniel, C.W., 1983. Mammary ductal elongation: differentiation of myoepithelium and basal lamina during branching morphogenesis. *Developmental biology*, ***97*****(2)**, pp.274-290.

Wilm, M., 2009. Quantitative proteomics in biological research. *Proteomics*, ***9*****(20)**, pp.4590-4605.

Wiśniewski, J.R., Zougman, A., Nagaraj, N. and Mann, M., 2009. Universal sample preparation method for proteome analysis. *Nature methods*, ***6*****(5)**, pp.359-362.

Xu, G., Paige, J.S. and Jaffrey, S.R., 2010. Global analysis of lysine ubiquitination by ubiquitin remnant immunoaffinity profiling. *Nature biotechnology*, ***28*****(8)**, pp.868-873.

Yamaji, D., Na, R., Feuermann, Y., Pechhold, S., Chen, W., Robinson, G.W. and Hennighausen, L., 2009. Development of mammary luminal progenitor cells is controlled by the transcription factor STAT5A. *Genes & development*, **23(20)**, pp.2382-2387.

Yan, W. and Chen, S.S., 2005. Mass spectrometry-based quantitative proteomic profiling. *Briefings in Functional Genomics*, ***4*****(1)**, pp.27-38.

Yang, C., Hayashida, T., Forster, N., Li, C., Shen, D., Maheswaran, S., Chen, L., Anderson, K.S., Ellisen, L.W., Sgroi, D. and Schmidt, E.V., 2011. The integrin αvβ3-5 ligand MFG-E8 is a p63/p73 target gene in triple-

negative breast cancers but exhibits suppressive functions in ER+ and erbB2+ breast cancers. *Cancer research*, **71(3)**, pp.937-945.

Yang, M.H. and Wu, K.J., 2008. TWIST activation by hypoxia inducible factor-1 (HIF-1): implications in metastasis and development. *Cell cycle*, **7(14)**, pp.2090-2096.

Yates, J.R., Ruse, C.I. and Nakorchevsky, A., 2009. Proteomics by mass spectrometry: approaches, advances, and applications. *Annual review of biomedical engineering*, ***11***, pp.49-79.

Ye, X., Tam, W.L., Shibue, T., Kaygusuz, Y., Reinhardt, F., Eaton, E.N. and Weinberg, R.A., 2015. Distinct EMT programs control normal mammary stem cells and tumour-initiating cells. *Nature*, **525(7568)**, pp.256-260.

Yu, Q., Geng, Y. and Sicinski, P., 2001. Specific protection against breast cancers by cyclin D1 ablation. *Nature*, **411(6841)**, pp.1017-1021.

Zhao, Q.J., Yu, Y.B., Zuo, X.L., Dong, Y.Y. and Li, Y.Q., 2012. Milk fat globule-epidermal growth factor 8 is decreased in intestinal epithelium of ulcerative colitis patients and thereby causes increased apoptosis and impaired wound healing. *Molecular Medicine*, ***18*(3)**, pp.497-506.

Zhou, B.P., 2004. Deng J, Xia W, Xu J, Li YM, Gunduz M, Hung MC. Dual regulation of Snail by GSK-3beta-mediated phosphorylation in control of epithelial-mesenchymal transition. *Nat Cell Biol*, **6**, pp.931-940.

Appendices

APPENDIX-I

1. Dulbecco's minimal essential medium (DMEM)

Dulbecco's minimal essential medium (Sigma, D2906-1L, without $NaHCO_3$ & Phenol red) was dissolved in sterile water (15.6g/l) and supplemented with sodium bicarbonate (1.2g/l). The pH of the resulting solution was adjusted to 7.3 using IN NaOH and filtered through 0.22 µm Millex – GV filter unit (Millipore). The medium was aliquoted in sterilized 100ml reagent bottles and stored at 4 ºC in refrigerator.

2. Determination of cell concentration in cell suspension by Haemocytometer

A. Neubauer counting chamber/haemocytometer

A haemocytometer enclose two Neubauer chambers. Each chamber is ruled into nine major squares, and each square is having height=1 mm, width=1 mm and depth=0.1 mm. Thus when coverslipped, the volume of each major square is = 1 x 1 x 0.1 mm^3 = 0.1 mm^3 or 0.1 µL. Since 1 mm^3 = 1 µL.

N = Average number of cells per major square

= Average number of cells per 0.1 µL

Hence, no. of cells per 1 µL = N x 10

Number of cells per 1000 µL (1 mL) = N x 10 x 1000 = N x 10^4

B. Method

The haemocytometer was placed on a levelled surface and cover slipped. The cells suspension was loaded into the channel (Hchannel) of the counting chamber by capillary action. Care was taken not to overload the chamber so that both the chamber draws the liquid uniformly. The counting chamber was viewed under a light microscope with 200x magnification and the cell numbers were counted in, lower left (LL: 16 small squares) and lower right (LR: 16 small squares) and the middle/central square (C: 25 small squares containing 25 x 16 smallest squares). Similarly, the cells of 5 each of four corner squares: upper left (UL: 16 small squares), and upper right (UR: 16 small squares) major squares of other chamber were also counted. The average no. of cells per major square was obtained by dividing the total no. of cells of 10 major squares by 10 and that gave the value of N.

C. Calculation of cell concentration in suspension:

No. of cells present in 0.1 µL of 1:400 diluted cell sample = N

No. of cells present in 1 mL of 1:400 diluted cell sample = N x 10^4

No. of cells present in 1 mL of original (undiluted) cell sample

= N x 10^4 x Dilution Factor (DF)

D. Adjusting the cells concentration suspension to 100 x 10^6 cells/mL

Concentration of original stock = N x 10^6 cells/mL

Concentration of required stock = 100 x 10^6 cells/mL

Let, 1 mL of original cell sample should be diluted to **(X)** mL to get 100 x 10^6 cells/mL

Hence, using the formula N1 x V1 = N2 x V2

Where,

N1 = Concentration of required cell sample

V1 = Final volume of required cell sample

N2 = Concentration of original (undiluted) cell sample

V2 = Volume of original cell sample to be diluted

N1 (100 x 10^6cells/mL) x V1 (**X** mL) = N2 (N x 10^6cells/mL) x V2 (1 mL)

100 x 10^6cells/mL x **(X)** mL = N x 10^6cells/mL x 1 mL

Hence, 1 mL of original cell sample should be diluted to N/100 mL to get cell concentration of 10^8cells/mL

E.g. If in one cell suspension N = 250, then

X = (1 x 250)/100 = 2.5 mL i.e 1 mL of original sample should be diluted to 2.5 mL to have cell concentration 100 x 10^6cells/mL

APPENDIX-II

1. **MTT:** 5 mg MTT/mL of PBS
2. **Neutral red (NR)**: 50µg/mL in serum free media

Formal calcium:

1) 10mL 40% formaldehyde
2) 10mL of 10%anhydrous calcium chloride
3) 80mL DW

Acetic acid and ethanol mixture: 1mL glacial acetic acid in 50% ethanol

3. **DCFH-DA dye:** Dilute 50 mg DCF-DA in 2.565 mL DMSO to make 40 mM
4. **Trypan Blue (1%):** 10 mg of trypan blue was weighed in 1.5 ml of centrifuge tube and dissolved in 1 mL of media on the day of experiment.
5. **Phosphate Buffer Solution (PBS 1x500mL):** 4 g of NaCl (137mM), 0.1 g of KCl (2.7mM), 0.575 g of Na2HPO4 (8.1mM) and 0.1 g of KH2PO4 (1.5mM) were dissolved in distilled water and make upto 500 mL for 1x concentration and finally adjust the pH 7.4 with 1M NaOH and stored at 4^0C.

6.1 M Potassium Phosphate Buffer (Reagent A): Prepared in 10 ml deionized water using Potassium Phosphate, Monobasic, Anhydrous. Adjust to pH 7.7 at 30°C with 1 M KOH.)

7. **100 mM Ethylenediaminetetraacetic Acid (Reagent B):** Prepared in 10 ml deionized water using Ethylenediaminetetraacetic Acid, Disodium Salt,Dihydrate
8. **TBE buffer (for gel electrophoresis**

Stock solution of 0.5M EDTA (500mL):

1) 93.03 g EDTA
2) Dissolve in 200mL deionized water (use magnetic stirrer before p^H titration)
3) Add NaOH until solution becomes clear inside fume hood. Adjust p^H 8.
4) Adjust the volume to 500 mL with deionized water.

Stock solution of TBE 10% (1Liter):

1) Dissolve (use magnetic stirrer) 108g Tris and 55g Boric acid in 800mL distilled water

2) Add 40mL 0.5 M Na_2EDTA (p^H 8.0)

3) Adjust volume to 1Liter

4) Store at room temperature

Preparation of working solution of TBE:

For agarose gel electrophoresis, TBE can be used at a concentration of 0.5X (1:10 dilution of the concentrated stock). Dilute the stock solution by 10X in deionized water.

APPENDIX-III

No.	Equipments	Company
1	Centrifuge	Remi R-8C Laboratory Centrifuge
2	CO_2 Incubator	NuAire water jacketed CO2 Incubator
3	Light microscope	CK-RFL, Olympus Optical Co. Ltd., Japan
5	Neubauer Chamber	Superior Merienfeld, Germany
6	Weighing Balance	Sartorins
7	pH meter	Genei. Pvt. Ltd, India
8	Power supply	Genei Digital, PS 500, Bangalore
10	Serological Water Bath	Popular India
11	Sonicator	Branson Sonic Power Company, Danbury
12	Spectrophotometer	UVD-3500 double beam UV/visible spectrophotometer (Labomed, USA)
13	ELISA plate reader	Epoch™ Microplate reader
14	Nanodrop	Thermo Scientific NanoDrop 2000 spectrophotometer
15	PCR	Thermo Scientific
16	Real time PCR	Applied Biosystems 7500 Real-Time PCR System
17	Magnetic stirrer	Perfit India
18	Phase contrast microscope	Olympus,CK40
19	Electrophoresis System	Biorad horizontal Mini-Sub Cell GT
20	Tissue Homogeniser	Perfit India
21	Cold centrifuge	Hermle Z 446 tabletop centrifuge
22	Orbitrap Fusion™ Tribrid™ Mass Spectrometer	Thermo Scientific™
23	Q-TOF Maxis HD	Bruker Daltonics